

ANALYSIS OF
ALTERNATIVE SPLICING REGULATION IN THE
HYPERVARIABLE RECEPTOR *DSCAM*

By
YASH RAMESH HEMANI

A thesis submitted to the
University of Birmingham
for the degree of
DOCTOR OF PHILOSOPHY

School of Biosciences
College of Life and Environmental Sciences
University of Birmingham
September 2012

UNIVERSITY OF
BIRMINGHAM

University of Birmingham Research Archive

e-theses repository

This unpublished thesis/dissertation is copyright of the author and/or third parties. The intellectual property rights of the author or third parties in respect of this work are as defined by The Copyright Designs and Patents Act 1988 or as modified by any successor legislation.

Any use made of information contained in this thesis/dissertation must be in accordance with that legislation and must be properly acknowledged. Further distribution or reproduction in any format is prohibited without the permission of the copyright holder.

Abstract

The pattern recognition receptor Dscam is a key molecule mediating innate immunity and wiring of the nervous system in *Drosophila*. Intriguingly, massive molecular diversity is generated by alternative splicing in three exon clusters of *Dscam*.

Upon pathogen exposure in *Anopheles gambiae*, the *AgDscam* splicing pattern changes to express isoforms that bind pathogens with higher affinity. In order to test the generality of *Dscam* splicing regulation in *Drosophila*, similar experiments involving microbial exposure were carried out, which also showed changes in *Dscam* splicing pattern. Mutants in RNA regulatory pathways and in the RNA binding protein ELAV were analyzed due to their similar mutant phenotypes in nervous system development as *Dscam*. In each of these mutants, alterations of *Dscam* alternative splicing in a cluster specific manner were observed, eluding a unique mechanism for any of the analyzed pathways. In ELAV mutants, one of the three clusters of alternatively spliced exons is dramatically mis-regulated.

Since no ELAV binding site is present in this cluster, genes downstream of ELAV could mediate mis-regulation of alternative splicing. From the analysis of mutants in ELAV differentially regulated genes it was concluded that *Dscam* alternative splicing is most prominently affected by chromatin remodeling factors, along with RNA binding proteins, DNA binding proteins and small-RNA processing factors. A heterologous transgene for expression of *Dscam* pre-mRNA in *Drosophila* was also developed to characterize the role of the chromatin state in alternative splicing.

Dedicated to

Pujyashri Gurudev

Baa

Mom and Dad

and the entire Hemani family

Acknowledgements

I would like to sincerely thank my PhD supervisor, Dr. Matthias Soller for guiding me throughout the course of my PhD. This project would not have been possible without your remarkable insights and technical prowess. Thank you for instilling in me the importance of efficient time management, multi-tasking and proaction. I earnestly thank The Darwin Trust of Edinburgh for funding my PhD.

I am very grateful to all members of the Soller lab namely Irmi, Emma, Min and Pinar for their support and cooperation without which this experience would have been far more difficult. Thanks to Irmi for her expert advice and useful discussions. Thanks to Emma for teaching me the basics of fly genetics and for being a great companion for all these years. Thanks to Min for teaching me fly transgenesis and for being a great listener in times of stress. I would like to extend my gratitude to all the past and present members of the Brogna, Hidalgo and Dove labs for making the '6th floor' such a fun place to work in.

I sincerely thank Mr. Suresh Patel, Mrs. Nirmala Patel and the entire Patel family for your support and blessings. All of you have been so kind and loving towards me. Thank you for making my stay in the UK such a memorable experience. Thanks to Dr. Apporva Bhatt and Dr. Kiran Bhatt for your advice and invaluable inputs during my PhD.

Lastly, I would like to thank Nawsheen Damree and Riddhi Shah for being fantastic housemates with whom I shared my daily experiences. Thank you, Nawsheen for being my pillar of strength during this entire journey. Thank you for always believing in me and providing me with solace in times of anxiety and pressure. Thank you, Riddhi for being a great friend, a confidante and my cooking buddy!

Table of Contents

CHAPTER 1: INTRODUCTION	1
1.1. Pre-mRNA processing	2
1.2. Pre-mRNA splicing	3
1.3. Alternative splicing	6
1.3.1. Modes of alternative splicing	8
1.3.2. Regulation of alternative splicing	10
1.3.2.1. Splice site strength regulates alternative splicing	11
1.3.2.2. Splicing regulatory elements and RNA binding proteins regulate alternative splicing	11
1.3.2.3. Cellular signaling regulates alternative splicing	12
1.3.2.4. Tissue-specific regulatory proteins affect alternative splicing regulation	13
1.3.2.5. Co-transcriptional regulation of alternative splicing	13
1.3.2.6. Promoter type can regulate alternative splicing	14
1.3.2.7. RNA pol II processivity can regulate alternative splicing	15
1.3.2.8. Nucleosome occupancy suggests a role in alternative splicing regulation	17
1.3.2.9. Histone modifications and chromatin structure can regulate alternative splicing	20
1.4. Mechanisms of mutually exclusive splicing	23
1.5. The <i>Dscam</i> gene	26
1.5.1. Gene organization and protein structure	26
1.5.2. <i>Dscam</i> mutually exclusive splicing and its regulation	28
1.5.2.1. RNA secondary structures mediate <i>Dscam</i> variable exon selection	28
1.5.2.2. <i>Dscam</i> variable exon clusters are in a repressed state	32
1.5.2.3. RNA binding proteins regulate inclusion of <i>Dscam</i> variable exons	35
1.6. Biological role of <i>Dscam</i> in invertebrates	37
1.6.1. Role of <i>Dscam</i> in <i>Drosophila</i> nervous system	37
1.6.1.1. Development of <i>Drosophila</i> nervous system	37
1.6.1.2. <i>Dscam</i> isoforms exhibit homophilic binding	38
1.6.1.3. Role of <i>Dscam</i> in axon guidance and dendritic field organization	41
1.6.1.4. Diversity of <i>Dscam</i> intracellular domain is important for neuronal development	45
1.6.2. Overview of the immune system	47
1.6.2.1. Insect immune system	48
1.6.2.2. Evidence for 'trained immunity' in invertebrates	49
1.6.2.3. <i>Dscam</i> splicing regulation provides 'trained immunity' in invertebrates	51
1.7. Model for <i>Dscam</i> splicing regulation	53
1.8. Aims	54
1.9. Objectives	54

CHAPTER 2: MATERIALS AND METHODS	57
2.1 <i>Drosophila</i> husbandry and genetics	57
2.1.1. Fly food	57
2.1.2. Fly maintenance	57
2.1.3. Embryo collection	57
2.1.4. Fly transgenesis with <i>UAS Dscam 9L</i>	58
2.2. Molecular biology	61
2.2.1. RNA isolation	61
2.2.2. Reverse transcription (RT)	62
2.2.3. Polymerase chain reaction (PCR)	63
2.2.3.1. Single fly PCR	63
2.2.4. Agarose gel electrophoresis	64
2.3. Radioactivity used to label primers	64
2.3.1. Primer radiolabeling	65
2.3.2. Restriction enzyme digests of PCR products from <i>Dscam</i> variable regions	65
2.3.3. Denaturing polyacrylamide gel electrophoresis	67
2.3.4. Quantification of bands	69
2.4. Molecular cloning	69
2.4.1. Media preparation	69
2.4.2. Preparation of competent cells	70
2.4.2.1. Chemically competent cells	70
2.4.2.2. Electro-competent cells	70
2.4.3. Primer phosphorylation	72
2.4.4. Phenol-chloroform extraction of PCR products	72
2.4.5. Restriction enzyme digests of PCR products	73
2.4.6. Gel extraction of digested DNA fragments	73
2.4.7. Ligation	74
2.4.8. Bacterial transformation	74
2.4.8.1. Heat shock transformation	74
2.4.8.2. Electro-transformation	75
2.4.9. Recombineering	75
2.4.9.1. Generation of pRed/ET electro-competent cells	76
2.4.9.2. Generation of <i>Dscam</i> BAC/pRed/ET electro-competent cells	76
2.4.9.3. Preparation of <i>Dscam</i> BAC/pRed/ET host for DNA retrieval	77
2.4.10. Plasmid DNA mini prep	78
2.4.11. Plasmid DNA midi prep	78
2.4.12. DNA sequencing	80
2.4.13. Cloning of <i>pAc5.1A Dscam Mut Exons 4-9</i>	80
2.5. Cell culture	86
2.5.1. Pathogen infection of <i>Drosophila</i> haemocytes	86
2.5.2. Treatment of <i>Drosophila</i> haemocytes with drugs affecting transcription and RNA pol II processivity	88
2.5.3. Transfection of <i>pAc5.1A Dscam Mut Exons 4-9</i> in <i>Drosophila</i> haemocytes	88
2.6. Western Blotting	90
2.6.1. Sample preparation	90

2.6.2. Sodiumdodecylsulphate polyacrylamide gel electrophoresis (SDS-PAGE)	90
2.6.3. Transfer	91
2.6.4. Blocking	91
2.6.5. Blotting	91
2.6.6. Development	92
CHAPTER 3: RESULTS	93
3.1. <i>Dscam</i> variable exons in clusters 4, 6 and 9 have similar sizes	93
3.2. Separation of <i>Dscam</i> variable exons based on sequence variation	93
3.3. <i>Dscam</i> splicing pattern changes on exposure to pathogens in S2 cells	101
3.4. Variation in <i>Dscam</i> splicing between different developmental stages, strains and sexes	106
3.5. Analysis of <i>Dscam</i> splicing in mutants of genes involved in small RNA and mRNA processing	115
3.6. Analysis of <i>ago1</i> and <i>rrp6</i> maternal mutants and redundancy between Agos and <i>rrp6</i> in <i>Dscam</i> splicing regulation	118
3.7. Overexpression of a single <i>Dscam</i> isoform does not reinforce selection of the same variable exons	126
3.8. <i>Dscam</i> intracellular signaling is not involved in regulating its own splicing pattern	128
3.9. Analysis of mRNA methylation for a role in <i>Dscam</i> splicing regulation	131
3.10. Analysis of <i>Dscam</i> exon 9 splicing regulation in mutants of genes differentially regulated in <i>elav</i> mutants	134
3.11. RNA pol II processivity does not influence splicing of <i>Dscam</i>	138
3.12. <i>Dscam</i> diversity is not generated by differential stability of isoforms	140
3.13. Development of a <i>Dscam</i> exon 9 reporter transgene recapitulating endogenous exon 9 splicing	140
CHAPTER 4: DISCUSSION	144
4.1. Future work	148
Appendices	151
A1. Separation of <i>Dscam</i> 4 variants	151
A2. Separation of <i>Dscam</i> 9 variants	152
A3. Separation of <i>Dscam</i> 6 variants	153
A4. Crossing scheme showing generation of zygotic <i>ago1</i> mutants	155
A5. Crossing scheme showing generation of zygotic <i>rrp6</i> mutants	156
A6. Crossing scheme showing generation of zygotic <i>elav</i> mutants	161
A7. Crossing scheme showing generation of <i>ago1/Df; ago2/ago2</i> double mutants	158
A8. Crossing scheme showing generation of <i>ago1/Df; rrp6/Df</i> double mutants	159
A9. Crossing scheme showing generation	

of <i>ago1</i> zygotic and maternal mutants	160
A10. Crossing scheme showing generation of <i>rrp6</i> zygotic and maternal mutants	162
A11. Analysis of <i>Dscam</i> exon 9 splicing in mutants of genes that are differentially regulated in <i>elav</i> mutants	164
A12. List of primers	172
A13. List of fly stocks	173
List of references	175

List of figures

Figure 1: Spliceosome assembly and pre-mRNA splicing	4
Figure 2: Transesterification reactions involved in pre-mRNA splicing	7
Figure 3: Modes of alternative splicing	9
Figure 4: Mechanisms of mutually exclusive splicing	25
Figure 5: Dscam gene organization and protein structure	27
Figure 6: Complementarity between the docking site and selector sequences consensus	30
Figure 7: Proposed model for <i>Dscam</i> exon 4 mutually exclusive alternative splicing	31
Figure 8: Proposed model for <i>Dscam</i> exon 17 mutually exclusive alternative splicing	33
Figure 9: Proposed model for <i>Dscam</i> exon 6 mutually exclusive alternative splicing	34
Figure 10: Regulation of <i>Dscam</i> exon 4 mutually exclusive alternative splicing by the iStem	36
Figure 11: Molecular mechanism of homophilic interactions between identical Dscam isoforms	40
Figure 12: Role of <i>Dscam</i> diversity in mushroom body development	43
Figure 13: Role of <i>Dscam</i> diversity in dendritic field organization of dendritic arborization (da) neurons	44
Figure 14: A schematic diagram of post-scutellar (pSc) mechanosensory neuron projections into the adult fly thoracic central nervous system (CNS)	46
Figure 15: Specification of <i>Dscam</i> isoform expression	55
Figure 16: Diagrammatic representation of <i>Dscam</i> Ex 7-11 in <i>pUC 3GLA 2.5 HA UAS</i>	59
Figure 17: Diagrammatic representation of the initial cloning steps to generate <i>pAc5.1A Dscam Mut Exons 4-9</i>	82
Figure 18: Diagrammatic representation of the final cloning step to generate <i>pAc5.1A Dscam Mut Exons 4-9</i>	83
Figure 19: Amplification of <i>Dscam</i> variable exons by RT-PCR	94
Figure 20: Diagrammatic representation showing the separation of <i>Dscam</i> exon 4 variants	96
Figure 21: Resolution of <i>Dscam</i> exon 4 cluster	97
Figure 22: Resolution of <i>Dscam</i> exon 9 cluster	98
Figure 23: Resolution of <i>Dscam</i> exon 6 cluster	100
Figure 24 (A,B): <i>Dscam</i> exon 4 splicing pattern changes on exposure to heat inactivated pathogens in S2 cells	103
Figure 24 (C,D): <i>Dscam</i> exon 4 splicing pattern does not change in naïve S2 cells over a period of 12 hr	104
Figure 24 (E,F): <i>Dscam</i> exon 9 splicing pattern changes on exposure to heat inactivated pathogens in S2 cells	105
Figure 25: Variation in <i>Dscam</i> exon 4 splicing pattern between different developmental stages, strains, sexes and tissues	107-110
Figure 26: Variation in <i>Dscam</i> exon 9 splicing pattern between different developmental stages, strains, sexes	112-114
Figure 27: <i>ago1</i> and <i>elav</i> show similar <i>Dscam</i> mutant phenotype	116

Figure 28: Analysis of <i>Dscam</i> exon 4 splicing in mutants of genes involved in small RNA and mRNA processing	119
Figure 29: Analysis of <i>Dscam</i> exon 9 splicing in mutants of genes involved in small RNA and mRNA processing	120
Figure 30: Analysis of <i>Dscam</i> exon 6 splicing in mutants of genes involved in small RNA and mRNA processing	121
Figure 31: Schematic representation of generating germ line clones using the dominant female sterile (DFS) technique	123
Figure 32: PCR validation showing recombined FRT sites on the same chromosome as the (A) <i>ago1</i> and (B) <i>rrp6</i> lethal mutation	124
Figure 33: Analysis of <i>ago1</i> and <i>rrp6</i> maternal mutants and redundancy between Agos and <i>rrp6</i> in <i>Dscam</i> splicing regulation	125
Figure 34: Diagrammatic representation of distinguishing the endogenous <i>Dscam</i> exon 4 variants from the exogenously overexpressed <i>Dscam</i> single isoform, containing exon variant 4.6	127
Figure 35: Overexpression of a single <i>Dscam</i> isoform does not reinforce selection of the same variable exons	129
Figure 36: <i>Dscam</i> intracellular signaling is not involved in regulating its own splicing pattern	130
Figure 37: Analysis of mRNA methylation for a role in <i>Dscam</i> splicing regulation	132-133
Figure 38: Graphical representation of proportions of genes differentially regulated in <i>elav</i> mutants	135
Figure 39: Heat map representation of <i>Dscam</i> exon 9 splicing analysis in mutants of genes that are differentially regulated in <i>elav</i> mutants	136
Figure 40: RNA pol II processivity does not influence splicing of <i>Dscam</i>	139
Figure 41: <i>Dscam</i> diversity is not generated by differential stability of isoforms	141
Figure 42: Development of a <i>Dscam</i> exon 9 reporter transgene recapitulating endogenous exon 9 splicing	143

List of tables

Table 1: Denaturing polyacrylamide gel composition.	68
Table 2: List of antibiotics used during the study.	71
Table 3: Estimation of DNA amounts corresponding to size for DNA sequencing (Beckman Coulter).	81
Table 4: List of pathogens used to challenge S2 cells.	87
Table 5: List of drugs affecting transcription and RNA pol II processivity used during the study.	89

Abbreviations

ActD	Actinomycin D
ago1	Argonaute 1
ago2	Argonaute 2
AMPs	Antimicrobial peptides
attB	Bacterial attachment site
attP	Phage attachment landing site
BAC	Bacterial artificial chromosome
BBP	Branch point binding protein
bp	Base pairs
BSA	Bovine serum albumin
CAMs	Cell adhesion molecules
cDNA	complementary DNA
CELF4	CUG-BP and ETR3-like factor 4
ChIP	Chromatin immunoprecipitation
Ci	Curies
CNS	Central nervous system
Cpm	Counts per minute
CPSF	Cleavage and polyadenylation specificity factor
CstF	Cleavage stimulating factor
CTCF	CCCTC-binding factor
CTD	Carboxy terminal domain
CUG-BP	CUG-repeat-binding protein
da	Dendritic arborization
DDAB	Didecyltrimethylammonium bromide
ddH ₂ O	Double distilled water
DEPC	Diethylpyrocarbonate
DFS	Dominant female sterile
dNTPs	deoxyribonucleotides
dpm	Disintegrations per minute
dps	Disintegrations per second
DRB	Dichlororibofuranosylbenzimidazole
DSCAM	Down Syndrome Cell Adhesion Molecule
DSE	Downstream sequence element
Dsx	Doublesex
DTT	Dithiothreitol
E	Counting efficiency
EDI	Extra domain I
EDII	Extra domain II
EDTA	Ethylenediaminetetraacetic acid
ELAV	Embryonic lethal abnormal visual system
ESEs	Exonic splicing enhancers
ESSs	Exonic splicing silencers
ETR3	Elav-type RNA-binding protein 3
Ewg	Erect wing
FBS	Foetal bovine serum

<i>FGFR2</i>	Fibroblast growth factor receptor 2
FNIII	Fibronectin type III
FRT	FLP-recombinase target
GFP	Green fluorescent protein
GMCs	Ganglion mother cells
hnRNPs	Heterogeneous nuclear ribonucleoproteins
HP1 α	Heterochromatin-associated protein 1 α
Ig	Immunoglobulin
ISEs	Intronic splicing enhancers
ISSs	Intronic splicing silencers
iStem	Inclusion stem
LB	Luria Bertani
LPS	Lipopolysaccharide
MOPS	3-morpholinopropane-1-sulfonic acid
mRNA	Messenger RNA
msl-2	Male-specific-lethal-2
Na-valproate	Sodium valproate
NM	Non-muscle
NMD	Nonsense-mediated mRNA decay
nt	Nucleotides
OD ₆₀₀	Optical density at 600 nm
PAMPs	Pathogen-associated molecular patterns
PAP	Poly A polymerase
PBS	Phosphate-buffered saline
PCR	Polymerase chain reaction
PGNs	Peptidoglycans
PP1	Protein phosphatase 1
pre-mRNA	Precursor messenger RNA
proPO	Prophenoloxidase
PRRs	Pattern recognition receptors
pSc	Post-scutellar
PTB	Polypyrimidine tract-binding protein
PTC	Premature termination codon
(Py) _n	Polypyrimidine tract
RBP	RNA binding proteins
RNA pol II	RNA polymerase II
RNAi	RNA interference
RNAsin	Ribonuclease inhibitor
RNS	Reactive nitrogen species
ROS	Reactive oxygen species
RT	Reverse transcription
RT-PCR	Reverse transcription polymerase chain reaction
SDS-PAGE	Sodiumdodecylsulphate polyacrylamide gel electrophoresis
SF2	Splicing factor 2
siRNAs	Small interfering RNAs
SM	Smooth muscle
snRNPs	Small nuclear ribonucleoproteins
SOC	Super optimal broth

SR	Serine/arginine
SREs	Splicing regulatory elements
SRPK1	Serine-arginine protein kinase 1
ss	Splice sites
STET	Sucrose-Tris-EDTA-Triton-X 100
sxl	Sex-lethal
T4-PNK	T4 polynucleotide kinase
TAE	Tris-acetate-EDTA
TBE	Tris-borate-EDTA
TBS	Tris-buffered saline
TBST	Tris-buffered saline-Tween 20
TE	Tris-EDTA
TEMED	Tetramethylethylenediamine
tra	Transformer
TRAMP	Trf4/Air2/Mtr4p polyadenylation
U2AF	U2 auxiliary factor
ubx	Ultrabithorax
VEGF	Vascular endothelial growth factor
VSP	Variant-specific surface protein
WSSV	White spot syndrome virus

CHAPTER 1

INTRODUCTION

Sections 1.4 and 1.5 have been published as 'Mechanisms of *Drosophila* Dscam mutually exclusive splicing regulation' in the Biochemical Society Transactions with myself as first author and Dr. Matthias Soller as corresponding author. Both of us planned the topics and the layout of the manuscript. I wrote the manuscript and drew the figures. Dr. Soller proofread the manuscript prior to submission. For the full article please see (Hemani and Soller, 2012).

1.1. Pre-mRNA processing

Eukaryotic genes are characterized by the presence of protein-coding sequences called exons and non-coding sequences called introns. However, not all exons are located in the coding regions. Transcription of a gene by RNA polymerase II (RNA pol II) results in the formation of a single stranded precursor messenger RNA (pre-mRNA) molecule, which undergoes many complex modifications in the nucleus to form a mature messenger RNA (mRNA). The pre-mRNA processing reactions include capping, editing, splicing and 3' end processing. The resulting mRNA is then transported from the nucleus to the cytoplasm where it serves as a template for protein synthesis via translation (Soller, 2006).

The first pre-mRNA processing reaction is capping which involves the addition of an N⁷-methyl GMP at the 5' end of the pre-mRNA by an atypical 5'-5' triphosphate linkage (McCracken et al., 1997). Nucleotides adjacent to the 5' cap are also methylated to various degrees at the 2'-hydroxyl positions of their ribose sugars (Bisaillon and Lemay, 1997). Capping is important for protecting the mRNA from 5'-3' exonucleases, enhancing splicing of the first intron and 3' end processing, and for translation initiation (Flaherty et al., 1997; Fortes et al., 2000; Izaurralde et al., 1994; Lewis et al., 1996).

RNA editing is a process of altering the sequence of nucleotides within an RNA transcript of a gene by either modification or insertion/deletion of bases, to a sequence, which does not correspond to the sequence of that gene. Editing by modification of bases is largely achieved by deamination of adenosine to inosine (A to I) or cytidine to uridine (C to U) by specialized deaminases. Editing by insertion involves a guide RNA, which is partially complementary to the pre-mRNA transcript;

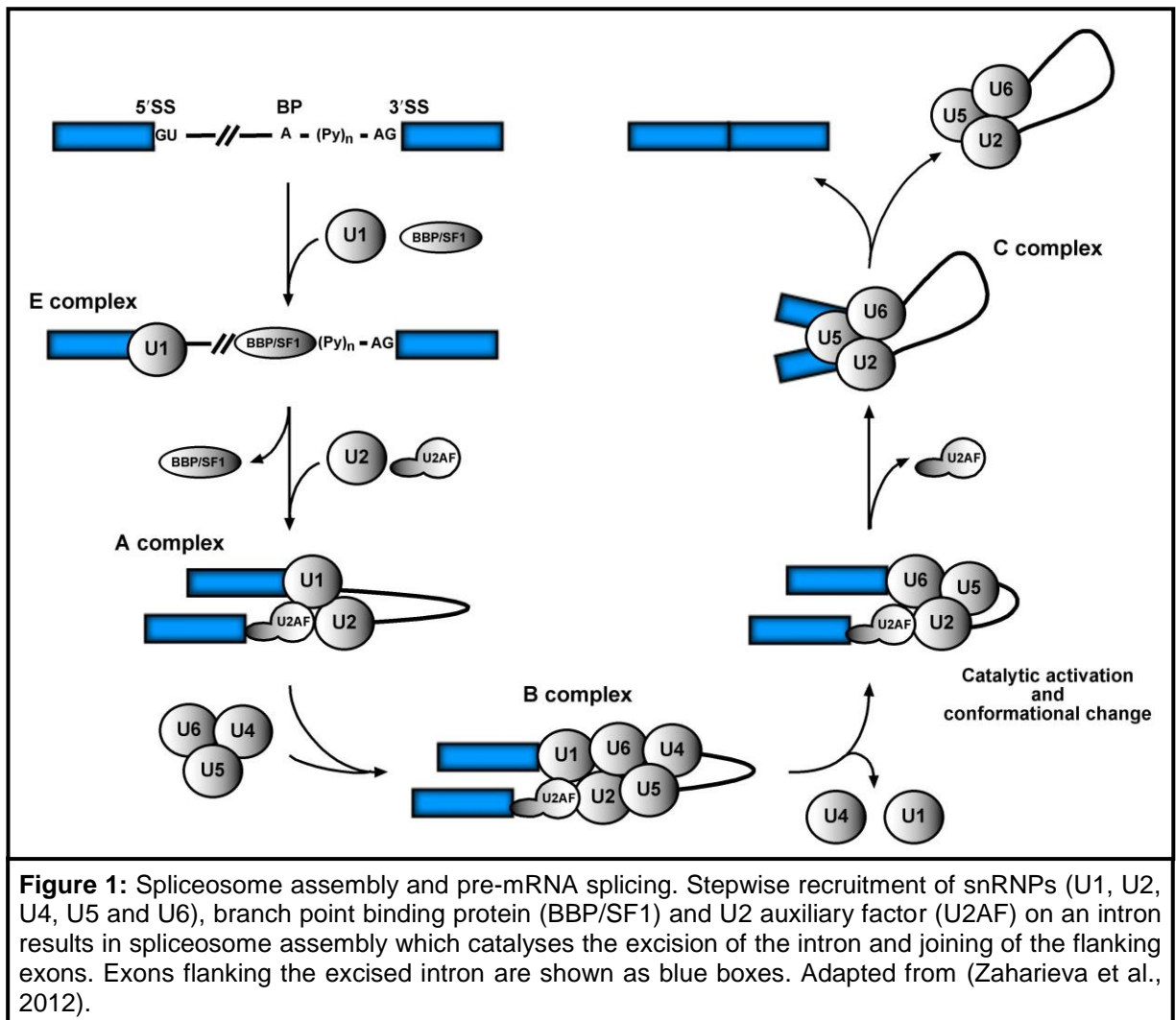
interrupted by additional adenosine residues. The guide RNA acts as a template for the synthesis of an edited transcript with additional uridines as observed in the mitochondria of trypanosomes. Only a few transcripts are edited in most eukaryotes (Smith et al., 1997).

Splicing is a process whereby introns, interspaced between the exons, are removed by the spliceosome, a multimeric RNA-protein complex, to produce an mRNA containing contiguous exons (Black, 2003). The mechanism of splicing and its regulation is explained in more detail from 1.2. to 1.4.

The final step of pre-mRNA processing involves cleavage and polyadenylation at the 3' end. Conserved sequence elements, which determine 3' processing comprise an AAUAAA hexamer, a CA dinucleotide located upstream of the cleavage site and a U- or GU-rich downstream sequence element (DSE). These sequence elements are identified by two multiprotein complexes; cleavage and polyadenylation specificity factor (CPSF) and cleavage stimulating factor (CstF) that trigger cleavage by cleavage factors I and II (CFI and CFII) and polyadenylation by poly A polymerase (PAP) together with CPSF (~200 adenosines). All RNA pol II transcripts have a poly-A tail except histone RNAs (Proudfoot, 2004; Venkataraman et al., 2005; Wahle and Ruegsegger, 1999; Zhao et al., 1999).

1.2. Pre-mRNA splicing

Pre-mRNA splicing comprises a series of reactions catalyzed by a multimeric RNA-protein complex called the spliceosome (Figure 1). The spliceosome is composed of small nuclear ribonucleoprotein (snRNP) subunits, which consist of five core structural RNAs namely U1, U2, U4, U5 and U6 and over 150 accessory proteins



(Jurica and Moore, 2003; Luhrmann and Stark, 2009). The orderly binding and release of these U snRNPs and auxiliary proteins results in excision of introns and joining of adjacent exons (Staley and Guthrie, 1998). Specific sequence elements in the pre-mRNA at the exon-intron junctions called splice sites (ss) are recognized by particular snRNPs and splicing factors. The 5' ss (splice donor site) and 3' ss (splice acceptor site) consensus sequences are defined by AG-guragu and yag-N (- designates the ss), respectively, however, only the first G of the 5' ss and the AG of the 3' ss are strictly conserved (Hertel, 2008; Smith et al., 1989). Additional sequence elements that mediate RNA splicing are the polypyrimidine tract ((Py)_n) immediately before the 3'ss and a branch point (ynyurac), containing a conserved adenine nucleotide, located upstream of the (Py)_n (Black, 2003).

The splicing reaction commences with the recruitment of U1 snRNP to the 5' ss, followed by the attachment of the branch point binding protein (BBP/SF1) to the branch point sequence to form the E complex. U2 auxiliary factor (U2AF), a heterodimeric splicing factor, binds to both the (Py)_n via its larger subunit (65-kDa) and the 3' ss via its smaller subunit (35-kDa). This binding triggers the recruitment of U2 snRNP, which binds to the branch point after the release of BBP/SF1, to form the A complex. The U4/U6.U5 heterotrimeric complex binds to the A complex to form the B complex (Soller, 2006).

At this point, a conformational rearrangement occurs within the B complex which results in the release of U1 and U4 snRNPs to eventually form the catalytic C complex. This complex catalyzes the removal of the intervening intron and joining of the adjacent exons via two transesterification steps. The first transesterification reaction occurs with the cleavage of the 5' end of the intron from the proximal exon

and its consequent ligation to the 2' hydroxyl group of the adenine in the branch point to form an unusual 2'-5' phosphodiester bond. At this point, there are two intermediates – the detached 5' exon and the intron-3' exon in the form of a lariat. The second transesterification reaction occurs with the nucleophilic attack on the phosphate at the 3' end of the intron by the 3' hydroxyl group of the separated exon. This results in the release of the intron, in the form of a lariat, and ligation of the two exons. The U2, U5 and U6 snRNPs release from the lariat, which is eventually linearized on hydrolysis of the 2'-5' phosphodiester bond by the lariat debranching enzyme (Black, 2003; Soller, 2006) (Figure 2). This mechanism underlies the function of the major class of spliceosomes, which removes introns flanked by conserved elements, 'gu' at the 5' end and 'ag' at the 3' end (Patel and Steitz, 2003). There is however, a minor class of spliceosome, which is involved in removal of introns with 'au' at the 5' end and 'ac' at the 3' end. Apart from recognizing different splicing signals, the minor spliceosome has different yet functionally equivalent snRNPs for U1, U2, U4 and U6, which are respectively called U11, U12, U4atac and U6atac (Patel and Steitz, 2003).

1.3. Alternative splicing

Alternative splicing is a process by which exons in the same pre-mRNA are differentially spliced to produce more than one variety of mature mRNA generating different protein isoforms from the same gene (Soller, 2006). Humans are estimated to have 22,000 genes, only a fraction more than the 20,000 genes postulated for the simple nematode, *Caenorhabditis elegans*, whereas grapevine (*Vitis vinifera*) has

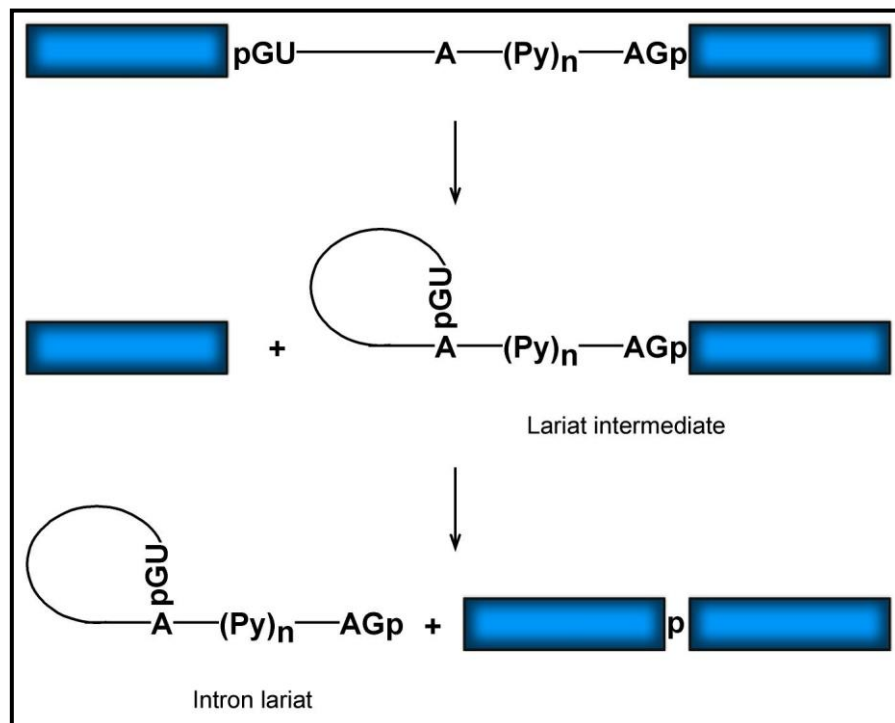


Figure 2: Transesterification reactions involved in pre-mRNA splicing. The catalytic C complex performs two transesterification reactions to result in efficient splicing of introns and subsequent ligation of flanking exons. The first transesterification step results in two reaction intermediates: the upstream exon and an intron/downstream exon fragment in a lariat conformation. The second transesterification step joins the two exons and excises the intron lariat. Exons flanking the excised intron are shown as blue boxes. Adapted from (Black, 2003).

~30,000 genes suggesting that gene number alone does not entirely define organismal complexity (Claverie, 2001; Zaharieva et al., 2012).

The variability in splicing pattern via alternative splicing is a major mechanism to generate molecular diversity (transcriptomic and proteomic) and organismal complexity from the limited number of genes present in higher eukaryotes. Alternative splicing occurs in ~25% of *C. elegans* genes, ~60% of *Drosophila melanogaster* genes and ~95% of human genes, which accounts for the disparity between the estimated 22,000 genes in the human genome and the proposed 100,000 proteins synthesized from them. Thus, organisms with more cell and tissue type complexity exhibit more alternative splicing (McManus and Graveley, 2011).

1.3.1. Modes of alternative splicing

Alternative splicing events occur in a number of different ways (Keren et al., 2010):

- *Use of cassette exons:* A cassette exon can either be included or excluded in the final mRNA transcript (Figure 3A). When the exon is excised from the pre-mRNA, the splicing event is termed exon skipping which constitutes nearly 40% of all alternative splicing events in higher eukaryotes.
- *Alternative 3' splice selection:* Using an alternative splice acceptor site changes the 5' end of the downstream exon (Figure 3B). Alternative 3' splice selection accounts for 18.4% of alternative splicing events in higher eukaryotes.
- *Alternative 5' splice selection:* Using an alternative splice donor site changes the 3' end of the upstream exon (Figure 3C). Alternative 5' splice selection accounts for 7.9% of all alternative splicing events in higher eukaryotes.

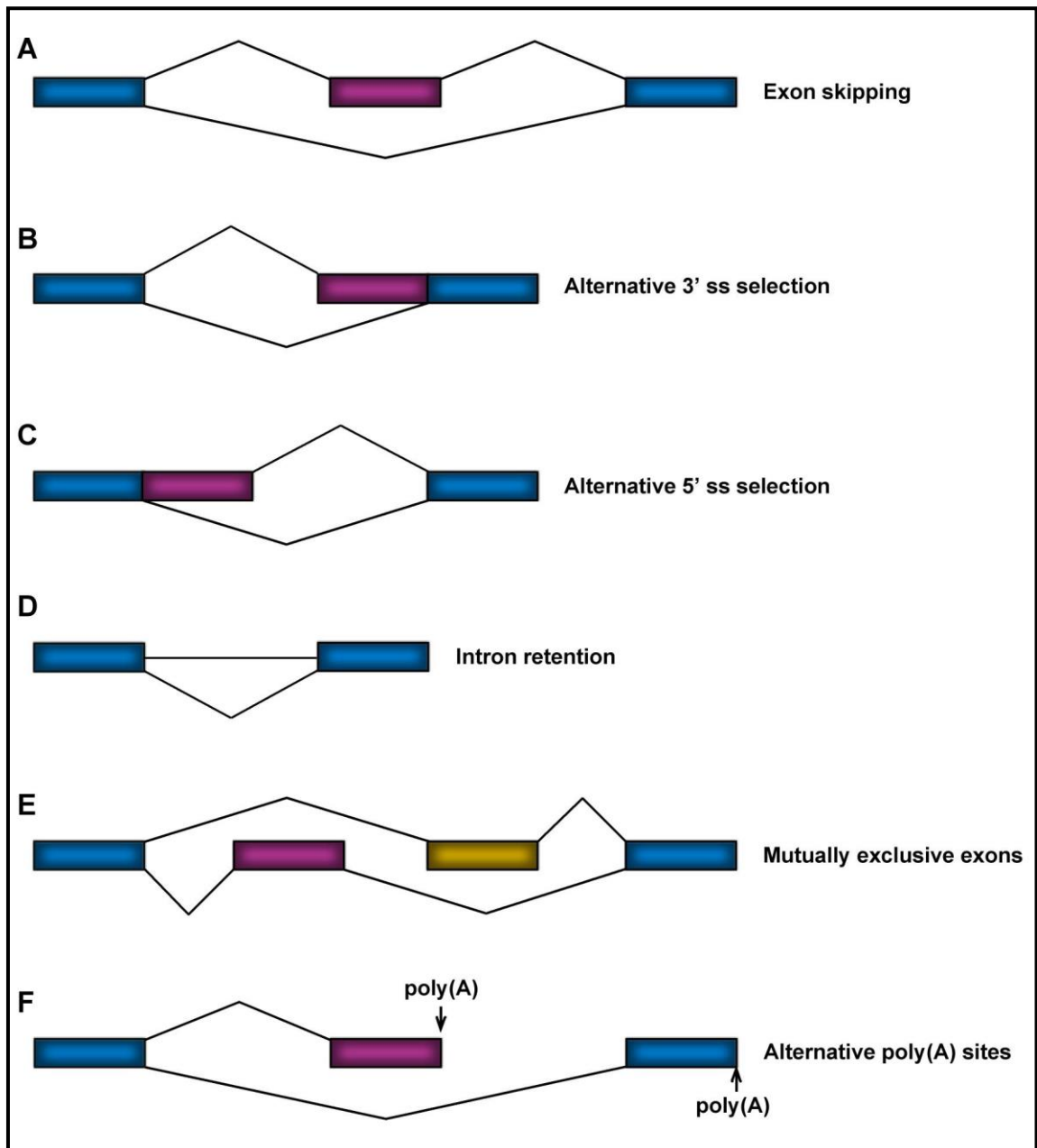


Figure 3: Modes of alternative splicing. (A) A cassette exon can either be included in or be excised from an mRNA. (B and C) Alternative 3' ss or 5' ss selection alters the 5' or 3' end of the downstream or upstream exon, respectively. (D) Intron retention can either result in exclusion or inclusion of an intron in the mRNA. (E) Mutually exclusive splicing of a group of exons allows the splicing of only one exon at a time. (F) Alternative poly A sites alter the 3' most exons in an mRNA transcript. Constitutive exons are shown as blue boxes and alternative exons as pink or yellow boxes. Solid lines represent splicing options. Adapted from (Keren et al., 2010).

- *Intron retention*: The intron can either be excluded or can be retained in the mRNA transcript (Figure 3D). Intron retention is the rarest form of alternative splicing in vertebrates and invertebrates constituting less than 5% of known alternative splicing events but is the most preferred mode of alternative splicing in plants, fungi and protozoa.
- *Mutually exclusive splicing*: Two or more cassette exons are spliced in a mutually exclusive manner such that only one exon will be included from the whole variable cluster (Figure 3E).
- *Alternative terminal exons*: Frequently, genes have alternative terminal exons, which is a different form of mutually exclusive exon usage. Here, regulation can occur at the level of splicing, 3' end processing or both. Use of alternative 3' ss and/or alternative polyadenylation sites result in a switch in the 3' most exon of the mRNA transcript (Figure 3F).

1.3.2. Regulation of alternative splicing

Recognition of an intron by the spliceosomal components and their consequent assembly around its ss determines the splicing of that intron. These reactions are under the control of combinatorial interactions between *cis*-acting elements and *trans*-acting factors. Disruption of these interactions affects alternative splicing, which has been associated with many human disease conditions such as cancer and neurodegeneration. Hence, developing a better understanding of mechanisms which regulate alternative splicing might help rectify erroneous splicing, potentially leading to novel molecular therapies (Garcia-Blanco et al., 2004; House and Lynch, 2008; Zaharieva et al., 2012).

1.3.2.1. Splice site strength regulates alternative splicing

The strength of 5' and 3' ss is proportional to the degree of complementarity with U1 small nuclear RNA (snRNA) and the extent of polypyrimidine tract, respectively. Accordingly, an intron having stronger ss is removed more readily than an intron with weaker ss. Conversely, an alternative cassette exon flanked by stronger ss is included more frequently than an adjacent exon flanked by weaker ss (Hertel, 2008).

1.3.2.2. Splicing regulatory elements and RNA binding proteins regulate alternative splicing

Auxiliary sequences called splicing regulatory elements (SREs) regulate recognition and consequent splicing of nearby ss (Voelker et al., 2012). These *cis*-acting elements occur within both exonic and intronic regions and bind directly or indirectly to *trans*-acting RNA binding proteins (RBPs) that function as splicing activators or repressors (House and Lynch, 2008).

SREs are divided into four categories based on location and function: exonic splicing enhancers (ESEs), intronic splicing enhancers (ISEs), exonic splicing silencers (ESSs) and intronic splicing silencers (ISSs). ESEs characteristically bind members of the serine/arginine-rich (SR) family of splicing factors and promote spliceosome assembly and exon inclusion (Garcia-Blanco et al., 2004). Sex-specific inclusion of *Drosophila doublesex (dsx)* exon 4 is mediated by the presence of an ESE in the exon, which binds RBP1 (SR protein) and transformer (Tra, an RNA binding protein), amongst other proteins, promoting spliceosome assembly and exon inclusion in females (Demir and Dickson, 2005; Manoli et al., 2005; Usui-Aoki et al., 2000). ESSs, however, typically bind heterogeneous nuclear ribonucleoproteins (hnRNPs)

and block spliceosome assembly and suppress exon inclusion (Garcia-Blanco et al., 2004). Variable exon 4 of the human *CD45* gene contains an ESS, which binds to hnRNP L and results in exon skipping (Rothrock et al., 2005). SR proteins (splicing activators) and hnRNPs (splicing repressors) function antagonistically but exist in a balance and a change in concentration and/or activity of one factor affects the splicing outcome (Long and Caceres, 2009). SR proteins and hnRNPs are functionally flexible and in some cases are also associated with exon skipping and inclusion, respectively (Han et al., 2011; Hofmann and Wirth, 2002; Konig et al., 2011). ISEs and ISSs function similarly to their exonic counterparts and are known to regulate splicing of exon 8 splicing in human fibroblast growth factor receptor 2 (*FGFR2*) pre-mRNA (Black, 2003; Wagner and Garcia-Blanco, 2002).

1.3.2.3. Cellular signaling regulates alternative splicing

Post-translational modifications such as methylation or phosphorylation in RBPs are important for determining RNA binding specificities. The most abundant class of phosphorylated RBPs is the one that includes SR proteins. SR proteins are active upon phosphorylation, which is important for alternative splicing regulation. Global shut down of splicing during mitosis or heat shock due to dephosphorylation of SRSF10 exemplifies such a splicing regulation where 5' splice site recognition and subsequent spliceosome assembly is hampered (Shin et al., 2004). Inhibition of SRPK1 (serine-arginine protein kinase 1) causes hypophosphorylation of SF2 (splicing factor 2) which regulates alternative splicing of VEGF (vascular endothelial growth factor) from pro- to anti-angiogenic spliceforms beneficial in inhibiting progression of diabetic nephropathy and tumour growth (Oltean et al., 2012). C6

pyridinium ceramide, a potential anti-cancer drug, inhibits dephosphorylation of various splicing regulatory proteins (including, SF2/ASF and Tra2-beta1) by binding to the protein phosphatase 1 (PP1) catalytic subunit thereby changing alternative splicing patterns of several endogenous genes such as *drf1*, *tau* and *syk* (Sumanasekera et al., 2012).

1.3.2.4. Tissue-specific regulatory proteins affect alternative splicing regulation

Regulation of alternative splicing can also be mediated by tissue-specific factors, which are present in one cell type but not in the other. Embryonic lethal abnormal visual system (ELAV), a neuron-specific RBP binds to and regulates alternative splicing of *Drosophila erect wing (ewg)* and *neuroglian (nrg)* genes (Lisbin et al., 2001; Soller and White, 2003). Sex-lethal (Sxl), an RBP expressed only in females, is a key regulator of the *Drosophila* sex determination pathway. Sxl regulates the splicing of *Drosophila tra* exon 2 and autoregulates its own exon 3 splicing. In both the cases, binding of Sxl blocks 3' splice recognition and suppresses exon inclusion to produce active Tra and Sxl proteins in females but not in males, where exon inclusion produces truncated and inactive proteins. Sxl also mediates X chromosome dosage compensation by blocking splicing of the first intron in *Drosophila male-specific-lethal-2 (msl-2)*, and also translation of *msl-2* to prevent transcriptional upregulation on the X chromosome as observed in males (Black, 2003; Lopez, 1998; Maniatis and Tasic, 2002; Schutt and Nothiger, 2000).

1.3.2.5. Co-transcriptional regulation of alternative splicing

Regulation of alternative splicing not only depends on the interaction of splicing

factors with their target pre-mRNA sequences but also transcription. Transcription and pre-mRNA processing were thought to be independent processes. However, studies in the *Drosophila* chorion genes (*s36-1* and *s38-1*) showed that transcripts appear to be shorter while still being attached to the chromatin via RNA pol II suggesting co-transcriptional pre-mRNA splicing (Osheim et al., 1985). Moreover, nascent RNA sequencing data in *Drosophila* revealed that eighty-seven percent of the introns manifest >50% co-transcriptional splicing (Khodor et al., 2011). Key to coupling of transcription and splicing is the carboxy terminal domain (CTD) of RNA pol II which comprises 52 tandem repeats of the 7 amino acid consensus sequence YSPTSPS and is subject to post-translational phosphorylation of serine residues, which affects co-transcriptional alternative splicing by recruiting splicing factors. CTD promotes skipping of human fibronectin extra domain I (EDI) exon, independent of RNA elongation rate, by recruiting SR protein SRp20 demonstrating that alternative splicing regulation does not solely depend on regulatory element-specific *trans*-acting factors (de la Mata and Kornblihtt, 2006).

1.3.2.6. Promoter type can regulate alternative splicing

Different RNA pol II promoters alter splicing outcome of the same exon provided very strong evidence towards coupling of transcription and alternative splicing. Transcription under the α -globin promoter results in a ten-fold reduction in the inclusion of human fibronectin EDI exon than when transcription is driven by the cytomegalovirus promoters suggesting that splicing can be influenced by RNA pol II transcription (Cramer et al., 1997). A similar regulatory function of promoters has also been observed in splicing of human *CD44* and cystic fibrosis transmembrane

regulator genes (Auboeuf et al., 2002; Pagani et al., 2003). These effects are not a result of differences in promoter strength but due to qualitative properties attributed to the RNA processing machinery. This observation is in line with microarray data showing that transcription based on promoter strength acts independently of alternative splicing on different sets of genes to result in tissue-specific expression profiles (Pan et al., 2004).

Promoter type affecting splicing outcome could function as a result of differences in promoter occupancy by factors varying in activation moieties and mechanistic properties (Kornblihtt, 2005). A possible mechanism that could explain such an effect is that the promoter itself recruits factors with functional domains for both transcription and splicing to the transcription site, via transcription factors that physically associate with the promoter or transcriptional enhancer elements within the promoter. The splicing of human fibronectin extra domain II (EDII) exon exemplifies such a mechanism where the promoter with a DR-1 transcriptional enhancer element binds transcription factor PPAR γ , which subsequently recruits the transcriptional co-activator PGC-1. Due to its dual functionality, PGC-1 interacts with RNA pol II and the splicing factor SRp40, which results in EDII exon skipping. Conversely, when PGC-1 is not a part of a promoter-binding complex, EDII exon is included (Monsalve et al., 2000).

1.3.2.7. RNA pol II processivity can regulate alternative splicing

RNA pol II elongation rates or processivity can regulate alternative splicing outcomes. A putative model suggests that for an alternative exon, flanked by a weaker upstream and a stronger downstream ss, low RNA pol II elongation rates or

internal stalling sites, commonly called pause sites, would favour exon inclusion, whereas a high RNA pol II elongation rate or absence of pause sites would result in exon skipping (Nogues et al., 2003). A lower elongation rate between the two ss would allow more time for spliceosomal components to assemble on the weaker ss and delay the synthesis of the stronger downstream ss, thus favouring excision of the upstream intron and exon inclusion. A higher elongation rate would expose both the ss simultaneously before the splicing machinery, which would choose the stronger 3' ss resulting in exon skipping. In the case of two constitutive strong ss, as observed in constitutive splicing, RNA pol II elongation rates do not affect splicing (Kornblihtt et al., 2004).

Altering RNA pol II elongation rates influences alternative splicing of human fibronectin EDI exon. Cells treated with dichlororibofuranosylbenzimidazole (DRB), a potent inhibitor of RNA pol II elongation showed a three-fold elevation in EDI inclusion (Nogues et al., 2002; Price, 2000). Also, the C4 RNA pol II mutant, which has a lower elongation rate due to a single amino acid substitution (741Arg-His) in its largest subunit, provided a direct evidence for the kinetic coupling of transcription and splicing. This slow polymerase was shown to cause a three-fold increase in fibronectin EDI exon inclusion in human cells. This mutation also affected the splicing of adenovirus E1a by favouring the inclusion of the most upstream exon out of the three alternative 5' donor sites (de la Mata et al., 2003).

The *Drosophila Hox* gene *Ultrabithorax (ubx)*, responsible for wing and leg formation in adult flies, can give rise to six different spliceforms by differential inclusion of its three variable exons: the B element and two microexons, mI and mII that are separated by very large introns. Joining of either mI or mII to the 5' constitutive exon

regenerates a consensus 5' ss which is subsequently recognized by the splicing machinery to result in exon skipping and shorter isoforms by a mechanism of recursive splicing (Burnette et al., 2005).

In C4 embryos, *Ubx* pre-mRNA splicing shows an enhancement in shorter isoforms, which translates as a mutant phenotype termed 'Ubx effect'. This increase in recursive splicing is attributed to the lowered RNA pol II elongation rate which allows more time for the newly formed 5' ss to be recognized by the spliceosome before the downstream 5' ss can be synthesized. Contrary to EDI and E1a, *ubx* shows exon skipping under the influence of a slow polymerase. Splicing of other alternative exons, such as exon 7B of the *Drosophila hnRNPA1* gene is not affected by the slow polymerase (de la Mata et al., 2003). Inhibition of RNA pol II elongation in Jurkat T cells revealed that RNA pol II occupancy was enhanced on introns flanking variable exons that became more included. This observation, at a genome-wide level, supports the RNA pol II elongation model (Ip et al., 2011).

1.3.2.8. Nucleosome occupancy suggests a role in alternative splicing regulation

DNA is packaged together with an octamer of highly evolutionarily conserved proteins called histones (two each of histones H2A, H2B, H3 and H4) to form the fundamental repeating unit of chromatin called nucleosome. Early sequence data from human and mouse genes suggested a relationship between nucleosome positioning and exon-intron architecture based on regular distribution of ss. Since splicing and transcription were regarded as independent processes then, no conclusion was derived from this study (Beckmann and Trifonov, 1991).

Deep-sequencing data from human and *C. elegans* genomes and computationally based predictions of nucleosome positioning in humans, *D. melanogaster* and *C. elegans* reveal that sequences favouring nucleosome positioning are located in exons and disfavouring sequences are a part of 50 nt intronic regions immediately before and after exons as if nucleosome-free regions delimit exon-intron boundaries (Schwartz et al., 2009). Studies in *Arabidopsis thaliana* and *Oryzias latipes* (Japanese killifish) have shown the enrichment of nucleosomes on internal exons (Andersson et al., 2009; Chodavarapu et al., 2010; Nahkuri et al., 2009). A nucleosome accommodates 147 bp of DNA around it, which interestingly is very similar to the average length of exons in higher eukaryotes (Venter et al., 2001). These findings might explain the mean exon length of 140-150 nt as it would facilitate wrapping around a nucleosome and possibly improve exon recognition (Beckmann and Trifonov, 1991). Nucleosomes have also been reported to cover ss junctions, which may protect them against mutations thereby facilitating efficient splicing (Hapala and Trifonov, 2011; Kogan and Trifonov, 2005).

Exons are known to contain a slightly higher GC content than introns. In addition, nucleosomes preferentially occupy GC-rich sequences. However, intronic regions with a much higher GC content than exons show lower levels of nucleosome occupancy and true exons show higher levels of nucleosome positioning, despite having the same level of GC content as pseudo-exons; intronic sequences flanked by strong ss but not included in the mRNA. These findings eliminate a possible bias of nucleosomes towards GC-rich sequences (Tilgner et al., 2009). Tilgner et al., (2009) also showed that nucleosomes are particularly enriched over exons flanked by weak ss. In contrast, exons with strong ss show reduced nucleosome occupancy but have

an extended region of nucleosomes upstream of the acceptor site. This inverse correlation between nucleosome occupancy and ss strength suggests an interplay between chromatin architecture and ss choice during pre-mRNA splicing (Tilgner et al., 2009). Schwartz et al. suggested a positive correlation between nucleosome occupancy and exon inclusion when analyzing splicing of three categories of exons: alternative exons with less than 50% inclusion, those with more than 50% inclusion and constitutive exons (Schwartz et al., 2009). In parallel, exon inclusion is disfavoured in pseudo-exons despite the presence of strong ss, possibly due to low nucleosome occupancy (Tilgner et al., 2009).

The link between chromatin architecture and ss choice is the CTD – a key component of transcription and splicing. *In vivo* data shows enhanced occupancy of RNA pol II over exons compared to introns (Brodsky et al., 2005; Dhami et al., 2010; Spies et al., 2009). These observations suggest a cross-talk between nucleosome positioning, RNA pol II occupancy and general/alternative splicing regulation. Nucleosomes positioned on alternative exons might act as natural hurdles or ‘speed-bumps’ for the transcribing RNA pol II and lower its elongation rate. This might delay the synthesis of competing downstream ss and consequently allow more time for spliceosome assembly and exon recognition eventually promoting exon inclusion (Churchman and Weissman, 2011; Hodges et al., 2009). In contrast, depletion of nucleosomes from alternative exons would result in a faster RNA pol II and hence, faster synthesis and recognition of the stronger downstream competing ss by the nucleosome resulting in exclusion of alternative exons (Carrillo Oesterreich et al., 2011).

1.3.2.9. Histone modifications and chromatin structure can regulate alternative splicing

Histones are post-translationally modified at many positions, particularly in the N-terminal tails that extend out of the nucleosomal core, by enzymes that write a 'histone code' by either adding or removing chemical groups. These histone marks primarily include methylation, acetylation and phosphorylation. A change in the degree of these modifications has been shown to regulate alternative splicing events (Hnilicova and Stanek, 2011).

Enrichment of specific histone modifications on nucleosomes helps distinguish exons from introns to facilitate efficient splicing. In order to analyse chromatin structure and function in *C. elegans*, a genome-wide map of histone H3 tail methylations, using chromatin immunoprecipitation (ChIP) -on-chip and ChIP sequence (ChIP-Seq) data, have shown that exons are preferentially marked with H3K36me3 relative to introns. Moreover, constitutive exons have higher H3K36me3 signal than alternative exons. Other modifications such as H3K4me3 and H3K9me3 do not exhibit this difference in levels (Kolasinska-Zwierz et al., 2009). H3K36me3 occurrence on alternative exons correlates with exon inclusion on a genome wide scale in humans suggesting interplay between H3K36me3 marking and alternative splicing regulation (Hon et al., 2009). Other histone methylations such as H3K27me1, H3K27me2, H4K20me1, H3K79me1 and H2BK5me1 have also been reported to favourably mark exons suggesting a possible role of chromatin structure in exon definition and regulation of alternative splicing (Andersson et al., 2009; Dhimi et al., 2010; Huff et al., 2010; Spies et al., 2009).

RNA pol II serves as a link between the transcribed pre-mRNA and chromatin structure and promotes cross-talk between them such that chromatin remodeling can alter RNA elongation rate and consequently regulate alternative splicing. Membrane depolarization causes hyperacetylation of H3K9 and relaxation of chromatin around the mouse *NCAM* alternative exon 18 favouring exon skipping (Schor et al., 2009). Conversely, inhibiting histone deacetylases with trichostatin A results in enhanced skipping of exon 18. Moreover, a slow RNA pol II mutant promotes exon 18 inclusion, suggesting the role of histone acetylation in increasing RNA pol II elongation rate and regulating alternative splicing in mouse *NCAM*. Similar effects are observed in HeLa cells where inhibiting deacetylase activity results in skipping of human fibronectin EDII exon (Hnilicova et al., 2011).

On the contrary, small interfering RNAs (siRNAs) complementarily binding an intron, downstream of the alternative human fibronectin EDI exon, enhances local H3K9me2 and H3K27me3 marks on the exon, which promotes heterochromatin formation via recruitment of heterochromatin-associated protein 1 α (HP1 α), reduces RNA pol II elongation rate and as a consequence enhances inclusion of EDI exon (Allo et al., 2009). These examples suggest a correlation between chromatin structure and alternative splicing regulation where histone acetylation results in more open chromatin architecture around an alternative exon, allowing faster RNA pol II processivity and consequential skipping of the alternative exon. Histone methylation, on the other hand, results in a more compact chromatin structure, which slows down RNA pol II elongation rate and hence allows more time for spliceosome assembly around the alternative exon resulting in an increase in its inclusion.

Specific histone modifications are suggested to recruit certain splicing factors, which mediate alternative splicing regulation. Indeed, MRG15, an adaptor protein, recognizes and binds to H3K36me3 modification on human *FGFR2* exon IIIb and recruits the polypyrimidine tract-binding protein (PTB), a splicing repressor. PTB binds to its intronic splicing silencer sites and causes exon skipping. Conversely, knockdown of MRG15 and reduction in H3K36me3 results in enhanced exon inclusion (Luco et al., 2011).

In human *CD44*, H3K9 trimethylation on variant exons recruits more HP1 γ , a transcriptional repressor, in the phosphorylated form (HP1 γ S83p), which binds to the *CD44* mRNA and slows down RNA pol II. A decrease in elongation rate in turn recruits splicing factors such as U2AF65 and PRP8 that facilitate inclusion of *CD44* variant exons. Apart from regulating *CD44* splicing, HP1 γ affects alternative splicing of a few other genes such as *PNK2*, *TAF4B*, *GLS*, *BRCA1* and *DSN* (Saint-Andre et al., 2011).

Chromatin and RNA binding factors, independent of recruitment by histone modifications, regulate alternative splicing of variable exons. CCCTC-binding factor (CTCF) binds to alternative human *CD45* exon 5 and promotes inclusion by local pausing of RNA pol II at the variable exon. DNA methylation on exon 5, however, inhibits CTCF binding and favours exon skipping (Shukla et al., 2011). Splicing regulators ELAV/Hu proteins, bind to RNA pol II and their target pre-mRNA sequences around alternative exons of mouse *FAS1* and *Nf1* genes and stimulate local histone hyperacetylation. This modification increases RNA pol II elongation rate which promotes variant exon skipping. Moreover, Hu proteins also directly bind and inhibit histone deacetylase 2 activity, which favours local histone acetylation. These

observations suggest a 'reach back' mechanism wherein splicing regulators remodel chromatin structure when recruited to their target pre-RNA sequences cotranscriptionally to ensure efficient regulation of alternative splicing (Zhou et al., 2011).

1.4. Mechanisms of mutually exclusive splicing

Mutually exclusive splicing results in inclusion of only one exon from two or more variable exons (Keren et al., 2010). Mechanisms explaining mutually exclusive splicing involve steric hindrance due to overlapping signals required for splicing, incompatibility of splicing signals for the major and the minor spliceosome, regulation by *trans*-acting factors and removal of transcripts with premature stop codons by nonsense-mediated mRNA decay (NMD).

In mammalian introns, a minimum of 50 nt are required between the 5' ss and the branch point for splicing. A shorter distance will not allow spliceosome assembly due to steric hindrance. Between exons 2 and 3 of human *α -tropomyosin* gene, the distance between the 5' ss and the branch point is only 41nt resulting in inclusion of either exon 2 or 3 (Smith, 2005; Smith and Nadal-Ginard, 1989) (Figure 4A).

Although most introns are spliced by the major spliceosome using GU/AG splicing signals, a minor spliceosome is present where U1 and U2 snRNPs are substituted by U11 and U12 snRNPs, which use AU/AC as splicing signals. The ss for major and minor spliceosomes are incompatible and cannot be spliced together to include adjacent exons. The intron between mutually exclusive exons 6a and 6b in human *JNK2* contains a U12-type 5' ss and a U2-type 3' ss and accordingly these exons cannot be spliced together (Chang et al., 2007) (Figure 4B).

In some exon pairs, tissue-specific expression or activity of *trans*-acting factors can favour inclusion or force exclusion of only one from two variable exons, which under certain conditions could also be spliced together. Such a situation is found in the rat *α-actinin1* gene where the smooth muscle (SM) exon is preferentially included and the non-muscle (NM) exon is preferentially excluded in smooth muscles. Here, CUG-repeat-binding protein (CUG-BP) and elav-type RNA-binding protein 3 (ETR3) activate the SM exon but together with CUG-BP and ETR3-like factor 4 (CELF4) they also suppress the NM exon. Inclusion of the SM exon also involves removal of PTB to relieve repression from the SM exon indicating that combinatorial interaction of multiple RBPs is required to regulate this complex alternative splicing event (Gromak et al., 2003) (Figure 4C).

In some genes, alternative splicing generates isoforms, which contain a premature termination codon (PTC) due to a frame shift. Such PTC containing isoforms can be efficiently removed by NMD thus disguising the absence of an isoform as mutually exclusive splicing. This situation is observed in mammalian *FGFR2* gene, where transcripts containing both mutually exclusive exons IIIb and IIIc, harbor a PTC and are therefore degraded (Jones et al., 2001) (Figure 4D).

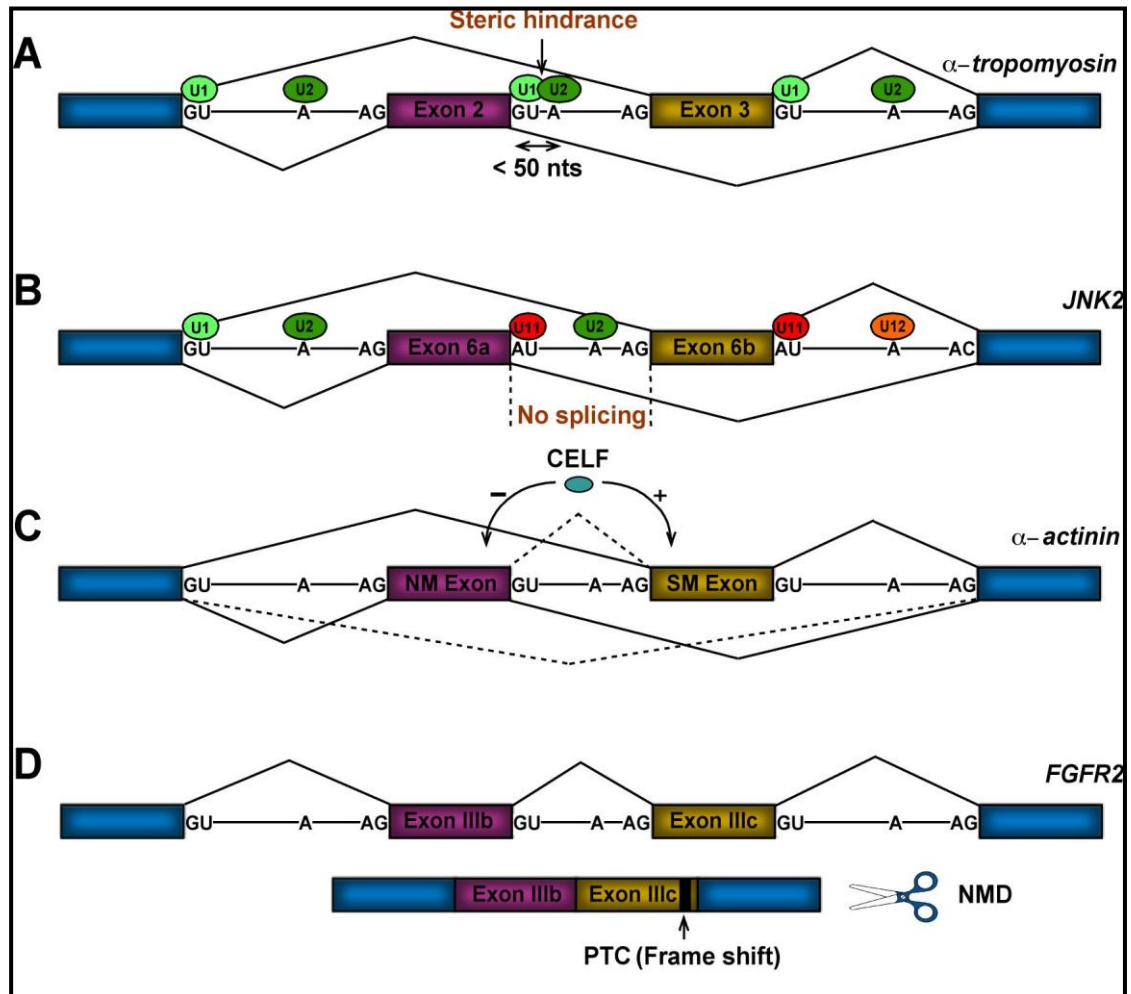


Figure 4: Mechanisms of mutually exclusive splicing. (A) Steric hindrance in spliceosome assembly is imposed by insufficient distance between 5' ss and the branch point resulting in mutually exclusive splicing of adjacent exons 2 and 3 in the *α-tropomyosin* gene. (B) The GU/AG splicing signals used by major spliceosomal U1/U2 snRNPs are incompatible with the AU/AC splicing signals used by minor spliceosomal U11/U12 snRNPs. An intron with a U12-type 5' ss and a U2-type 3' ss cannot be spliced due to spliceosomal incompatibility as observed between exons 6a and 6b of *JNK2* gene. (C) *Trans*-acting factors can regulate mutually exclusive splicing by acting as both promoters and inhibitors of mutually exclusive exon pairs to prevent them from being spliced together. CELF proteins regulate splicing of SM and NM exons of *α-actinin* gene resulting in mutually exclusive splicing. Disfavoured, but observed splicing is shown as dotted lines. (D) Inclusion of multiple mutually exclusive exons can result in generation of a PTC due to a frame shift. Such aberrant transcripts are removed by NMD as observed in *FGFR2* transcripts containing both IIIb and IIIc exons. Constitutive exons are shown as blue boxes, and pairs of mutually exclusive exons are shown as pink and yellow boxes. Adapted from (Hemani and Soller, 2012).

1.5. The *Dscam* gene

Dscam, a *Drosophila* homolog of human Down Syndrome Cell Adhesion Molecule (DSCAM) was first isolated by its affinity to Dock, an SH3/SH2 adaptor protein required for axon guidance (Schmucker et al., 2000). *Drosophila Dscam* is expressed in the developing nervous system and in immune cells. *Dscam* is important for its role in wiring of the nervous system and pattern recognition in the immune system (Hattori et al., 2007; Watson et al., 2005).

1.5.1. Gene organization and protein structure

Dscam structure resembles that of an immunoglobulin (Ig) receptor and is related to other cell adhesion molecules (CAMs). The Ig superfamily is known to be the largest group of related cell surface receptors (Harpaz and Chothia, 1994; Williams and Barclay, 1988). They contain ten Ig domains and six fibronectin type III (FNIII) domains. Nine out of the ten Ig domains are arranged in tandem whereas the tenth domain is located between FN4 and FN5. It also contains a transmembrane domain and a unique cytoplasmic domain with multiple tyrosine phosphorylation sites (Schmucker et al., 2000; Yamakawa et al., 1998) (Figure 5).

The *Dscam* gene comprises 115 exons of which 95 exons are alternatively spliced. These 95 variable exons are organized into four exon clusters namely exon 4 (encoding the N-terminal half of Ig2 domain), exon 6 (encoding the N-terminal half of Ig3 domain), exon 9 (encoding the entire Ig7 domain) and exon 17 (encoding transmembrane domains) clusters. Alternative splicing of individual exons takes place in a mutually exclusive and combinatorial manner resulting in tens of thousands of *Dscam* isoforms. Each of the exon clusters can generate 12, 48, 33 and

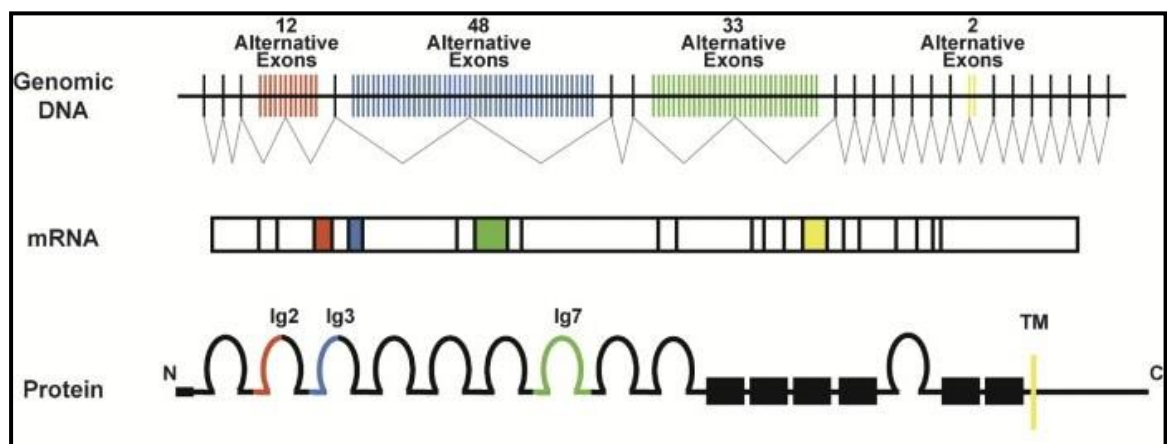


Figure 5: Dscam gene organization and protein structure. The *Dscam* gene comprises four exon clusters spliced in a mutually exclusive manner generating a repertoire of upto 38,016 isoforms. Variable exon clusters are shown in colour: exon 4 cluster (red, 12 variables), exon 6 cluster (blue, 48 variables), exon 9 cluster (green, 33 variables), exon 17 cluster (yellow, 2 variables). The Dscam protein comprises ten Ig domains and six FN type III domains. Nine out of the ten Ig domains are arranged in tandem and the tenth Ig domain is present between FN4 and FN5 domains. Exons 4 and 6, code for the N-terminal halves of Ig2 and Ig3, respectively. Exons 9 and 17, code for the entire Ig7 and transmembrane domain, respectively. Adapted from (Wojtowicz et al., 2004).

two alternative forms, respectively. If all combinations were allowed, 38,016 different isoforms could be generated by inclusion of a single exon in each of the variable regions (Schmucker et al., 2000).

1.5.2. *Dscam* mutually exclusive splicing and its regulation

Alternative splicing of *Dscam* is extraordinary considering not only the resultant protein diversity but also its unique mechanism. Each variable exon cluster can give rise to multiple alternative exons, however; only one variant is included in the functional *Dscam* isoform.

The mechanisms of mutually exclusive splicing discussed previously do not seem to apply to splicing of the *Dscam* variable exons comprising the extracellular domain. Introns in the variable clusters are longer than the minimal size of about 59 nt in *Drosophila* and contain splicing signals for the major spliceosome (Graveley, 2005). Although splicing together of exons from the exon 6 cluster would result in a premature termination codon, removal of such isoforms by nonsense mediated mRNA decay would seem a highly inefficient way to remove isoforms with multiple inclusions due to the large number of possibilities. Hence, a mechanism is postulated whereby RNA secondary structure mediates the inclusion of a specific exon by relieving the variable cluster from its default repressed state (Graveley, 2005; Olson et al., 2007).

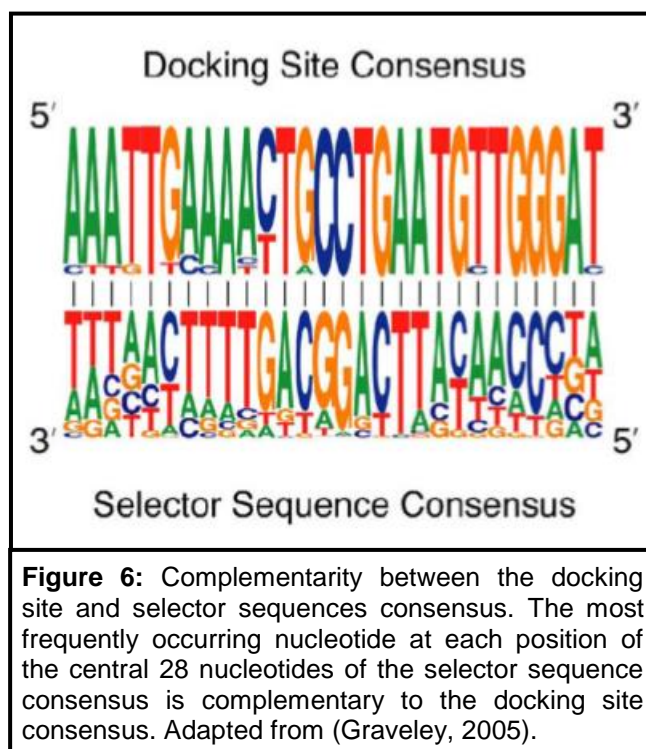
1.5.2.1. RNA secondary structures mediate *Dscam* variable exon selection

Extensive sequence analysis and phylogenomics have initially identified evolutionary conserved intronic sequences in the exon 6 cluster consisting of a 66 nt sequence in

the intron after exon 5 termed the “docking site” and a partially complementary shorter sequence called “selector sequence” in front of each exon 6 variant (Figure 6). Base pairing between the docking site and the selector site is then postulated to bring a specific variable exon into the proximity of the preceding constant exon resulting in splicing of the intron by the release of a repressor (e.g. hrp36 for exon 6, explained in 1.5.2.2.), subsequently triggering splicing to the distal constant exon. Since the selector sequences overlap with one another to a certain extent, the docking site is thought to interact with only one selector sequence at a time (Graveley, 2005).

The function of the docking site is evolutionary conserved and is required for exon 6 splicing. Deletions in the docking site increase exon 6 skipping and alter inclusion frequencies of exon 6 variables. Also, swapping selector sequences from rarely to frequently encoded variable exons, and vice versa, alters inclusion accordingly (May et al., 2011). Further support for the involvement of RNA secondary structure has recently come from sequence analysis of the variable clusters 4 and 9, where the docking site is present in the intron between the entire variable cluster and the downstream constitutive exon and the selector sequences are located in the introns after each exon variant (Yang et al., 2011) (Figure 7).

Most introns in *Drosophila* are spliced co-transcriptionally (Khodor et al., 2011). Although the variable exon 4, 6 and 9 clusters extend over 6, 12 and 15 kb respectively, a “polar effect” leading to preferential inclusion of variable exons closer to the proximal constant exon is not observed arguing for dedicated mechanisms regulating the inclusion of a single variable exon.



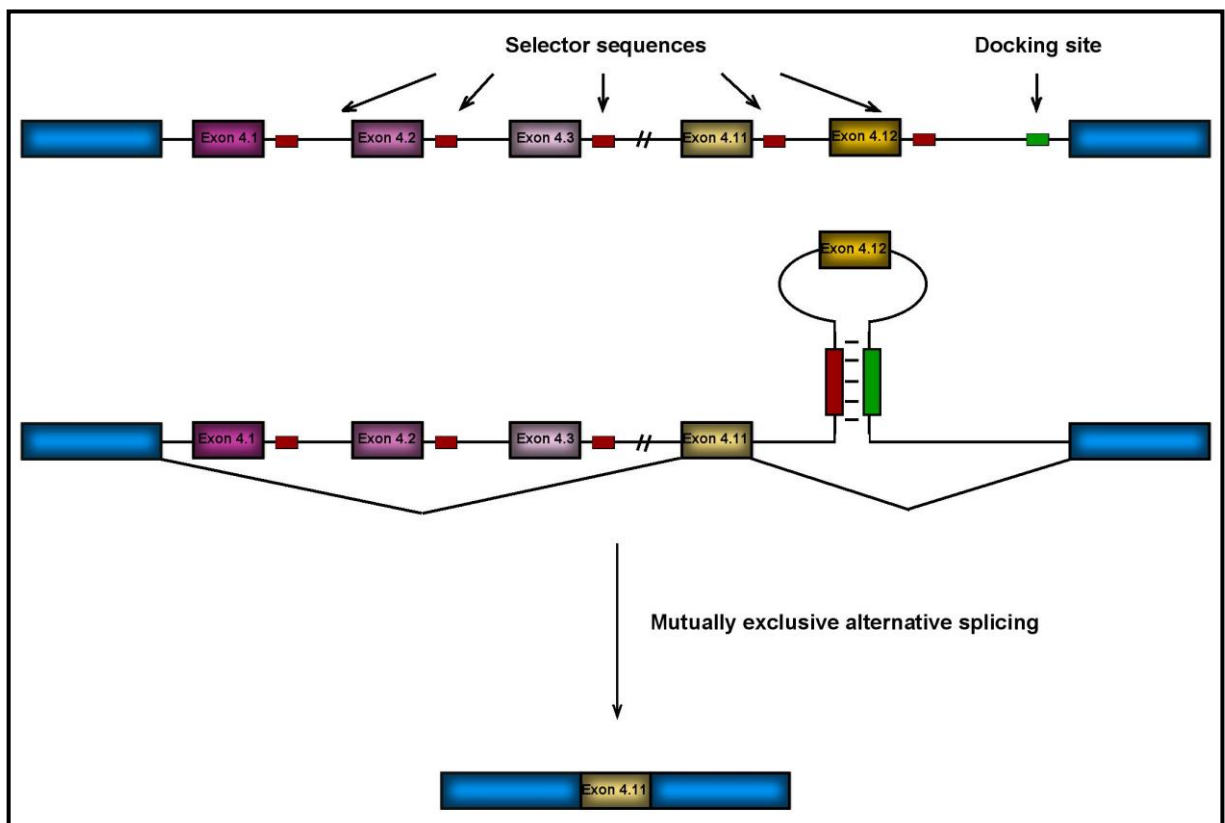


Figure 7: Proposed model for *Dscam* exon 4 mutually exclusive alternative splicing. Once an exon is chosen for inclusion, an RNA stem loop is formed by complimentary base pairing between the docking site (green box) and the selector sequence (red box) downstream of the chosen exon. For simplicity, only five exon 4 variables are shown. Constant exons are shown in blue and variable exons in a gradient from pink to yellow. Adapted from (Yang et al., 2011).

RNA secondary structure is also postulated to govern mutually exclusive splicing of the transmembrane domain encoded by the two exon 17 variables (Anastassiou et al., 2006; McManus and Graveley, 2011). Here, four conserved sequences that can form two competing RNA stem-loop structures are present in the intron distal of constitutive exon 16 (Figure 8). Mutually exclusive splicing of variable exon 17 is functionally important to localize Dscam isoforms either to dendrites (exon 17.1) or axons (exon 17.2) of mushroom bodies (Wang et al., 2004).

1.5.2.2. *Dscam* variable exon clusters are in a repressed state

Adjacent exons in each variable cluster have ss close to the consensus sequence; however they are not spliced together. Through RNA interference (RNAi) mediated knockdown of RBPs in *Drosophila* S2 cells (cell-line of haematopoietic origin), an hnRNP called hrp36 has been identified to specifically repress the joining of multiple exons throughout the exon 6 cluster but not the other clusters (Figure 9). An RT-PCR flanking the exon 6 cluster in cells depleted of hrp36 show multiple bands in contrast to a single band in the presense of hrp36. Although hrp36 also binds to the exon 4 and 17 cluster, no joining of multiple exons is observed when RNAi reduces hrp36 levels. Thus, hrp36 regulates mutually exclusive splicing of exon 6 in a cluster-specific and cluster-wide manner.

Other hnRNPs such as hrp38, hrp40 and hrp48 do not regulate splicing fidelity of exon 6. Moreover, hrp36 acts antagonistically to SR proteins to prevent ectopic inclusion of multiple exon variants. These observations suggest a mechanism, which keeps the variable exon cluster in a repressed state until one exon is chosen for inclusion. Though very compelling, the role of hrp36 in repressing splicing together of

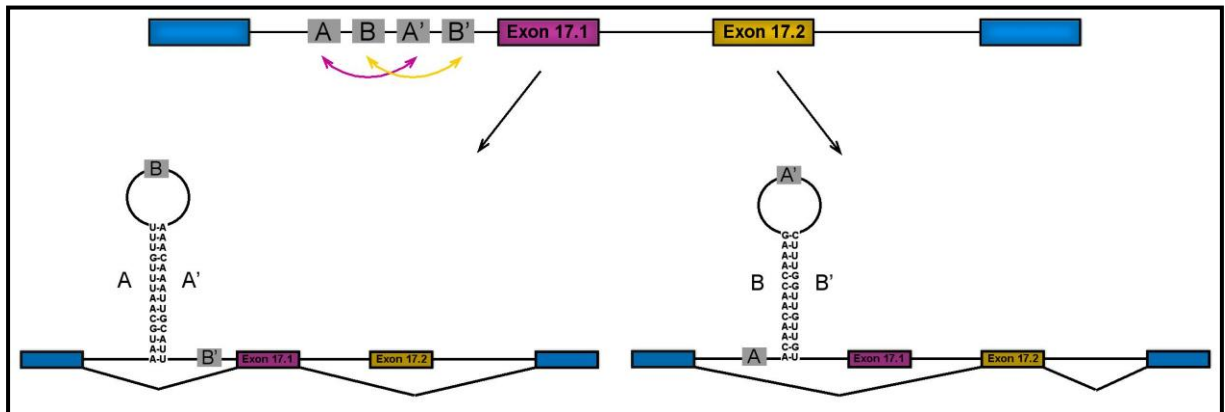


Figure 8: Proposed model for *Dscam* exon 17 mutually exclusive alternative splicing. Four conserved intronic sequence elements are located upstream of *Dscam* exon 17 cluster, which have the capacity to form RNA secondary structures by complimentary base pairing. These stem-loop structures allow the inclusion of only one of the two exon 17 variable exons. Adapted from (McManus and Graveley, 2011).

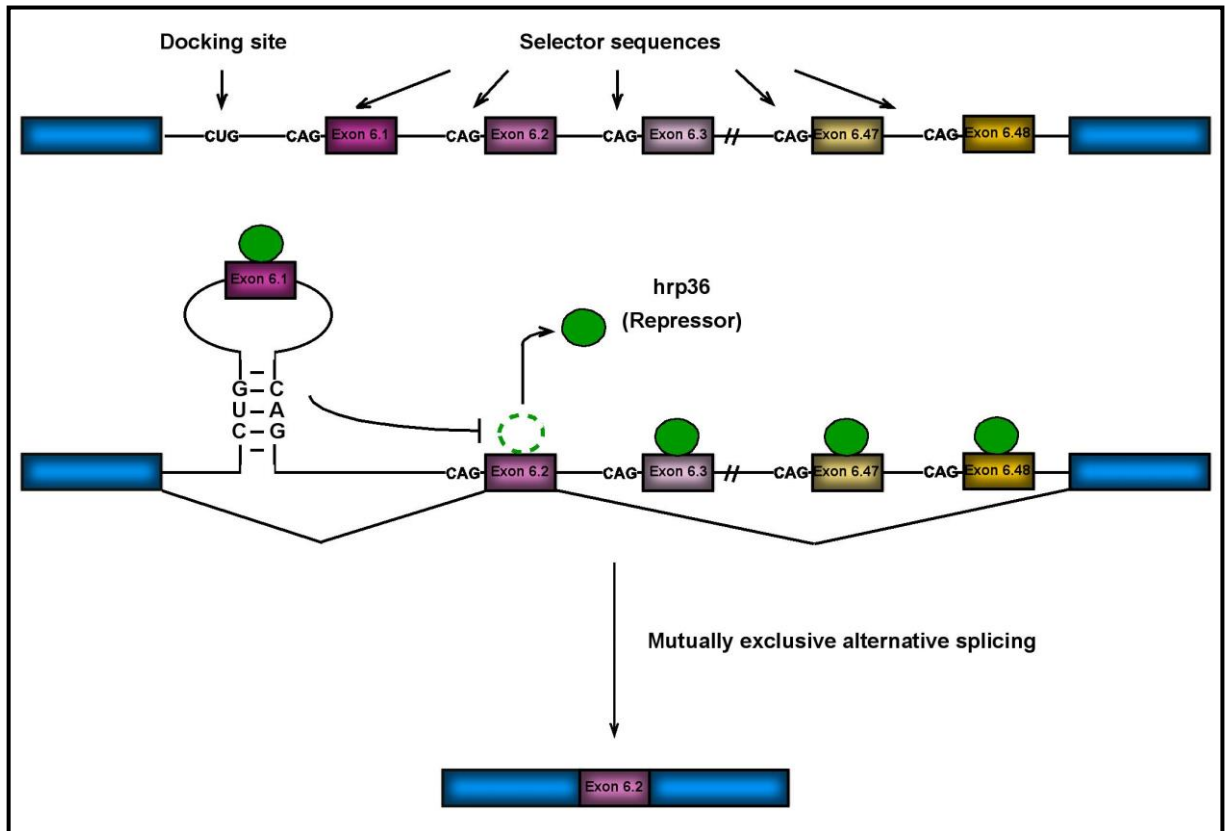
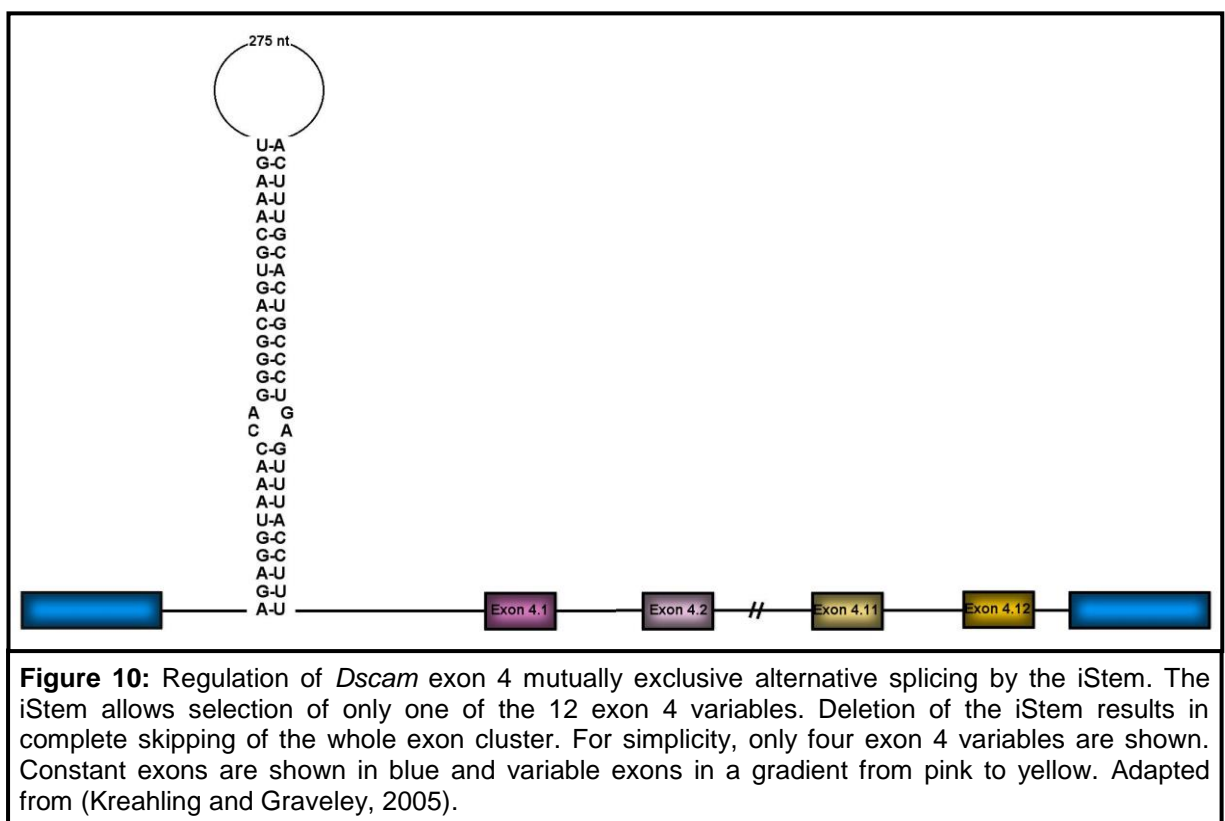


Figure 9: Proposed model for *Dscam* exon 6 mutually exclusive alternative splicing. Once an exon is chosen for inclusion, an RNA stem loop is formed by complimentary base pairing between the docking site and the selector sequence preceding the chosen exon, the repressor hrp36 is released to allow for its inclusion. Only the most frequently occurring nucleotides of the core consensus docking site (CUG) and selector sequences (CAG) are shown. For simplicity, only five exon 6 variables are shown. Constant exons are shown in blue and variable exons in a gradient from pink to yellow. Adapted from (Hemani and Soller, 2012).

multiple exons in the exon 6 cluster seems not to extrapolate to the whole organism. No splicing repressor has been associated with other variable exon clusters (Olson et al., 2007). Recent work in shrimp (*Litopenaeus vannamei*) demonstrated the role of Lvhrp36 as a splicing repressor of Ig2, Ig3 and Ig7 variable regions (Lee et al., 2012). The repression of the exon 4 cluster is governed by an RNA secondary structure, wherein a 27 nt stem with a 2 nt bulge and a 275 nt loop structure, called inclusion stem (iStem), located in the intron 18 nt after exon 3 is functionally relevant for inclusion of one variable exon (Figure 10). Deletion or mutation of the double stranded part of the iStem results in skipping of the entire exon 4 cluster (in cell culture) but the length and sequence of the loop in the iStem seem not to play a role in regulating splicing in the exon 4 cluster. It is also unknown how this loop interacts with the spliceosome. The iStem plays a role in repression but is not involved in exon choice. Genome sequence comparison showed that the iStem is evolutionarily conserved in all eleven *Drosophila* species known. This study suggests that a fine balance exists between choosing a variant exon and repression of the entire exon 4 cluster (Kreahling and Graveley, 2005).

1.5.2.3. RNA binding proteins regulate inclusion of *Dscam* variable exons

Regulation of *Dscam* diversity is required to provide unique identities to individual neurons in mushroom bodies and to increase levels of high affinity binding isoforms that fight against pathogens in the immune system (Dong et al., 2006; Zhan et al., 2004). Prime candidates to regulate inclusion of individual variants are RBPs. RNAi knock down of 250 RBPs in S2 cells reveals 36 proteins that have an effect on the splicing of exon 4 cluster, but only eight proteins that affect alternative splicing of



exon 17 cluster. All eight proteins involved in splicing of exon 17 cluster also affect splicing of exon 4 cluster (Park et al., 2004).

These results suggest combinatorial control in the regulation of *Dscam* mutually exclusive variable exon splicing by RBPs, but surprisingly those RBPs identified mostly affect inclusion of the same small set of variable exons implying that a large proportion of *Dscam* diversity is unutilized. Currently, it is not clear how specific exons are included over others to establish neuronal patterning and how a few exons are included more frequently on pathogen exposure.

1.6. Biological role of *Dscam* in invertebrates

1.6.1. Role of *Dscam* in *Drosophila* nervous system

1.6.1.1. Development of *Drosophila* nervous system

The insect central nervous system (CNS) comprises the ventral nerve cord and the brain. After gastrulation, neurogenic regions of the ectoderm are determined to form the neuroectoderm, a sheet of undifferentiated epithelial cells. The ventral neurogenic region gives rise to the ventral nerve cord and the procephalic neurogenic region gives rise to the brain. In each hemisegment, a few selected cells delaminate from the neuroectoderm as CNS progenitor stem cells, also called neuroblasts that divide asymmetrically by restoring themselves and producing a chain of secondary precursor cells called ganglion mother cells (GMCs). A single GMC divides to give rise to two progeny cells that differentiate into neurons and/or glia. Each hemisegment has ~30 neuroblasts that generate a total of 350 embryonic progeny cells which include ~290 interneurons, 30 motorneurons and 30 glial cells (Technau et al., 2006; Urbach and Technau, 2004). Subsequently, the axons and

dendrites branches from these neurons must find their target cells via axon pathfinding and dendritic field organization, respectively (Kaprielian et al., 2000; Nichols, 2006). The adult fly brain comprises highly organized neuropile structures such as mushroom bodies, optic lobes, antennal lobes and the central complex. The ventral nerve cord is relatively simpler, composed of a series of uniform segments called neuromeres (8 abdominal, 3 thoracic and 3 gnathal) (Technau et al., 2006).

Neural patterning in the nervous system comprises many different neurons that are interconnected by a complex network of synaptic connections. Precise assembly of these neural circuits depends on interactions between cell surface recognition proteins expressed on projecting neurons and specific guidance signals from target neurons (Zipursky et al., 2006). In *Drosophila* there are ~250,000 different neurons and only ~15,000 genes which clearly suggest that each cell recognition event cannot be governed by a different gene product. Despite the limited number of genes, several mechanisms facilitate complex neuronal wiring, including combinatorial use of guidance cues such as attractants, repellants or modifiers, diffusible gradient labels and coordinated firing activity between neurons (Schmucker and Flanagan, 2004). Alternative splicing of *Drosophila Dscam* serves as a mechanism to generate thousands of neuronal cell surface proteins with distinct recognition properties from a single gene, which could be used to establish connections within the fly neural circuitry (Schmucker et al., 2000; Shapiro, 2007).

1.6.1.2. Dscam isoforms exhibit homophilic binding

It would be interesting to know how these isoforms, expressed on the surface of one neuron, are recognized and interpreted by neighboring neurons. *In vitro* biochemical

binding assays reveal that 95% of Dscam isoforms, like many Ig superfamily proteins, exhibit isoform-specific homophilic binding (Wojtowicz et al., 2007). The first eight N-terminal Ig domains, including all three variable domains, form a symmetric S shaped bend and determine binding specificity of Dscam isoforms. Strong homophilic interactions require matching of all the three variable Ig domains. Isoforms with even a single variable Ig domain mismatch fail to engage in heterophilic binding (Wojtowicz et al., 2004) (Figure 11).

The Ig 1-4 domains form a horseshoe shaped 'head' wherein Ig2 and Ig3 comprise two distinct binding elements on opposite sides of the ectodomain - epitope I and epitope II. Dimerization and consequently homophilic interactions involve symmetric antiparallel pairing of epitope I but not epitope II (Sawaya et al., 2008). These striking observations suggest that the vast repertoire of Dscam isoforms mediates cell-surface recognition important for neural circuit assembly in *Drosophila* nervous system development.

Although isoform-specific homophilic interactions might appear to mediate adhesion forces to establish neuronal connectivity, it has been established that binding of identical Dscam isoforms on isoneuronal dendritic branches triggers cytoplasmic signaling events that result in repulsion forces between sister dendrites (Hughes et al., 2007; Soba et al., 2007). Accordingly, deletion of the cytoplasmic domain results in adhesion rather than repulsion, promoting ectopic self-crossing and formation of stable bridges between dendritic branches. Such contact dependent repulsion also underlies axonal branch segregation in mushroom body neurons. The signaling mechanisms downstream of Dscam however remain to be elucidated (Matthews et al., 2007).

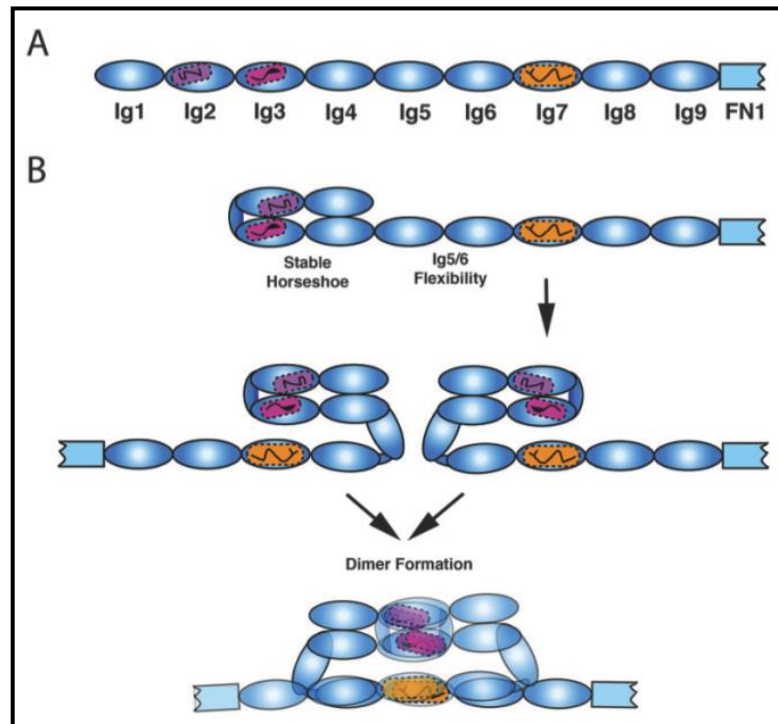


Figure 11: Molecular mechanism of homophilic interactions between identical Dscam isoforms. (A) Dscam protein structure showing nine of ten Ig domains and one half of FN1 domain. Ig2, Ig3 and Ig7 domains are encoded by variable exon clusters 4, 6 and 9, respectively. (B) Ig2, Ig3 and Ig7 domains determine the binding specificity between Dscam isoforms. Ig 1-4 domains comprise a 'horseshoe' conformation and a strong skew between Ig 4-5 domains results in an S-shaped conformation important for dimer formation. Matching of all three variable Ig domains is necessary for strong homophilic interactions. Adapted from (Schmucker and Chen, 2009)

1.6.1.3. Role of *Dscam* in axon guidance and dendritic field organization

Dscam loss-of-function mutants show axon guidance defects in the embryonic central nervous system, disruption of axonal extension and sister branch segregation in mushroom body neurons, interrupted axon arborization within the ellipsoid body and altered olfactory receptor neuron target specificity and dendritic patterning of projection neurons in the antennal lobe (Hummel et al., 2003; Schmucker et al., 2000; Wang et al., 2002; Zhu et al., 2006). Although, these findings show the involvement of *Dscam* in *Drosophila* nervous system development, they do not address the question of whether isoform diversity is essential for *Dscam* function.

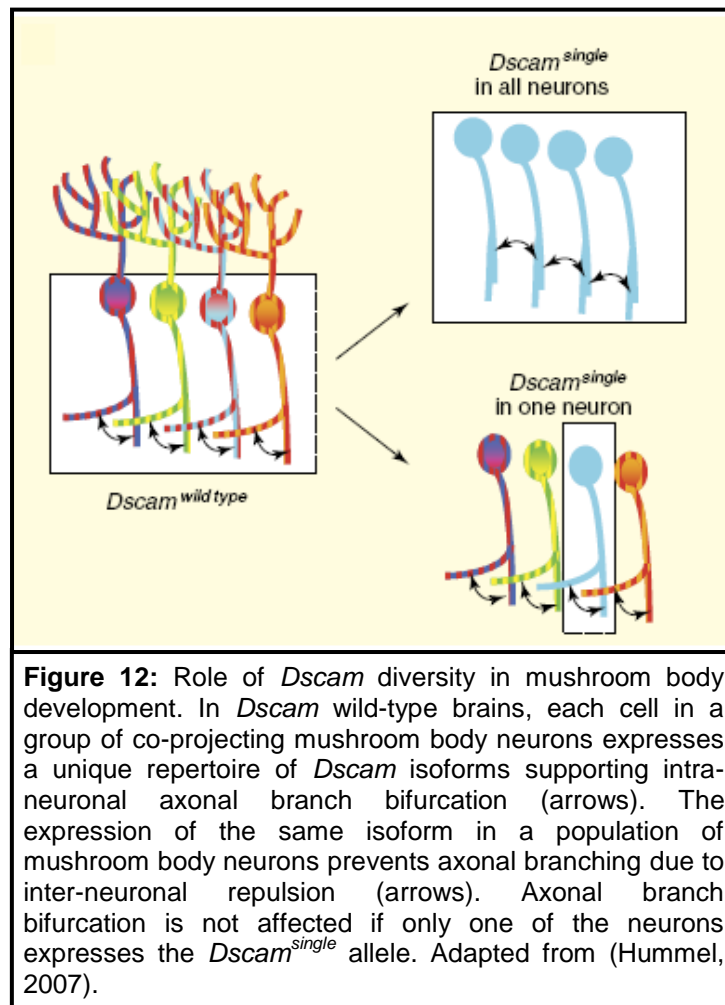
Indeed, individual cells express a stochastic yet biased repertoire of *Dscam* isoforms as observed in photoreceptor neurons and S2 cells (14-50 isoforms) and mushroom body neurons (8-30 isoforms) (Du Pasquier, 2005; Neves et al., 2004; Zhan et al., 2004). Hence, *Dscam* diversity provides each neuron with a unique cell surface 'tag', which allows it to distinguish between 'self' and 'non-self' essential for intra-neuronal avoidance and inter-neuronal recognition (Zipursky et al., 2006).

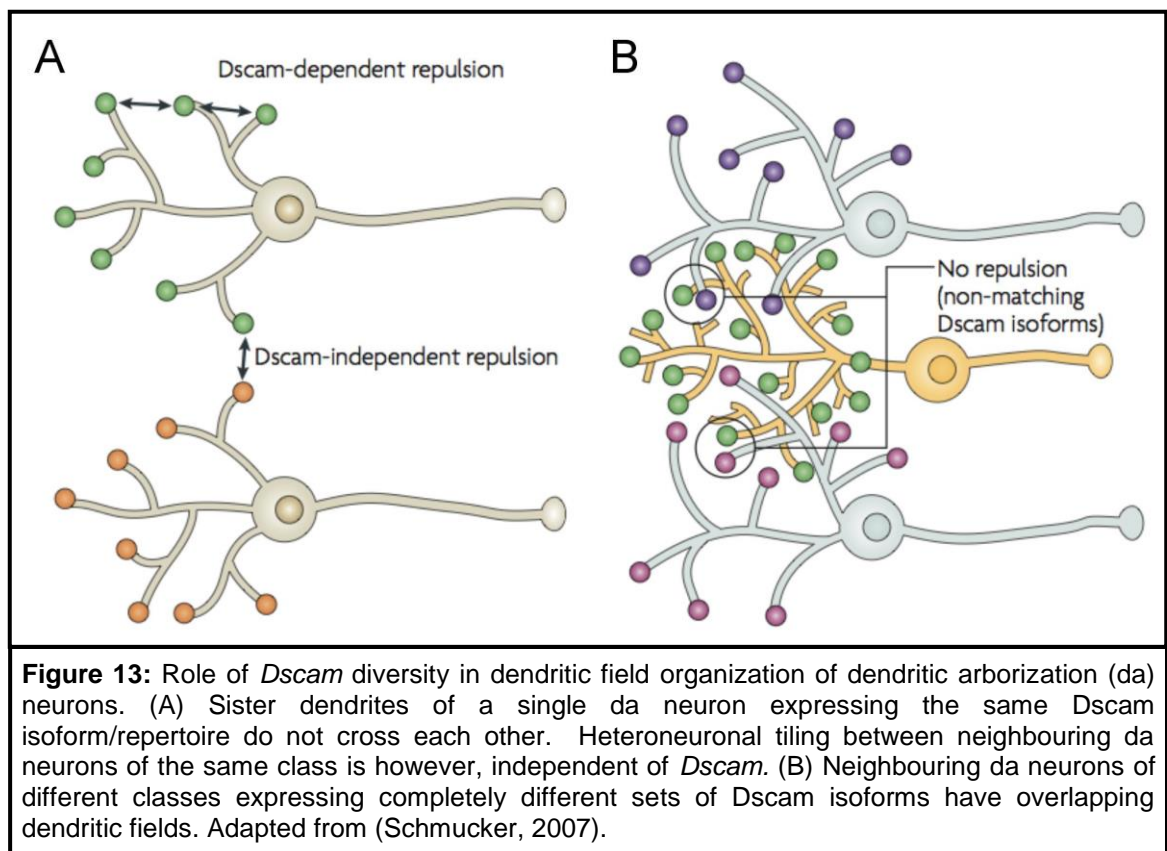
Different mushroom body neurons express several isoforms in varying combinations such that no two neurons share the exact *Dscam* repertoire. *Dscam* null mushroom body neurons exhibit defects in axon extension. *Dscam* diversity reduced to ~11,000 isoforms by deleting various subsets of Ig2 variants, does not affect mushroom body development (Wang et al., 2004). Intriguingly, single isoforms of *Dscam*, differing only in their ectodomains or transmembrane domains, substantially rescue loss-of-function defects in *Dscam* null mushroom bodies (Neves et al., 2004; Zhan et al., 2004). These results imply functional redundancy between *Dscam* isoforms and hence no requisite for isoform diversity. However, expression of a single *Dscam*

isoform in a bundle of co-projecting neurons causes defasciculation in larval and adult mushroom body. Conversely, expression of a *Dscam* isoform in a single mutant neuron in an otherwise wild type environment rescues axonal sister branch segregation (Hattori et al., 2007; Zhan et al., 2004) (Figure 12). *Dscam* diversity is thus essential to provide neighboring neurons with distinct isoforms for normal mushroom body morphogenesis, but a single *Dscam* isoform is sufficient for sister branch segregation in individual neurons. Moreover, no specific isoform or a subset of isoforms is required for mushroom body development (Hattori et al., 2009; Wang et al., 2004).

Dscam diversity also ensures dendritic field organization in dendritic arborization (da) neurons. Here, da neurons of different classes, sharing the same dendritic territory, need to express different *Dscam* isoforms. Expression of one *Dscam* isoform in single mutant da neurons significantly rescues dendritic self-avoidance but over-expressing the same isoform in da neurons of different classes forces spatial segregation of the once overlapping dendritic fields. *Dscam*, however, does not play a role in heteroneuronal tiling between da neurons of the same class (Hughes et al., 2007; Matthews et al., 2007; Soba et al., 2007) (Figure 13).

In contrast, the role of *Dscam* diversity is seemingly different in mechanosensory neurons. Expression of randomly chosen single isoforms can restore initial axonal extension and early branching but cannot rescue connectivity. These neurons show impaired secondary and tertiary axonal branching and fail to cross the midline in the central nervous system to reach their target cells. Also, two independent deletions of five Ig2 variants show allele-specific connectivity defects, which suggest functional differences between different isoforms. Thus, in contrast to mushroom body neurons



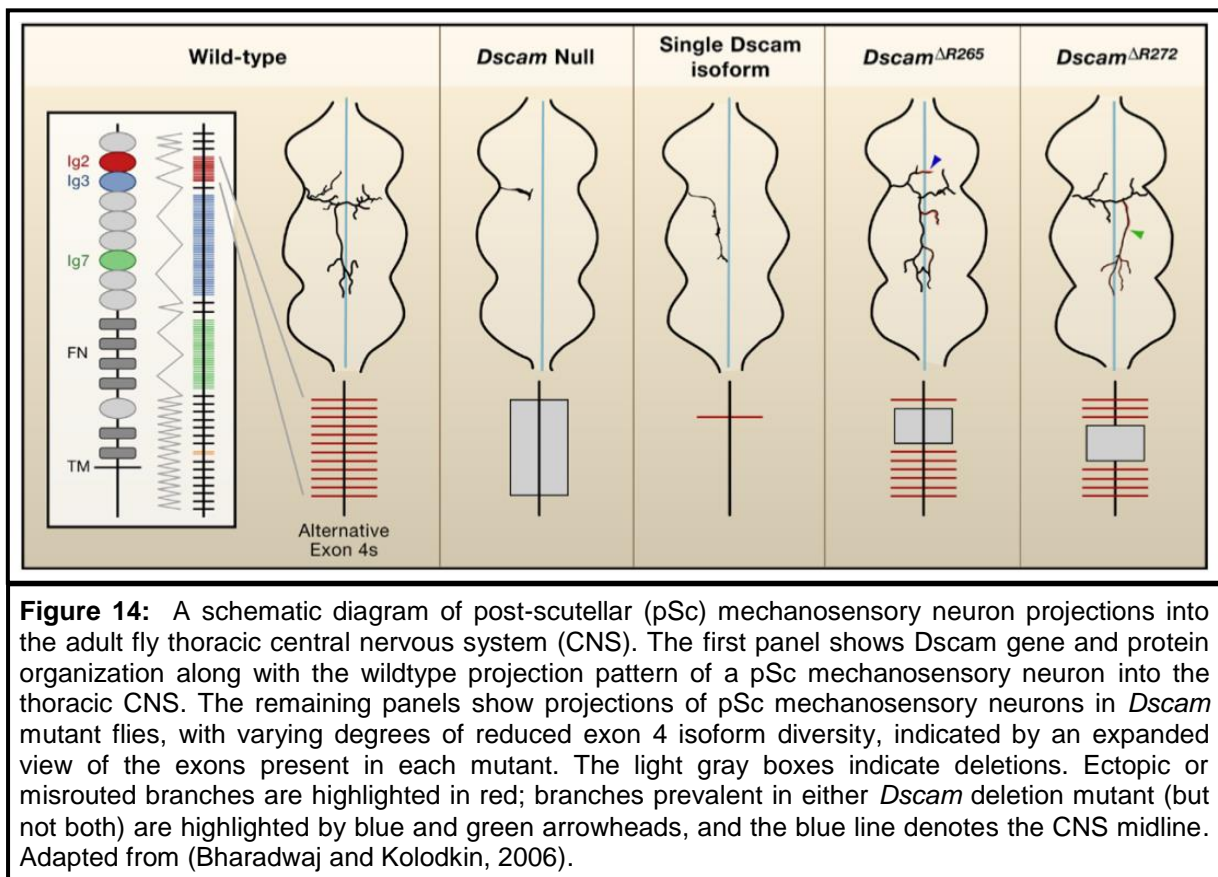


where a larger deletion of Ig2 variants does not affect axonal bifurcation, mechanosensory neurons require a greater Dscam diversity for axonal branching and connectivity with their target cells (Chen et al., 2006) (Figure 14). A model whereby mechanosensory neurons and their corresponding target cells require expression of identical Dscam isoforms to establish neuronal connectivity via homophilic adhesion forces remains plausible.

In summary, axonal sister branch bifurcation and dendritic field organization require the expression of any one Dscam isoform which underlies a strictly cell-intrinsic process of repulsion between isoneuronal neurites. Fasciculation between co-projecting neurons and overlapping heteroneuronal dendritic fields require each cell to express a different set of isoforms to allow co-existence of neighboring neurons arguing for adhesion forces between them (Hughes et al., 2007; Matthews et al., 2007; Soba et al., 2007). An exceptional case of homophilic binding leading to target connectivity via attractive forces is also conceivable.

1.6.1.4. Diversity of Dscam intracellular domain is important for neuronal development

An additional level of Dscam endodomain diversity due to skipping of exon 19 and/or exon 23 has profound impact in neuronal development. RNAi silencing of exon 19 containing transcripts prevents neurites from crossing the midline in *Drosophila* embryos. Intriguingly, silencing of transcripts lacking exons 19 and 23 disrupts neural wiring in adult flies. Moreover, isoforms without exon 19 are localized in neurites of mushroom body neurons, contrary to exon 19 containing isoforms that localize in cell bodies as well (Yu et al., 2009). Similarly, exon 17.1 containing isoforms are targeted



to dendrites and exon 17.2 containing isoforms are enriched in axons, supporting the evidence that ectopic expression of exon 17.2 containing Dscam rescues axonal branching in mushroom body (Wang et al., 2004). Unlike the ectodomain diversity, no mechanism has been proposed to explain location dependent neuronal function of Dscam isoforms, arising due to alternatively spliced intracellular and transmembrane domains.

1.6.2. Overview of the immune system

The immune system is a collection of defense mechanisms within an organism, which protects it against disease by identifying and combating foreign particles (bacteria, fungi, viruses and parasitic worms) and tumour cells. Importantly, it distinguishes them from the organism's own healthy cells and tissues – ‘self’ from ‘non-self’ (Kvell et al., 2007).

The immune system has two components: innate immunity and adaptive immunity. The innate immune system, present in all organisms, is the first line of defense against any invading foreign particle and is believed to be largely invariable without immunological memory (as explained in 1.6.2.1.). In contrast, adaptive immunity, present exclusively in jawed vertebrates, generates variability in the form of antibodies by somatic recombination to cause an intruder-specific response coupled with immunological memory. Phagocytes, responsible for engulfing foreign particles, and B-lymphocytes, producing antibodies, are key players in the innate and adaptive immune responses, respectively (Kvell et al., 2007; Pham et al., 2007).

1.6.2.1. Insect immune system

Insects do not have antibodies, but have a potent innate immune system. Pattern recognition receptors (PRRs) help insects to recognize pathogen-associated molecular patterns (PAMPs) such as lipopolysaccharide (LPS), peptidoglycans (PGNs) and double stranded RNA (Ghosh et al., 2011). Haemocytes are central to cell-mediated immune responses and induce wound healing and blood coagulation to prevent further entry of invading pathogens.

On penetrating this barrier, pathogens are killed by phagocytosis upon recognition, engulfment and intracellular disintegration by haemocytes. Encapsulation wraps multicellular parasites with a thick wall of haemocytes and eradicates them. Nodulation around a microorganism comprises a central core of melanised haemocytes surrounded by a layer of flattened haemocytes, which also effectively clears pathogens (Marmaras and Lampropoulou, 2009; Rowley and Powell, 2007).

Antimicrobial peptides (AMPs) produced under the control of two evolutionarily conserved pathways – TOLL and IMD, are key immunomodulators in the insect humoral immune response. The prophenoloxidase (proPO) cascade produces a dark pigment called melanin, which deposits around pathogens and facilitates capsule and nodule formation. Insects also produce cytotoxic reactive oxygen species (ROS) and reactive nitrogen species (RNS), which eliminate host pathogens (Kurata, 2006; Marmaras and Lampropoulou, 2009). Other effectors such as lectins, which bind pathogen associated sugar molecules, and complement-like factors also function in destroying infectious agents (Beck and Habicht, 1996).

1.6.2.2. Evidence for ‘trained immunity’ in invertebrates

Due to the mostly short lifespan of invertebrates, their immune system has been assumed to lack any adaptive capacity. In recent years, however, evidence has accumulated indicating development of pathogen specific responses and immunological memory, which provides invertebrates with a defense system, independent of somatic recombination, called ‘trained’ immunity. One of the earliest works in this direction showed that earthworms were able to recognize and reject grafts from other earthworms. These worms demonstrated a faster graft rejection upon second exposure (Cooper and Roch, 1986).

A later study reported that male American cockroaches (*Periplaneta Americana*) that were first immunized and later challenged with a lethal dose of *Pseudomonas aeruginosa*, survived better (upto 14 days) than saline injected controls. Animals primed with other microbes (*Serratia marcescens*, *Enterobacter cloacae*, *Micrococcus lysodeikticus* and *Streptococcus lactis*) failed to show similar protection when challenged with *P. aeruginosa* (Faulhaber and Karp, 1992). Similarly, bumblebees (*Bombus terrestris*) that were initially primed with *Pseudomonas fluorescens*, *Paenibacillus alvei* or *Paenibacillus larvae* showed higher survival rates on receiving a homologous challenge (same bacteria) as compared to a heterologous challenge (different bacteria) (Sadd and Schmid-Hempel, 2006). These results suggest that insects primed with a particular species of bacteria, show a long-term pathogen-specific immune protection.

Intriguingly, priming *Drosophila* with a sub-lethal dose of *Streptococcus pneumoniae* or *Beauveria bassiana* (fungal pathogen) protected it against a subsequent lethal challenge, but such protection was not observed in flies immunized with *Salmonella*

typhimurium, *Listeria monocytogenes* or *Mycobacterium marinum*. These findings suggest that protection by priming is not a general mechanism against all pathogens in *Drosophila*. Also, for the first time, phagocytes were shown to rapidly clear microbial challenge from the haemolymph and provide such 'trained' immunity (Pham et al., 2007).

An interesting phenomenon observed in arthropods involves maternal transfer of pathogen-specific immunity onto the progeny. The water flea *Daphnia magna* were primed with two strains of pathogenic bacterium *Pasteuria ramosa*, strain A and strain G. The offsprings of these two groups when exposed to homologous challenge (primed and challenged with strain A or strain G) showed increased survival over those exposed to a heterologous challenge (primed with strain A and challenged with strain G and vice versa) (Little et al., 2003). Such transgenerational immune priming has also been observed in flour moths, bumblebees and mealworms (Moret, 2006; Rahman et al., 2004; Sadd et al., 2005). However, no studies have been carried out to explain the mechanism behind these observations.

The discovery of 'trained' immunity in invertebrates serves as a means to assess the importance of cellular versus humoral defenses in providing pathogen-specific long-term protection. The investigations involving *P. fluorescens* and *S. pneumoniae* challenge in previously primed bumblebees and fruit flies, respectively, found no role of AMPs in pathogen-specific immune response (Sadd and Schmid-Hempel, 2006). *In vivo* studies in *Drosophila* showed that activation of proPO pathway is not required for their survival against infectious challenge (Leclerc et al., 2006). Relish/NF- κ B double mutant *Drosophila* with fewer or no circulating haemocytes, and hence reduced phagocytic activity, but with fully functional AMP synthesis did not survive

opportunistic bacterial or fungal infections (Matova and Anderson, 2006). Moreover, homologous pathogen challenge post-immunization in lobsters (*Homarus americanus*) resulted in enhanced phagocytic activity of haemocytes (Mori and Stewart, 2006; Paterson and Stewart, 1979). These findings provide convincing evidence about the direct involvement of phagocytosis in challenge-specific long-term immunity in invertebrates. It is thus imperative to further explore the mechanism underlying the recent paradigm shift in invertebrate immunity from being completely innate to being ‘trained’.

Giardia lamblia, a human intestinal parasite, undergoes variation in antigen expression to escape the host’s immune system. It transcribes many of its variant-specific surface protein (VSP) coding genes (~190 genes) but expresses only one VSP at any given time and can switch to express another VSP. Silencing of the RNAi machinery, results in the expression of multiple VSPs in individual parasites (Prucca et al., 2008). Generally, RNA-dependent mechanisms could represent ways to generate molecular diversity to evade external pathogenic challenges in invertebrates.

1.6.2.3. *Dscam* splicing regulation provides ‘trained immunity’ in invertebrates

Immunoglobulin domain containing proteins comprise the largest group of cell surface receptors, which play a role in antigen recognition, cell adhesion and signaling in vertebrates and invertebrates. In higher vertebrates, Ig containing B and T cell receptors and antibodies exhibit enormous diversity via somatic recombination and clonal selection (Watson et al., 2005). Invertebrates employ alternative splicing

of *Dscam*, a well-known PRR, to generate a vast repertoire of spliceforms to recognize and protect against a variety of host pathogens (Kurata, 2006).

Watson et al., (2005) showed that *Dscam* is expressed in *Drosophila* larval haemocytes, fat bodies and brain tissue and is also secreted in the haemolymph. Haemocytes from hypomorphic and transgenic *Dscam* RNAi larvae; and *Drosophila* S2 cells show reduced phagocytic uptake of *E. coli* by ~25-35%. Moreover, *Dscam* directly binds to live *E. coli in vitro* via its extracellular domain. This study demonstrates a role of *Dscam* in phagocytic uptake of bacteria by direct binding and potentially also opsonizing circulating pathogens in the haemolymph via isoforms cleaved from the membrane. However, the specificity of this observation was not examined with different pathogenic exposures (Watson et al., 2005).

In *Anopheles gambiae*, Sua5B cells (haemocyte-like cell line), on challenge with bacteria (*E. coli*, *Pseudomonas veronii* or *Staphylococcus aureus*) and bacterial cell surface determinants (lipopolysaccharide or peptidoglycan), causes rapid change in *AgDscam* exon 4 splicing pattern to yield high affinity binding isoforms in a pathogen-specific manner. RNAi against these isoforms decreases bacterial binding, phagocytic uptake by ~55-60% and survival rates on exposure to the same pathogen (Dong et al., 2006). Also, injecting *E. coli* and *S. aureus* in crayfish (*Pacifastacus leniusculus*) induces pathogen-specific, high affinity binding isoforms of *PIDscam*. Moreover, coating bacteria with these *PIDscam* recombinant isoforms hides the binding sites required for bacterial clearance by phagocytosis (Wattanasurorot et al., 2011). Feeding mosquitoes with blood meal infected with either one, two or three genotypes of *P. falciparum* results in increased *AgDscam* diversity (Smith et al., 2011). The change in splicing pattern and increase in diversity suggests a

mechanism of increasing the probability to recognize, bind and defend against the invading pathogen.

Intriguingly, shrimp (*Litopenaeus vannamei*) *LvDscam* lacks the characteristic transmembrane and intracellular membrane domains associated with *Dscam* in other arthropods. Haemocytes express a total of 39 individual *LvDscam* isoforms – 12 isoforms in white spot syndrome virus (WSSV)-free, 11 isoforms in WSSV-persistent and 16 isoforms in WSSV-acute infection conditions. This result suggests a unique mechanism adopted by shrimps to choose *LvDscam* isoforms exclusively associated with the intensity of viral infection (Chou et al., 2009).

In conclusion, the results from these studies suggest that change in *Dscam* splicing pattern plays a key role in the putative invertebrate ‘trained’ immunity. Nonetheless, the mechanism, which regulates this splicing switch, is not understood.

1.7. Model for *Dscam* splicing regulation

Regulation of *Dscam* diversity by mutually splicing is quintessential for neural circuit formation, organization of dendritic fields and clearance of pathogens by *Dscam* mediated phagocytosis. For all these functions, expression of a small unique set of *Dscam* isoforms is required in individual cells of an otherwise identical population.

Single cell analysis in R7 photoreceptor neurons and haemocytes reveals that each cell expresses a distinct set of about 14 to 50 *Dscam* isoforms (Neves et al., 2004). Hence, every cell in a population of neurons or haemocytes contributes towards an overall unique *Dscam* identity. Diversification of *Dscam* could potentially be achieved in the nervous system and the immune system during independent events. In the nervous system, an extensive array of *Dscam* isoforms present in undifferentiated

neurons is reduced to a cell-specific complement during differentiation, or a limited diversity of *Dscam* isoforms present initially is altered during differentiation to provide a unique neuronal identity. In the immune system, experimental evidence argues that the initial diversity present in a population of haemocytes diversifies into a different complement of isoforms on encountering pathogens.

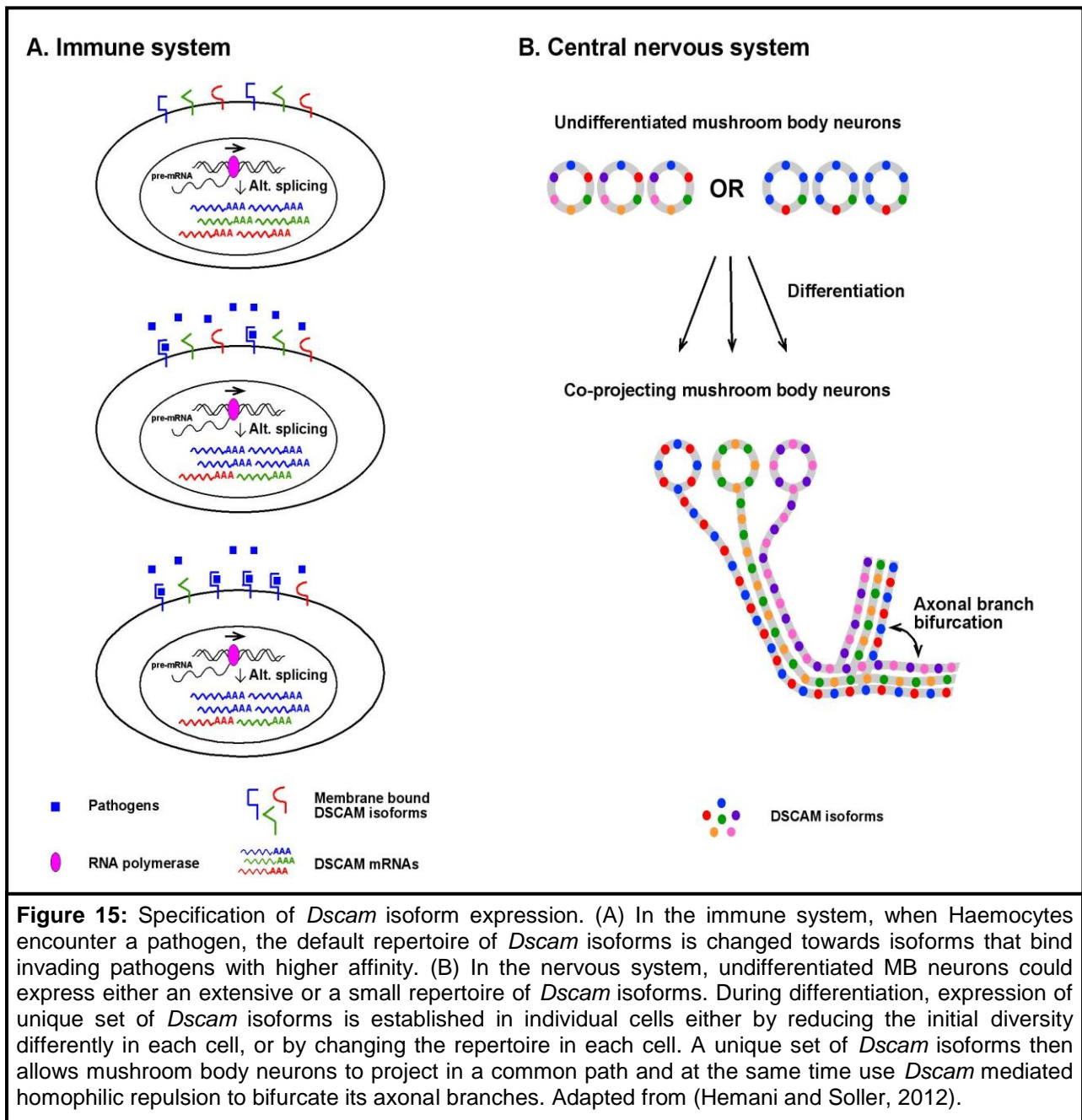
The mechanism underlying the choice and inclusion of specific exons is however, poorly understood. Particularly intriguing, signals from the cell surface seem to relay to the splicing machinery to regulate *Dscam* diversity. Encountering a pathogen causes high affinity binding *Dscam* isoforms to feedback positive selection and amplification of the same isoform. Contrarily, *Dscam* homophilic repulsion sends negative feedback to exclude selection of identical isoforms between neighbouring neurons (Figure 15).

1.8. Aims

This project is integrated in the long-term aim to identify the mechanisms, which regulate the choice of a single or a specific set of *Dscam* isoforms in the *Drosophila* immune system and the nervous system by alternative splicing.

1.9. Objectives

In order to mount an immune response, host organisms must first recognize the pathogen after infection. Despite the importance of this process, little is known about the mechanisms of pathogen recognition in invertebrates. Upon pathogen exposure in mosquitoes, the *Dscam* splicing pattern changes to express isoforms that bind the pathogens with higher affinity (Dong et al., 2006). To validate the generality of *Dscam*



splicing regulation on pathogen exposure, *Drosophila* S2 cells were challenged with different microbes. Potentially, *Dscam* isoforms binding to the pathogens could signal from the membrane to the nucleus through their associated mRNAs to induce the inclusion of the same exons. In support, *Giardia lamblia* employs RNAi to establish antigenic variation on its surface such that at any given time, it expresses only one out of ~190 variant-specific surface proteins (Prucca et al., 2008). Accordingly, a single *Dscam* isoform was expressed in *Drosophila* S2 cells to test if the endogenous *Dscam* splicing pattern changes to enhance the inclusion of exons present in the exogenous isoform. To further explore RNA based mechanisms in altering *Dscam* alternative splicing, mutants of *ago1* and *elav*, which have a similar nervous system defect as observed in *Dscam* mutants were tested. In addition, mutants of other RNA processing factors such as *ago2*, involved in siRNA-directed RNAi and members of the exosome and Trf4/Air2/Mtr4p polyadenylation (TRAMP) complexes such as *rrp6* and *trf4* respectively that are involved in removal of cryptic RNA transcripts were also tested. Since ELAV has no obvious binding site in *Dscam* pre-mRNA, an indirect role of ELAV in regulating *Dscam* splicing was assumed. Consequently, mutants of RNA binding proteins, DNA binding proteins and chromatin remodeling factors that are differentially regulated in *elav* mutants were tested for changes in *Dscam* splicing. To further understand the regulation of *Dscam* splicing, transgenic flies containing a construct heterologously expressing an entire variable cluster were made, which will enable us to identify sequence elements that could play a role in selection of specific exons.

CHAPTER 2

MATERIALS AND METHODS

2.1. *Drosophila* husbandry and genetics

2.1.1. Fly food

Flies were reared in glass vials containing 11 ml of standard cornmeal-agar food (8.5% dextrose (w/v), 6% cornmeal (w/v), 2.5% nipagin (v/v), 1% agar (w/v) in tap water). Once solidified, the food was supplemented with live yeast to encourage egg laying.

2.1.2. Fly maintenance

Stocks and crosses were maintained in a 12 hr day/12 hr night photoperiod at 25°C and 70% relative humidity. Crosses were flipped every second day and stocks were flipped every three weeks to allow healthy development of offsprings. The vials were monitored regularly to prevent overcrowding and dehydration.

2.1.3. Embryo collection

14-18 hr old, stage 17 embryos were used for experiments. A cylindrical chamber sealed at the bottom with a wired mesh and covered on top with grape juice plates (3% agar (w/v) and 25% grape juice (v/v) (Ritchies) in tap water with a smear of live yeast) was used to collect embryos. Flies were acclimatized in the chamber for 2-3 d prior to embryo collection. Flies were allowed to lay eggs on a plate in the evening for

four hr. This plate was incubated at 25° for 14 hr after which the embryos (14-18 hr old) were collected and dechorionated by immersing them in 50% sodium hypochlorite solution (v/v) for 90 sec. The dechorionated embryos were washed with tap water on a fine mesh using an aspirator (UniEquip) and then observed under a light microscope or a fluorescent microscope (Leica) if green fluorescent protein (GFP) expression was desired. Embryos similar in gut morphology were selected and stored in 10 µl of double distilled water (ddH₂O) at -80°C.

2.1.4. Fly transgenesis with *UAS Dscam 9L*

UAS Dscam 9L (containing *Dscam Ex 7-11*, obtained from M. Soller, Figure 16) was prepared by using the Qiagen plasmid purification kit (as explained in 2.4.11). Integration of *UAS Dscam 9L* in the *Drosophila* genome was achieved by φC31 mediated germline transformation system (Bischof et al., 2007). *UAS Dscam 9L* carries a bacterial attachment site (*attB*), which allows its site-specific incorporation into the genome of flies containing a pre-determined phage attachment landing site (*attP*) at position 76A2 (*PBac(y[+]-attP-9A)VK00013*). The recombination reaction is initiated by a constitutively expressed φC31 integrase encoded on the X chromosome (*y₁ w⁺ M(vasint.Dm)ZH2A*).

The injection mix was prepared by adding 2.5 µg of *UAS Dscam 9L*, 1X injection buffer (5 mM KCl, 0.1 mM Na₃PO₄, pH 7.8), 1 mM MgCl₂ and 0.2 µM filtered food dye in a total volume of 10 µl. The mixture was centrifuged at 16,000g for ten min to remove of any interfering particles and placed on ice. The needles used for microinjection were made from fine borosilicate glass capillary tubes (Intracel), with an internal filament (0.22 mm in diameter), by a micropipette puller (Narishige).

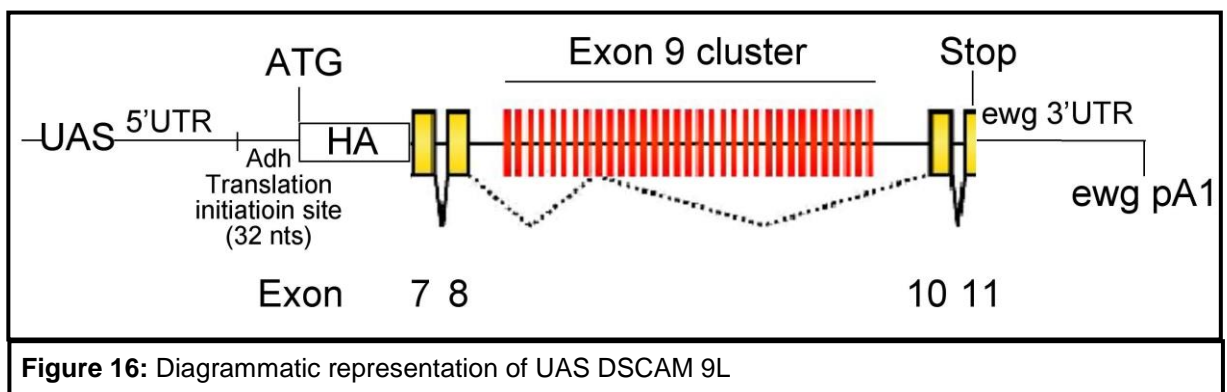


Figure 16: Diagrammatic representation of UAS DSCAM 9L

A capillary was placed in a vertical position and melted by a heating filament and subsequently pulled by attached weights under the force of gravity. Needles were filled with DNA from one end, which spread along the whole filament up till the tip, by capillary action.

Approximately 300-500 flies from the $y_1 w^* M(vasint.Dm)ZH2A ; PBac(y[+]-attP-9A)VK00013$ stock were transferred into an egg laying chamber (as explained in 2.1.3.) and allowed to acclimatize for 2-3 d before injection. Grape juice plates were changed twice a day during this period. The following steps were carried out in an 18°C room. Embryos were harvested after a 20-25 min laying period and washed with tap water using a squeeze bottle. They were dechorionated in 33% sodium hypochlorite solution (v/v) for two min and thoroughly rinsed with tap water. Dechorionated embryos (~80 embryos) in the pre-blastoderm were aligned with a paintbrush along the edge of a glass coverslip. Care was taken to align the embryos in the same orientation for ease of injection. Embryos were picked up by gently lowering a coverslip coated with heptane glue such that the embryos stuck to the coverslip. The affixed embryos were dehydrated for ~15 min in a desiccation chamber containing silica gel. This time period was adjusted according to relative humidity levels in the desiccation chamber such that a gap developed between the posterior end of the embryo and the vitelline membrane when observed under a phase contrast. The dehydrated embryos were covered in a thin layer of halocarbon 700 oil (Sigma). The coverslip was fixed onto a glass slide and then placed on the stage of an inverted microscope (Nikon) fitted with a micromanipulator (Nikon). The microscope was also attached to a microinjector (Narishige) and a compressor (Jun-Air) via a needle holder. Embryos were focused such that their posterior ends faced

the needle on the same focal plane. The micromanipulator was used to move the embryos against the static needle. Microinjection was achieved by inserting the tip of the needle inside the posterior end of the embryos by expelling a fixed volume of DNA solution under a fixed air pressure. Embryos exhibiting cellularization were destroyed to avoid unnecessary work after eclosion. The injected slide was tilted for 15 min to run out the excess oil. The slide was then placed in a hydration chamber and larvae were collected after 48 hr. These larvae were transferred in special soft food (1% agar (w/v), 5% sucrose (w/v), 4% yeast extract (w/v), 2% inactivated yeast (w/v), 0.5% 9:1 propionic acid: phosphoric acid (v/v)). Eclosed flies from the injected embryos were out-crossed with *yw*. Apart from the attB site, *UAS Dscam 9L* has GFP as a positive transformation marker. Progeny from the outcross were screened for GFP expression in the eyes, indicating that transgenesis has occurred. To stabilize the transgenic line, transformants were crossed to a doubly balanced strain (*yw*; TM3 Sb/TM6b) and a homozygous transgenic stock was established.

2.2. Molecular biology

2.2.1. RNA isolation

Flies/embryos/tissues/cells were homogenized with a pestle in 50 µl of Trizol reagent (Sigma). The pestle was washed off any bound RNA with 450 µl of Trizol reagent. The homogenized mixture was vortexed for 2 min. Then, 200 µl of chloroform:isoamyl alcohol (49:1) was added to the mixture and again vortexed for 2 min. The tube was kept on ice for five min until the phases separated. The mixture was centrifuged at 16,000g for ten min. Then, 200 µl of the aqueous phase (containing RNA) was carefully transferred into a new tube containing 1 µl of

glycogen. Care was taken to avoid contamination of the aqueous phase from the interphase (DNA) or the organic phase (proteins/lipids). Then, 200 µl of absolute isopropanol was added to the aqueous phase and vortexed for a few seconds. The solution was centrifuged at 16,000g for ten min. The supernatant was discarded and the pellet was washed with 750 µl of 70% ethanol (v/v) at 16,000g for ten min. The supernatant was removed and the RNA pellet was left to air dry for ~5 min. The pellet was dissolved in autoclaved diethylpyrocarbonate (DEPC) treated de-ionized water and stored at -20°C. DEPC treated water was made by adding 0.1% DEPC (v/v) to de-ionized water and allowing it to stand for 2 hours at room temperature with intermittent shaking. DEPC was inactivated by autoclaving.

2.2.2. Reverse transcription (RT)

For a total RT reaction volume of 20 µl, a master mix (13 µl) containing the isolated RNA (9.5 µl), 1 µl of 10X RT buffer (200 mM Tris-HCl, 500 mM KCl, pH 8.3), 1 µl of 100 mM dithiothreitol (DTT), 20 units of ribonuclease inhibitor (RNAsin, Promega) and 1 µl of 10 pM oligo(dT) or 1 µl of 20 µM gene-specific probe was kept at 70°C for 15 min in a thermal cycler (Eppendorf). A second master mix (6 µl) containing 1 µl of 10X RT buffer, 1 µl of 100 mM DTT, 1 µl of 100 mM MgCl₂, 1 µl of 10 mM deoxyribonucleotides (dNTPs) and 20 units of RNAsin were added to the reaction mixture just before the temperature reached 50°C. After ten min of incubation at 50°C the reaction mixture was kept at 46°C when 20 units of Superscript II Reverse Transcriptase (Invitrogen) were added and reverse transcription was carried out for one hr. The final extension was carried out at 70°C for 15 min.

2.2.3. Polymerase chain reaction (PCR)

For a total reaction volume of 50 μ l, a master mix was prepared containing 1 μ l of template (genomic DNA/cDNA/plasmid), 1X Dream Taq buffer (10mM Tris-HCl, 50 mM KCl, 2 mM $MgCl_2$, pH 8.3, Fermentas), 0.4 μ M forward and reverse primers, 0.2 mM dNTPs and 1.25 units of Dream Taq DNA polymerase (Fermentas). This reaction mixture was placed in a thermal cycler (Applied Biosystems) when temperature was $>90^\circ C$ and subjected to an initial denaturation at $94^\circ C$ for 30 sec, then 30-40 cycles of denaturation at $94^\circ C$ for 30 sec, annealing at $56^\circ C$ for 40 sec and synthesis at $72^\circ C$ for 45 sec and a final extension for one min (annealing temperature and synthesis time varied with primer type and length of PCR product, respectively). PCRs for cloning were carried out using Phusion DNA polymerase (Finnzymes), a proofreading enzyme, in 1X Phusion buffer. Care was taken to prevent mixing of primers before introducing the tubes in the thermal cycler to avoid primer dimer formation.

2.2.3.1. Single fly PCR

One male fly was introduced into a PCR tube and frozen at $-20^\circ C$ for 30 min. Then, 200 μ l of isopropanol was added to the tube and incubated at room temperature for one hr. The isopropanol was removed by suction under vacuum for 30 min in a speed vacuum concentrator (Thermo Scientific). A master mix was immediately added to the tube and placed in a thermal cycler to proceed for a PCR reaction (as explained in 4.2.3.).

2.2.4. Agarose gel electrophoresis

To prepare 1% and 2.5% agarose gels (w/v), 1 g and 2.5 g of electrophoresis quality agarose was melted in 100 ml of 1X TAE buffer (40 mM Tris, 1 mM EDTA, 20 mM glacial acetic acid, pH 8.0), respectively. Care was taken to fully dissolve the agarose. Ethidium bromide (5 μ l per 100 ml of gel) was added and mixed by shaking. The gel mixture was poured into a gel cast (with combs) and allowed to solidify at room temperature. The PCR products were mixed with 2 μ l of 9X loading buffer (43.5% glycerol (w/v), 50 mM EDTA pH 8.0-8.5, 10 mM Tris pH 7.5, 0.05% xylene cyanol (w/v), 0.05% bromophenol blue (w/v)) and loaded into the gels. The samples were run at 150-200 V for 30 min.

2.3. Radioactivity used to label primers

^{32}P γ -ATP (143 $\mu\text{Ci}/\mu\text{l}$, 6000 Ci/mmol, Perkin Elmer) was used for all experiments involving radioactivity. Specific activity of ^{32}P γ -ATP was measured using a scintillation counter with a counting efficiency (E) of 0.5. The counts per minute (cpm) reading from the counter was used to calculate disintegrations per minute (dpm) using the equation $\text{dpm} = \text{cpm}/E$. The dpm value was converted to disintegrations per second (dps) by using the equation $\text{dps} = \text{dpm}/60$. Activity of the radiolabel was calculated in curies (Ci) using the equation $\text{Ci} = \text{dps}/3.7 \times 10^{10}$ (1 Ci = 3.7×10^{10} dps). Specific activity of the radiolabel was calculated by determining curies per millimole (Ci/mmol) of the radiolabel measured in the scintillation counter (Packard).

2.3.1. Primer radiolabeling

For a total reaction volume of 20 μl , 10 units of T4 polynucleotide kinase (T4-PNK) were used to label 10 μM primers with 143 μCi ^{32}P γ -ATP in 1X PNK buffer (70 mM Tris-HCl, 10 mM MgCl_2 , 5 mM DTT, pH 7.6). The reaction mixture was incubated at 37°C for 30 min. The enzyme was inactivated by incubating the reaction mixture at 80°C for ten min. For a radioactive PCR, either the forward or the reverse primer (as required) was radiolabeled. All of the ^{32}P γ -ATP in the reaction mixture was incorporated into the 10 μM of primers used.

2.3.2. Restriction enzyme digests of PCR products from *Dscam* variable regions

5 μl of PCR product was precipitated using 0.3 M sodium acetate and 2.5 volumes of absolute ethanol at -80°C for ten min. The solution was centrifuged at 16,000g for ten min. The supernatant was discarded and the DNA pellet was washed with 500 μl of 70% ethanol (v/v) at 16,000g for ten min. The pellet was air dried for ~5 min and resuspended in 30 μl of ddH₂O. The precipitated PCR product was digested using appropriate enzyme combinations and buffers depending on the amplified *Dscam* variable exon cluster (as explained below). For a reaction volume of 50 μl , 5 units of each enzyme were used to carry out restriction digests. The digested product was precipitated (as explained above) and dissolved in 20 μl of denaturing gel loading buffer (98% de-ionized formamide (v/v), 10 mM EDTA pH 8.0, 0.025% xylene cyanol (w/v), 0.025% bromophenol blue (w/v)). The samples were denatured at 95°C for 90 sec and immediately placed on ice before loading into the gel.

Exon 4 cluster was digested with *Mbol*, *Alul* and *HinPI* in 1X NEBuffer 4 (50 mM potassium acetate, 20 mM Tris-acetate, 10 mM magnesium acetate, 1 mM DTT, pH 7.9) and 1X bovine serum albumin (BSA) at 37°C for one hr in a total reaction volume of 50 µl. Then, *Taq^{II}* was added to the digest mixture and incubated at 65°C for 1 hr.

Exon 6 cluster was digested with *Mbol*, *Alul* and *Mspl* in 1X NEBuffer 2 (50 mM NaCl, 10 mM Tris-HCl, 10 mM MgCl₂, 1 mM DTT, pH 7.9) and 1X BSA at 37°C for one hr in a total reaction volume of 50 µl. Then, the reaction volume was adjusted to 75 µl with 1X NEBuffer 2 and 1X BSA and digested with *BstUI*, *BstM* and *Taq^{II}* at 60°C for 1 hr.

Exon 9 cluster with the forward primer radio-labeled was digested with *HpyCH4IV* in 1X NEBuffer 1 (10 mM Bis-Tris-Propane-HCl, 10 mM MgCl₂, 1 mM DTT, pH 7.0) and 1X BSA at 37°C for one hr in a total reaction volume of 50 µl. Then, the reaction volume was adjusted to 75 µl with 1X NEBuffer 2 and 1X BSA and digested with *HaeIII*, *XmnI* and *Mspl* at 37°C for 1 hr. Finally, the reaction volume was adjusted to 100 µl with 1X NEBuffer 2 and 1X BSA and digested with *BstUI* and *BstM* at 60°C for 1 hr.

Exon 9 cluster with the reverse primer radio-labeled was digested with *HpyCH4IV* in 1X NEBuffer 1 and 1X BSA at 37°C for one hr in a total reaction volume of 50 µl. Then, the reaction volume was adjusted to 75 µl with 1X NEBuffer 2 and 1X BSA and digested with *Mbol*, *Alul* and *HinPI* at 37°C for 1 hr. Finally, the reaction volume was adjusted to 100 µl with 1X NEBuffer 2 and 1X BSA and digested with *BstUI* and *Taq^{II}* at 60°C for 1 hr. All restriction enzymes and buffers were bought from New England Biolabs (NEB).

2.3.3. Denaturing polyacrylamide gel electrophoresis

Denaturing polyacrylamide gel electrophoresis was carried out using the SequaGel System (National Diagnostics). For a total volume of 60 ml of 8% gel, SequaGel concentrate (1.07 M acrylamide, 26 mM methylene bisacrylamide (40:1 acrylamide:bisacrylamide), 2.4 M urea), SequaGel diluent (4.35 M urea) and SequaGel buffer (89 mM Tris-borate, 2 mM EDTA, pH 8.3 and 0.75 M urea) were mixed together. Appropriate proportions of the concentrate, diluent and buffer for a range of gel percentages are listed in Table 1 (National Diagnostics). 0.04% TEMED (v/v) and 0.8% freshly prepared ammonium persulfate (v/v) were added to allow polymerization of acrylamide. The un-polymerized gel was gently mixed and cast between two clean glass plates (one of them silanized on one side) separated by plastic spacers. The comb was inserted at one end and the gel was left to polymerize for 1-2 hr. After polymerization, the gel was made to pre-run at 800-1000V for 15-20 min until the temperature reached 55-60°C after which the samples were loaded. 1X TBE (89 mM Tris-borate, 2 mM EDTA, pH 8.3) buffer was used as running buffer. After the completion of the run (at 1300V for ~2.5-3 hr), the glass plates were separated using a spatula. The gel, still stuck on the silanized surface, was fixed with fixing solution (10% methanol (v/v), 10% glacial acetic acid (v/v)) for ten min. The fixed gel was then transferred onto a clean wet filter paper and heat vacuum dried at 85°C for 1 hr. A Kodak imaging screen (Biorad) was exposed to the radioactive gel for 14 hr before scanning it in a molecular imager (Biorad) using Quantity One software (Biorad). The radioactive signal on the imaging screen was erased against a screen eraser (Biorad).

DNA Fragment Size (bp)	% Monomer	SequaGel Concentrate	SequaGel Diluent	SequaGel Buffer
>200	4	16ml	74ml	10ml
80-200	5	20ml	70ml	10ml
60-150	6	24ml	66ml	10ml
40-100	8	32ml	58ml	10ml
0-50	12	48ml	42ml	10ml
<20	20	80ml	10ml	10ml

Table 1: Denaturing polyacrylamide gel composition. The table shows volumes of SequaGel concentrate, diluent and buffer (total gel volume = 100 ml) for commonly used polyacrylamide gel percentages required to resolve corresponding DNA fragments (National Diagnostics).

2.3.4 Quantification of bands

The average intensity of each band was calculated by using the volume rectangle tool in Quantity One software. It measures the total signal intensity within a defined border drawn around the band by adding the intensities of all pixels within the volume boundary multiplied by the pixel area (intensity units x mm²). The background intensity was subtracted from the band intensity using the local background subtraction method. This tool adds the intensities of all pixels in a 1-pixel boundary around the border drawn and divides it by the total number of boundary pixels. This gives a measure of the average background intensity around each volume drawn, which is then subtracted from the intensity of each pixel within the volume. The intensities of resolved exon bands (digested fragments) were divided with the intensity of their input bands (undigested PCR products) to obtain their respective inclusion levels, which were normalized against the input of the control experiment. Regulation of splicing changes was analyzed by determining fold differences between the normalized inclusion levels of a variant exon against corresponding exon bands in the control experiment. The quantified data were represented as best-fit heat-maps, which were generated using the Matrix2png interface.

2.4. Molecular cloning

2.4.1. Media preparation

Luria Bertani (LB) medium was prepared by dissolving peptone (1% (w/v)), yeast extract (0.5% (w/v)) and sodium chloride (0.5% (w/v)) in ddH₂O. The pH was adjusted to 7.0 with 5 M sodium hydroxide (~1.0 ml). The medium was then autoclaved.

2YT medium was prepared by dissolving peptone (1.6% (w/v)), yeast extract (1% (w/v)) and sodium chloride (0.5% (w/v)) in ddH₂O. The pH was adjusted to 7.0 with 5 M sodium hydroxide (~1.0 ml). The medium was then autoclaved. LB plates were made by adding technical quality agarose (1.5% (w/v)) to LB medium and autoclaving. Appropriate antibiotic selection was added to the medium after it cooled to < 50°C. A list of antibiotics used is mentioned in Table 2.

2.4.2. Preparation of competent cells

2.4.2.1. Chemically competent cells

From a single colony of *DH5α* cells, an overnight culture was set up at 37°C with vigorous shaking. An inoculum of 2.5 ml from the fresh overnight culture was added to 250 ml of LB medium and grown at 37°C with vigorous shaking until OD₆₀₀ reached 0.4-0.5. Care was taken to not overgrow the culture above an OD₆₀₀ of 0.5. The following steps were carried out at 4°C. Cells were harvested by centrifugation at 1,000g for five min. The supernatant was removed and the pellet was carefully resuspended in 100 ml of 50 mM ice-cold CaCl₂. After a recovery time of 20 min, the cells were centrifuged at 1,000g for five min. The supernatant was removed and the pellet was resuspended in 8 ml of 100 mM CaCl₂ to which 2.4 ml of ice-cold 87% glycerol (w/v) was slowly added whilst constant mixing. Aliquots of this suspension were stored at -80°C.

2.4.2.2. Electro-competent cells

From a single colony of *DH5α* cells, an overnight culture was set up at 37°C with vigorous shaking. An inoculum of 10 ml from the fresh overnight culture was added to

Antibiotic	Stock Concentration	Solvent	Working solution
Ampicillin	100 mg/ml	Water	100 µg/ml
Chloramphenicol	34 mg/ml	Ethanol	25 µg/ml for plasmids; 12.5 µg/ml for BACs
Tetracycline	50 mg/ml	Ethanol	12.5 µg/ml; 3 µg/ml for low copy number

Table 2: List of antibiotics used during the study. The table shows the stock concentrations (mg/ml), solvents and working solutions (µg/ml) of all antibiotics used during the study.

1 lit of LB medium and grown at 37°C with vigorous shaking until OD₆₀₀ reached 0.6. Care was taken to not overgrow the culture above an OD₆₀₀ of 0.6. The following steps were carried out at ~0°C. Cells were harvested by centrifugation at 1,000g for 15 min. The supernatant was removed and the pellet was carefully resuspended in 1 lit of ice-cold 10% glycerol. The suspension was centrifuged at 1,000g for 15 min. This step was subsequently repeated with 0.5 lit and 250 ml of ice-cold 10% glycerol. The final pellet was resuspended in ice-cold 10% glycerol such that the concentration of cells was 1-3x10¹⁰ cells/ml. Aliquots of this suspension were stored at -80°C.

2.4.3. Primer phosphorylation

For a total volume of 20 µl, 10 units of T4-PNK were used to phosphorylate 20 µM primers in 1X T4 DNA ligase buffer (50 mM Tris-HCl, 10 mM MgCl₂, 10mM DTT, 1 mM ATP, pH 7.5). The reaction mixture was incubated at 37°C for 30 min.

2.4.4. Phenol-chloroform extraction of PCR products

The PCR product was made (as explained in 4.2.3.) upto a final volume of 200 µl with ddH₂O. An equal volume of phenol/chloroform/isoamyl alcohol (50:49:1) was added to the diluted PCR product, mixed and centrifuged at 16,000g for ten min. The upper phase was carefully taken and an equal volume of chloroform/isoamyl alcohol (49:1) was added. The solution was mixed and centrifuged at 16,000g for ten min. DNA was precipitated using 0.3 M sodium acetate and 2.5 volumes of absolute ethanol at -80°C for ten min. The solution was then centrifuged at 16,000g for ten min. The supernatant was discarded and the DNA pellet was washed with 500 µl of

70% ethanol (v/v) at 16,000g for ten min. The pellet was air dried for ~5 min and resuspended in ddH₂O to proceed with appropriate restriction enzyme digests.

2.4.5. Restriction enzyme digests of PCR products

All restriction enzyme digests for cloning procedures were performed as 16-fold over-digestion where 1 unit of enzyme digests 1 µg of plasmid DNA/ PCR product per hr. All digestion reactions were set in a 50 µl reaction volume. Enzymatic reactions were inactivated by adding 100 µl of phenol/chloroform/isoamyl alcohol (50:49:1) and centrifugation at 16,000g for five min. From the supernatant, 50 µl was run on a 1% agarose gel (w/v) to proceed with gel extraction of the desired band.

2.4.6. Gel extraction of digested DNA fragments

Gel purification of digested DNA fragments was done using the gel extraction kit from Fermentas as follows. After running restriction digests in a 1% agarose gel (w/v), the desired DNA fragment was excised from the gel and weighed. For every 100 mg of agarose gel, 100 µl of binding buffer was added. The gel mixture was incubated at 55°C for five min until the gel piece was completely dissolved. Silica powder suspension was then added to the mixture (5 µl of silica powder suspension for ≤2.5 µg of DNA and an additional 2 µl of silica powder suspension for every µg if DNA ≥2.5 µg). The mixture was incubated at 55°C for five min with intermediate mixing to allow DNA binding to the silica beads. The mixture was then centrifuged at 16,000g for 5 sec to form a silica pellet. The supernatant was removed and the pellet was resuspended in 500 µl of ice cold washing buffer (2.5% concentrated washing buffer (v/v), 50% absolute ethanol (v/v)). This process was repeated three times after which

the silica pellet was air dried until all ethanol evaporated. Finally, the pellet was resuspended in a desired volume of ddH₂O or 1X TE (10 mM Tris pH 7.5, 1 mM EDTA pH 8.0), incubated at 55°C for five min and centrifuged at 16,000g for 1 min. The recovered supernatant was placed in a new tube and centrifuged again to remove residual silica before being used for setting up ligation reactions.

2.4.7. Ligation

Gel purified vector backbone and inserts were run on an agarose gel to determine the relative concentrations of each DNA fragment. Appropriate ratios of the backbone and inserts (total DNA amount of 100-120 ng) were ligated in a final volume of 10 µl using 400 cohesive units of T4-DNA ligase in 1X T4-DNA ligase buffer. The ligation mixture was incubated overnight at 16°C.

2.4.8. Bacterial transformation

2.4.8.1. Heat shock transformation

Heat shock transformation was used only to obtain higher yields of plasmids. Chemically competent *E. coli* (DH5α strain) cells were thawed on ice. Approximately 0.5-1µg of plasmid DNA was mixed with 20 µl of *E. coli* cells and incubated on ice for 30 min. The mixture was incubated at 42°C for 90 sec and the tube was immediately placed on ice for 1 min. Subsequently, 400 µl of SOC medium (2% Bacto tryptone (w/v), 0.5% Bacto yeast extract (w/v), 10 mM NaCl, 2.5 mM KCl, 10 mM MgCl₂, 10 mM MgSO₄, 20 mM glucose) was added and the cells were regenerated at 37°C for 1 hr. The bacteria were then plated on agar plates with appropriate antibiotic selection and incubated overnight at 37°C.

2.4.8.2. Electro-transformation

Electro-transformation was used while cloning fragments to obtain new constructs. Electro-competent *E. coli* (*DH5α* strain) were thawed on ice. The ligation mixture was dialyzed on membranes (0.025 μm, Millipore) against ddH₂O for 30 min. The dialyzed mixture was washed off the membrane using 8 μl of ddH₂O and this step was repeated thrice. The mixture was gently added to 25 μl of bacterial cells and the final volume was made up to 90 μl with ddH₂O. This suspension was carefully transferred into a cold 1 mm electroporation cuvette (0.2cm, Cell Projects) without introducing any air bubbles. The cuvette was placed in a chilled safety slide of a pulser apparatus (Biorad) and pushed into the chamber until the cuvette was seated between the contacts at the base of the chamber. The cells were pulsed once with 2.0 kV, 200 Ω and 25 μF. The capacitance extender and time constant were expected to be 125 μF and 4.5-5 ms, respectively. The pulsed cells were resuspended gently in 500 μl of SOC medium and incubated at 37°C for 1 hr. The bacteria were then plated onto agar plates with appropriate antibiotic selection and incubated overnight at 37°C.

2.4.9. Recombineering

Recombineering is a technique to obtain a fragment from the donor DNA in the host cell by transforming in a linearized vector with homologous regions (200-250 nts) at each end. For homologous recombination to occur the host cell requires the pRed/ET plasmid which encodes the genes of proteins required for recombination, which are induced by L-arabinose at 30°C. The plasmid is lost at 37°C due to temperature

sensitive origin of replication. In order to detect efficient recombination, the donor vector needs to have a different selection than the receiving vector.

2.4.9.1. Generation of pRed/ET electro-competent cells

From a single colony of pRed/ET plasmid (Gene Bridges) containing cells (agar plates containing 3 µg/ml tetracycline), an overnight culture was set up at 30°C with vigorous shaking. An inoculum of 5 ml from the fresh overnight culture was added to 500 ml of LB medium (3 µg/ml tetracycline) and incubated at 30°C until OD₆₀₀ reached ~0.2. Care was taken to not overgrow the culture above an OD₆₀₀ of 0.2. Immediately, 15 µl of 10% L-arabinose (w/v) was added to the culture and placed in a 37°C water bath and then in a 37°C shaker for one hr until OD₆₀₀ reached 0.35-0.4. Care was taken to not overgrow the culture above an OD₆₀₀ of 0.4. Cells from this culture were washed with 10% glycerol (w/v) to generate electro-competent cells (as explained in 4.4.2.2.). Linearized donor and recipient fragments with homologous flanking sequences (200-400 bp) were co-transformed to allow recombineering of the insert.

2.4.9.2. Generation of Dscam BAC/pRed/ET electro-competent cells

From a single colony of Dscam BAC (Pacman Resources) containing cells (agar plates containing 12.5 µg/ml chloramphenicol) an overnight culture was set up at 37°C with vigorous shaking. An inoculum of 30 µl from the fresh overnight culture was added to 1.4 ml of LB medium (12.5 µg/ml chloramphenicol) and grown at 37°C with vigorous shaking until OD₆₀₀ reached 0.6. Care was taken to not overgrow the culture above an OD₆₀₀ of 0.6. The following steps were carried out at ~0°C. Cells

were harvested by centrifugation at 10,000g for 30 s. The supernatant was removed and the pellet was carefully resuspended in 1 ml of ice-cold 10% glycerol (w/v). This step was repeated once again and the supernatant was tipped out and dripped on a paper towel. The cells were resuspended in the ~30 μ l of glycerol left behind. Cells were electro-transformed using 1-5 ng of pRed/ET and grown at 30°C for 70 min before plating (3 μ g/ml tetracycline; 12.5 μ g/ml chloramphenicol). The cells were grown on plates in the dark at 30°C for 24 hr.

2.4.9.3. Preparation of Dscam BAC/pRed/ET host for DNA retrieval

From a single colony of Dscam BAC/pRed/ET containing cells (3 μ g/ml tetracycline; 12.5 μ g/ml chloramphenicol) an overnight culture was set up at 30°C with vigorous shaking. An inoculum of 30 μ l from the fresh overnight culture was added to 1.4 ml LB medium (3 μ g/ml tetracycline; 12.5 μ g/ml chloramphenicol) and grown at 30°C with vigorous shaking until OD₆₀₀ reached 0.2. Care was taken to not overgrow the culture above an OD₆₀₀ of 0.2. Then, 15 μ l of 10% L-arabinose (w/v) was added to the culture and immediately placed in a 37°C shaker for one hr until OD₆₀₀ reached 0.35-0.4. Care was taken to not overgrow the culture above an OD₆₀₀ of 0.4. The following steps were carried out at ~0°C. Cells were harvested by centrifugation at 10,000g for 30 s. The supernatant was removed and the pellet was carefully resuspended in 1 ml of ice-cold 10% glycerol (w/v). This step was repeated once again and the supernatant was tipped out and dripped on a paper towel. The cells were resuspended in the ~30 μ l of glycerol left behind and electro-transformed with linearized fragments with flanking sequences (200-400 bp) homologous to sequences flanking the region of DNA to be retrieved from Dscam BAC clone.

2.4.10. Plasmid DNA mini prep

From 12-48 individual colonies picked randomly from agar plates, overnight cultures were set up in 3 ml of 2YT medium with appropriate antibiotic selection and grown at 35.5°C for 16-18 hr with vigorous shaking. The shaker was set at 35.5°C and not 37°C because incase the temperature goes above 37°C (due to inconsistency of the thermostat), it has been observed that bacteria produce non-digestible DNA and also cause unwanted recombination events with large plasmids. From the overnight culture, 1.5 ml was centrifuged at 800g for five min. The supernatant was discarded and the cells were lysed with STET (8% sucrose (w/v), 0.1% Triton-X 100 (v/v), 50 mM EDTA, 50 mM Tris pH 8-8.5) and lysozyme (0.7 µg/µl, 0.7µM Tris pH 7.5). The solution was vortexed and allowed to stand at room temperature for five min after which it was boiled for 1-3 min and centrifuged at 16,000g for ten min. The protein pellet was removed with a toothpick after which RNaseA (0.04 µg/µl, 0.2 mM Tris pH 7.5, 0.3 mM NaCl, Roche) and 0.3 M sodium acetate (pH 5.2) was added to the supernatant and allowed to stand at room temperature for five min. Thereafter, 500 µl of absolute isopropanol was added and the solution was centrifuged at 16,000g for ten min. The supernatant was discarded and the pellet was washed with 650 µl of 70% ethanol (v/v) at 16,000g for ten min. The pellet was air dried for ~ five min and then dissolved in 50 µl 1X TE out of which 20 µl was used for analytical restriction enzyme digests to screen for the right clone.

2.4.11. Plasmid DNA midi prep

Plasmid DNA midi preps were done using the Qiagen plasmid purification kit as follows. On obtaining the right clone, a starter culture was inoculated from its

corresponding colony in 3 ml of LB medium with appropriate antibiotic selection. After six hr of culturing, it was transferred into 32 ml of LB medium and incubated overnight at 35.5°C for 16-18 hr in a shaker. Subsequently, the cells were harvested by centrifugation at 800g at 4°C for 15 min. The bacterial pellet was resuspended in 4 ml of buffer P1 (50 mM Tris-Cl, 10 mM EDTA, 100 µg/ml RNase, pH 8.0). Then, 4 ml of chilled buffer P2 (200 mM NaOH, 1% SDS (v/v)) was added and the suspension was mixed thoroughly by inverting the tube 4-6 times and incubated at room temperature for five min. Then, 4 ml of buffer P3 (3 M potassium acetate, pH 5.5) was added and immediately mixed by inverting the tube 4-6 times. The lysate was poured into the barrel of the QIAFilter Cartridge and incubated at room temperature for ten min. In the mean time, the QIAGEN-tip 100 was equilibrated with 4 ml of buffer QBT (750 mM NaCl, 50 mM 3-morpholinopropane-1-sulfonic acid (MOPS), 15% isopropanol (v/v), 0.15% Triton X-100 (v/v), pH 7.0) and the column was emptied by gravity flow. A plunger was inserted in the previously equilibrated cartridge and the lysate was filtered into the QIAGEN-tip 100 and allowed to enter the resin by gravity flow. The QIAGEN-tip 100 was washed two times with 10 ml of buffer QC (1 M NaCl, 50 mM MOPS, 15% isopropanol (v/v), pH 7.0) by gravity flow. Finally, the DNA was eluted from the column by 5 ml of buffer QF (50 mM Tris-Cl, 1.25 M NaCl, 15% isopropanol (v/v), pH 8.5). The eluted DNA was precipitated by adding 3.5 ml of room temperature absolute isopropanol and centrifugation at 2,500g for 30 min. The supernatant was discarded and the DNA pellet was washed with 2 ml 70% ethanol (v/v) by centrifugation at 2,500g for ten min. The supernatant was discarded and the DNA pellet was air dried for ~5 min and dissolved in 50-100 µl of 1X TE.

2.4.12. DNA sequencing

All plasmid DNA midi preps were sequenced in the Functional Genomics, Proteomics and Metabolomics Facility in the School of Biosciences, University of Birmingham. For a total reaction volume of 11 μ l, 0.5 μ M of the primer was mixed with appropriate amounts of DNA as suggested by Beckman Coulter (Table 3).

2.4.13. Cloning of *pAc5.1A Dscam Mut Exons 4-9*

The complete cloning strategy is diagrammatically represented in Figures 17 and 18.

For cloning of the *pAc5.1A Dscam Mut Exons 4-9* construct, the 3'UTR of Dscam was amplified from *pcDNA3(-MCS)/F.L. Dscam 7.27.25.2* (kindly provided by Dr. Woj Wojtowicz, University of California) with primers Dscam cDNA end F1 NotI EcoRV (GTGCTGCGGCCGCGATATCCCGCCAACTGTGCCGAAGAGGACCAATATCG)

and Dscam cDNA end R1 (AAATGCCACGCCCCACCGCCGCAGAGGGCGCTTACAAATTACACTG) and the 3'

end of the endogeneous poly A site was amplified from the Dscam BAC clone with primers Dscam 6kb frag F1

(AAATGTTTTTGTACATCAATTTTCGTGTCTGTGGTCCG) and Dscam 6kb frag R1 Xho Spe

(GCGTCCTCGAGACTAGTCTGATAACTGCTCCCGCTGATCCTGCTAATCCCTTG).

and cloned into *pAc5.1A* (Invitrogen) using NotI and SalI/XhoI sites to generate

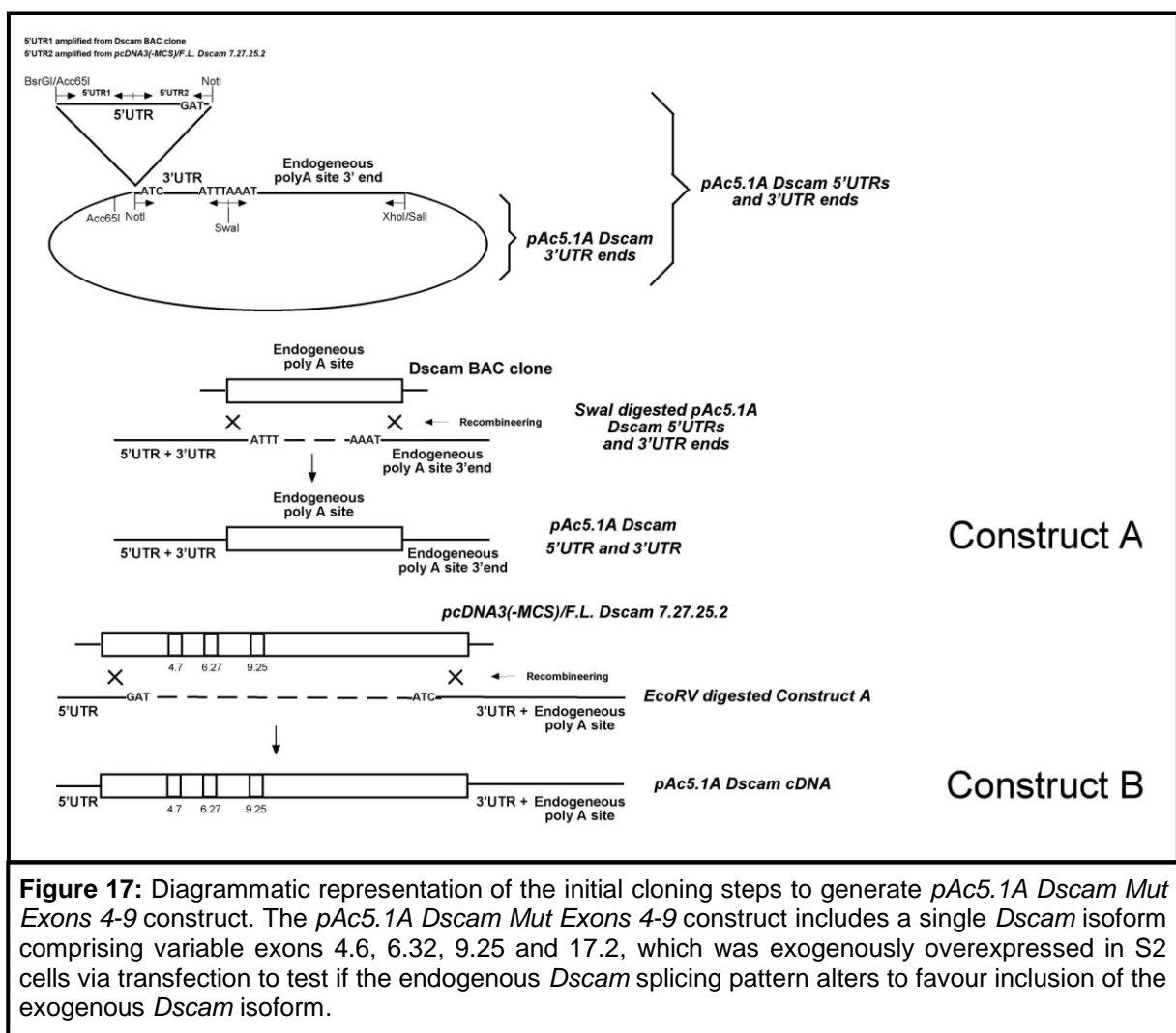
pAc5.1A Dscam 3'UTR ends. The first part of Dscam 5'UTR was amplified from the Dscam BAC clone with primers Dscam 5'UTR1 F1 BsrGI SalI BglII

(GCGTCTGTACAGTCGACAGATCTAGAACCGGATTTTCAGCGCTAGTCGGCG) and

Dscam 5'UTR1 R1

Size (kbp)	ng for 100 fmol
0.20	13
0.30	20
0.40	26
0.50	33
1	65
2	130
3	195
4	260
5	325
6	390
8	520
10	650
12	780
14	910
16	1040
18	1170
20	1300
48	1500

Table 3: Estimation of DNA amounts corresponding to size for DNA sequencing (Beckman Coulter).



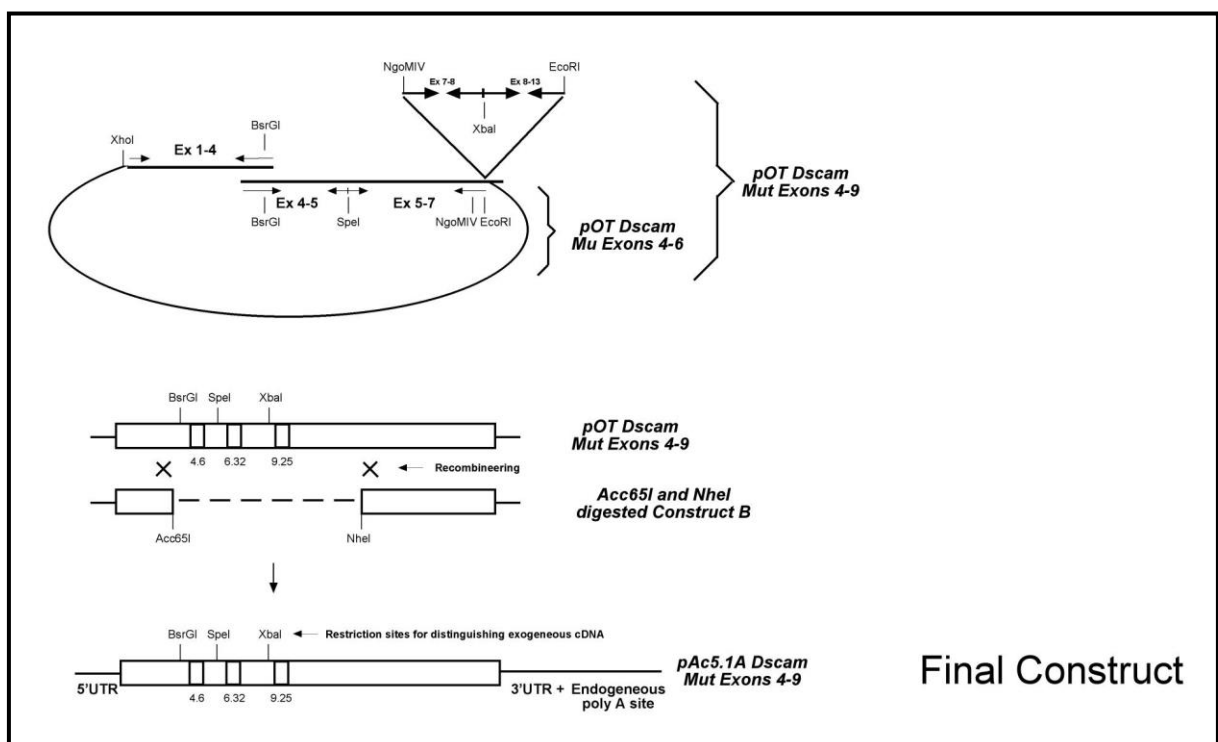


Figure 18: Diagrammatic representation of the final cloning step to generate *pAc5.1A Dscam Mut Exons 4-9* construct. The *pAc5.1A Dscam Mut Exons 4-9* construct includes a single *Dscam* isoform comprising variable exons 4.6, 6.32, 9.25 and 17.2, which was exogenously overexpressed in S2 cells via transfection to test if the endogenous *Dscam* splicing pattern alters to favour inclusion of the exogenous *Dscam* isoform.

(ATTGTTAACACTCACACACACACACTTGTGAGAGTGGTG) and the second part of Dscam 5'UTR was amplified from *pcDNA3(-MCS)/F.L. Dscam 7.27.25.2* using primers Dscam 5'UTR2 F2 (TAATCGCATT TAAAAACAATTTGGCCAGCCGCAG) and Dscam 5'UTR2 R2 (GCGTCGCGGCCGCGATATCTCGGGCATGGGATTGCCGCTGGCCTTG). Both the 5'UTR fragments were cloned into *pAc5.1A Dscam 3'UTR ends* using Acc65I/BsrGI and NotI sites to generate *pAc5.1A Dscam 5'UTRs and 3'UTR ends*. The entire 6kb inter-genic fragment from the Dscam BAC clone was recombined into *pAc5.1A Dscam 5'UTRs and 3'UTR ends* cut with Swal to generate *pAc5.1A Dscam 5'UTR and 3'UTR* (Construct A). The Dscam cDNA region was recombined from *pcDNA3(-MCS)/F.L. Dscam 7.27.25.2* into *pAc5.1A Dscam 5'UTR and 3'UTR* cut with EcoRV to generate *pAc5.1A Dscam cDNA* (Construct B). In parallel to the above steps, the *pOT Mut Exons 4-9* construct was cloned. To achieve this, a fragment encoding exons 1-4 was amplified from *pcDNA3(-MCS)/F.L. Dscam 7.27.25.2* with primers Dscam Exon 1-4 F1 (GCGTCCTCGAGACGCGGCCGCGAGTCTAGAAATAAGCTTGCATTAATCGCATT TAAAAACAATTTGGCCAGCCGCAG) and Dscam Exon 1-4 R1 (GATATCGGCGCCGTAAACTGATTCACAACGGCTCGCACATGTACATCCCGG). Exons 4-5 were amplified from embryonic Dscam cDNA with primers Dscam Exon 4-5 F1 (CCGGGATGTACATGTGCGAGCCGTTGTGAATCAGTTTTACGGCGCCGATATC) and Dscam Exon 4-5 R1 (GTCGTCCTTTTGTGGCACTTAATCGGGTTTCTCCG). These two fragments were fused together by an overlapping PCR with primers Dscam Exon 1-4 F1 (GCGTCCTCGAGACGCGGCCGCGAGTCTAGAAATAAGCTTGCATTAATCGCATT TAAAAACAATTTGGCCAGCCGCAG) and Dscam Exon 1-4 R1 (GATATCGGCGCCGTAAACTGATTCACAACGGCTCGCACATGTACATCCCGG).

(GCGTCCTCGAGACGCGGCCGCAGTCTAGAATAAGCTTGCATTAATCGCATTTA
AAAAACAATTTGGCCAGCCGCAG) and Dscam Exon 4-5 R1
(GTCGTCCTTTTGTGGCACTTAATCGGGTTTCTCCG). Exons 5-7 were amplified
from embryonic Dscam cDNA with primers Dscam Exon 5-7 F1
(TAGTCATCACAGAGCCCGTTAGCAGTAGTCCGCCCAAATCAATG) and Dscam
Exon 5-7 R1 NgoMIV Spe Mlu BglII EcoRI
(GCGTCGAATTCAGAGATCTGCACGCGTAGACTAGTGCGCCGGCGACGCACTT
GAGGAATACACTTGGTCCGGGTTCATG). These two PCR products were cloned
into *pOT* (kindly provided by Dr. Saverio Brogna, University of Birmingham) using
XhoI and EcoRI sites to give *pOT Dscam Mut Exons 4-6*. Exons 7-8 were amplified
from *pcDNA3(-MCS)/F.L. Dscam 7.27.25.2* with primers Dscam Exon 7-8 F1 NgoMIV
(GCGAGTGCTGAGCTGAAGCTCGGAGGCCGTTTTCG) and Dscam Exon 7-8 R1
(GAGATCCTCGAGCAGAGTATCCTTCCTGATTCTTGGC). Similarly, Exons 8-13
were amplified from *pcDNA3(-MCS)/F.L. Dscam 7.27.25.2* with primers Dscam Exon
8-13 F1 (TAGAAGTGCAAGTCATGGTTCACCCAAAATTACGCCCTTCGACTTTCG)
and Dscam Exon 8-13 R1 EcoRI
(GTTGGCACTGAATTCGACGCCCTTGATCTTCCATGTG). The above two PCR
products were cloned into *pOT Dscam Mut Exons 4-6* using NgoMIV and EcoRI sites
to generate *pOT Dscam Mut Exons 4-9*. Finally, the mutated Dscam cDNA from *pOT
Mu Exons 4-9* was recombined into *pAc 5.1A Dscam cDNA* cut with Acc65I and NheI
and end filled with T4 DNA pol to generate *pAc5.1A Dscam Mut Exons 4-9* (Final
construct) (Figure 18). The midi prep of the final construct was confirmed by
sequencing the region of the insert carrying the mutations.

2.5. Cell culture

2.5.1. Pathogen infection of *Drosophila* haemocytes

The type and culture conditions of pathogens used are listed in Table 4. *Drosophila* Schneider 2 (S2) cells were cultured in Insect Express medium supplemented with 10% heat inactivated foetal bovine serum (FBS) and 1% L-glutamine/penicillin/streptomycin (w/v) at 27°C with 0% CO₂. They were sub-cultured in a ratio of 1:4 (cells:medium) to maintain 3-5x10⁶ healthy cells/ml and to avoid growth. They were plated at a density of 3x10⁶ cells/well in six well tissue culture plates (Corning), 24 hr prior to pathogen infection. Pathogens, used in the study, were harvested from an overnight culture by centrifugation at 800g for five min, for an inoculum size of 1x10⁶ cells/ml and washed with sterile 1X PBS (137 mM NaCl, 2.7 mM KCl, 8 mM Na₂HPO₄, 1.76 mM KH₂PO₄, pH 7.4). Pathogens were resuspended in 1X PBS and heat inactivated at 70°C for 30 min, 60°C and 57°C each for 2.5 min and five min. S2 cells were replenished with serum free and antibiotic free Insect Express medium immediately before pathogen exposure. S2 cells were then exposed to either live pathogens or inactivated pathogens at an infection ratio 1:10 (S2 cell:pathogen) and incubated at 27°C with 0% CO₂ for 12 hr.

After exposure, the infected S2 cells were harvested and resuspended in 1X PBS. RNA was extracted from infected S2 cells for downstream analysis of alternative splicing. PBS treated cells were used as controls. S2 cells and *S. pombe* were kindly provided by Dr. Saverio Brogna, University of Birmingham and the *Mycobacterium* sp. and *C. glutamicum* was kindly provided by Dr. Apoorva Bhatt, University of Birmingham.

Pathogens	Strain	Medium	Temperature
<i>Escherichia coli</i>	DH5 α	Luria Bertani broth	37°C
<i>Saccharomyces pombe</i>	040	Yeast extract with supplements + 3% glucose (w/v)	30°C
<i>Mycobacterium smegmatis</i>	MC155	Luria Bertani broth + 0.05% Tween 80 (v/v)	37°C
<i>Mycobacterium marinum</i>	Wild type	7H9 broth + 0.05% Tween 80 (v/v)	30°C
<i>Corynebacterium glutamicum</i>	13032	Luria Bertani broth	37°C

Table 4: List of pathogens used to challenge S2 cells. The table shows pathogen strains with their culture conditions used to challenge S2 cells to test changes in *Dscam* alternative splicing.

2.5.2. Treatment of *Drosophila* haemocytes with drugs affecting transcription and RNA pol II processivity

S2 cells were cultured as mentioned in 4.5.1. S2 cells were then exposed to working concentrations of 10 µg/ml Actinomycin D (ActD), 100 µg/ml 6-Azauracil, 100 µg/ml DRB and 0.83 mg/ml sodium valproate and incubated at 27°C with 0% CO₂ for 12 hr (Table 5). After exposure, the infected S2 cells were harvested and resuspended in 1X PBS. RNA was extracted from treated S2 cells for downstream analysis of alternative splicing.

2.5.3. Transfection of *pAc5.1A Dscam Mut Exons 4-9* in *Drosophila* haemocytes

Transfection of S2 cells with *pAc5.1A Dscam Mut Exons 4-9* was done by using either didecyldimethylammonium bromide (DDAB) or TransIT-LT1 (non-liposomal formulation of lipid and protein/polyamine mixture with low toxicity, Mirus). One day prior to transfection, 3x10⁶ S2 cells were seeded per well at a concentration of 1.5x10⁶ cells/ml of complete Insect Express medium supplemented with 10% heat inactivated FBS and 1% L-glutamine/penicillin/streptomycin (w/v). On day two, transfection was commenced when S2 cells reached a confluency of 50-80%. For transfection with DDAB, 62.5 µl of serum free medium was mixed with 26 µl of 1X DDAB (0.4 mg/ml) in one tube. In another tube, 62.5 µl of serum free medium was mixed with 3 µg of the *pAc5.1A Dscam Mut Exons 4-9* construct. Both these solution mixtures were incubated separately at room temperature for 30 min and were later mixed together. For transfection with TransIT-LT1, 200 µl serum free medium was

Drugs	Stock Concentration	Solvent	Working solution
Actinomycin D	50 mg/ml	DMSO	10 µg/ml
6-Azauracil	50 mg/ml	NH ₄ OH	100 µg/ml
DRB	24 mg/ml	DMSO	100 µg/ml
Sodium valproate	50 mg/ml	H ₂ O	0.83 mg/ml

Table 5: List of drugs affecting transcription and RNA pol II processivity used during the study. The table shows the stock concentrations (mg/ml), solvents and working solutions of all drugs used during the study.

mixed with 3 μ l of TransIT-LT1 and 3 μ g of the *pAc5.1A Dscam Mut Exons 4-9* construct and incubated at room temperature for ten min. To the DDAB/DNA and TransIT-LT1/DNA mixtures, 580 μ l and 700 μ l of serum free medium was added respectively. These mixtures were then added separately to S2 cells and incubated at 27°C without CO₂ for three hr. After transfection, any floating cells in the wells were removed using a Pasteur pipette attached to an aspirator. The cells were replenished with 2 ml of complete Insect Express medium and incubated at 27°C without CO₂ for 2 days. The cells were then harvested for RNA extraction and downstream analysis of alternative splicing.

2.6. Western Blotting

2.6.1. Sample preparation

In order to check if the transgene *UAS Dscam 9L* expresses protein, Western blotting was done on larval progeny from a cross between homozygous transgenic *UAS Dscam 9L* and *Elav Gal4* flies. Five *UAS Dscam 9L/Elav Gal4* larvae were homogenized in 50 μ l of 1X PBS. The homogenized sample was mixed with 50 μ l of 2X sample buffer (125 mM Tris-HCl pH 6.8, 4% SDS (v/v), 0.01% bromophenol blue (w/v), 100 mM DTT, 15% glycerol (w/v)) and heat inactivated at 95°C for four min.

2.6.2. Sodiumdodecylsulphate polyacrylamide gel electrophoresis (SDS-PAGE)

Proteins were resolved by SDS-PAGE (Resolving gel: 8% acrylamide (w/v), 0.1% ammonium persulphate (APS) (w/v) and 0.001% TEMED (v/v) in 1X resolving buffer

containing 375 mM Tris, 0.125% SDS (v/v), pH 8.8; Stacking gel: 3% acrylamide (w/v), 125 mM Tris-HCl pH 6.8, 0.1% SDS (v/v), 0.1% APS (w/v) and 0.001% TEMED (v/v); Running buffer: 25 mM Tris, 191 mM glycine, 0.1% SDS (v/v), pH 8.3), The samples were run at 20 mA in the stacking gel and then 25 mA in the resolving gel.

2.6.3. Transfer

A nitrocellulose membrane and eight strips of 0.53 mm blotting paper (Whatman blotting paper 3MM) cut to the size of the gel were pre-wet in the transfer buffer. A sandwich of these components was assembled in a semi dry blotting apparatus (Biorad) in the following order (from cathode to anode) – four strips of blotting paper, nitrocellulose membrane, SDS gel, four strips of blotting paper. The transfer was carried out at 0.8 mA/cm² for 20-30 min and the membrane was then air dried.

2.6.4. Blocking

After re-wetting the nitrocellulose membrane in 1X TBST, it was washed using 5% dry milk (w/v) dissolved in 1X TBST (0.05% Tween 20 (v/v) in 1X TBS buffer - 25 mM Tris, 137 mM NaCl, 2.68 mM KCl, pH 7.4) at room temperature for 30 min on a shaker.

2.6.5. Blotting

After blocking, the membrane was incubated in 1X TBST/0.5% dry milk solution (w/v), containing anti-HA primary antibody (Roche) in a 1:100 dilution for 1.5 hr on a shaker. After the primary antibody incubation, the membrane was briefly washed

twice followed by four ten min washes in 1X TBST. The membrane was then incubated in 1X TBST/0.5% dry milk solution (w/v), containing a peroxidase-conjugated anti-rat secondary antibody (Amersham) in a 1:10,000 dilution on a shaker for 1.5 hr.

2.6.6. Development

Before developing the blot, the membrane was briefly washed twice followed by four ten min washes in 1X TBST. The blot was exposed to an X-ray film and developed by chemiluminescence (ECL Super Signal West femto, Thermo Scientific).

Note: All commonly used chemicals were bought from Sigma or Fischer Scientific.

CHAPTER 3

RESULTS

3.1. *Dscam* variable exons in clusters 4, 6 and 9 have similar sizes

The *Dscam* gene comprises four variable exon clusters 4, 6, 9 and 17 containing 12, 48, 33 and 2 alternative exons, respectively, that are spliced in a mutually exclusive manner (Figure 5, page 27). RT-PCR (reverse transcription polymerase chain reaction) with primers in constitutive exons flanking each variable cluster resulted in a single band on an agarose gel for exon clusters 4, 6 and 9 (Figure 19). These bands represent a population of variable exons that are indistinguishable due to their identical or very similar lengths. Exon 4, 6 and 9 variants range between 159-171bp, 116-128bp and 279-306bp, respectively. The two exon 17 variants differ in 45bp (exon 17.1=168bp; exon 17.2=213bp) and appeared as two separate bands on an agarose gel.

3.2. Separation of *Dscam* variable exons based on sequence variation

To make regulation of *Dscam* alternative splicing possible, it is required to be able to distinguish inclusion levels of individual exon variants in a *Dscam* variable cluster. Analysis of sequence variation between alternative exons in each cluster revealed that their annotated sequences are divergent enough so that they can be

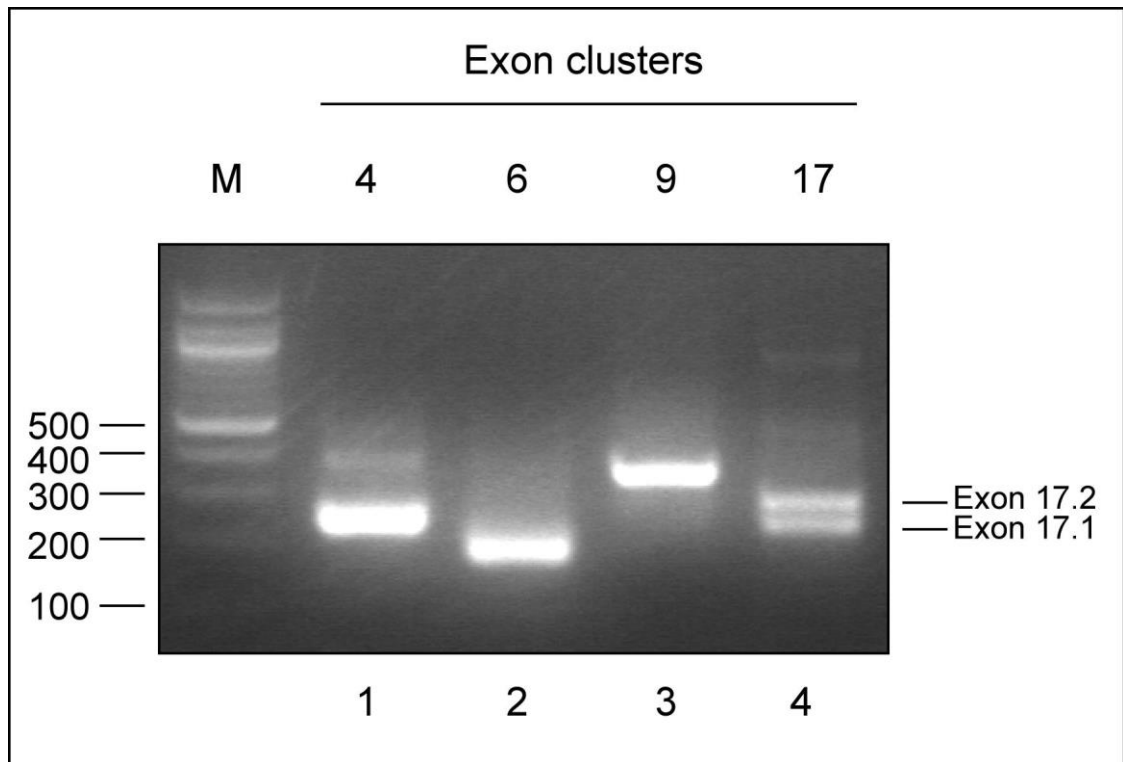


Figure 19: Amplification of *Dscam* variable exons by RT-PCR using RNA extracted from wild type embryos (*Canton S*), with primers in the constitutive exons flanking the variable exon clusters. Gene specific primer (Dscam YH 11RT1) was used in the RT reaction for cDNA (complementary DNA) synthesis. *Dscam* exon 4 variants were amplified using primers Dscam YH 3F2 and Dscam YH 5R1 (Lane 1), exon 6 variants with primers Dscam YH 5F1 and Dscam YH 7R1 (Lane 2), exon 9 variants with primers Dscam YH 8F1 and Dscam YH 10R1 (Lane 3) and exon 17 variants with primers Dscam YH 16F1 and Dscam YH 18R1 (Lane 4). The amplified products were run on a 2.5% agarose gel.

distinguished after digestion with a combination of restriction enzymes resulting in fragments of distinct lengths. To resolve shorter fragments, the forward primer was radiolabeled with ^{32}P and the digested exon variants were run on a denaturing polyacrylamide gel. Each band on the gel can be assigned its corresponding variable exon number based on the distance of the restriction site closest to the labeled end. A diagrammatic representation of separating exon 4 cluster variants is shown in Figure 20. Exon 4 variants were identified by digestion with restriction enzymes *Mbol*, *Alul*, *HinP1I* and *Taq^qI*. All 12 exon 4 variants were separated by this combination of restriction enzymes according to their annotated sequence as follows (Figure 21; Lane 5 - refer to A1 in appendix). Exons 4.3 and 4.8 were identified by *Mbol* (Figure 21; Lane 1), exon 4.9 by *Alul* (Figure 21; Lane 2), exons 4.6 and 4.12 by *HinP1I* (Figure 21; Lane 3) and exons 4.1, 4.4, 4.5, 4.7, 4.10 and 4.11 by *Taq^qI* (Figure 21; Lane 4). Exon 4.2 was identified by its full length due to the absence of a restriction site. An unspecific band, likely due to PCR artifacts was detected and is indicated by a “*” band. Often, two closely spaced bands were observed in the size range expected for exons 4.10 and 4.12. This could likely be due to incomplete denaturation of these fragments thus affecting their mobility on the gel. To avoid ambiguity, both bands were considered for exons 4.10 and 4.12 when analyzing *Dscam* exon 4 splicing regulation.

Exon 9 variants were identified by digestion with restriction enzymes *HpyCH4IV*, *HaeIII*, *XmnI*, *MspI*, *BstUI* and *BstNI*. Theoretically, this combination of enzymes would separate 24 out of the 33 exon 9 variants. Experimentally, however, only 17 variable exons were identified as follows (Figure 22; Lanes 7, 8 and 9 - refer to A2 in appendix). Exons 9.7 and 9.10 were identified by *BstUI* (Figure 22; Lane 2), exons



Figure 20: Diagrammatic representation showing the separation of *Dscam* exon 4 variants. The green box represents the population of *Dscam* exon 4 variants. Red boxes represent the flanking constitutive exons 3 and 5. The solid circle (•) indicates the ^{32}P radiolabel at the 5' end of the forward primer. Coloured arrows show the combination of enzymes that digest *Dscam* exon 4 variants at distinct sites resulting in fragments of different lengths that can be separated on a denaturing polyacrylamide gel. Note that exon 4 fragments are not drawn to scale.

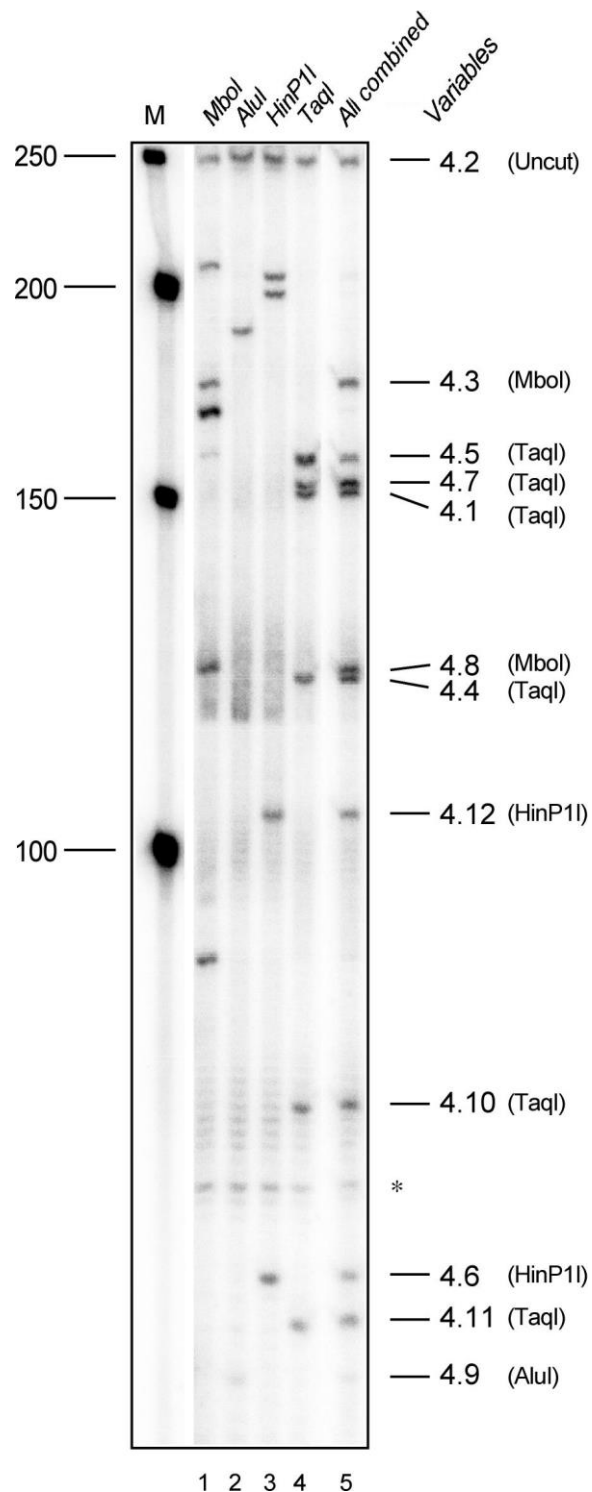


Figure 21: Resolution of *Dscam* exon 4 cluster. Separation of *Dscam* exon 4 variants after RT-PCR using RNA extracted from wild type embryos (*Canton S*), with primers *Dscam* YH 3F2, radiolabeled with ^{32}P , and *Dscam* YH 5R1 located in constitutive exons 3 and 5, respectively. The population of *Dscam* exon 4 variants was digested with *Mbol*, *Alul*, *HinP1I* and *TaqI* (Lane 5). Each band is assigned its corresponding variable exon number and identifying enzyme in brackets. The population of *Dscam* exon 4 variants was digested individually with *Mbol*, *Alul*, *HinP1I* and *TaqI*, respectively (Lanes 1-4). Unspecific bands are indicated by asterisks (*). Samples were run on an 8% denaturing polyacrylamide gel. M=50bp ladder (NEB).

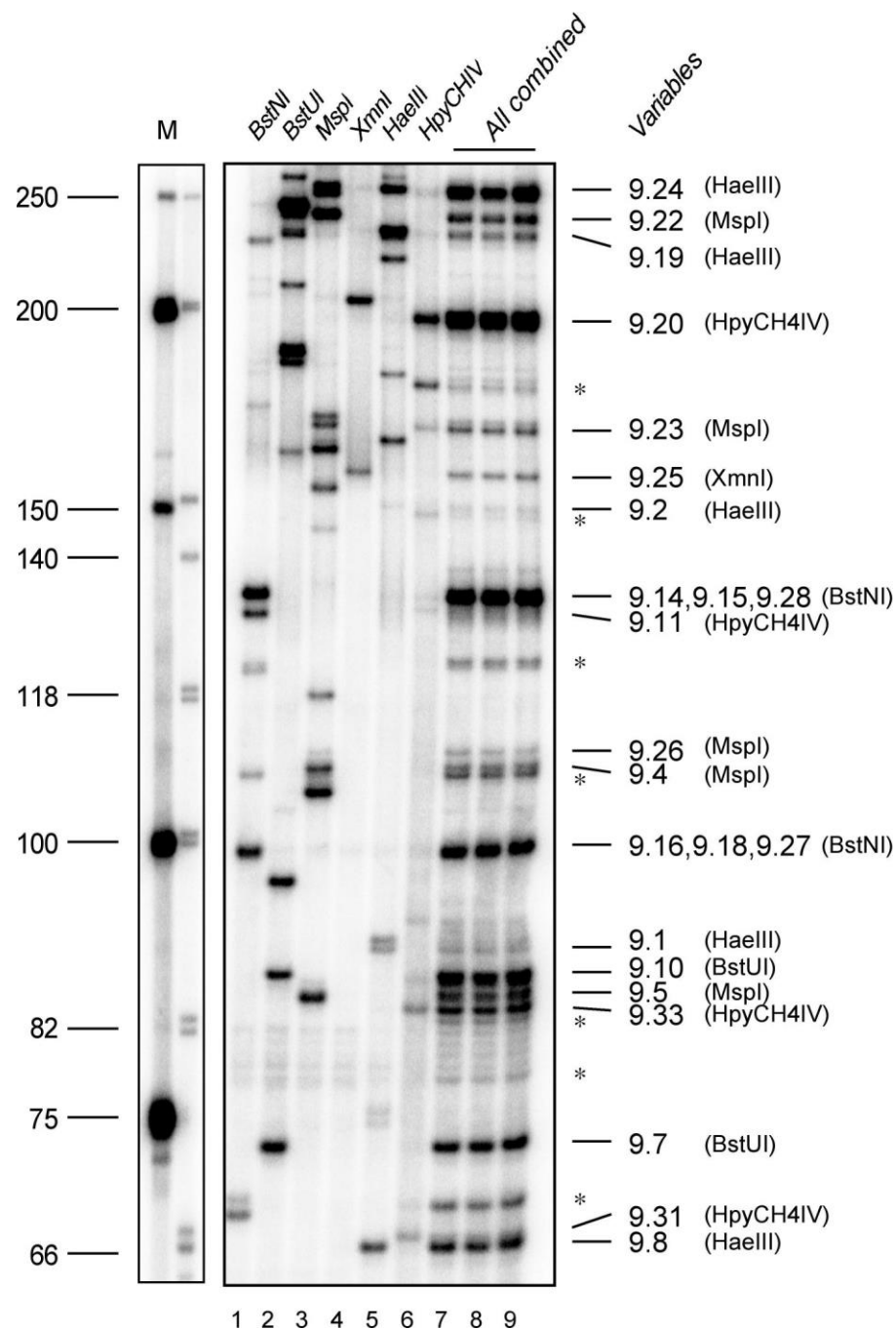


Figure 22: Resolution of *Dscam* exon 9 cluster. Separation of *Dscam* exon 9 variants after RT-PCR using RNA extracted from wild type embryos (*Canton S*), with primers *Dscam* YH 8F1, radiolabeled with ^{32}P , and *Dscam* YH 10R1 located in constitutive exons 8 and 10 respectively. The population of *Dscam* exon 9 variants was digested with *BstNI*, *BstUI*, *MspI*, *XmnI*, *HaeIII* and *HpyCH4IV* (Lanes 7-9, digest loaded three times). Each band is assigned its corresponding variable exon number and identifying enzyme in brackets. The population of *Dscam* exon 9 variants was digested individually with *BstNI*, *BstUI*, *MspI*, *XmnI*, *HaeIII* and *HpyCH4IV*, respectively (Lanes 1-6). Unspecific bands are indicated by asterisks (*). Samples were run on an 8% denaturing polyacrylamide gel. M=50bp ladder (NEB), phiX174 DNA/HinfI marker (Biotools).

9.4, 9.5, 9.22, 9.23 and 9.26 by *MspI* (Figure 22; Lane 3), exon 9.25 by *XmnI* (Figure 22; Lane 4), exons 9.1, 9.2, 9.8, 9.19 and 9.24 by *HaeIII* (Figure 22; Lane 5) and exons 9.11, 9.20, 9.31 and 9.33 by *HpyCH4IV* (Figure 22; Lane 6). Exons 9.11 and 9.31 were detected at a very low level and in close proximity to highly expressed exons 9.14, 9.15 and 9.28 and exon 9.8, respectively. To avoid the potential overlap of radioactive signal between strong and weak bands, exons 9.11 and 9.31 were excluded from the analysis of *Dscam* exon 9 splicing regulation. Exons 9.14, 9.15 and 9.28 as well as exons 9.16, 9.18 and 9.27 appeared as a single band as they were digested by *BstMI* to produce same sized fragments (Figure 22; Lane 1). Exons 9.3 and 9.32, digested by *BstMI*, and exon 9.9 digested by *BstUI* also appeared together as a single band (not shown in figure 22). The remaining seven exon variants, namely 9.6, 9.12, 9.13, 9.17, 9.21, 9.29 and 9.30 were not detected at the predicted size likely because of low level of inclusion. A few unspecific bands, likely due to PCR artifacts, were also detected and are shown as ‘*’ bands (Figure 22).

Although the focus of this study is on exon 4 and 9 clusters, a preliminary analysis of exon 6 cluster was also done. Exon 6 variants were identified by digestion with restriction enzymes *Mbol*, *AluI*, *MspI*, *BstUI*, *BstMI* and *TaqI*. Theoretically, this combination of enzymes would separate 28 out of the 48 exon 6 variants. Experimentally, however, only 23 variable exons were identified based on sequence annotation as follows (Figure 23 - refer to A3 in appendix). Exons 6.8, 6.17, 6.18 and 6.23 were identified by *Mbol*, exons 6.9, 6.13, 6.19, 6.21, 6.22, 6.32, 6.36, 6.38 and 6.39 by *AluI*, exons 6.16 and 6.28 by *MspI*, exons 6.10, 6.15, 6.35 and 6.41 by *BstUI*, exons 6.1, 6.6 and 6.24 by *BstMI* and exon 6.44 by *TaqI*. The unresolved exon variants appeared as single bands at distinct positions in groups of two or more

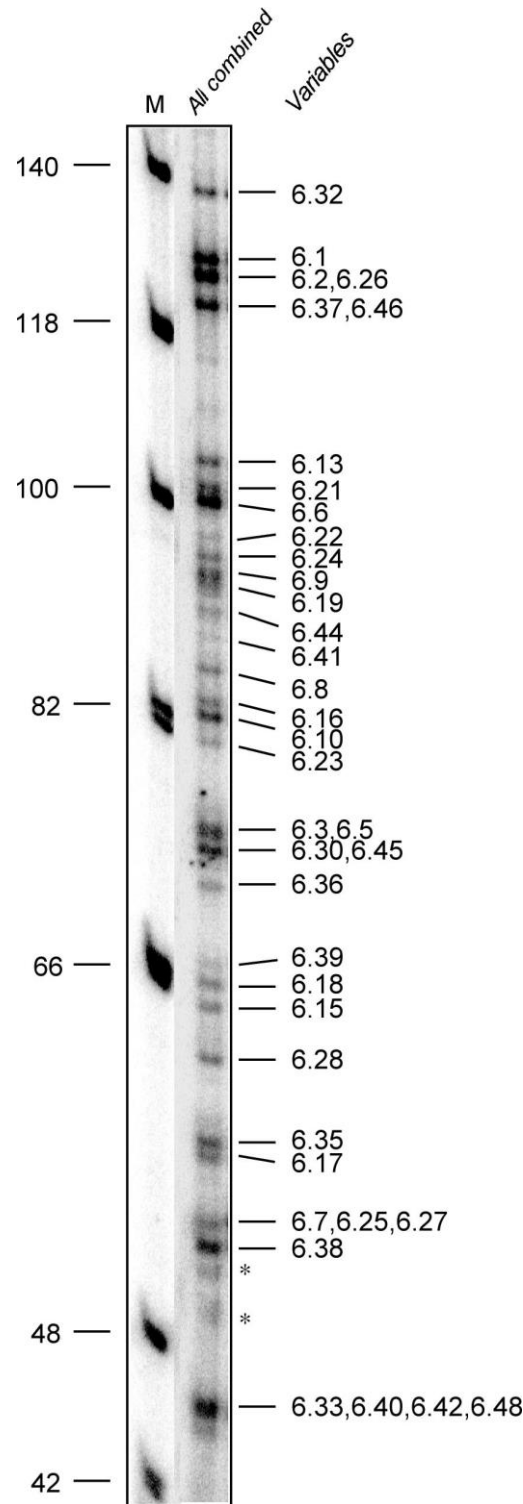


Figure 23: Resolution of *Dscam* exon 6 cluster. Separation of *Dscam* exon 6 variants after RT-PCR using RNA extracted from wild type embryos (*Canton S*), with primers Dscam YH 5F1, radiolabeled with ^{32}P , and Dscam YH 7R1 located in constitutive exons 5 and 7, respectively. The population of *Dscam* exon 6 variants was digested with *Mbol*, *Acl*, *MspI*, *Bst*UI, *Bst*MI and *Taq*I (Lane 2). Each band is assigned its corresponding variable exon number. Unspecific bands are indicated by asterisks (*). Samples were run on an 8% denaturing polyacrylamide gel. M=phiX174 DNA/Hinfi marker (Biotools).

exons because they were digested by enzymes to produce the same sized fragments. The exon variants that could not be separated include exons 6.2 and 6.26 digested by *AluI*, exons 6.37 and 6.46 digested by *BstM*, exons 6.3 and 6.5 digested by *BstUI*, exons 6.7, 6.25 and 6.27 digested by *MboI*, exons 6.33, 6.40, 6.42 and 6.48 digested by *AluI* and exons 6.30 and 6.45 digested by *Taq^{II}* and *AluI*, respectively. Exon 6.12 digested by *AluI* and exons 6.14 and 6.34 digested by *Taq^{II}*; and exons 6.4 and 6.31 digested by *MspI* also appeared together as single bands, respectively (not shown in the figure 23).

The remaining five exon variants, namely 6.11, 6.20, 6.29, 6.43 and 6.47 were not detected at the predicted size likely because of low level of inclusion. A few unspecific bands, likely due to PCR artifacts were detected and are shown as ‘*’ bands (Figure 23).

3.3. *Dscam* splicing pattern changes on exposure to pathogens in S2 cells

The splicing pattern of *AgDscam* exon 4 cluster in Sua5B cells has been shown to change on exposure to pathogens and pathogenic determinants to express challenge-specific high affinity binding isoforms. Silencing these isoforms by RNAi reduces binding of *AgDscam* to the inducing pathogen and compromises their phagocytic uptake. Also, RNAi-mediated depletion of *AgDscam* in mosquitoes reduces their viability after bacterial infection (Dong et al., 2006).

To test if the splicing pattern of *Dscam* exon 4 and 9 clusters changes upon pathogen exposure, S2 cells were challenged with *E. coli*, *S. pombe*, *C. glutamicum*,

M. smegmatis and *M. marinum* that were heat inactivated at 70°C for 30 min (Figures 24A and B). Naïve cells expressed all exon 4 cluster variables, but exons 4.3 and 4.6 were expressed at a very low level (Figure 24A; Lane 1). Challenges with all pathogens increased exon 4.7 inclusion, maximally with *S. pombe* and *M. marinum* by an 11.2-fold and 9.2-fold upregulation, respectively (Figure 24A; Lanes 3 and 6). *E. coli* and *C. glutamicum* challenge resulted in a 5.5-fold and 6.1-fold increase in exon 4.7 splicing, respectively (Figure 24A; Lanes 2 and 4). Splicing of exon 4.3 was downregulated by 5.8-fold in S2 cells exposed to *C. glutamicum* (Figure 24A; Lane 4). S2 cells infected with *M. smegmatis* showed the least overall change in *Dscam* exon 4 splicing (Figure 24A; Lane 5). To attribute the above changes in splicing pattern purely to the pathogenic exposure, *Dscam* exon 4 splicing was examined over 4 hr, 8 hr and 12 hr in naïve S2 cells to observe if *Dscam* splicing changes over time. This experiment revealed that *Dscam* splicing pattern is largely constant over a time period of 12 hours suggesting that changes in exon 4.7 splicing were purely due to the pathogen exposures (Figures 24C and D). Contrary to exon 4 cluster, S2 cells expressed a very limited repertoire of exon 9 cluster variants with exons 9.24, 9.20 and 9.8 being the predominant exons. A quantification of only these strongly expressed exons revealed no significant differences between different pathogen challenges (Figures 24E and F).

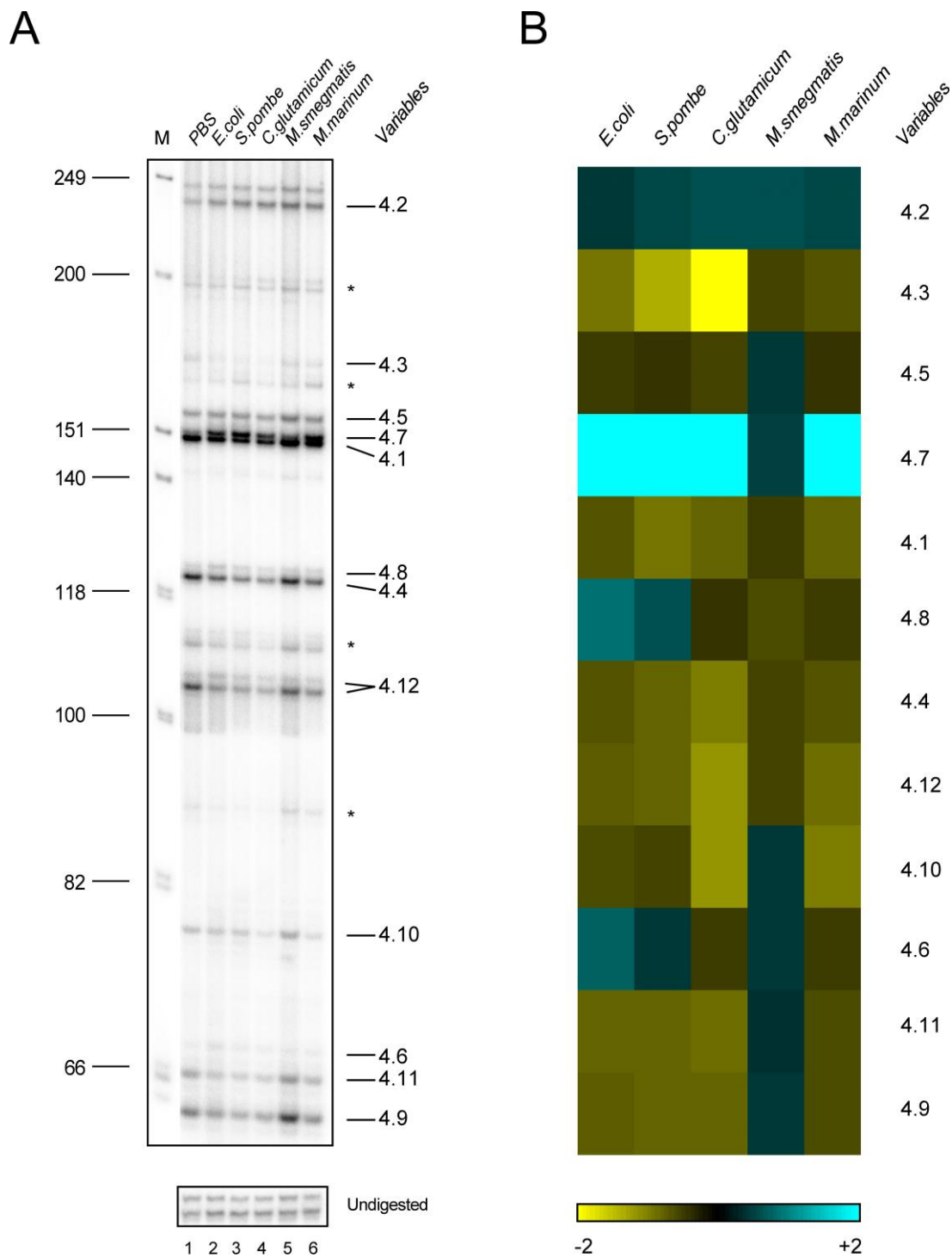
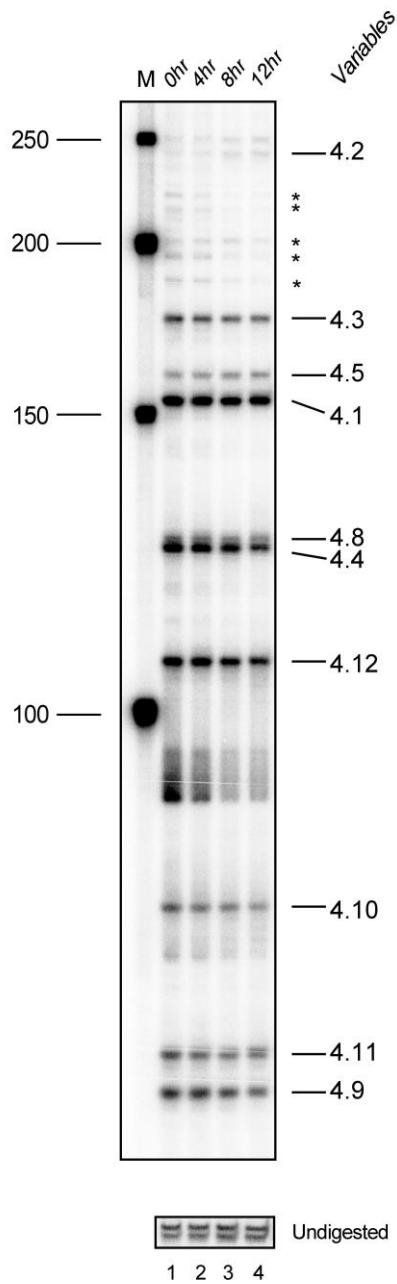


Figure 24 (A,B): *Dscam* exon 4 splicing pattern changes on exposure to heat inactivated pathogens in S2 cells. (A) Analysis of *Dscam* exon 4 splicing pattern using RNA extracted from S2 cells exposed to *E. coli* (Lane 2), *S. pombe* (Lane 3), *C. glutamicum* (Lane 4), *M. smegmatis* (Lane 5) and *M. Marinum* (Lane 6). PBS added to S2 cells served as controls (Lane 1). (B) Heat map representation of *Dscam* splicing changes observed in A. *Dscam* exon variants were separated as explained in figure legend 21. Unspecific bands are indicated by asterisks (*). Samples were run on an 8% denaturing polyacrylamide gel. M=phiX174 DNA/HinfI marker (Biotoools).

C



D

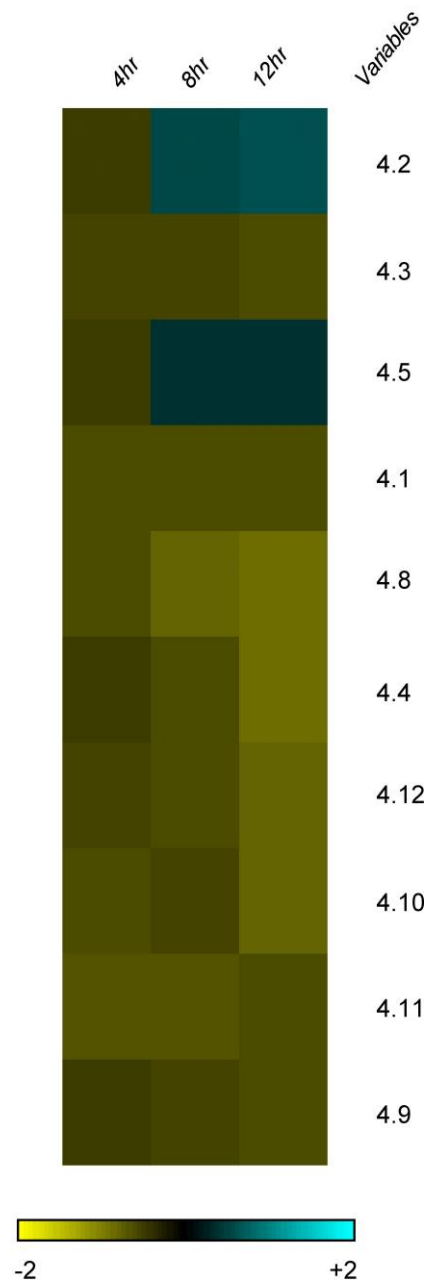
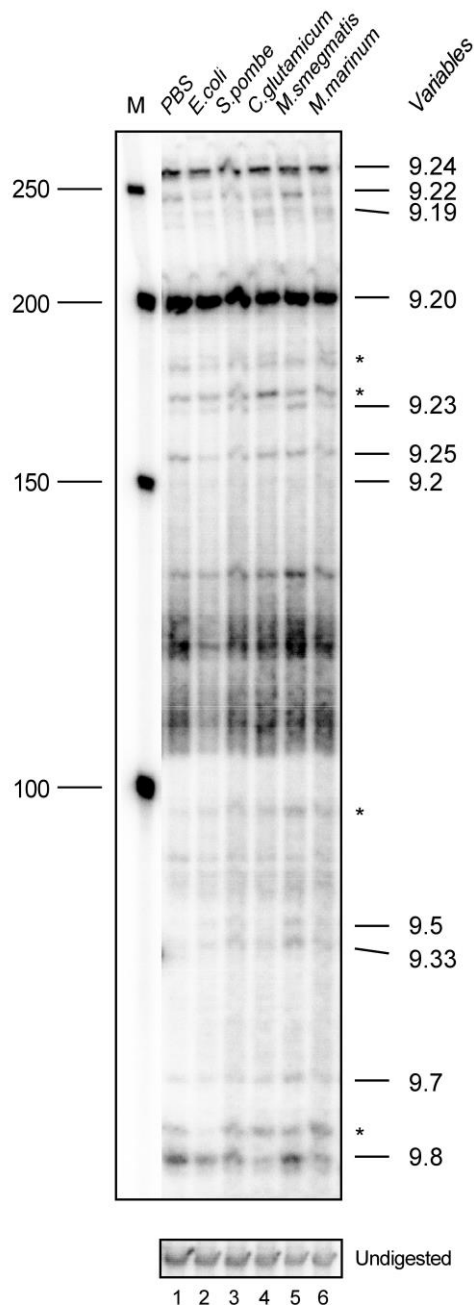


Figure 24 (C,D): *Dscam* exon 4 splicing pattern does not change in naïve S2 cells over a period of 12 hr. (C) Analysis of *Dscam* exon 4 splicing pattern over a time course of 0 hr (Lane 1), 4 hr (Lane 2), 8 hr (Lane 3) and 12 hr (Lane 4) in naïve S2 cells. (D) Heat map representation of *Dscam* splicing changes observed in C. *Dscam* exon variants were separated as explained in figure legend 21. Unspecific bands are indicated by asterisks (*). Samples were run on an 8% denaturing polyacrylamide gel. M=50bp ladder (NEB).

E



F

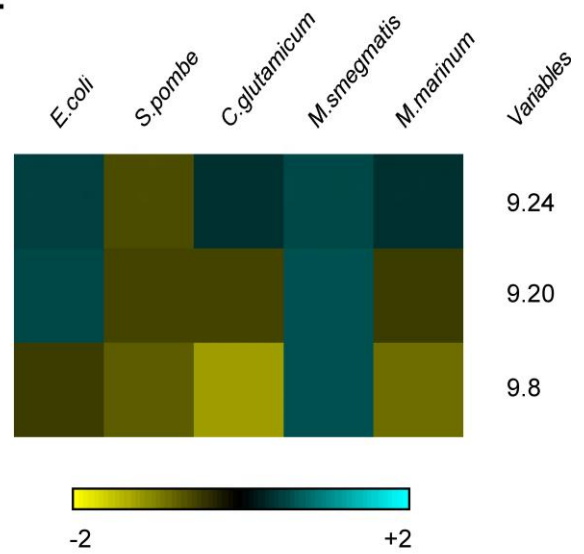


Figure 24 (E,F): *Dscam* exon 9 splicing pattern changes on exposure to heat inactivated pathogens in S2 cells. (E) Analysis of *Dscam* exon 9 splicing pattern using RNA extracted from S2 cells exposed to *E. coli* (Lane 2), *S. pombe* (Lane 3), *C. glutamicum* (Lane 4), *M. smegmatis* (Lane 5) and *M. Marinum* (Lane 6). PBS added to S2 cells served as controls (Lane 1). (F) Heat map representation of *Dscam* splicing changes observed in E. *Dscam* exon variants were separated as explained in figure legend 22. Unspecific bands are indicated by asterisks (*). Samples were run on an 8% denaturing polyacrylamide gel. M=50bp ladder (NEB).

3.4. Variation in *Dscam* splicing between different developmental stages, strains and sexes

To elucidate the mechanisms regulating *Dscam* splicing in adaptation to pathogen exposure or during neuronal development, it was thought to test mutants in candidate genes for splicing regulators. Since *Dscam* splicing in mushroom bodies and dendritic arborization neurons changes such that individual cells acquire a unique set of *Dscam* isoforms, it is possible that *Dscam* splicing is generally variable. To exclude that such variability is a key feature of *Dscam*, the pattern of *Dscam* splicing at various developmental stages and in individual flies was analysed. Consequently, *Dscam* exon 4 and 9 splicing pattern was analyzed between nine independent pools of ten *Canton S* embryos, ten individual *Canton S* males and eight individual *yw* females (Figures 25 and 26). These results of this analysis revealed that the choice of exon variants in *Dscam* exon 4 and 9 splicing followed a different trend between different developmental stages, wild type strains and sexes. For *Dscam* exon 4 splicing, exon 4.9 accounted for 10.3% of all spliced exons in *Canton S* embryos, where as in *Canton S* males and *yw* females it accounted for only 3.9%. In *Canton S* males, exon 4.5 represented 12.7% of all splicing events, which was only 6.9% in *yw* females. Similarly, exon 4.8 accounted for 12.5% of all spliced variable exons in *yw* females, which was only 6.9% in *Canton S* males (Figures 25A-G).

To attribute variation observed between *Canton S* males and *yw* females to strain or sex differences, and also to get a better understanding about tissue specific splicing, neuron rich head-thoraces were compared with neuron poor abdomens between *Canton S* and *yw* females. The results revealed that differences in proportions of exon variants included in *Canton S* and *yw* flies were due to strain differences as

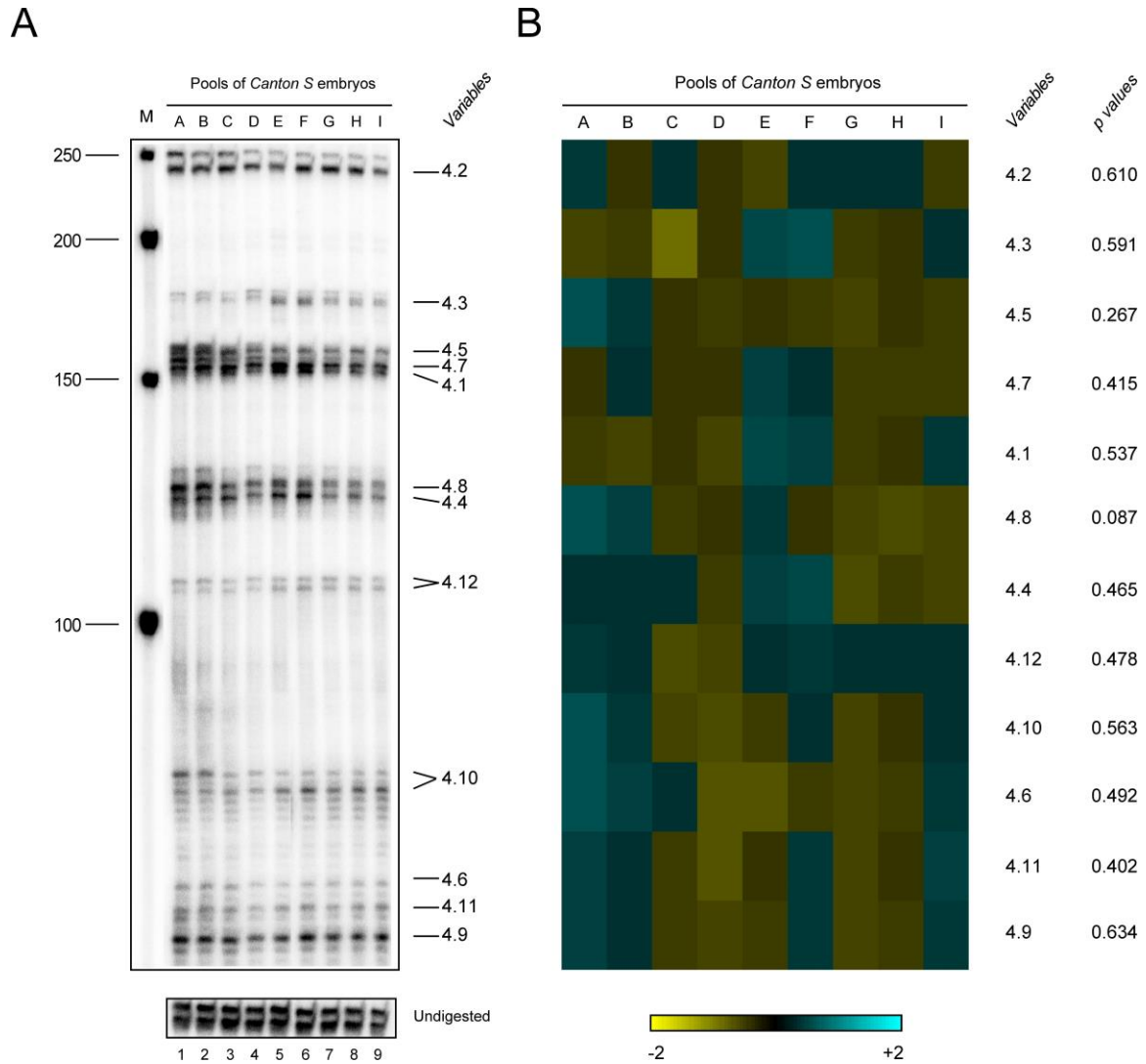
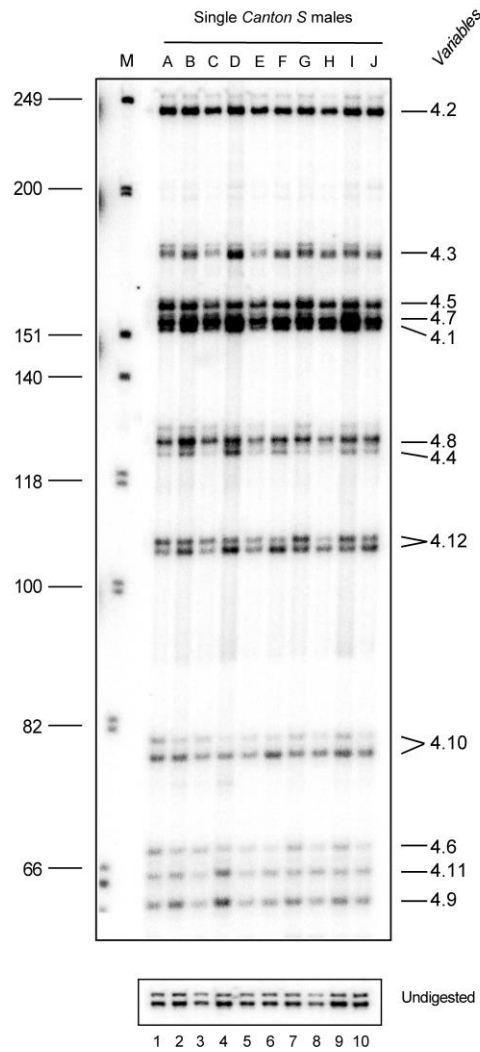


Figure 25 (A,B): Variation in *Dscam* exon 4 splicing pattern between different developmental stages, strains, sexes and tissues. (A) Analysis of *Dscam* exon 4 splicing pattern using RNA extracted from independent pools of ten 14-18 h old *Canton S* embryos (Lanes 1-9). (B) Heat map representation of *Dscam* splicing changes observed in A. *p* values for each exon variant are mentioned alongside. *Dscam* exon variants were separated as explained in figure legend 21. Samples were run on an 8% denaturing polyacrylamide gel. M=50bp ladder (NEB).

C



D

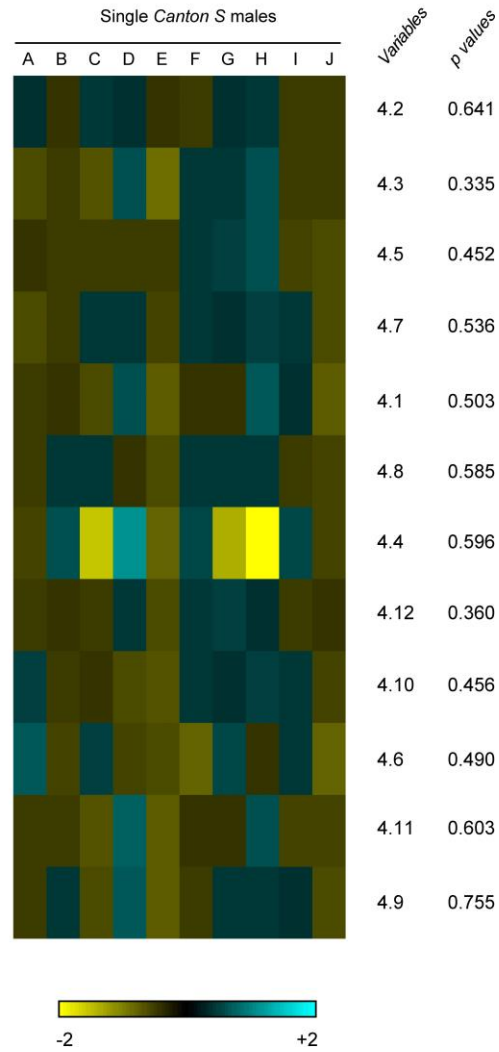


Figure 25 (C,D): Variation in *Dscam* exon 4 splicing pattern between different developmental stages, strains, sexes and tissues. (C) Analysis of *Dscam* exon 4 splicing pattern using RNA extracted from single *Canton S* males (Lanes 1-10). (D) Heat map representation of *Dscam* splicing changes observed in C. p values for each exon variant are mentioned alongside. *Dscam* exon variants were separated as explained in figure legend 21. Samples were run on an 8% denaturing polyacrylamide gel. M=phiX174 DNA/HinfI marker (Biotools).

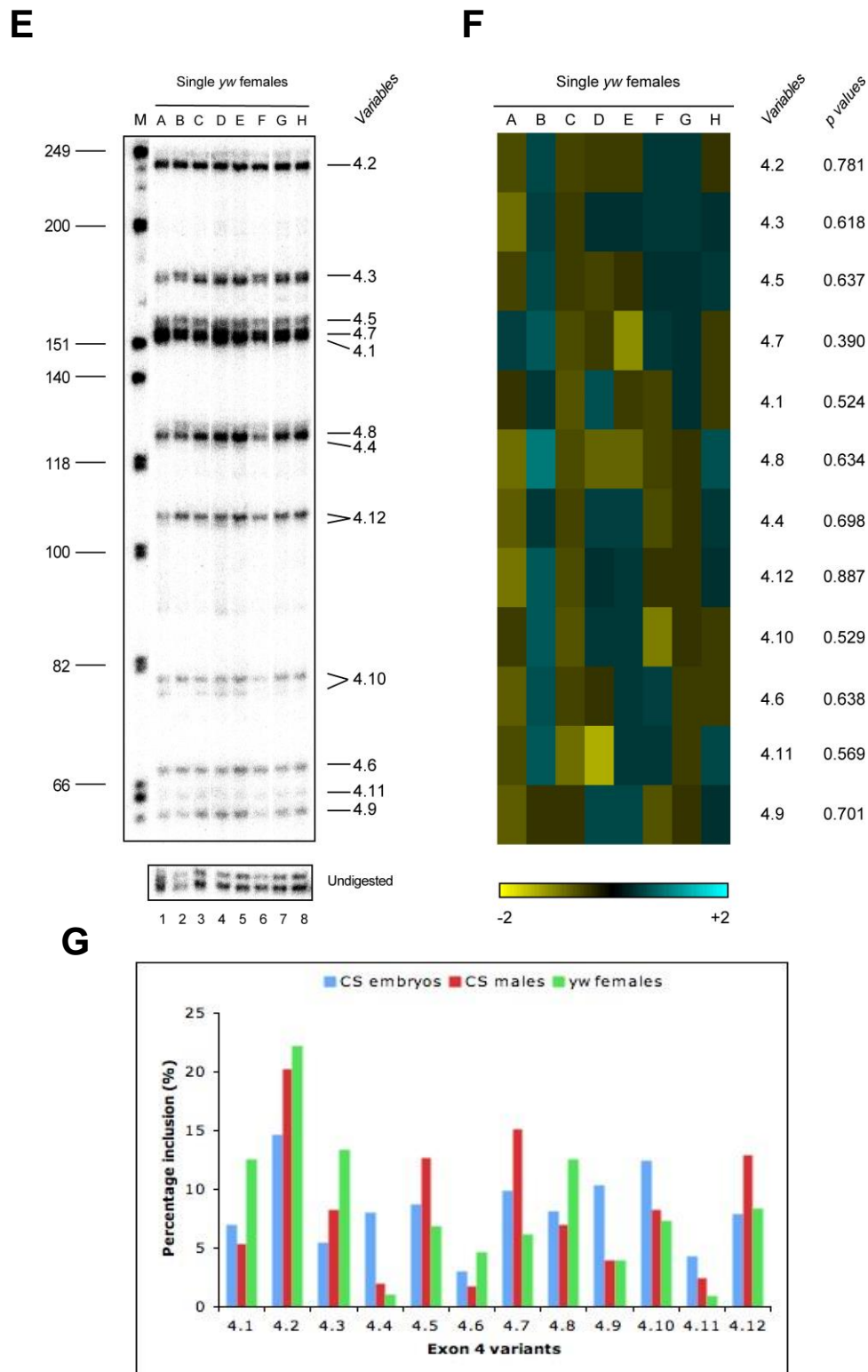
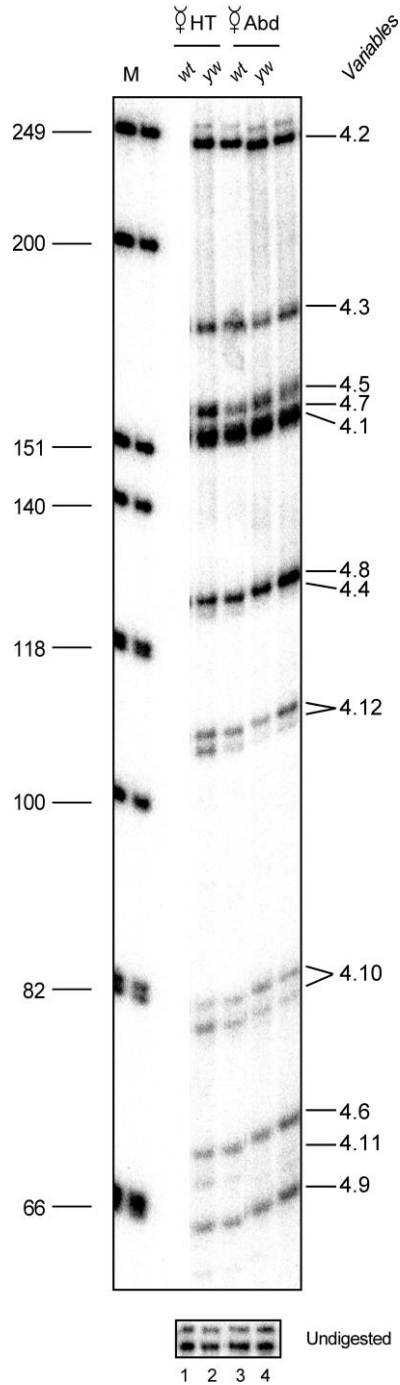
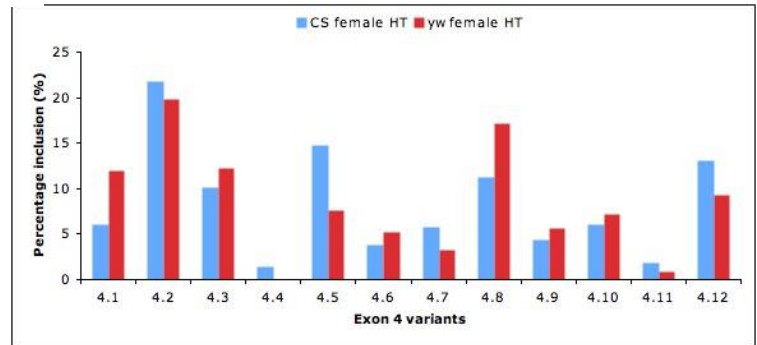


Figure 25 (E,F,G): Variation in *Dscam* exon 4 splicing pattern between different developmental stages, strains, sexes and tissues. (E) Analysis of *Dscam* exon 4 splicing pattern using RNA extracted from single yw females (Lanes 1-8). (F) Heat map representation of *Dscam* splicing changes observed in E. *p* values for each exon variant are mentioned alongside. *Dscam* exon variants were separated as explained in figure legend 21. Samples were run on an 8% denaturing polyacrylamide gel. (G) Graphical representation of percentage inclusion levels of each exon 4 variant observed in A, C and E. M=phiX174 DNA/Hinfl marker (Biotools).

H



I



J

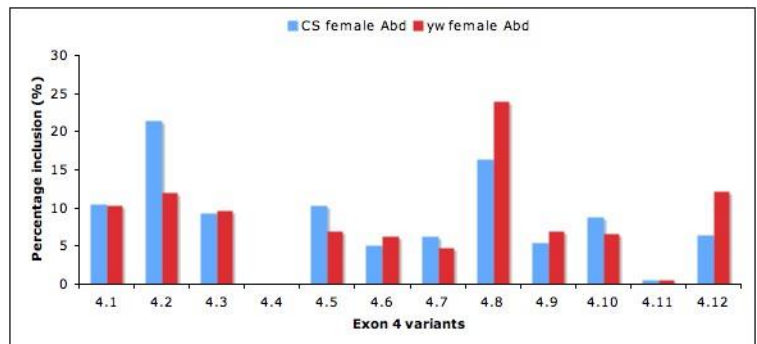


Figure 25 (H,I,J): Variation in *Dscam* exon 4 splicing pattern between different developmental stages, strains, sexes and tissues. (H) Analysis of *Dscam* exon 4 splicing pattern using RNA extracted from head-thorax from single *Canton S* female (Lane 1) and *yw* female (Lane 2); abdomen from single *Canton S* female (Lane 3) and *yw* female (Lane 4). (I and J) Graphical representation of percentage inclusion levels of each exon 4 variant observed in H. *Dscam* exon variants were separated as explained in figure legend 21. Samples were run on an 8% denaturing polyacrylamide gel. M=phiX174 DNA/HinfI marker (Biotools).

observed in exons 4.5, 4.8 and 4.12. The pattern between head-thoraces and abdomens was however, very similar within the same strain (Figures 25H-J). Similar levels of exon variants such as 4.2, 4.9 and 4.10 were also observed between *Canton S* males and *yw* females. Only exons 4.6 and 4.11 showed comparable levels of inclusion between all the three sample types (Figure 25G). For *Dscam* exon 9 splicing, exons 9.7 and 9.8 both accounted for 15.5% of all exon 4 variants in *Canton S* embryos, which were expressed at levels less than 8.6% and 4.1% in *Canton S* males and *yw* females, respectively. Exon 9.24 was maximally included in *yw* females representing 33.4% of all exons included within the cluster, where as in *Canton S* embryos and flies it was only 9.2% and 19.32% respectively. Overall, exon 9 cluster showed less variation between the three sample sources as compared to the exon 4 cluster (Figures 26A-G).

The splicing pattern between individual pools of *Canton S* embryos, *Canton S* males and *yw* females was highly reproducible. To investigate reproducibility of *Dscam* splicing pattern between independent experiments a 2-tailed t-test was performed for each of the resolved exon 4 and 9 variants by comparing their inclusion levels across all experiments. The data set was randomly divided into 3 different pairs of arrays and their mean *p value* was calculated. The obtained *p values* for all exon 4 and 9 variants were >0.05 , which suggested that the results obtained between independent experiments are very similar. Hence, *Dscam* splicing pattern is highly reproducible between individual samples of the same source such as embryo pools and individual flies. The *p values* are shown adjacent to each exon 4 and 9 variants in figures 25 and 26B, D and F, respectively. Between individual *Canton S* males, exons 4.4, 9.2,

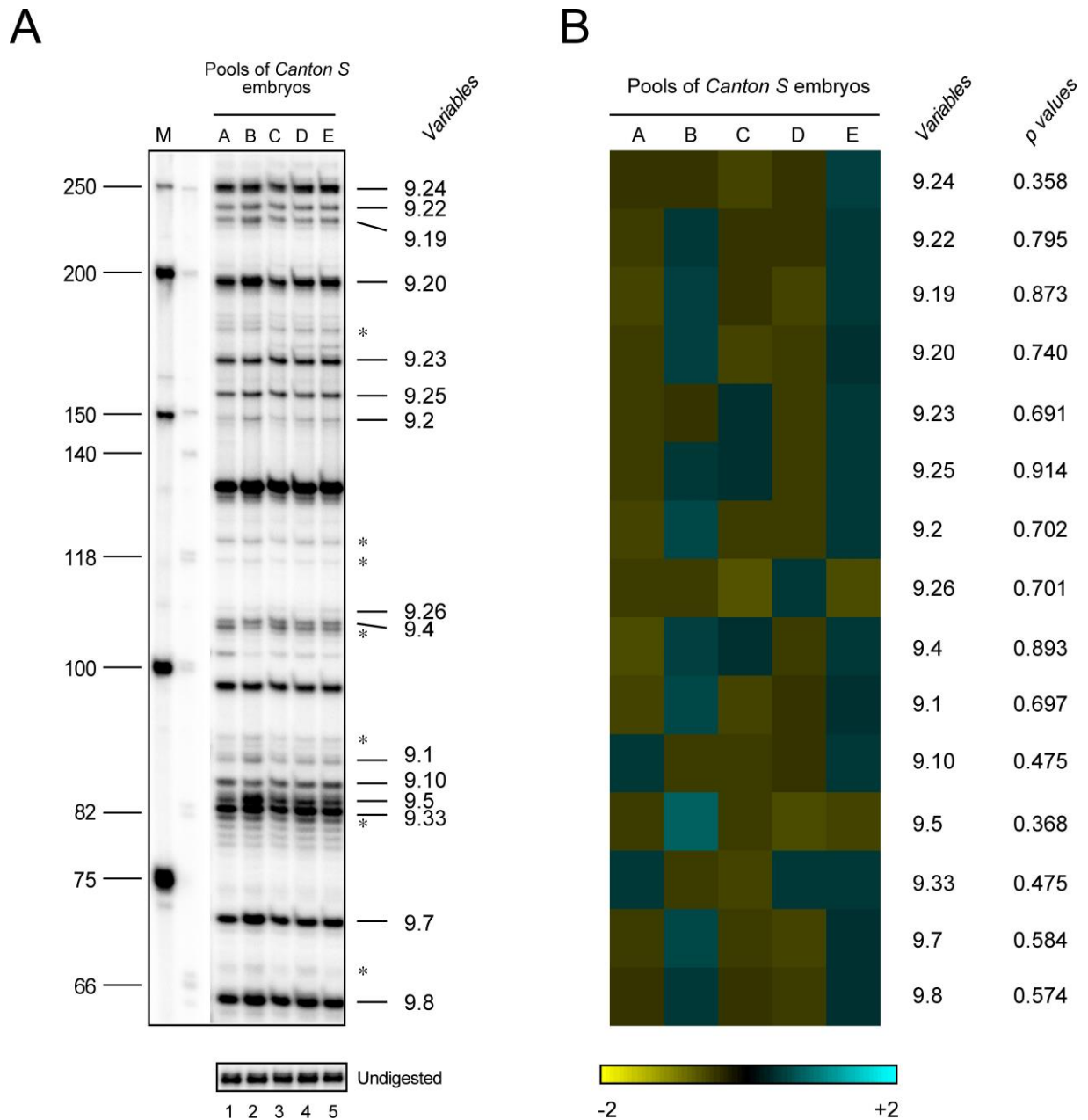


Figure 26 (A,B): Variation in *Dscam* exon 9 splicing pattern between different developmental stages, strains, sexes. (A) Analysis of *Dscam* exon 9 splicing pattern using RNA extracted from independent pools of ten 14-18 h old *Canton S* embryos (Lanes 1-5). (B) Heat map representation of *Dscam* splicing changes observed in A. *p* values for each exon variant are mentioned alongside. *Dscam* exon variants were separated as explained in figure legend 22. Unspecific bands are indicated by asterisks (*). Samples were run on an 8% denaturing polyacrylamide gel. M=phiX174 DNA/Hinfl marker (Biotools).

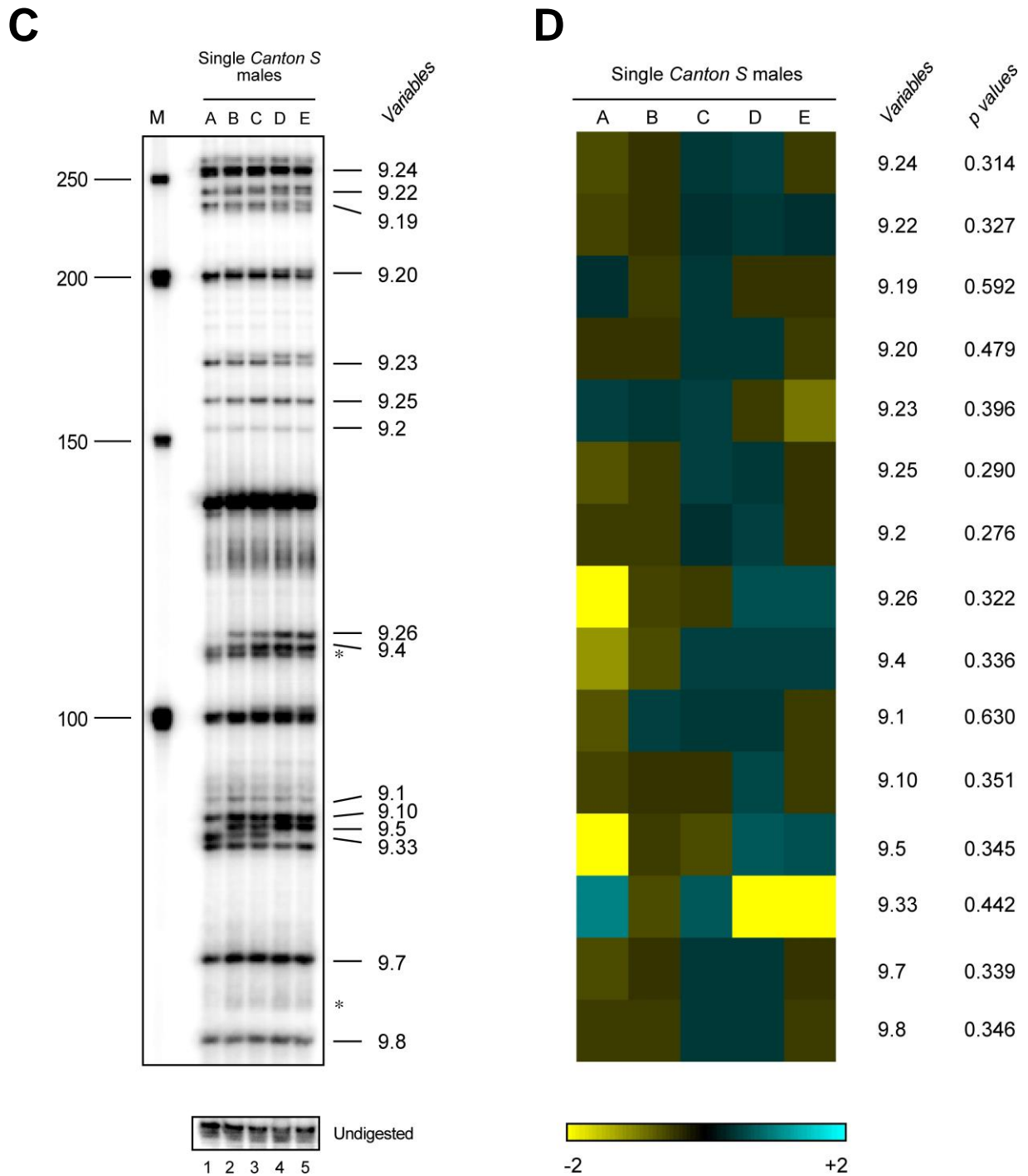


Figure 26 (C,D): Variation in *Dscam* exon 9 splicing pattern between different developmental stages, strains, sexes. (C) Analysis of *Dscam* exon 9 splicing pattern using RNA extracted from single *Canton S* males (Lnes 1-5). (D) Heat map representation of *Dscam* splicing changes observed in C. *p* values for each exon variant are mentioned alongside. *Dscam* exon variants were separated as explained in figure legend 22. Unspecific bands are indicated by asterisks (*). Samples were run on an 8% denaturing polyacrylamide gel. M=50bp ladder (NEB).

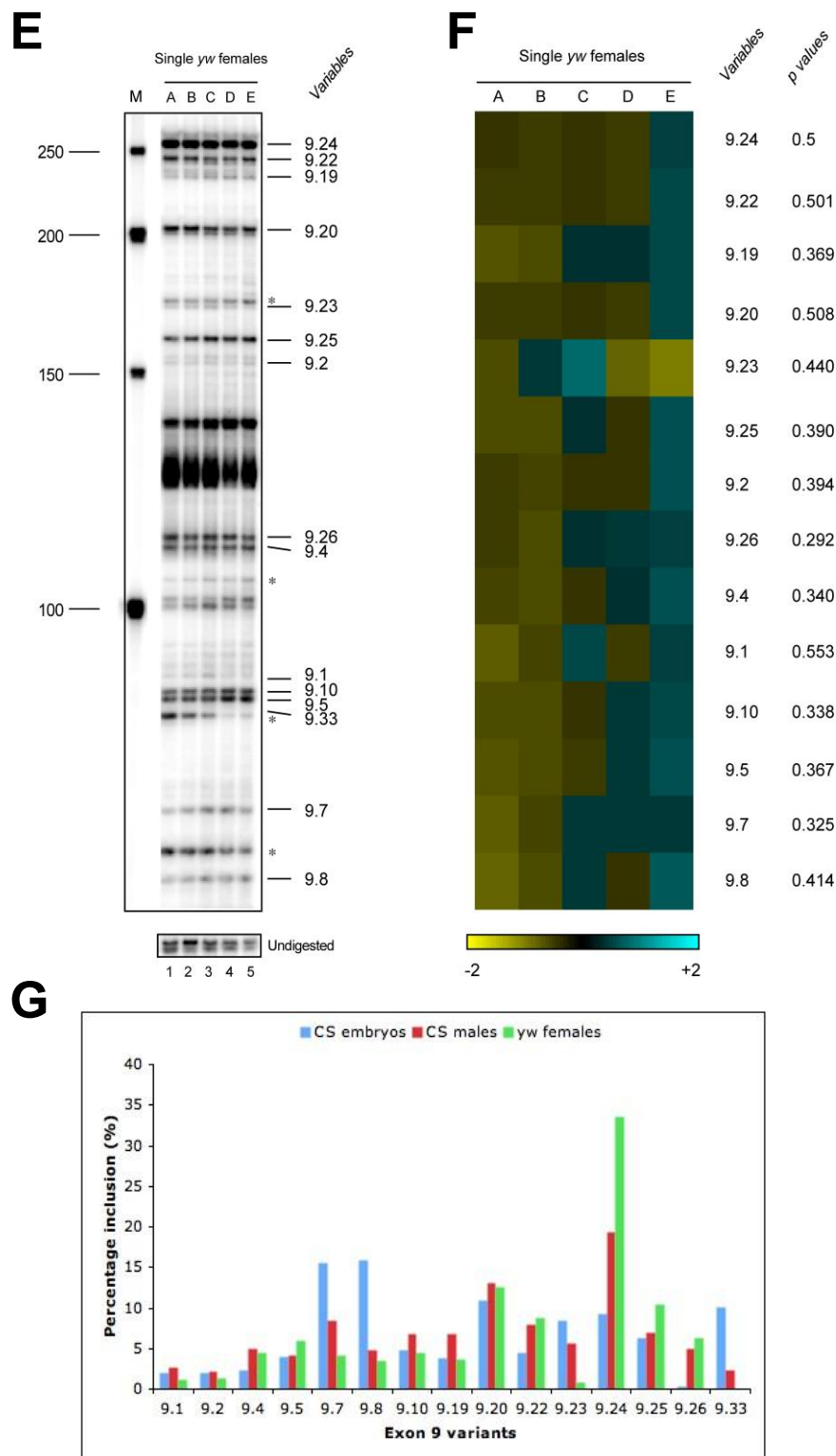


Figure 26 (E,F,G): Variation in *Dscam* exon 9 splicing pattern between different developmental stages, strains, sexes. (E) Analysis of *Dscam* exon 9 splicing pattern using RNA extracted from single yw females (Lanes 1-5). (F) Heat map representation of *Dscam* splicing changes observed in E. *p* values for each exon variant are mentioned alongside. (G) Graphical representation of percentage inclusion levels of each exon 9 variant observed in A, C and E. *Dscam* exon variants were separated as explained in figure legend 22. Unspecific bands are indicated by asterisks (*). Samples were run on an 8% denaturing polyacrylamide gel. M=50bp ladder (NEB).

9.5 and 9.33 showed the most variation. Females from the *yw* strain showed complete absence of exon 9.33.

3.5. Analysis of *Dscam* splicing in mutants of genes involved in small RNA and mRNA processing

Dscam mutants exhibit severe nervous system defects manifested in the disruption of connectives and commissures in the ventral nerve cord (Schmucker et al., 2000). Therefore, mutants of genes involved in RNA processing, which have similar nervous system defects to analyze *Dscam* splicing were searched. The genes that were identified with such a phenotype were *elav* and *ago1* (Kataoka et al., 2001; Simionato et al., 2007) (Figure 27). ELAV is a neuron-specific RNA binding protein that regulates alternative splicing of *erect wing* and *Neuroglian* by binding to their pre-mRNA (Lisbin et al., 2001; Soller and White, 2003). Ago1 is a key component of the RNAi machinery, which functions in the cytoplasm as a regulator of translation and RNA degradation, and in the nucleus as a regulator of chromatin remodeling (Bernstein and Allis, 2005; Hutvagner and Simard, 2008). Given Ago1's role in chromatin remodeling, it was further reasoned that the inclusion of a specific *Dscam* exon in the variable cluster might be mediated by its RNA sequence through Ago1 by signaling back to the nucleus, potentially involving chromatin remodeling. Thus, Ago1 might play a role in regulating *Dscam* splicing by an unknown RNA based mechanism of signaling from the cell surface to the nucleus to induce selection or repression of a particular *Dscam* isoform (shown later in Figure 35). In addition to Ago1, *Drosophila* has a second Argonaute protein; Ago2, which is primarily involved in siRNA-mediated silencing of exogenous genes in response to, for e.g. viruses or of

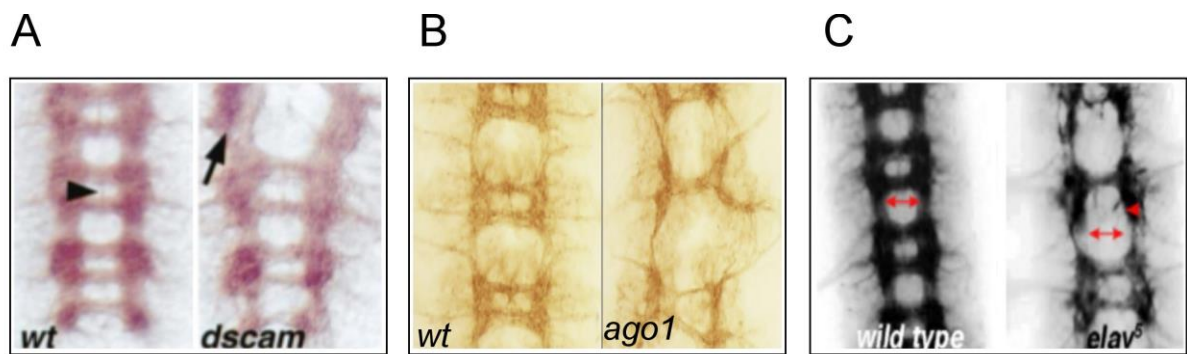


Figure 27: *ago1* and *elav* show similar *Dscam* mutant phenotype. Similar nervous system defects manifested in abnormal connectives and commissures observed in stage 16 mutant embryos of (A) *Dscam*, (B) *ago1* and (C) *elav*. Adapted from (Kataoka et al., 2001; Schmucker et al., 2000; Simionato et al., 2007).

endogenous genes primarily encoded by transposons (Chung et al., 2008; Okamura et al., 2004; van Mierlo et al., 2012).

In this study, mutants in *rrp6*, the activity determining component of the nuclear exosome and *trf4*, a component of the TRAMP complex, involved in degradation of aberrant RNAs and spurious transcripts termed, cryptic transcripts were also included (Callahan and Butler, 2010). It was reasoned that such transcripts might be involved in selection of exons in the *Dscam* variable region. In particular, spurious antisense transcription has been shown to silence genes and such a mechanism could also occur in the *Dscam* region to suppress inclusion of specific exon variants (Camblong et al., 2007).

Dscam splicing in mutants for the above genes in 14-18h old embryos were analyzed because *ago1*, *rrp6* and *elav* null mutants are embryonic lethal. To analyze *Dscam* splicing in *ago1* and *rrp6* mutants, a genetic trick was applied to select for null mutant embryos because no GFP labeled balancers were available at this time that would allow selection of homozygous mutant embryos. Therefore, the GAL4/UAS system was used to mark the chromosome carrying the mutation with *elav*GAL4 and a chromosome carrying a deficiency of the locus with UAS GFP (Brand and Perrimon, 1993). If these two strains are crossed together, only the mutant embryos will express GFP. This genetic selection system was used to identify *ago1* and *rrp6* mutants. For selection of *elav* null embryos, the C155 enhancer trap GAL4 inserted in the *elav* gene was used in combination with UAS GFP to label the *elav*⁺ progeny from the following cross, *elav/C155; UAS GFP/+* x *C155/Y; UAS GFP/UAS GFP* (refer to A4, A5 and A6 in appendix). Embryos of *ago2* and *trf4* mutants were directly collected from their stocks because they are homozygous viable.

Dscam exon 4, 6 and 9 splicing pattern was analyzed in *ago1*, *ago2*, *rrp6*, *trf4* and *elav* mutant embryos. Analysis of *Dscam* exon 4 splicing pattern revealed that *ago1* mutants produced a severe overall effect in altering *Dscam* splicing. Exons 4.5 and 4.11 were not detected (Figure 28A; Lane 3). Also, splicing of exons 4.3 and 4.10 was reduced by over two-fold. Exon 4.4 splicing was enhanced in *rrp6*, *ago2* and *elav* mutants by greater than five-fold (Figure 28A; Lanes 2, 5 and 6). Analysis of *Dscam* exon 9 splicing revealed that *elav* mutants produced the most dramatic changes. Exons 9.1, 9.4, 9.19, and 9.23 were all downregulated by over five-fold. The *ago2* mutants also showed downregulation of exons 9.19 and 9.20 by 4.5 and 6.8-fold, respectively (Figure 29A; Lane 3). Thus, exon cluster-specific effects in regulation of *Dscam* alternative splicing were observed with *ago1* affecting exon 4 and *elav* affecting exon 9 splicing. Also, a preliminary study on regulation of *Dscam* exon 6 splicing by the above mutants was carried out. None of the mutants produced any pronounced effects in splicing of exon 6 variants, except *ago1* mutants which downregulated exon 6.6 by 2.3-fold (Figure 30A; Lane 2).

3.6. Analysis of *ago1* and *rrp6* maternal mutants and redundancy between Agos and *rrp6* in *Dscam* splicing regulation

Although differences in *Dscam* exon 4 splicing were primarily observed in *ago1* mutants, the full effect of the Argonaute proteins might not have been seen because they might function redundantly in regulating *Dscam* splicing. To test if Ago1 and Ago2 play redundant roles in regulating *Dscam* splicing, double mutants of *ago1* and

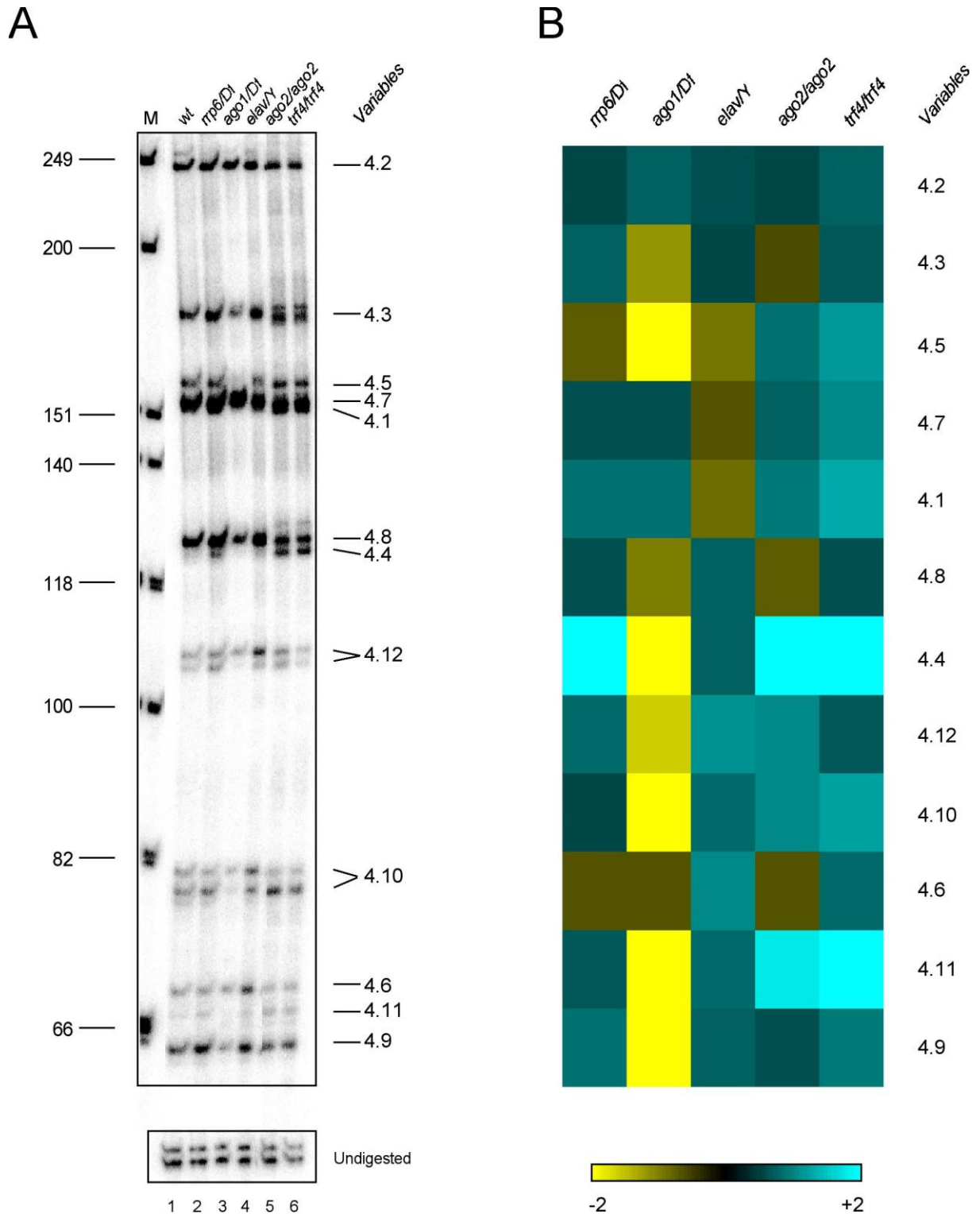


Figure 28: Analysis of *Dscam* exon 4 splicing in mutants of genes involved in small RNA and mRNA processing. (A) Analysis of *Dscam* exon 4 splicing pattern using RNA extracted from 14-18 h old mutant embryos of *rrp6/Df* (Lane 2), *ago1/Df* (Lane 3), *elav/Y* (Lane 4), *ago2/ago2* (Lane 5) and *trf4/trf4* (Lane 6). *Canton S* embryos served as control (Lane 1). (B) Heat map representation of *Dscam* splicing changes observed in A. *Dscam* exon variants were separated as explained in figure legend 21. Samples were run on an 8% denaturing polyacrylamide gel. M=phiX174 DNA/HinfI marker (Biotools).

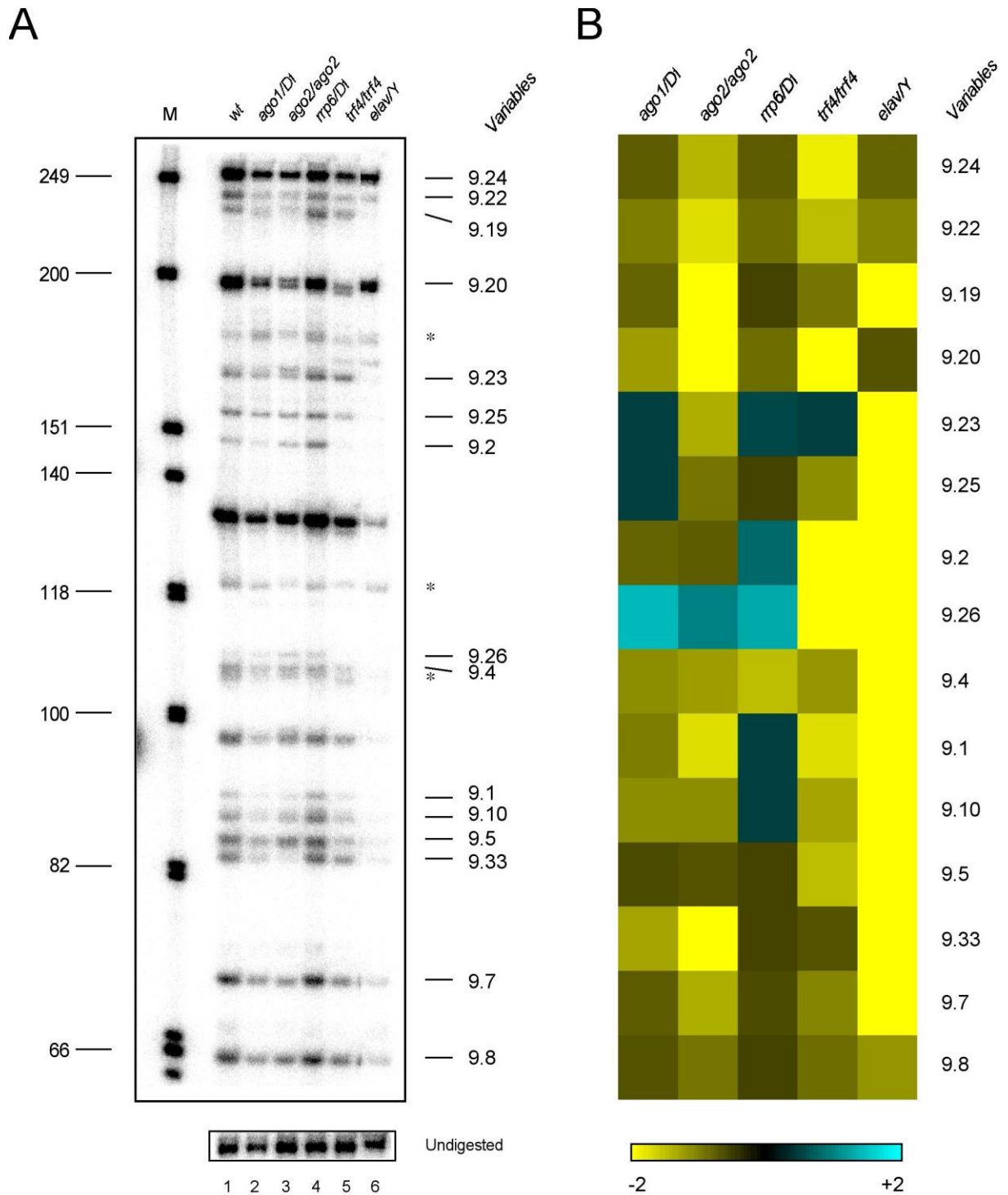
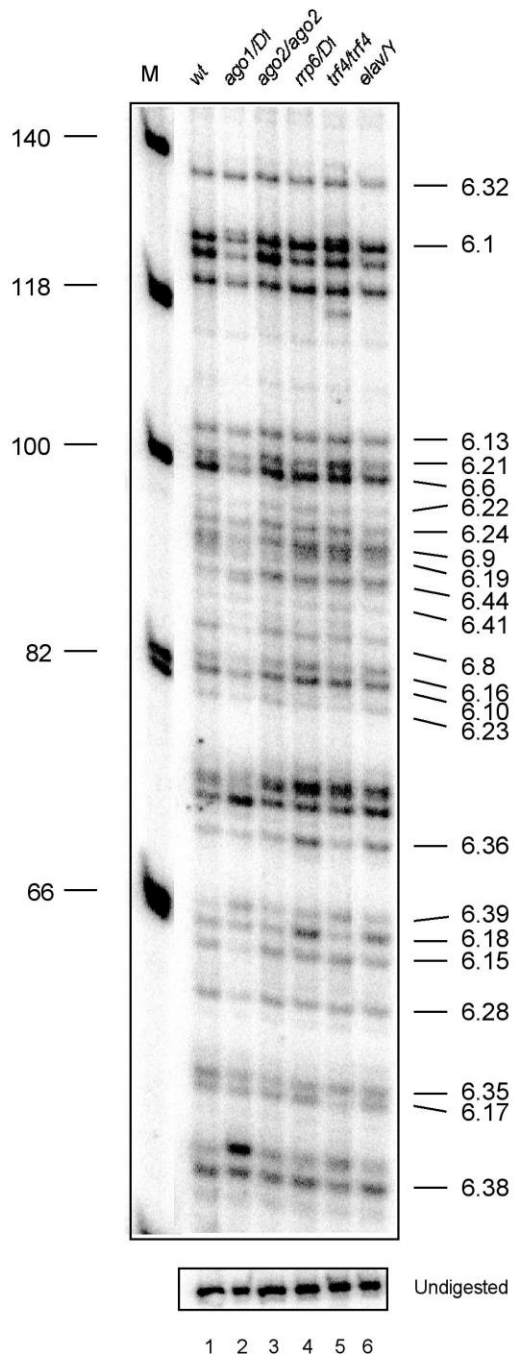


Figure 29: Analysis of *Dscam* exon 9 splicing in mutants of genes involved in small RNA and mRNA processing. (A) Analysis of *Dscam* exon 9 splicing pattern using RNA extracted from 14-18 h old mutant embryos of *ago1/Df* (Lane 2), *ago2/ago2* (Lane 3), *rrp6/Df* (Lane 4), *trf4/trf4* (Lane 5) and *elav/Y* (Lane 6). *Canton S* embryos served as control (Lane 1). (B) Heat map representation of *Dscam* splicing changes observed in A. *Dscam* exon variants were separated as explained in figure legend 22. Unspecific bands are indicated by asterisks (*). Samples were run on an 8% denaturing polyacrylamide gel. M=phiX174 DNA/HinfI marker (Biotools).

A



B

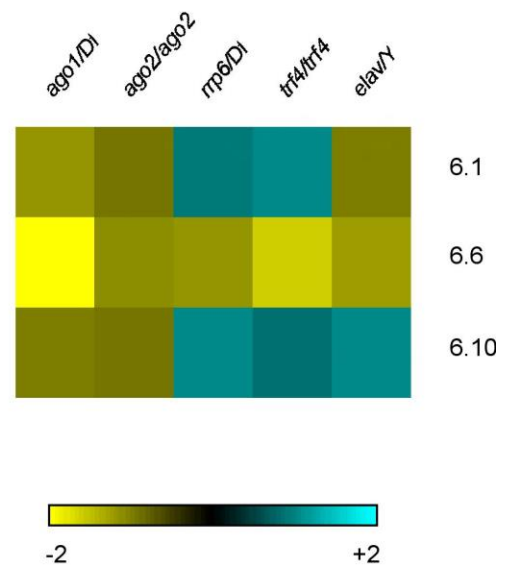


Figure 30: Analysis of *Dscam* exon 6 splicing in mutants of genes involved in small RNA and mRNA processing. (A) Analysis of *Dscam* exon 6 splicing pattern using RNA extracted from 14-18 h old mutant embryos of *ago1/Df* (Lane 2), *ago2/ago2* (Lane 3), *rrp6/Df* (Lane 4), *trf4/trf4* (Lane 5) and *elav/Y* (Lane 6). *Canton S* embryos served as control (Lane 1). (B) Heat map representation of *Dscam* most significant splicing changes observed in A. *Dscam* exon variants were separated as explained in figure legend 23. Samples were run on an 8% denaturing polyacrylamide gel. M= phiX174 DNA/HinfI marker (Biotools).

ago2 were generated. Since *ago2* is located on a different chromosome than *ago1* and *ago2* mutants are viable, the GAL4-UAS system could be used as before to recognize *ago1* mutants in an *ago2* background (refer to A7 in appendix). Potentially, *ago1* and *rrp6* could act redundantly in selection of *Dscam* isoforms and therefore double mutants were also tested. Testing these double mutants was possible because the genes are located on different chromosomes and GFP labeled balancers with no maternal expression of GFP were available (refer to A8 in appendix).

Both, *ago1* and *rrp6* are expressed during oogenesis. Therefore, both proteins are deposited in eggs and provide functionality during embryogenesis. Hence, zygotic null mutants still contain protein that can last up to the end of embryogenesis. To remove maternal *ago1* and *rrp6*, germ line clones for these mutants were generated (refer to A9 and A10 in appendix). The dominant female sterile technique utilizes the dominant *ovo^D* mutation that does not allow development of oocytes. Mitotic recombination mediated by flp-FRT site specific recombination between homologous chromosomes, containing either an *ovoD* transgene or a mutation of choice in female germ cells, will result in the loss of *ovoD* and hence development of functional oocytes (Perrimon, 1998) (Figure 31). To allow the generation of germ line clones, FRT sites were added to mutant chromosome arms by meiotic recombination and validated by PCR (Figures 32A and B).

Analysis of *Dscam* exon 4 splicing in *ago1/Df;ago2/ago2* double mutants showed no significant differences in the splicing pattern (Figure 33A; Lane 3). Also, *ago1/Df;rrp6/Df* double mutants revealed no obvious differences in the splicing pattern. Exon 4.12 showed a 1.8-fold decrease in inclusion (Figure 33A; Lane 5).

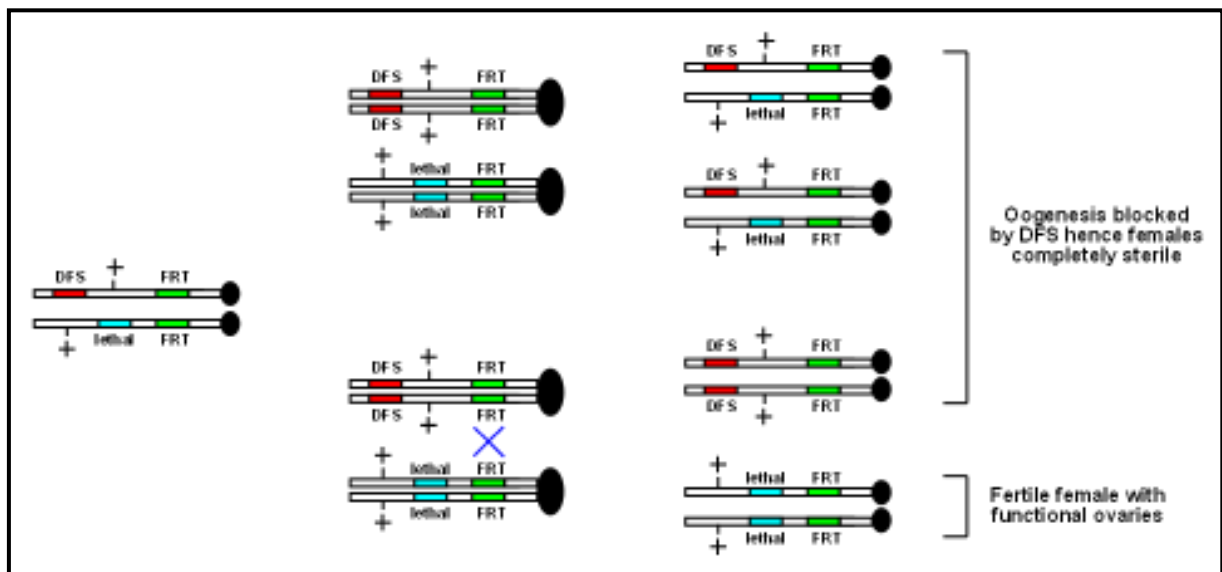


Figure 31: Schematic representation of generating germ line clones using the dominant female sterile (DFS) technique. Mitotic recombination occurs between chromosomes with genotypes DFS FRT/lethal FRT. The FRT is inserted proximally to both DFS and the lethal mutation. On heat shock treatment, the heat shock promoter (on another chromosome) gets activated and provides recombinase activity which catalyses the site-specific chromosomal exchange at the FRT sequences. FLP-recombinase target sequences (FRT). Dominant Female Sterile (DFS). Recessive zygotic lethal mutation (lethal) Adapted from (Perrimon, 1998).

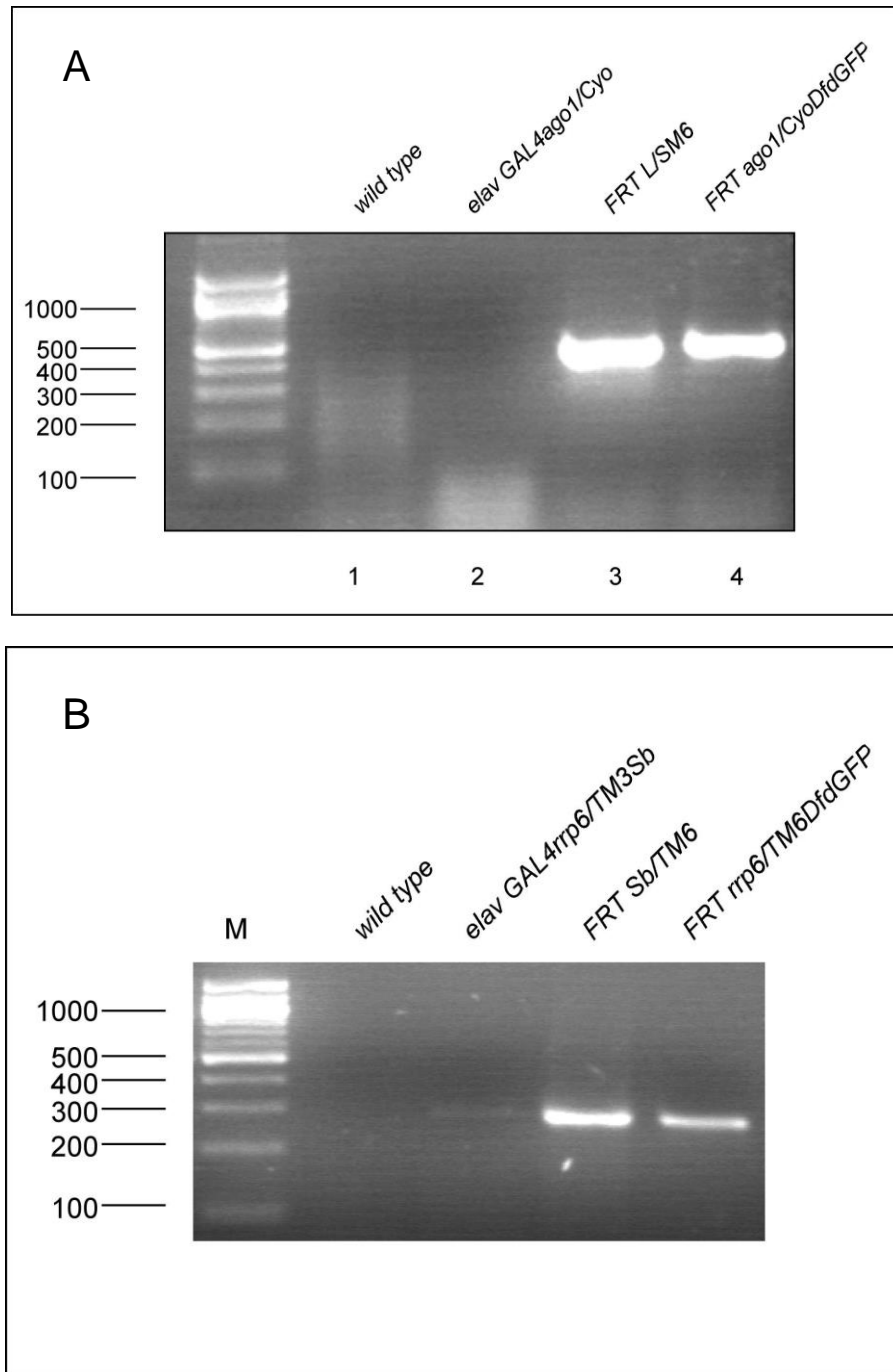


Figure 32: PCR validation showing recombined FRT sites on the same chromosome as the (A) *ago1* and (B) *rrp6* lethal mutation. Primers pUChneoF1 and pUChneoR1 flanking the FRT sites on 42B and primers FRT F1 and Car3'InvR1 flanking the FRT sites on 82B were used to carry out single fly PCRs on *FRTago1/CyODfdGFP* and *FRTrrp6/TM6DfdGFP* flies, respectively. The starting fly lines, *elavGAL4ago1/CyO* and *elavGAL4rrp6/TM3Sb* served as negative controls. The *FRTL/SM6* and *FRTSb/TM6* lines served as positive controls for FRT sites. In both the gels, *Canton S* males were used as negative controls.

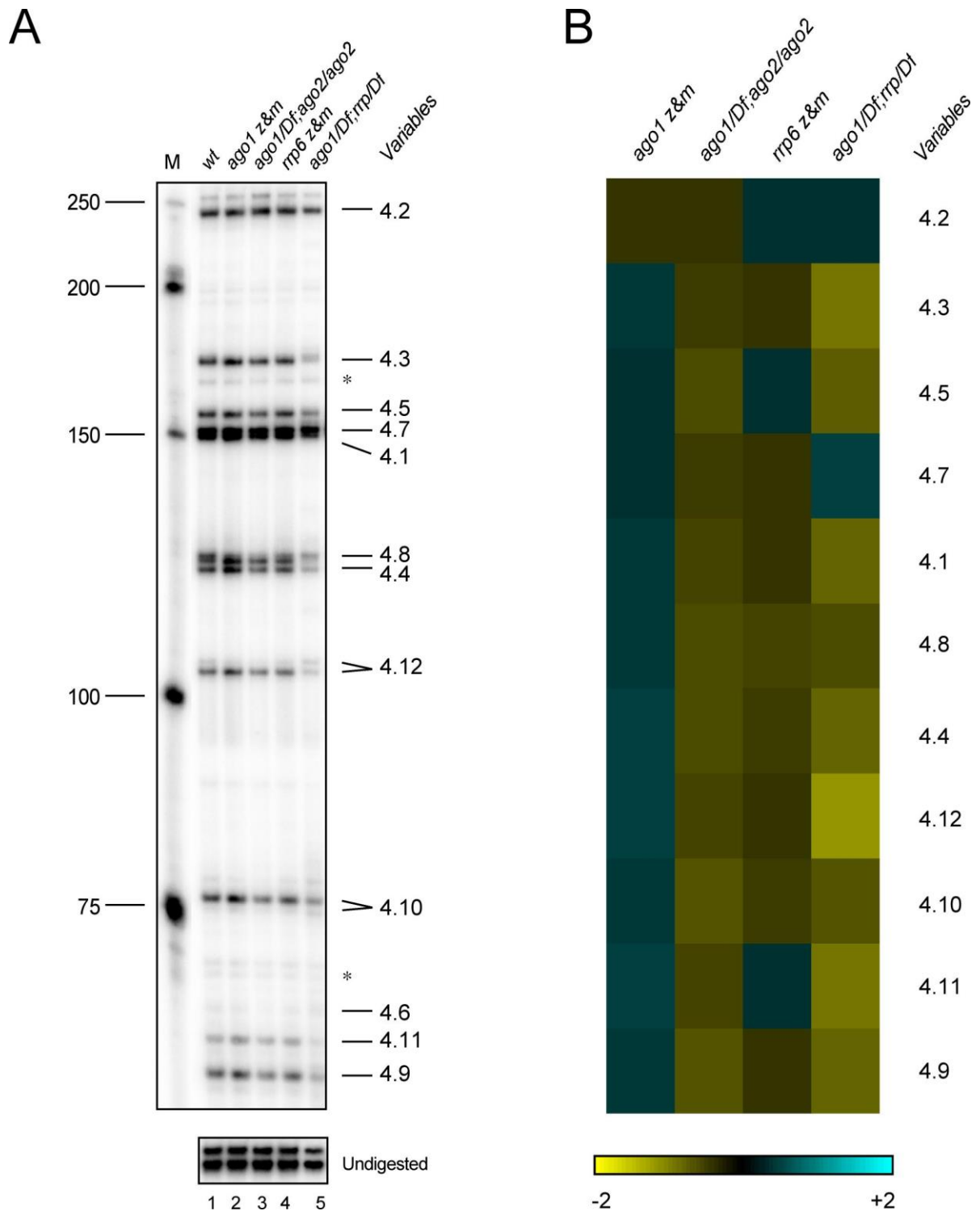


Figure 33: Analysis of *ago1* and *rrp6* maternal mutants and redundancy between Agos and *rrp6* in *Dscam* splicing regulation (A) Analysis of *Dscam* exon 4 splicing pattern using RNA extracted from 14-18 h old mutant embryos of *ago1 z&m* (Lane 2), *ago1/Df; ago2/ago2* (Lane 3), *rrp6 z&m* (Lane 4) and *ago1/Df; rrp6/Df* (Lane 5). *Canton S* embryos served as control (Lane 1). (B) Heat map representation of *Dscam* splicing changes observed in A. *Dscam* exon variants were separated as explained in figure legend 21. Unspecific bands are indicated by asterisks (*). Samples were run on an 8% denaturing polyacrylamide gel. z&m = zygotic and maternal mutants. M=50bp ladder (NEB).

Germline clones for *ago1* and *rrp6*, unexpectedly showed no obvious changes in *Dscam* exon 4 splicing pattern (Figure 33A; Lanes 2 and 4).

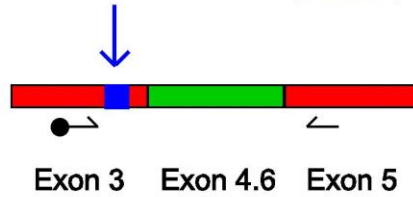
3.7. Overexpression of a single *Dscam* isoform does not reinforce selection of the same variable exons

The defects that were found in *ago1* and *rrp6* zygotic mutants were not conclusive regarding an RNA mediated mechanism involved in *Dscam* variable exon selection. Since this does not rule out that such a mechanism could apply, it was required to test if overexpression of a single *Dscam* transcript species can reinforce splicing of the same isoform. Therefore, a *Dscam* cDNA construct was generated that includes its entire 5'UTR and also includes the endogenous 3' end-processing site as it was reasoned that cytoplasmic cleavage and/or polyadenylation might be involved in producing a relay of expression information to the nucleus and force selection of specific exons. To be able to distinguish the endogenous *Dscam* transcripts from the overexpressed exogenous isoform, a restriction site was included in front of exon clusters 4, 6 and 9, which is absent in the variable downstream cluster to cut off the label from PCR products that originate from the transfected cDNA (Figure 34).

pAc5.1A Dscam Mut Exons 4-9, comprising a single *Dscam* isoform with variable exons 4.6, 6.32, 9.25 and 17.2, was transfected into S2 cells (as mentioned in 4.5.4). The splicing pattern of the endogenous *Dscam* was analyzed for exon clusters 4 and 9 as before, but also including *BsrGI* and *XbaI* to cut the label off from the exogenous transcripts originating from the transfected cDNA construct. This analysis revealed that the splicing pattern of endogenous *Dscam* exon 4 and 9 cluster did not change, in particular did not reinforce the inclusion of the exogenously expressed variable

Exogenous Isoform

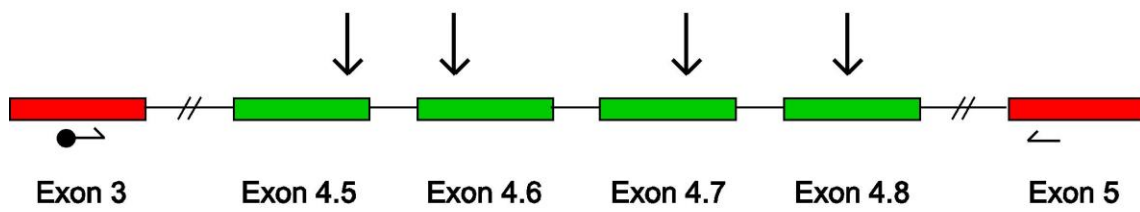
Restriction Site (*Bsr*GI)



↓ Restriction Digest + *Bsr*GI



Endogenous Isoform



↓ Restriction Digest + *Bsr*GI

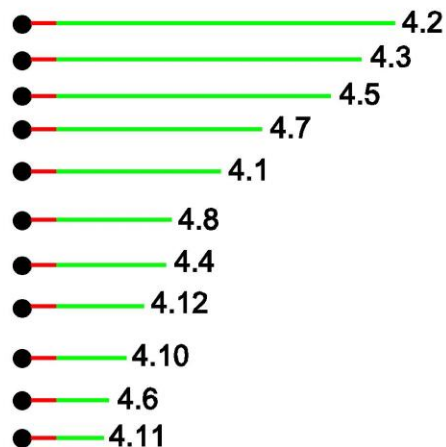


Figure 34: Diagrammatic representation of distinguishing the endogenous *Dscam* exon 4 variants from the exogenously overexpressed *Dscam* single isoform, containing exon variant 4.6. A *Bsr*GI restriction site added before the variable exon cluster was used to cut off the 5' radioactive label. The dark circle (•) represents ^{32}P used to label the forward primer YH *Dscam* 3F2.

exons 4.6 and 9.25, respectively (Figures 3A5 and B).

3.8. Dscam intracellular signaling is not involved in regulating its own splicing pattern

The cytoplasmic domain of *Dscam* interacts with Dock, an SH3-SH2 adaptor protein, and Pak, a serine threonine kinase, to translate the recognized guidance signals into changes in the actin-based cytoskeleton and promote axon guidance (Schmucker et al., 2000). Individual mushroom body and da sensory neurons from an otherwise identical population acquire a unique splicing pattern resulting in canalization of a broad variety of *Dscam* isoforms into just a few unique isoforms (Matthews et al., 2007; Zhan et al., 2004).

To test if *Dscam* intracellular signaling is involved in canalization or in any form of exon selection, a set of transposon inserts that result in secreted Dscam (Figure 36A; mutants *A* and *B*), membrane bound Dscam without intracellular domain (Figure 36A; mutants *C*, *D* and *E*) or signaling compromised Dscam (Figure 36A; mutant *F*) were used. Analysis of *Dscam* exon 9 splicing showed no pronounced effects in any of the analyzed mutants. Mutants *D* and *E* with transposons after the transmembrane domain behaved similarly, by upregulating exons 9.2 and 9.5 and downregulating exon 9.33 by over three-fold (Figure 36B; Lanes 5 and 6). Mutants *C* and *F* downregulated exon 9.7 by 7.2-fold. Although minor differences were observed, however, none of the changes observed in splicing pattern were striking (Figure 36B; Lanes 4 and 7). Mutants *A* and *B* produced the least effect in changing *Dscam* exon 9 splicing (Figure 36B; Lanes 2 and 3).

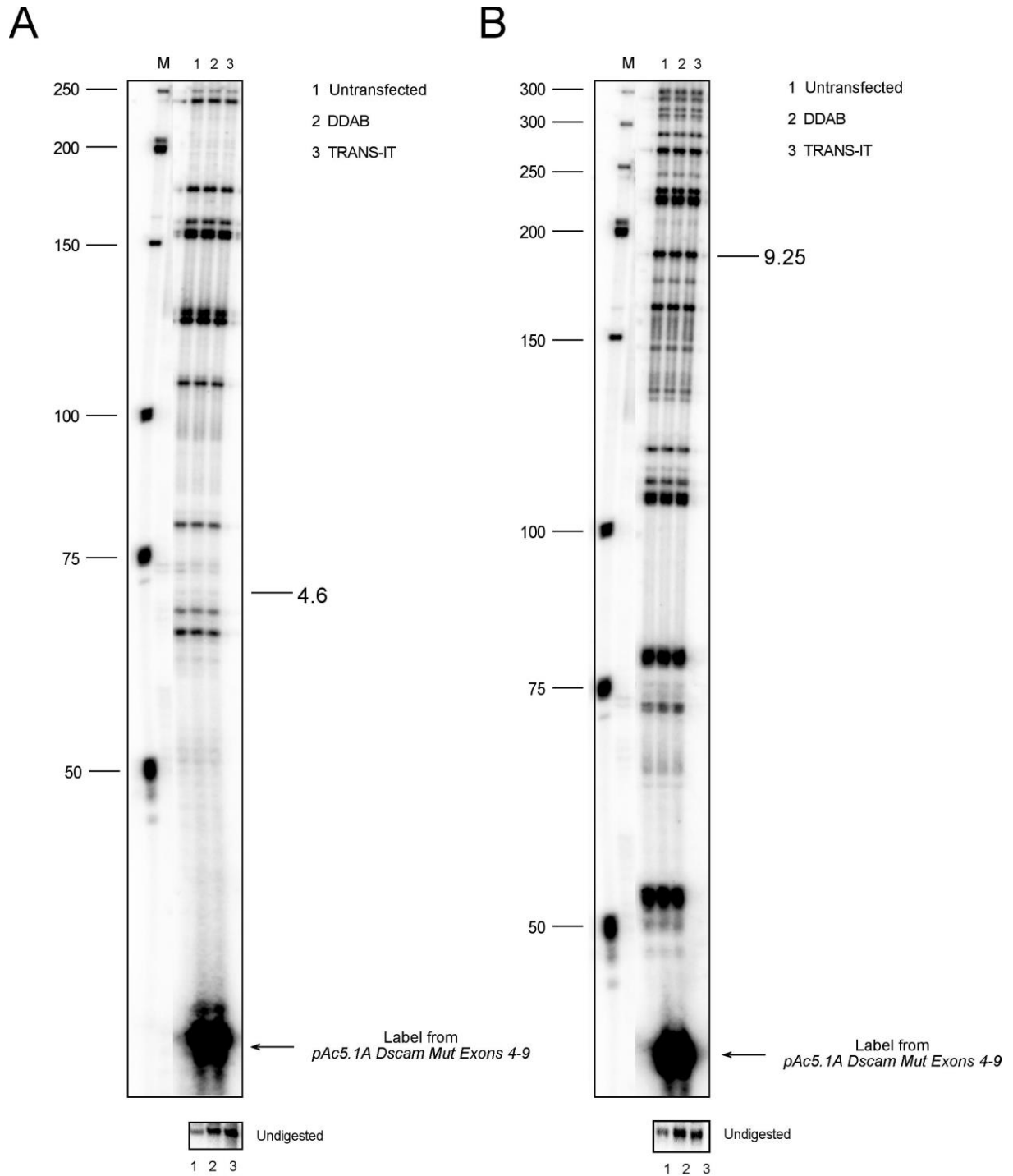


Figure 35: Overexpression of a single *Dscam* isoform does not reinforce selection of the same variable exons. Analysis of endogenous *Dscam* variable exon 4.6 (A) and variable exon 9.25 (B) splicing in response to transfection of exogenous *Dscam* construct *pAc5.1A Dscam Mut Exons 4-9* into S2 cells by using DDAB (Lane 2) or TRANS-IT (Lane 3). Untransfected S2 cells served as control (Lane 1). *Dscam* exon variants were separated in A and B as explained in figure legend 21 and 22, respectively. Samples were run on an 8% denaturing polyacrylamide gel. M=50bp ladder (NEB).

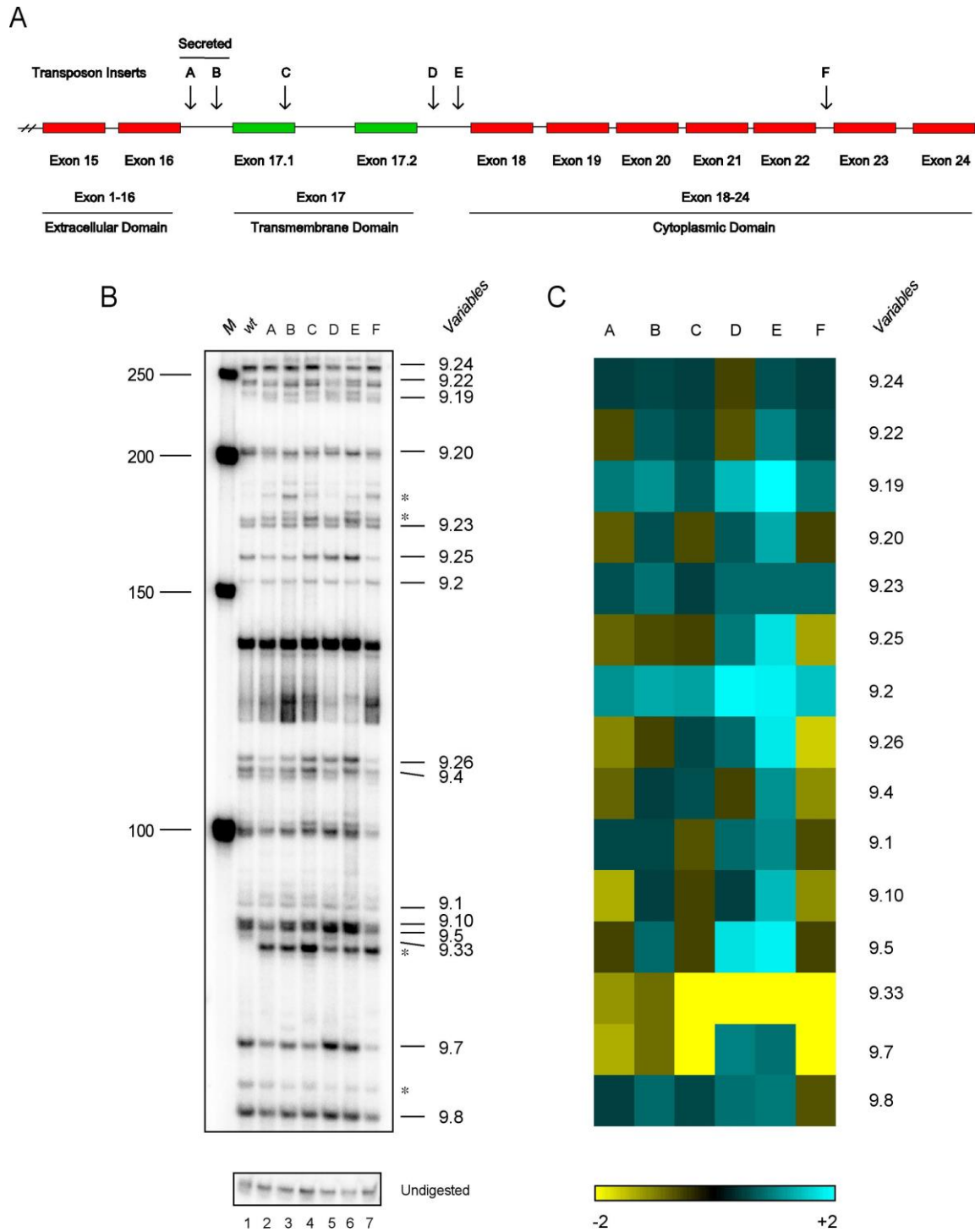


Figure 36: Dscam intracellular signaling is not involved in regulating its own splicing pattern. (A) Analysis of *Dscam* exon 9 splicing pattern using RNA extracted from 14-18 h old mutant embryos of *P[GawB]Dscam^{NP3327}* (mutant A; Lane 2), *P[RS3]Dscam^{CB-0486-3}* (mutant B; Lane 3), *P[XP]Dscam^{d10584}* (mutant C; Lane 4), *P[EPgy2]Dscam^{EY08820}* (mutant D; Lane 5), *PBac[SAstopDsRed]LL01770* (mutant E; Lane 6) and *PBac[RB]Dscam^{e04629}* (mutant F; Lane 7). *Canton S* embryos served as control (Lane 1). (B) Heat map representation of *Dscam* splicing changes observed in A. *Dscam* exon variants were separated as explained in figure legend 22. Unspecific bands are indicated by asterisks (*). Samples were run on an 8% denaturing polyacrylamide gel. M=50bp ladder (NEB).

3.9. Analysis of mRNA methylation for a role in *Dscam* splicing regulation

The mRNAs of higher eukaryotes can be variably methylated at the cap or internally (Motorin). At the cap, the ribose of the first and second nucleotides can be 2'-O-methylated sequentially by methyltransferases MTr1 and MTr2, respectively (Belanger et al., 2010; Kruse et al., 2011; Werner et al., 2011). The first 2'-O-methylation results in the formation of cap1 and the subsequent methylation results in the formation of cap2. Cap methylations are also present in U snRNAs and seem to be essential for splicing regulation (Donmez et al., 2004). Internally, mRNAs can be methylated at the N⁶ position of adenosine and this modification is introduced by a multimeric complex containing the catalytic activity of MT-A70 (Bokar et al., 1997). Intriguingly, the *Arabidopsis thaliana* homolog of MT-A70 interacts with the homolog of the *Drosophila* splicing regulator Female-Lethal 2D and m6A modification has been found in the vicinity of splice sites (Zhong et al., 2008). Thus, it was reasoned that nuclear mRNA methylation, either at the cap or internally might affect *Dscam* splicing by fixing a specific splicing pattern or positively marking specific exons for inclusion.

Analysis of *Dscam* exon 9 splicing in mutants for cap 2'-O-methyltransferases, *dMTr1* and *dMTr2* and double mutant *dMTr1/dMTr2* revealed no significant changes in splicing pattern (Figure 37C; Lanes 2, 3 and 4). Analysis of *Dscam* exon 9 splicing in mutants for m6A methylase (*dMT-A70*) and two other putative RNA methylases (*CG7818* and *CG14906*) downregulated the inclusion of exon 9.7 by less than two-fold (Figure 37A; Lanes 2, 3 and 4). No other significant differences were observed.

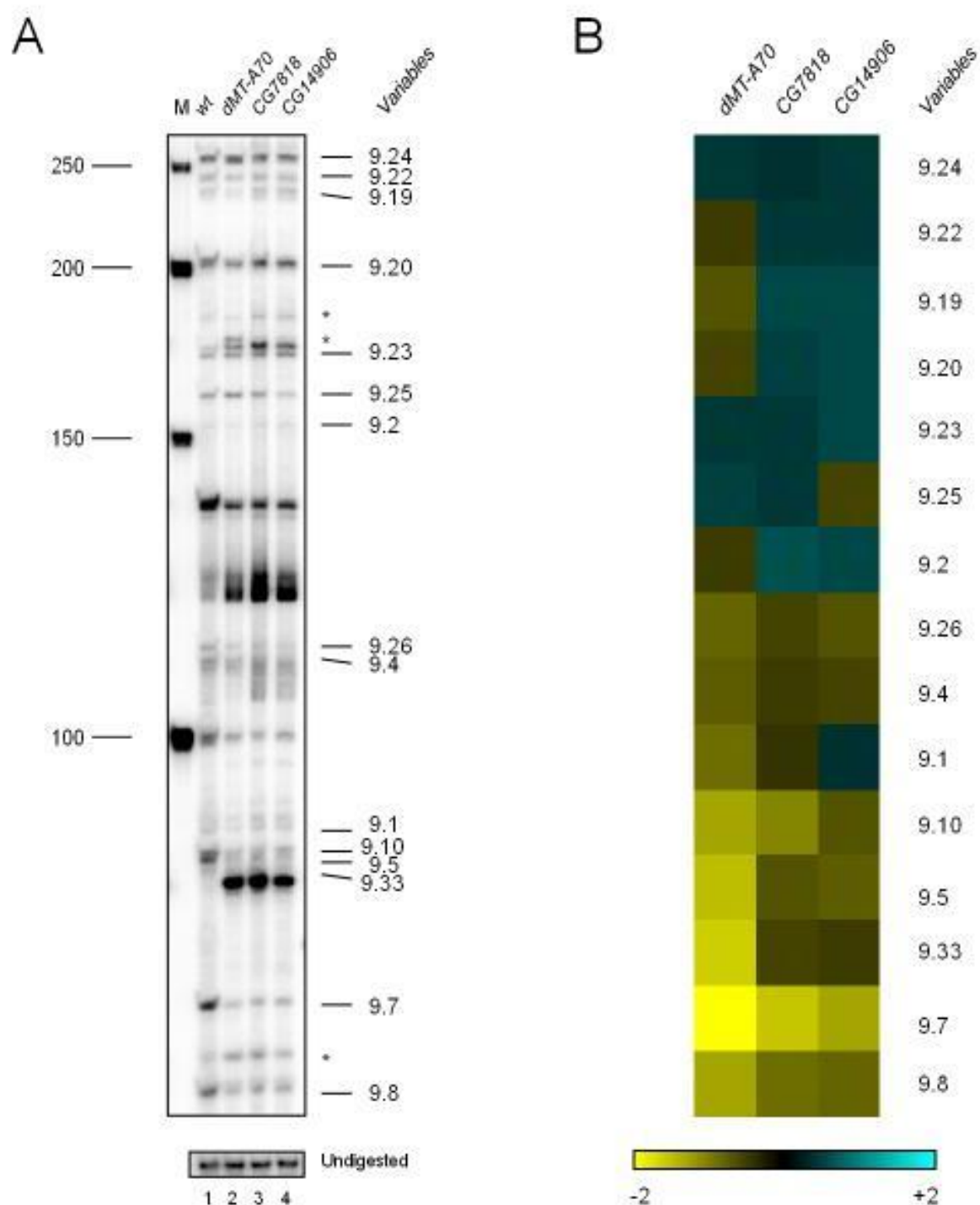


Figure 37 (A,B): Analysis of mRNA methylation for a role in *Dscam* splicing regulation. (A) Analysis of *Dscam* exon 9 splicing pattern using RNA extracted from 14-18 h old mutant embryos of internal mRNA methylases *dMT-A70* (Lane 2), *CG7818* (Lane 3) and *CG14906* (Lane 4). *Canton S* embryos served as control (Lane 1). (B) Heat map representation of *Dscam* splicing changes observed in A. *Dscam* exon variants were separated as explained in figure legend 22. Unspecific bands are indicated by asterisks (*). Samples were run on an 8% denaturing polyacrylamide gel. M=50bp ladder (NEB).

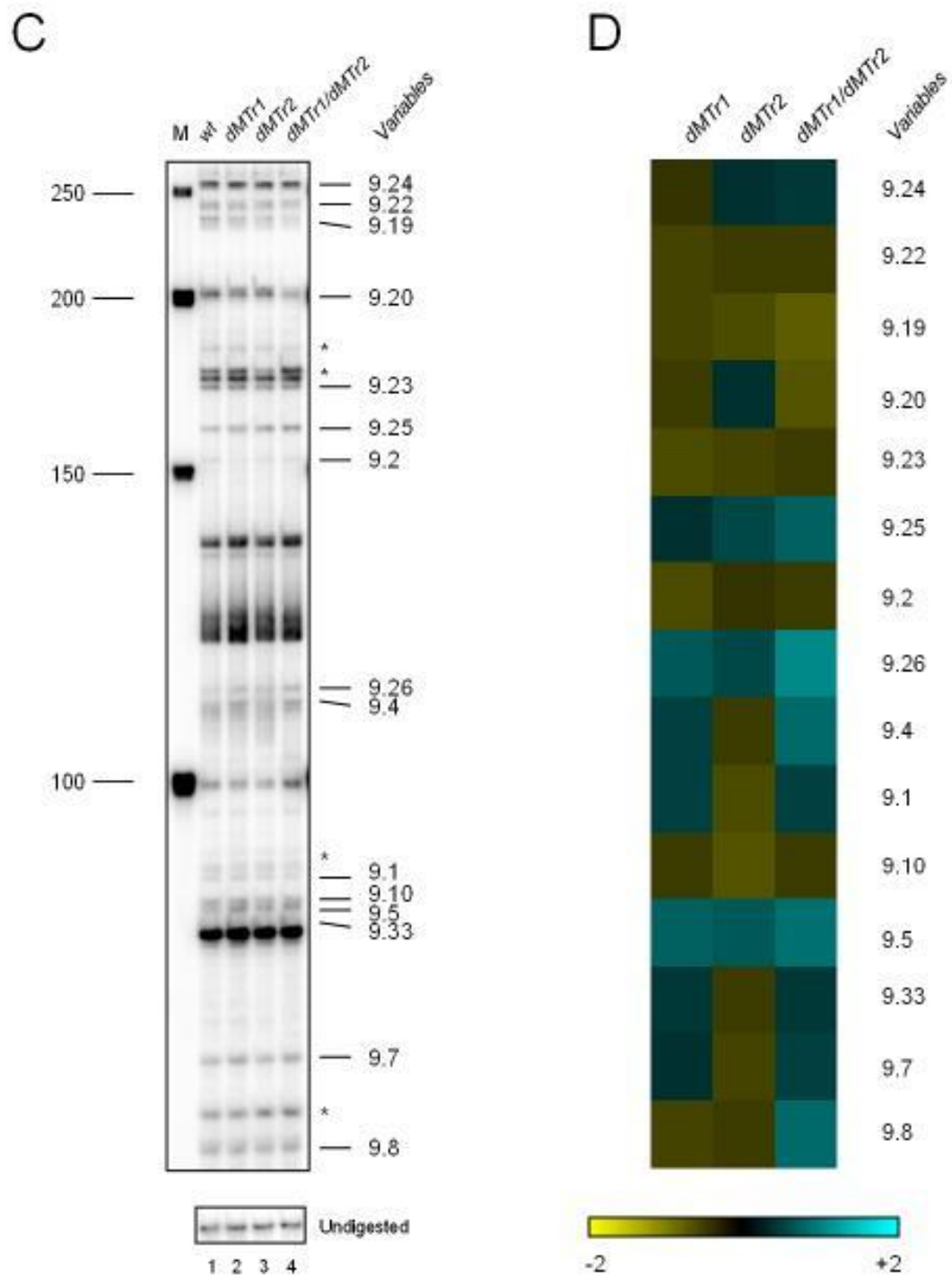


Figure 37 (C,D): Analysis of mRNA methylation for a role in *Dscam* splicing regulation. (C) Analysis of *Dscam* exon 9 splicing pattern using RNA extracted from 14-18 h old mutant embryos of internal cap methylases *dMTr1* (Lane 2), *dMTr2* (Lane 3) and *dMTr1/dMTr2* (Lane 4). *Canton S* embryos served as control (Lane 1). (D) Heat map representation of *Dscam* splicing changes observed in C. *Dscam* exon variants were separated as explained in figure legend 22. Unspecific bands are indicated by asterisks (*). Samples were run on an 8% denaturing polyacrylamide gel. M=50bp ladder (NEB).

3.10. Analysis of *Dscam* exon 9 splicing regulation in mutants of genes differentially regulated in *elav* mutants

Since *Dscam* exon 9 splicing is particularly affected in *elav* mutants, the introns of the exon 9 cluster were analyzed for potential ELAV binding sites. Although, some U-rich sequences are present in this exon cluster, these sequences are not *bona fide* ELAV binding sites and also no experimental evidence could be obtained so far which indicates that ELAV directly binds to *Dscam* pre-mRNA (Hausmann and Soller, unpublished). Gene expression analysis in *elav* mutants, however, has shown that numerous genes encoding RNA binding proteins, DNA binding proteins and proteins involved in chromatin remodeling are massively differentially expressed (Figure 38) suggesting that ELAV might regulate *Dscam* splicing indirectly. Therefore, all available mutants were obtained from these categories of genes (56 genes) that are differentially regulated in *elav* mutants to test their contribution in regulating *Dscam* splicing (refer A11 (A-H) in appendix). As a control to this analysis, mutants of metabolic genes were used that were differentially regulated in *elav* mutants as it was anticipated that these genes would not have a role in *Dscam* splicing regulation (Figure 39). Analysis of *Dscam* exon 9 splicing in mutants of genes differentially regulated in *elav* mutants revealed that *Dscam* splicing is affected by many genes, the pattern, however, is not random (refer A11 (A-H) in appendix). When taking exons into consideration that were two-fold or more differentially regulated, it was found that a group of exons tended to be preferentially upregulated in a set of mutants while a different group tended to be preferentially downregulated in a different set of mutants. For upregulated exons, it was found that exons 9.2, 9.7, 9.8, 9.25 and 9.26 (Figure 39; Columns 2, 5, 6, 13 and 14) were mostly upregulated in

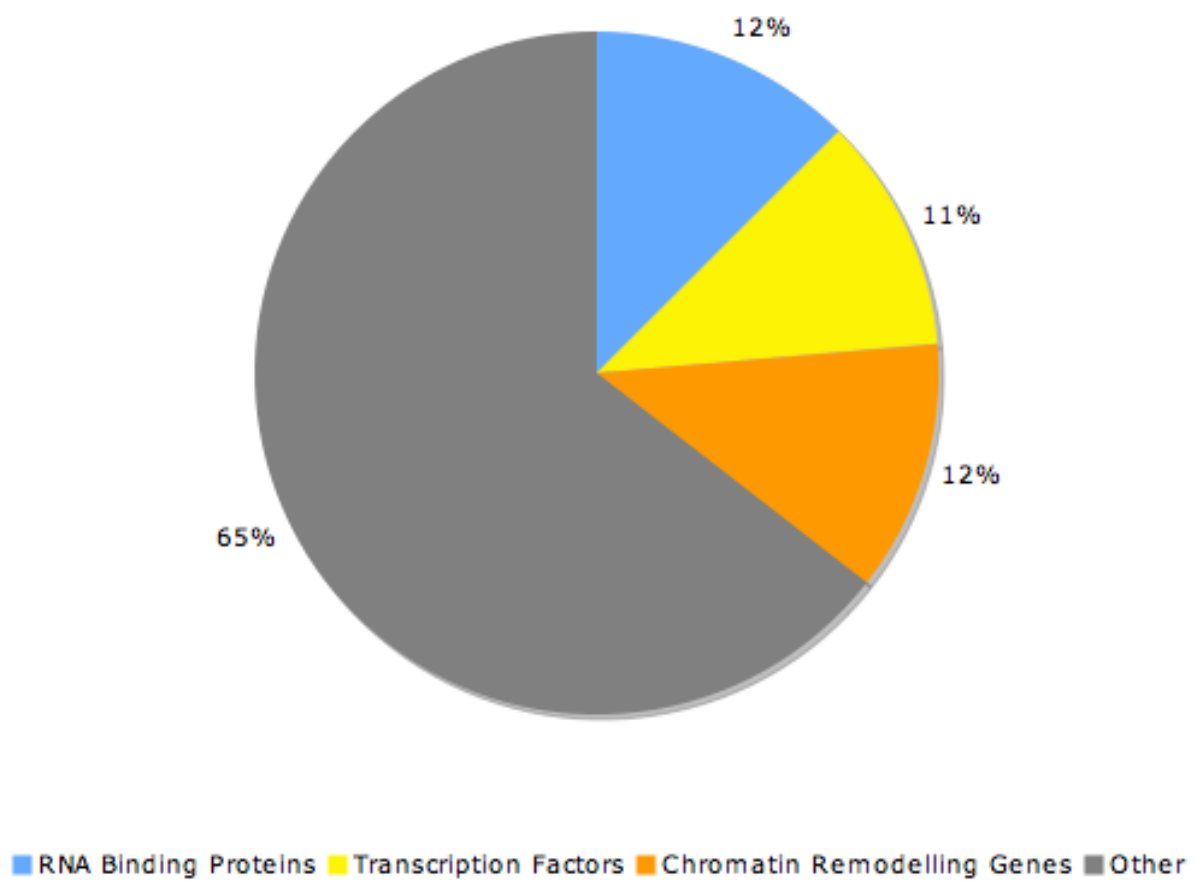


Figure 38: Graphical representation of proportions of genes differentially regulated in *e/av* mutants. RNA binding proteins, transcription factors and chromatin remodeling genes account for 12%, 11% and 12%, respectively of all genes differentially regulated in *e/av* mutants.

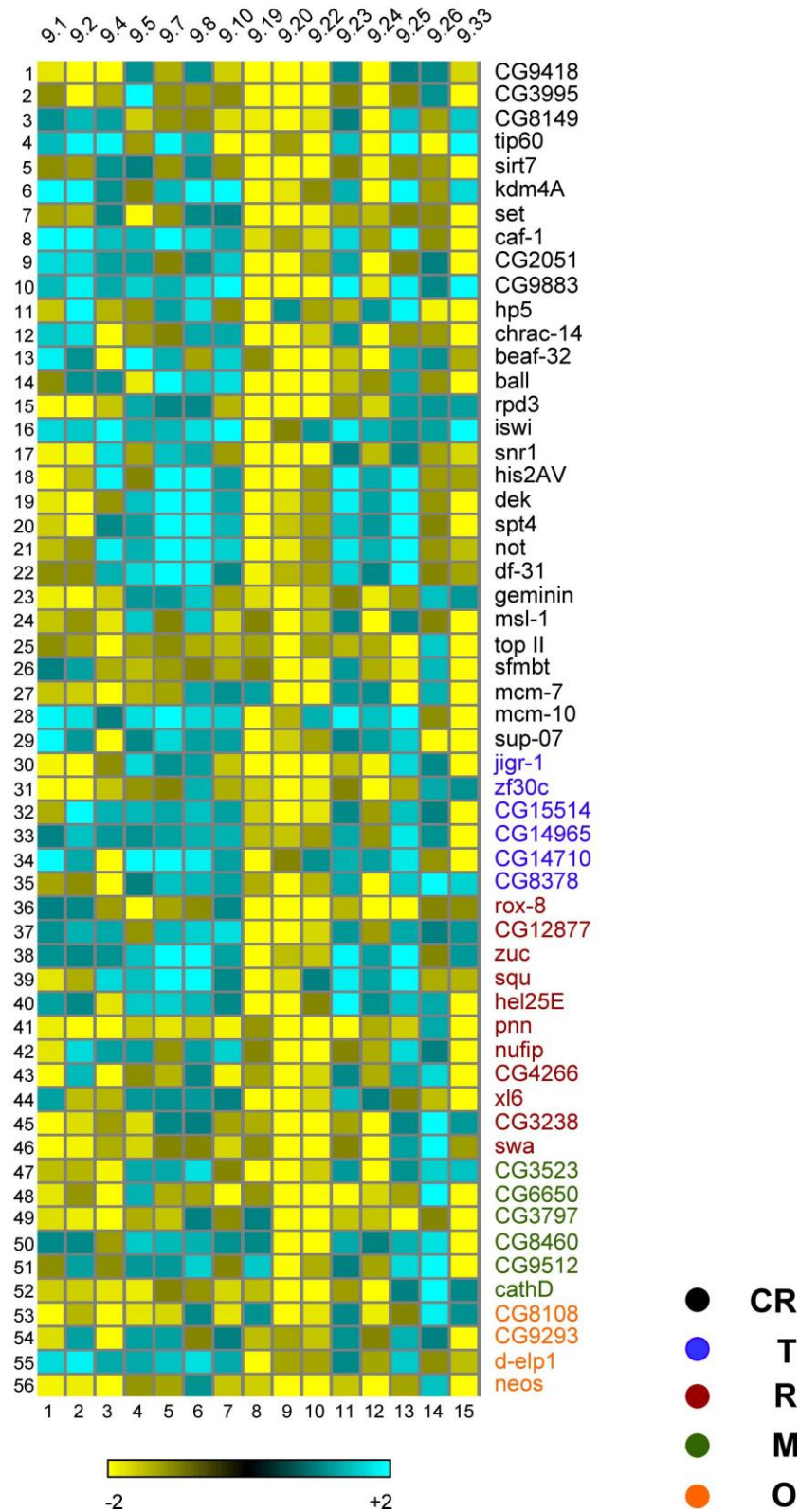


Figure 39: Heat map representation of *Dscam* exon 9 splicing analysis in mutants of genes that are differentially regulated in *elav* mutants. CR=chromatin remodeling; T=transcription factors; R=RNA binding proteins; M=metabolic genes; O=others, including zinc finger proteins (CG8108 and CG9293), RNA-dependent RNA polymerase (d-elp1), nuclear receptor coactivator (neos).

mutants of chromatin remodeling factors *caf1*, *His2AV* and *dek* (Figure 39; Rows 8, 18 and 19). Similar upregulation of these exons was also observed in mutants for RNA binding proteins *zuc* and *squ*, involved in rasiRNA generation (Figure 39; Rows 38 and 39, (Pane et al., 2007).

For downregulated exons, it was found that exons 9.4, 9.19, 9.20, 9.22, 9.24 and 9.33 (Figure 39; Columns 3, 8, 9, 10, 12 and 15) were mostly downregulated in mutants of chromatin remodeling factors *CG9418*, *CG3995* and *mcm7* (Figure 39; Rows 1, 2 and 27). Also, mutants for *pnn*, a splicing factor and *neos*, a nuclear receptor coactivator, showed a pronounced decrease in inclusion of most of these exons (Figure 39; Rows 41 and 56).

I also observed that some mutants regulated the splicing pattern of *Dscam* exon 9 in a similar manner by affecting the same groups of exons. Mutants of chromatin remodeling genes *snr1*, *His2AV*, *dek*, *spt4*, *not* and *Df-1* (Figure 39; Rows 17-22) showed a very similar *Dscam* exon 9 splicing pattern by upregulating inclusion of exons 9.7, 9.8, 9.23 and 9.25 (Figure 39; Columns 5, 6, 11 and 13) and downregulating inclusion of exons 9.1, 9.2, 9.19 and 9.20 (Figure 39; Columns 1, 2, 8 and 9). Also mutants of *zuc* and *squ* regulated *Dscam* exon 9 splicing pattern in a very similar way (Figure 39; Rows 38 and 39). Contrary to expectation, however, no mutants were found where only one exon variant was affected, e.g. one exon that was massively upregulated or downregulated. This suggested that exon choice is regulated by combinatorial interactions of RNA binding proteins, DNA binding proteins and chromatin remodeling factors. Furthermore, *Dscam* exon 9 splicing seems to be generally sensitive to genetic perturbation as changes were found in mutants of metabolic genes (Figure 39; Rows 47-52).

3.11. RNA pol II processivity does not influence splicing of *Dscam*

The processivity of RNA pol II has been shown to be critical for inclusion of the fibronectin EDI exon such that a slow polymerase favours inclusion while a fast polymerase results in preferential exclusion of the alternative exon (Kornblihtt et al., 2004). Accordingly, it was speculated that polymerase processivity might be important for *Dscam* variable exon selection. In particular, pausing of RNA pol II at a specific exon variant could relieve its repressed state and result in its inclusion. To test if there is a correlation between the speed of the polymerase and inclusion of *Dscam* variable exons, the *Drosophila* C4 mutant of the RNA pol II subunit 215, which has a lower elongation rate was used. In addition, two inhibitors of RNA pol II elongation rate namely, 6-Azauracil and dichlororibofuranosylbenzimidazole (DRB) were used to analyze *Dscam* exon 9 splicing in S2 cells (Hrzenjak et al., 2006; Iglesias-Gato et al.; te Poele et al., 1999). If indeed a slow polymerase would affect inclusion of variable exons, my expectation was to see preferential inclusion of cluster proximal exons over cluster distal exons resulting in a polar effect. Alternative splicing of exon 23a of *Nf1* gene has been shown to be affected by histone deacetylase activity such that inhibiting histone deacetylation results in an increased local RNA pol II elongation rate resulting in skipping of the alternative exon (Zhou et al., 2011). Thus, sodium valproate (Na-valproate), a potent inhibitor of histone deacetylase, was used to test if *Dscam* splicing is regulated by histone modifications. Analysis of *Dscam* exon 9 splicing in flies with a C4 mutation (Figure 40A; Lane 2) and S2 cells treated with 6-Azauracil, DRB or sodium valproate (Figure 40A; Lanes 4, 6 and 8) showed no significant difference in the overall splicing pattern. In the C4

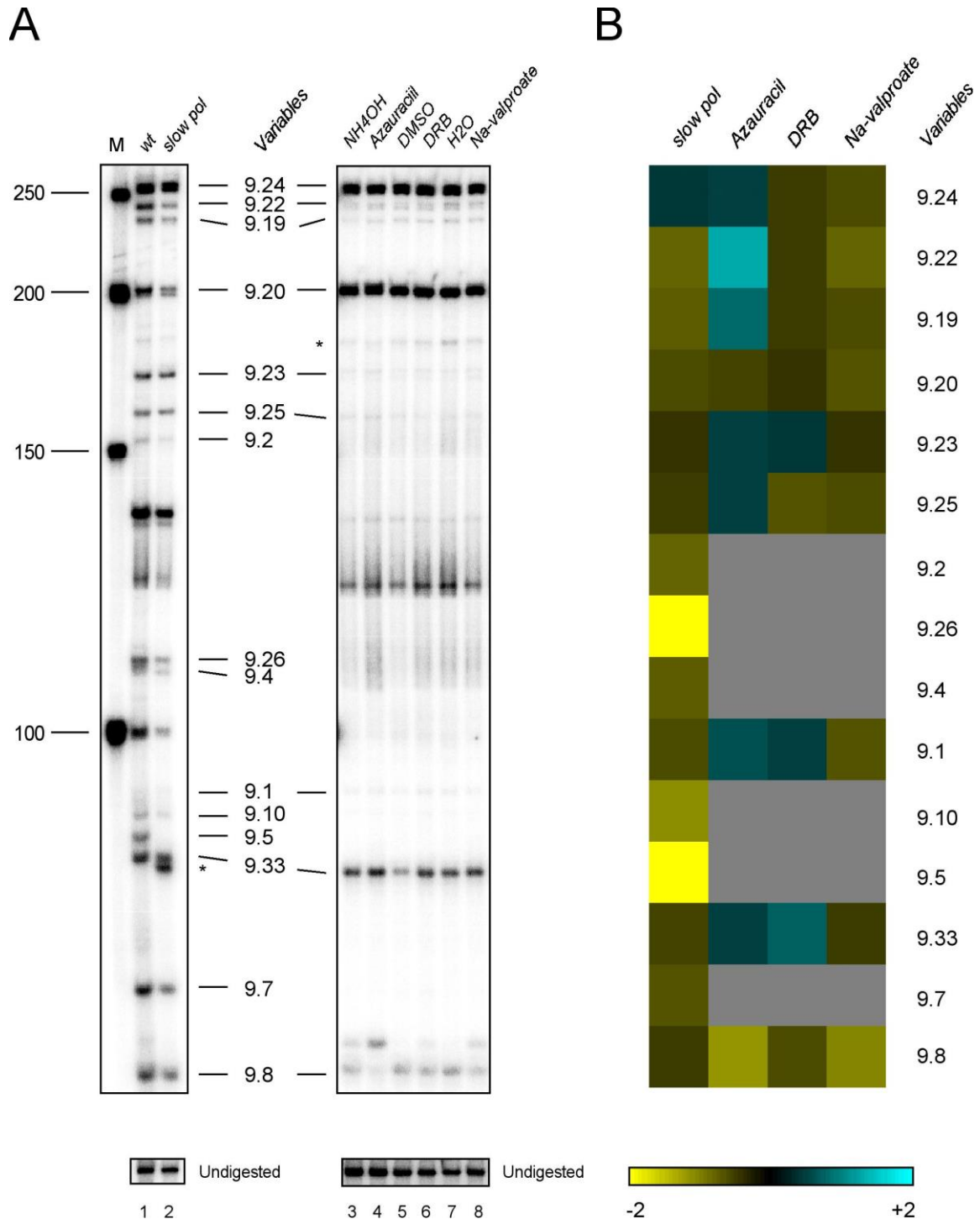


Figure 40: RNA pol II processivity does not influence splicing of *Dscam*. (A) Analysis of *Dscam* exon 9 splicing pattern using RNA extracted from 14-18 h old mutant embryos of C4 slow polymerase (Lane 2) and using RNA extracted from S2 cells after 12 h of exposure to 100 µg/ml azauracil (Lane 4), 100 µg/ml DRB (Lane 6) and 0.83 mg/ml Na-valproate (Lane 8). *Canton S* embryos served as control for the C4 mutant (Lane 1); solvents *NH*₄OH (Lane 3), DMSO (Lane 5) and water (lane 7) served as controls for azauracil, DRB and Na-valproate, respectively. (B) Heat map representation of *Dscam* splicing changes observed in A. Exon 9 variants not detected are represented in grey. *Dscam* exon variants were separated as explained in figure legend 22. Unspecific bands are indicated by asterisks (*). Samples were run on an 8% denaturing polyacrylamide gel. M=50bp ladder (NEB).

RNA pol II mutant, exon 9.26 was severely downregulated by over ten-fold and exon 9.5 was not detected. However, this change does not support the relation between lower elongation rate and increased inclusion of alternative exons as none of the exons showed significant upregulation.

3.12. *Dscam* diversity is not generated by differential stability of isoforms

Although the sequence contribution of variable exons to the overall length of *Dscam* mRNA is minor (<0.1%) and variable exons have very similar sequences, these sequences could affect stability of *Dscam* mRNAs. To test if sequence variation provided by the variable exons contributed to the stability of *Dscam* isoforms, and this way affected steady state levels of different isoforms, the stability of *Dscam* mRNAs was analyzed in S2 cells by stopping transcription with Actinomycin D (Murph et al., 2007). Analysis of *Dscam* exon 4 splicing pattern over a time course of 2 h, 4 h and 8 h post Actinomycin D treatment showed no significant change in the levels of *Dscam* exon 4 variants, which suggested that *Dscam* diversity, is not generated by differential stability of its isoforms (Figures 41A and B).

3.13. Development of a *Dscam* exon 9 reporter transgene recapitulating endogenous exon 9 splicing

To analyze the sequence elements directing the inclusion of exon 9 variants, a reporter gene is required. Therefore, the exon 9 variable cluster was inserted with

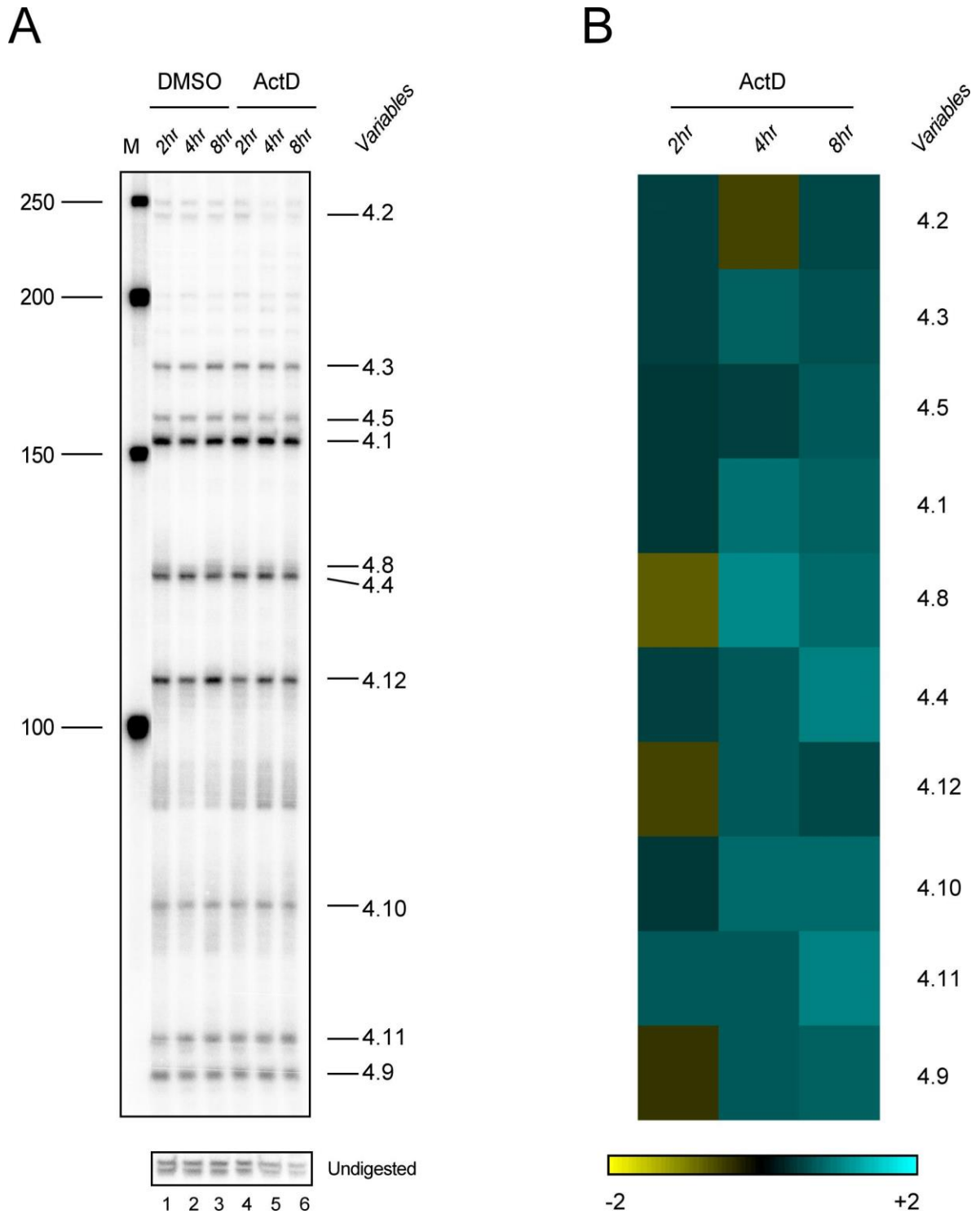
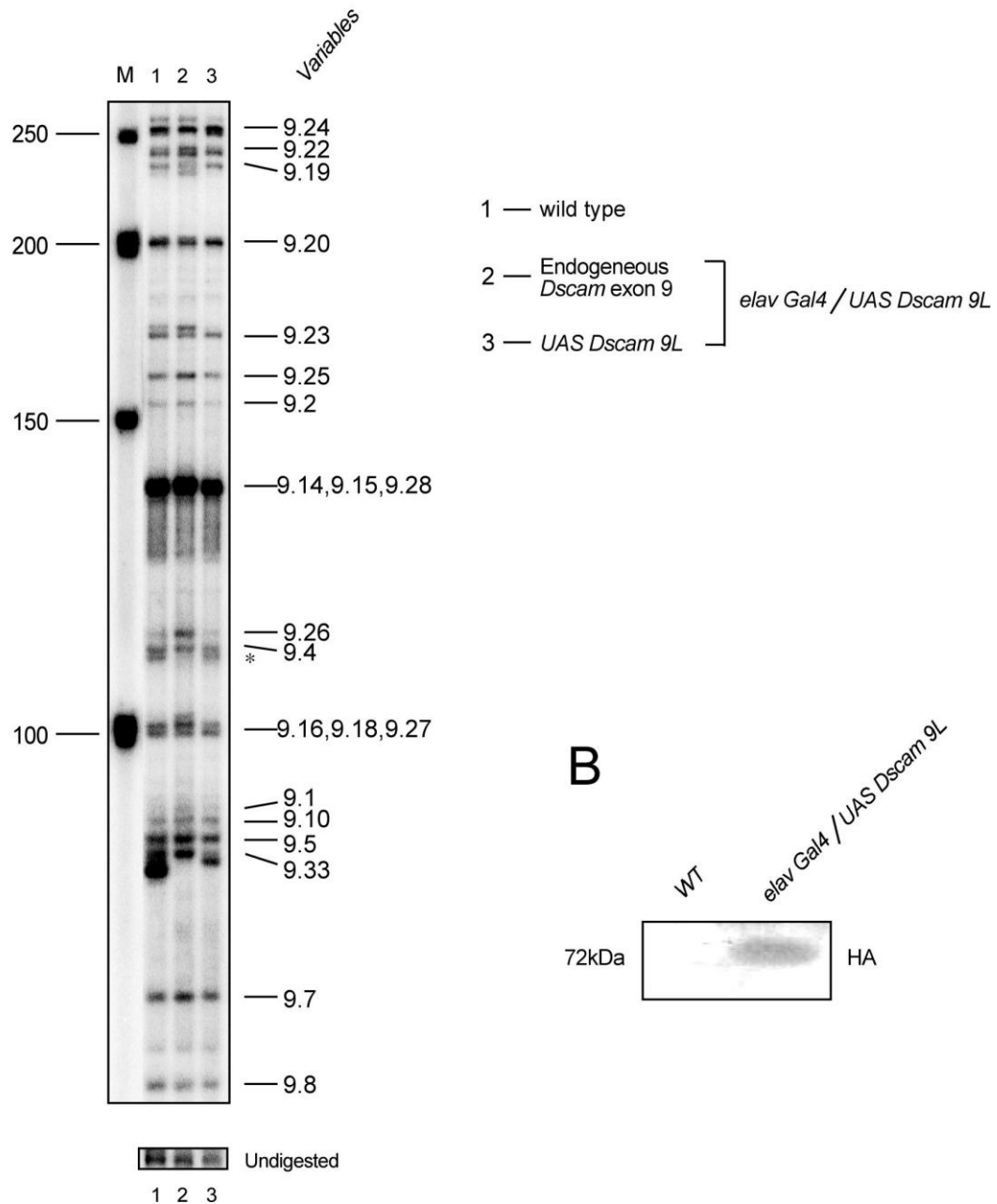


Figure 41: *Dscam* diversity is not generated by differential stability of isoforms. (A) Analysis of *Dscam* exon 4 splicing by using RNA extracted from S2 cells exposed to 10µg/ml Actinomycin D over a time course of 2 h (Lane 4), 4 h (Lane 5) and 8 h (Lane 6). S2 cells treated with DMSO over a time course of 2 h (Lane 1), 4 h (Lane 2) and 8 h (Lane 3) served as controls. (B) Heat map representation of *Dscam* splicing changes observed in A. *Dscam* exon variants were separated as explained in figure legend 21. Unspecific bands are indicated by asterisks (*). Samples were run on an 8% denaturing polyacrylamide gels. M=50bp ladder (NEB).

flanking constant exons 7 and 8 at the distal end and exons 10 and 11 at the proximal end into a UAS reporter construct and generated a transgenic line at a defined genomic location using phiC31 recombination (Bischof et al., 2007; Venken et al., 2006). Using the phiC31 transformation system, allows insertion of modified reporter transgenes at exactly the same position to control for position effects. To be able to distinguish endogenous *Dscam* transcripts originating from the reporter transgene, a reporter sequence for reverse transcription was included.

Analysis of a transgene inserted at the landing site at 76A2 on the third chromosome revealed that it recapitulated the splicing pattern observed from endogenous *Dscam* when expressed with elavGAL4 (Figures 42A; Lane 3 and 43B).

A



B

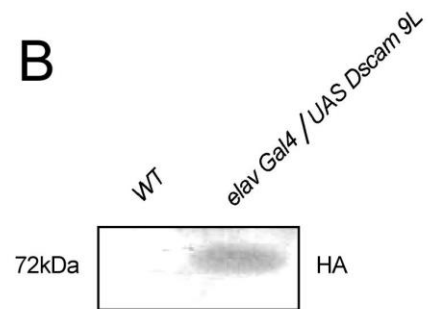


Figure 42: Development of a *Dscam* exon 9 reporter transgene recapitulating endogenous exon 9 splicing (A) Analysis of endogenous *Dscam* exon 9 splicing pattern using RNA extracted from 14-18 h old *Canton S* (Lane 1) and *elavGal4/UAS Dscam 9L* (Lane 2) embryos; and exogenous *Dscam* exon 9 splicing pattern in *elavGal4/UAS Dscam 9L* embryos (Lane 3). *Dscam* exon variants were separated as explained in figure legend 22. Samples were run on an 8% denaturing polyacrylamide gel. (B) Western blot confirming expression of *UAS Dscam 9L* transgene driven by *elavGal4*. M=50bp ladder (NEB).

CHAPTER 4

DISCUSSION

The most striking feature about the *Dscam* gene is its enormous molecular diversity generated by mutually exclusive splicing of its four variable exon clusters, namely 4, 6 and 9 and 17 comprising 12, 48, 33 and 2 variable exons, respectively. Although, all exons in the variable clusters have splice sites comparably similar to the consensus sequence, only one exon is included at a time and no splicing together of adjacent exons is observed (Schmucker et al., 2000). It is still unclear how these exon clusters are kept in a repressed state and how inclusion of specific exons by release of this repression is regulated. Particularly intriguing, pathogen exposure in mosquitoes results in a change of *AgDscam* splicing pattern favouring inclusion of isoforms that show higher binding affinity towards pathogen recognition (Dong et al., 2006). These experiments suggest that *Dscam* splicing is under strict regulation by exogenous and endogenous cues. In the immune system, these cues are pathogens, which are recognized by *Dscam* and endocytosed by haemocytes and in the nervous system they are the neighbouring neurons that need to acquire a different complement of *Dscam* isoforms to allow for axon bifurcation in mushroom body neurons and generation of overlapping dendritic fields in dendritic arborization sensory neurons (Dong et al., 2006; Matthews et al., 2007; Zhan et al., 2004).

The work described in the present thesis established a method to analyze *Dscam* splicing in the variable exon clusters where all exons have nearly the same length, but have sequences divergent enough to allow their separation on denaturing acrylamide gels by prior digestion with restriction enzymes. With this approach, the

exon 4 cluster was completely resolved and more than 50% of the exon 9 variants could be separated. However, the exon 6 cluster resolution was limited due to the large number of variables. The main limiting factor in exon 6 cluster is the short lengths of individual exon variants and their limited sequence variability, thus limiting the choice of restriction enzymes. Given that next generation sequencing techniques, (e.g. Illumina and 454 sequencing) are becoming cost effective, they can be applied to analyze *Dscam* splicing. One limitation to apply e.g. Illumina sequencing for amplicon analysis is the large capacity these machines have been currently designed for requiring combining multiple samples that are identified by unique bar codes. Next generation sequencing would also aid in recognizing the unexpected bands that were observed during the study, which could either be PCR artifacts or sequence associated mobility shifts. It is highly unlikely that the unexpected bands could be generated due to polymorphisms, resulting in generation or omission of a restriction site, because an almost identical *Dscam* splicing pattern was observed between numerous different strains.

A key feature of *Dscam* in mosquitoes is the change in its splicing pattern on pathogen exposure (Dong et al., 2006), and it was demonstrated that pathogen exposure also induced changes in *Dscam* splicing in *Drosophila*. Contrary to the expectation, however, the changes observed in *Dscam* splicing in *Drosophila* were rather mild with either heat inactivated or untreated *E. coli* resulting in differential regulation of only a few exons.

It remains to be shown that the isoforms that were highly upregulated show very high binding affinity with the treated *E. coli*. Adaptation to pathogen exposure by producing high affinity pathogen binding isoforms has also been observed in crayfish.

Moreover, coating pathogens with these high affinity binding isoforms allows the pathogens to escape phagocytosis (Watthanasurorot et al., 2011). Thus, *Dscam* splicing across arthropods appears to have a common feature of being sensitive to pathogenic triggers such that they alter *Dscam* diversity to generate a repertoire that allows better recognition, stronger binding and effective defense to the host against the invading pathogen.

Dscam splicing pattern changes upon pathogen exposure or in certain developing neurons to unique signatures of variable exons for immune defense or neuronal wiring, respectively (Dong et al., 2006; Matthews et al., 2007; Neves et al., 2004). However, it was found that the *Dscam* splicing pattern in individual flies is quite robustly maintained and seems not to change between individuals. This suggested that variation in *Dscam* splicing might be specific to certain cell types such haemocytes, mushroom body neurons and da sensory neurons. A different mode of *Dscam* splicing regulation is indeed indicated from the analysis of projection of mechanosensory neurons in the ventral nerve cord. Here, reduced *Dscam* variability results in projection defects, which intriguingly had no effect on axon branching in mushroom body neurons. These results indicate that isoforms, specific to certain neurons, have counterparts in the areas where these neurons project to establish connectivity with their target cells (Chen et al., 2006). In this context, *Dscam* would acquire a cell type specific splicing pattern, which would need to be recapitulated in those cells located in the remote location in the brain. Since many neurons and also their precursors migrate during neuronal development, a common origin could result in the same *Dscam* splicing pattern. For example, segmental identity generated by

hox gene expression might be sufficient to generate a regionalized *Dscam* spliceform repertoire.

The very reproducible splicing pattern observed in various developmental contexts, makes it possible to interrogate the regulation of *Dscam* splicing by using mutants in various candidate genes for splicing regulation. One such candidate that was analyzed is *ago1*, which has similar developmental defects in the nervous system as *Dscam* (Kataoka et al., 2001).

Argonautes are further attractive candidates as they suggest an RNA mediated mechanism involved in reinforcement of splicing to a specific isoform upon encounter of a trigger via a relay of signal from the cell surface to the nucleus. Further analysis of mutants in genes involved in RNA mediated regulation and over expression of a single isoform did not further support such a hypothesis of an RNA mediated mechanism in canalization of *Dscam* diversity. Rather, the effect of Argonautes, as well as of other factors identified in this study in the regulation of *Dscam* splicing are cluster specific suggesting unique regulatory mechanisms directed by cluster dedicated factors. In *Giardia lamblia*, an RNAi mechanism is involved in generating diversity of variant-specific surface protein (VSP) genes. Here, all VSP genes are transcribed at a similar rate but except for a single transcript, all others are degraded by RNAi. From time to time, expression of VSP protein switches from one to another by changing the transcript complements degraded by RNAi (Prucca et al., 2008). Such a mechanism could potentially also apply to generate *Dscam* diversity. If this was the case, it could be expected that different *Dscam* isoforms would have different half lives resulting in different levels of inclusion of variable exons. When analyzing stability of *Dscam* isoforms, however no evidence for such a mechanism.

elav mutants show nervous system defects similar to *Dscam* mutants (Simionato et al., 2007) and indeed it was found that *Dscam* splicing regulation is particularly affected in exon 9 cluster. Analysis of the sequence in exon 9 cluster together with the lack of experimental evidence so far obtained for the identification of ELAV targets argues that *elav* regulates *Dscam* splicing indirectly. Indeed, many of genes differentially regulated in *elav* mutants encode for regulators of gene expression involving RNA binding proteins, DNA binding proteins and chromatin remodeling factors. Analysis of *Dscam* exon 9 splicing by mutants of such genes revealed that *Dscam* splicing is very sensitive to changes in mutants of regulators of gene expression. Intriguingly, many exons were observed to be upregulated or downregulated in a specific set of mutants. However, none of the mutants regulated the splicing of just one exon variant. The screen revealed that *Dscam* splicing is very sensitive to genetic perturbation.

4.1. Future work

Given the biological complexity of higher vertebrates, it is assumed that mammalian genes involved in development of the nervous system are more in number and more complex than invertebrate genes. *Dscam* is an exceptional example of a highly complex gene in relatively simple arthropods. Despite vast structural differences between the insect *Dscam* and mammalian *DSCAM*, they share important roles in neuronal patterning. Understanding the molecular mechanisms of *Dscam* function in different organisms and species would reveal important clues about the evolution of CAMs into recognition units involved in neural wiring and immune recognition.

The key to understanding the dual role of *Drosophila Dscam* in the immune and nervous systems lies in its unique mechanism of generating extraordinary diversity. It is still unclear, which external cues trigger a change in alternative splicing of *Dscam*. Also, a unique mechanism whereby a neuronal or pathogenic trigger may result in the selection of a specific exon or set of exons in each variable cluster is unknown. Last but not the least, it would be interesting to determine if the *Dscam* sequence itself has a role to play in exon selection.

It is crucial to find an external cue which would trigger a signal for change in *Drosophila Dscam* alternative splicing. S2 cells could be exposed to pure microbial cell surface determinants such as lipopolysaccharides or peptidoglycans and analyzed for changes in *Dscam* alternative splicing. Isoforms undergoing a change in inclusion can be silenced in S2 cells to test their ability to phagocytose pathogens expressing the specific cue. Contrarily, pathogens that are mutant for the specific cue can be used to challenge S2 cells to observe, possibly, no splicing changes in the affected alternative exons. An alternative approach of investigating the role of *Dscam* in the *Drosophila* immune system could be to expose flies, mutant for genes that play a role in the immune system (e.g. *imd*, *relish*, *dorsal* and *Myd88*) with live or attenuated pathogens and subsequently test for *Dscam* splicing changes in their haemocytes.

In this study, an exon 9 reporter transgene (*UAS Dscam 9L*), expressed heterologously, has been shown to recapitulate endogenous exon 9 splicing pattern, which suggests that the information regulating exon 9 alternative splicing lies within the cluster sequence itself. To further speculate which sequence elements within the cluster are crucial for selection of particular exon variants, different sequence altering

strategies may be adopted. Firstly, deletion of combinations of consecutive introns and exons such as, deletion of an intron and its preceeding or succeeding exon or an exon and its flanking introns, resulting in fusion of two alternate exons, may affect splicing of neighbouring exons. Secondly, reversing the sequence of an intron may influence the splicing of its adjoining exons. Thirdly, mutating the sequence of a particular intron could disrupt its RNA secondary structure which may alter the splicing of its flanking exons. Finally, swapping selective intronic sequences of one variable cluster into another may regulate its default splicing pattern such that an intron, which causes enhanced inclusion of a particular exon 4 variant, when inserted in the exon 9 cluster before or after an exon variant showing low expression, may allow enhanced splicing of that exon 9 variant. Such an approach may help in understanding whether intronic or exonic sequences are important for selection of a particular *Dscam* exon variant.

Dscam is an extraordinary model to understand how a single gene plays vital roles in the nervous and immune systems. Unravelling the enigma around the splicing mechanism of this unique pattern recognition receptor may throw light on unexplored mechanisms of immune defence in vertebrates.

Appendices

A1. Separation of *Dscam* 4 variants. The table shows all *Dscam* exon 4 variants, their annotated lengths, identifying enzymes and expected lengths on a denaturing polyacrylamide gel after restriction digest.

Exon	Variable no.	Variable length	Enzyme	Fragment size
4	2	162	-	238
4	3	162	Mbol	173
4	5	162	TaqI	157
4	7	162	TaqI	152
4	1	162	TaqI	151
4	8	171	Mbol	124
4	4	171	TaqI	123
4	12	171	HinP1I	106
4	10	171	TaqI	79
4	6	162	HinP1I	67
4	11	159	TaqI	64
4	9	168	AluI	61

A2. Separation of *Dscam* 9 variants. The table shows all *Dscam* exon 9 variants, their annotated lengths, identifying enzymes and expected lengths on a denaturing polyacrylamide gel after restriction digest.

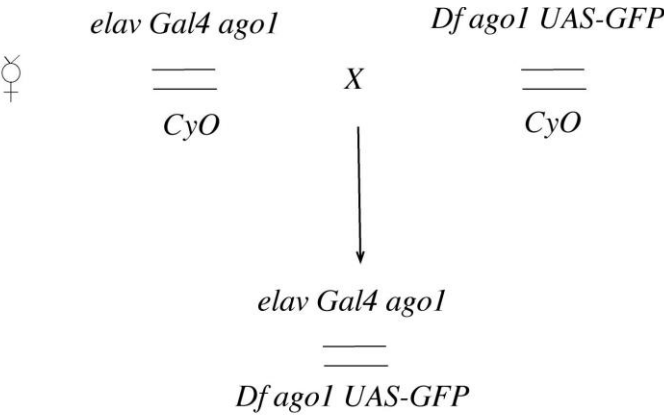
Exon	Variable no.	Variable length	Enzyme	Fragment size
9	24	288	HaeIII	261
9	13	299	MspI	253
9	22	288	MspI	241
9	21	288	HpyCH4IV	233
9	19	288	HaeIII	231
9	20	288	HpyCH4IV	197
9	6	291	XmnI	174
9	23	288	MspI	169
9	25	288	XmnI	158
9	2	288	HaeIII	151
9	14	288	BstNI	134
9	15	288	BstNI	134
9	28	288	BstNI	134
9	11	291	HpyCH4IV	132
9	26	288	MspI	109
9	17	288	BstNI	108
9	4	288	MspI	107
9	16	291	BstNI	99
9	18	288	BstNI	99
9	27	288	BstNI	99
9	1	306	HaeIII	90
9	10	291	BstUI	87
9	5	291	MspI	85
9	33	294	HpyCH4IV	82
9	7	291	BstUI	73
9	31	285	HpyCH4IV	67
9	8	291	HaeIII	66
9	12	285	HaeIII	63
9	29	294	MspI	52
9	3	288	BstNI	33
9	9	291	BstUI	33
9	32	279	BstNI	33
9	30	288	BstUI	32

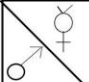
A3. Separation of *Dscam* 6 variants. The table shows all *Dscam* exon 6 variants, their annotated lengths, identifying enzymes and expected lengths on a denaturing polyacrylamide gel after restriction digest.

Exon	Variable no.	Variable length	Enzyme	Fragment size
6	20	124	-	152
6	29	124	AluI	145
6	32	121	AluI	136
6	1	124	BstNI	127
6	2	124	AluI	124
6	26	124	AluI	124
6	37	124	BstNI	121
6	46	124	BstNI	121
6	13	127	AluI	104
6	21	124	AluI	101
6	6	124	BstNI	100
6	22	124	AluI	95
6	24	124	BstNI	94
6	9	124	AluI	93
6	19	124	AluI	92
6	44	124	TaqI	91
6	41	124	BstUI	89
6	11	118	AluI	87
6	8	124	MboI	86
6	16	124	MspI	84
6	10	124	BstUI	83
6	23	124	MboI	81
6	3	124	BstUI	75
6	5	124	BstUI	75
6	30	124	TaqI	74
6	45	124	AluI	74
6	36	124	AluI	72
6	39	124	AluI	67
6	18	124	MboI	66
6	15	124	BstUI	65
6	28	124	MspI	62
6	47	116	MspI	61
6	35	124	BstUI	58
6	17	124	MboI	57
6	7	124	MboI	53
6	25	124	MboI	53

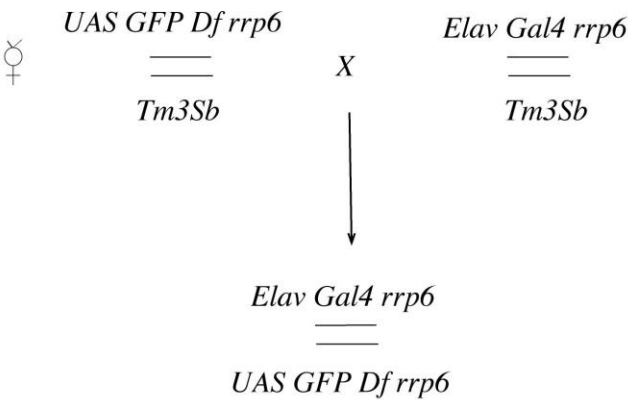
6	27	124	Mbol	53
6	38	124	Alul	52
6	33	127	Alul	46
6	40	128	Alul	46
6	42	124	Alul	46
6	48	121	Alul	46
6	43	124	BstNI	42
6	12	124	Alul	37
6	14	127	Mbol	37
6	34	121	TaqI	37
6	4	133	MspI	31
6	31	121	MspI	31

A4. Crossing scheme showing generation of zygotic *ago1* mutants



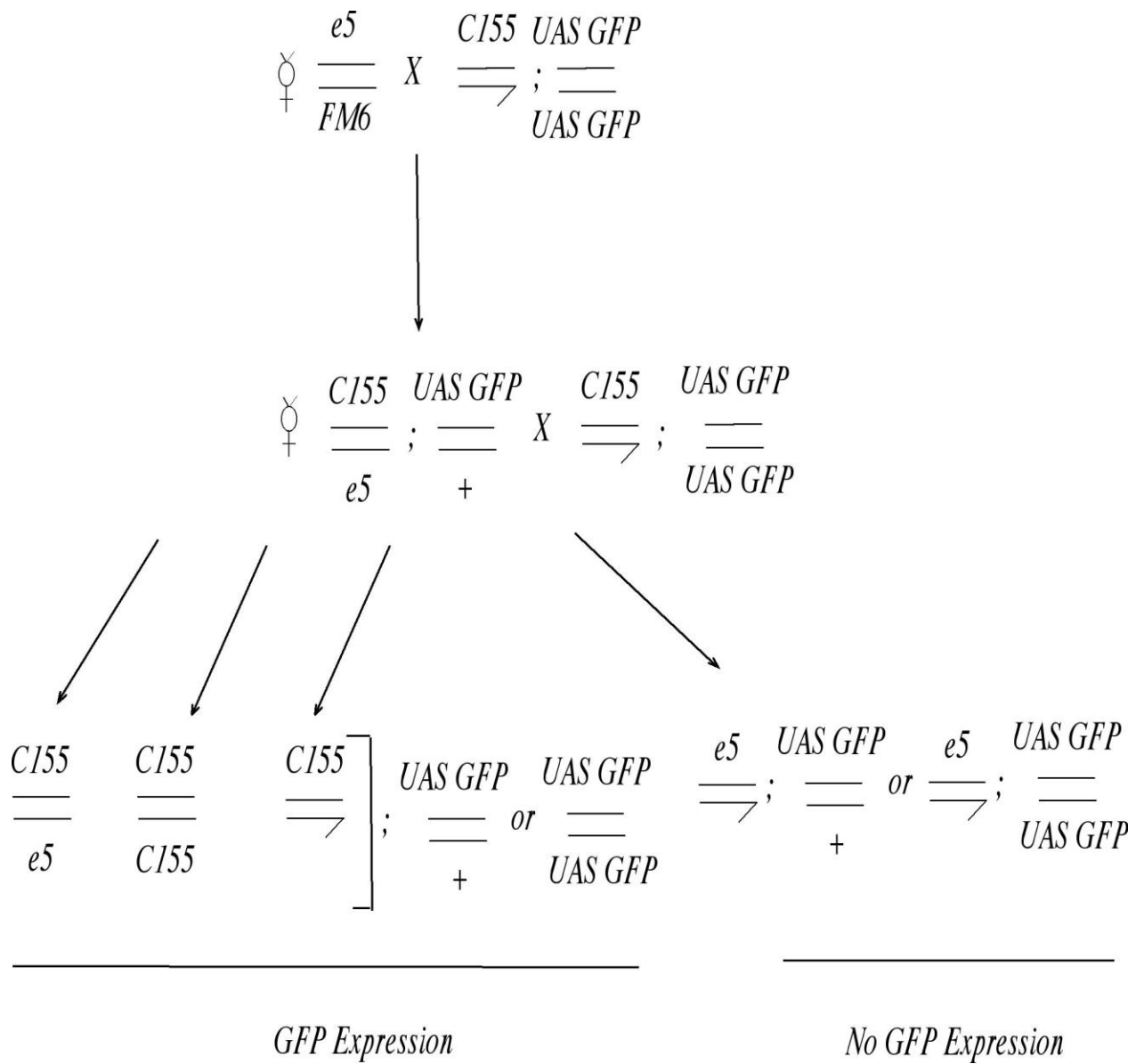
	<i>elav Gal4 ago1</i>	CyO
<i>Df ago1 UAS-GFP</i>	<i>elav Gal4 ago1</i> ===== <i>Df ago1 UAS-GFP</i> GFP Expression	<i>Df ago1 UAS-GFP</i> ===== CyO No GFP Expression
CyO	<i>elav Gal4 ago1</i> ===== CyO No GFP Expression	CyO ===== CyO Lethal

A5. Crossing scheme showing generation of zygotic *rrp6* mutants

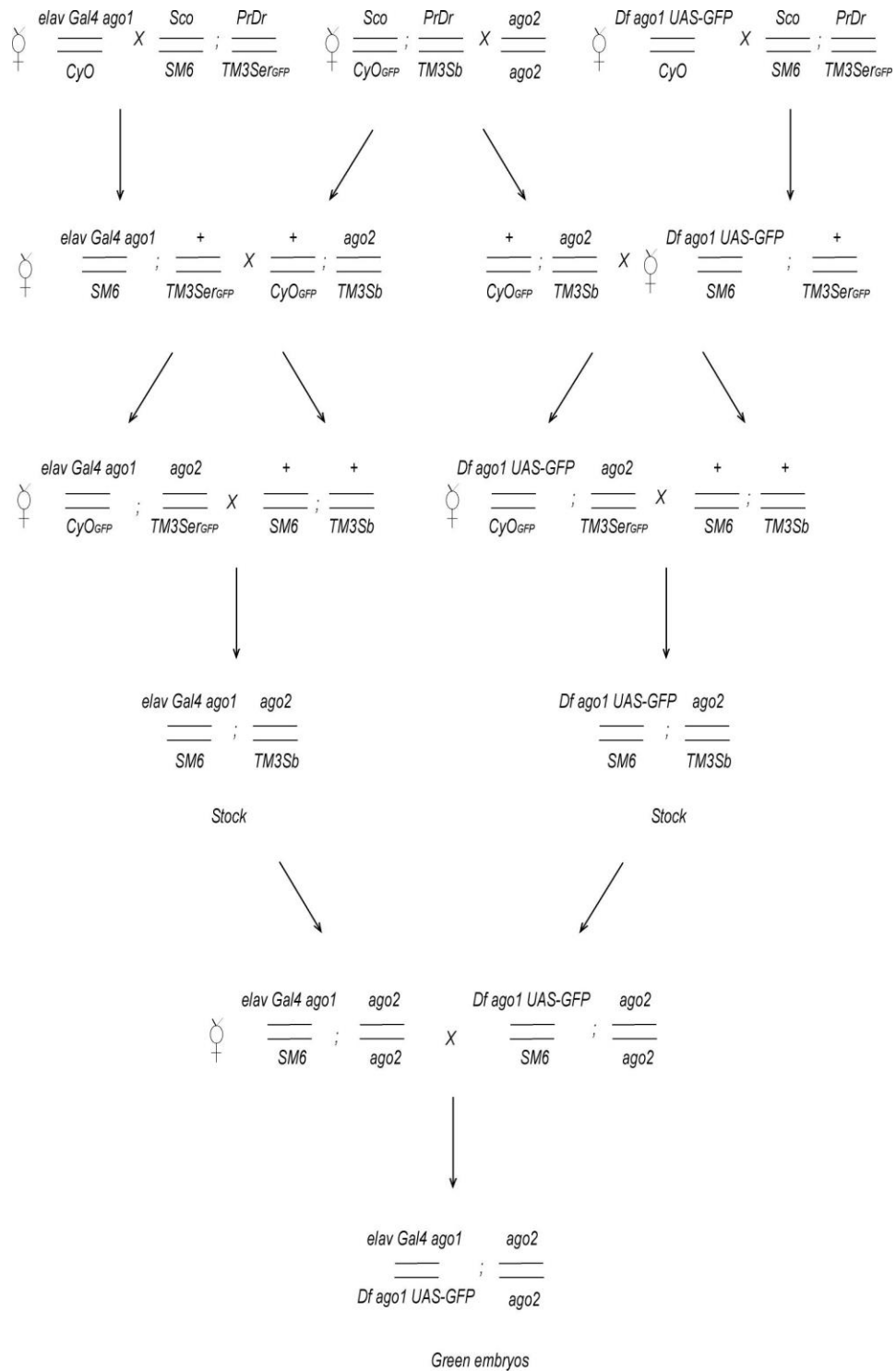


<div><div>♀</div><div>♂</div></div>	<i>UAS GFP Df rrp6</i> ==	<i>Tm3Sb</i> ==
<i>Elav Gal4 rrp6</i> ==	<div><i>Elav Gal4 rrp6</i> == <i>UAS GFP Df rrp6</i></div> <i>GFP Expression</i>	<div><i>Elav Gal4 rrp6</i> == <i>Tm3Sb</i></div> <i>No GFP Expression</i>
<i>Tm3Sb</i> ==	<div><i>UAS GFP Df rrp6</i> == <i>Tm3Sb</i></div> <i>No GFP Expression</i>	<div><i>Tm3Sb</i> == <i>Tm3Sb</i></div> <i>Lethal</i>

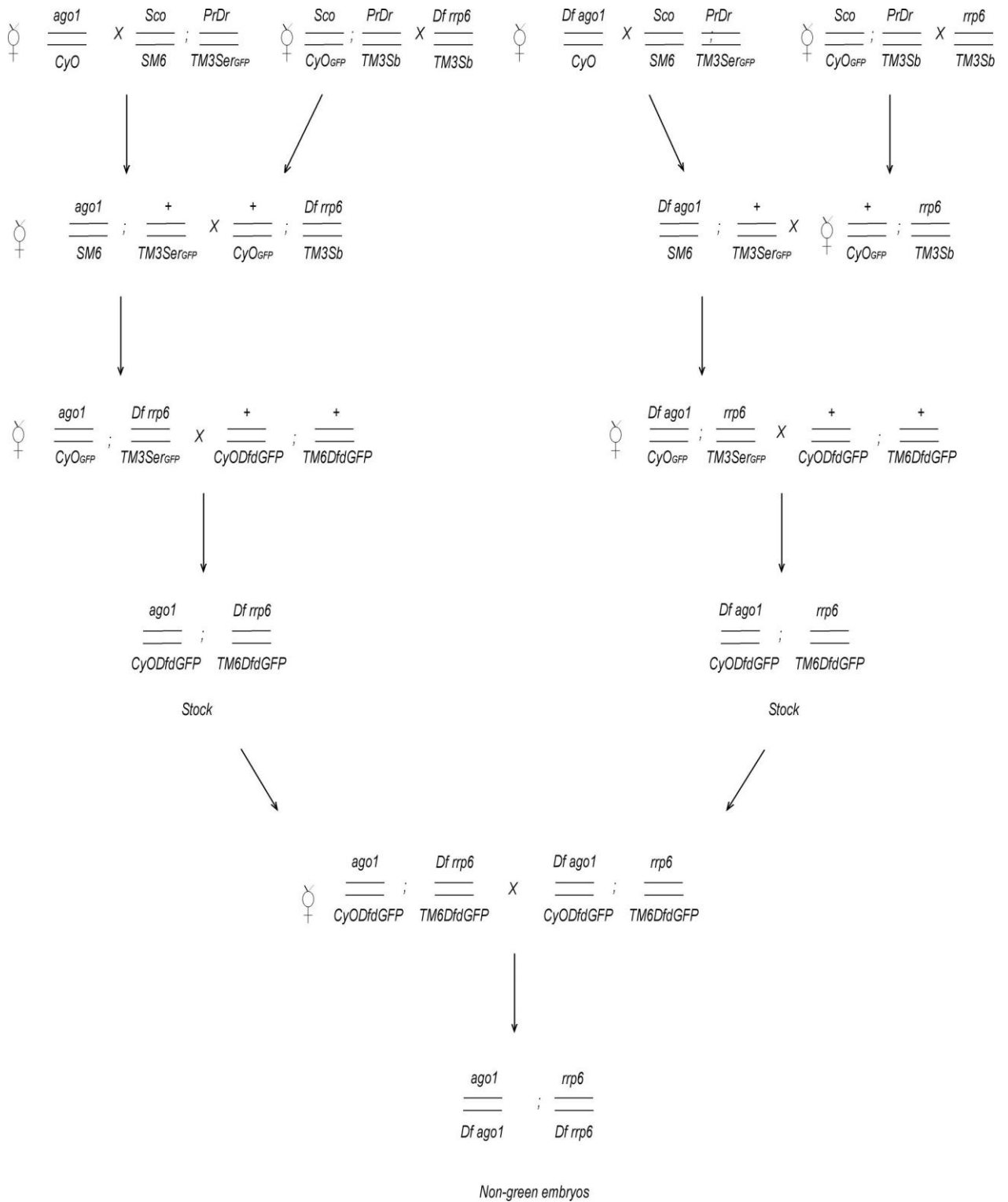
A6. Crossing scheme showing generation of zygotic *elav* mutants



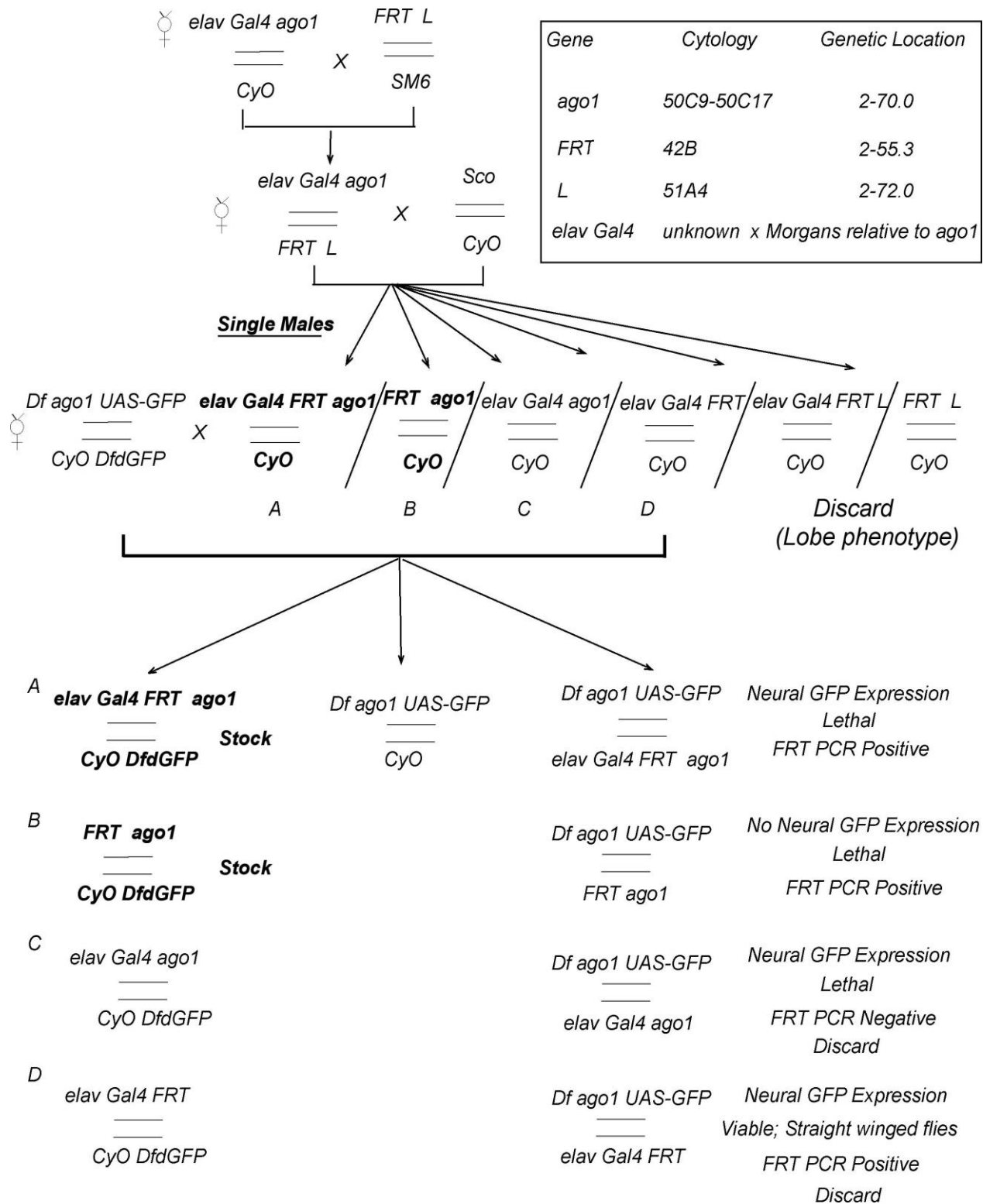
A7. Crossing scheme showing generation of *ago1/Df*; *ago2/ago2* double mutants



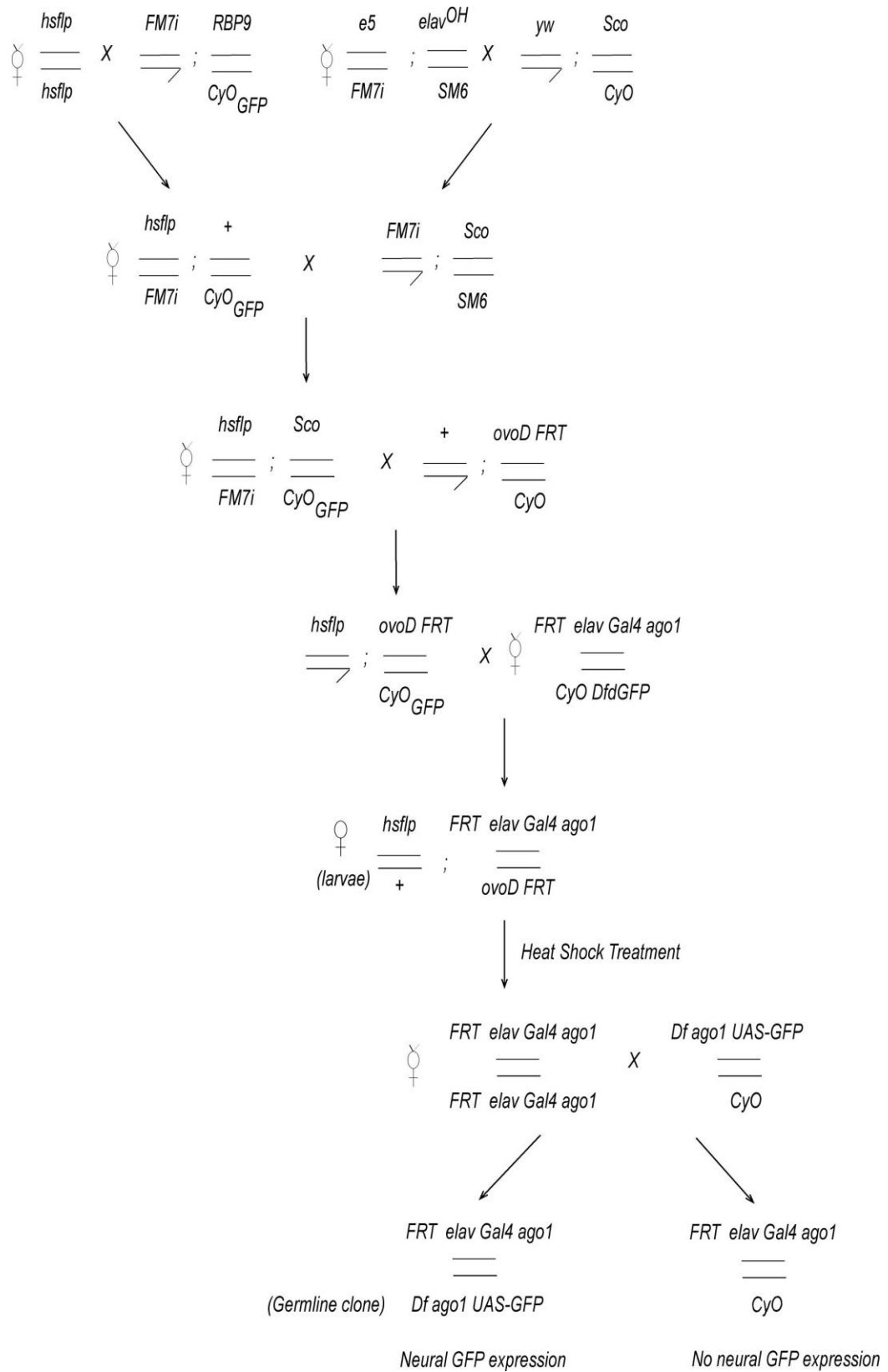
A8. Crossing scheme showing generation of *ago1/Df*; *rrp6/Df* double mutants



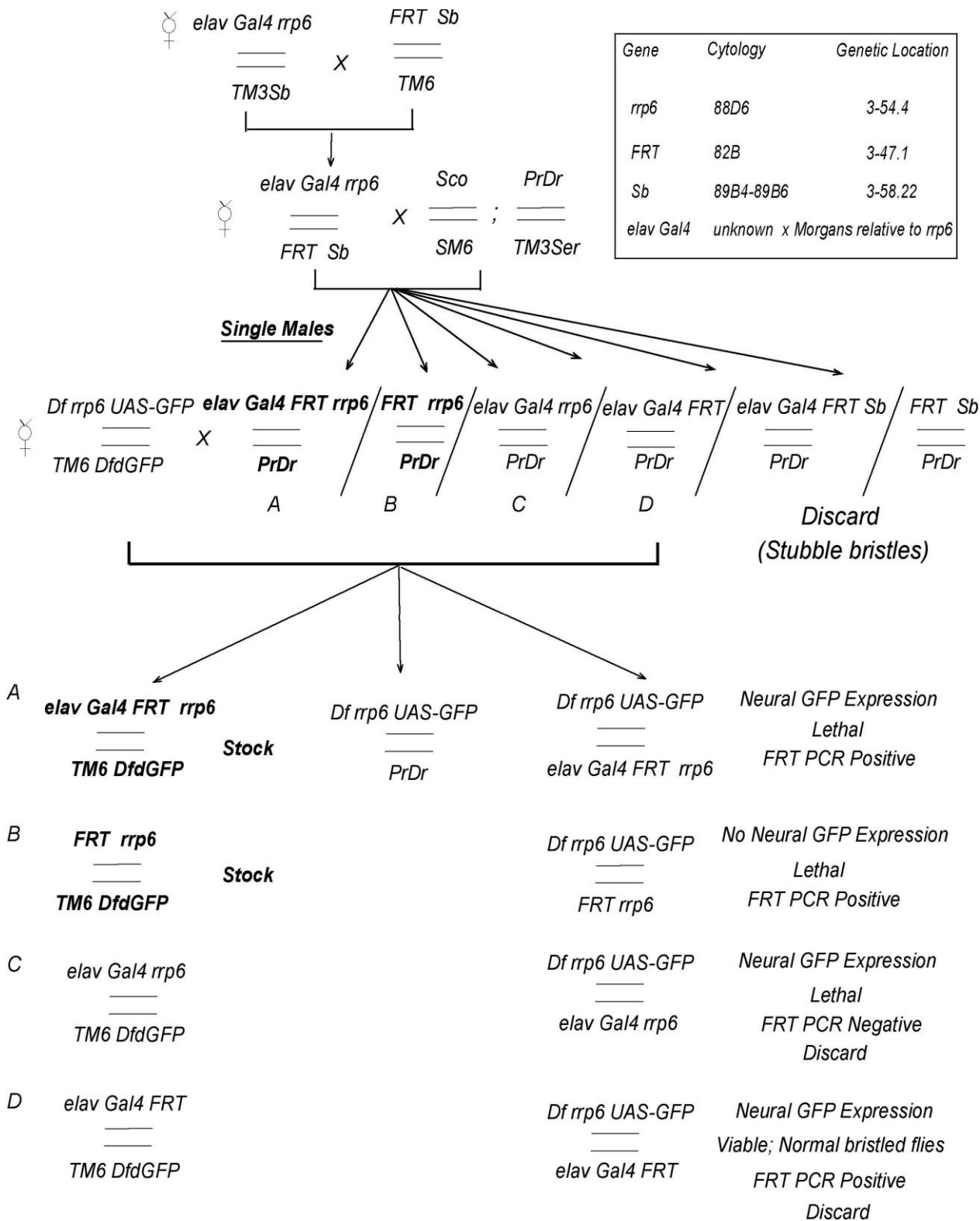
A9. Crossing scheme showing generation of *ago1* zygotic and maternal mutants



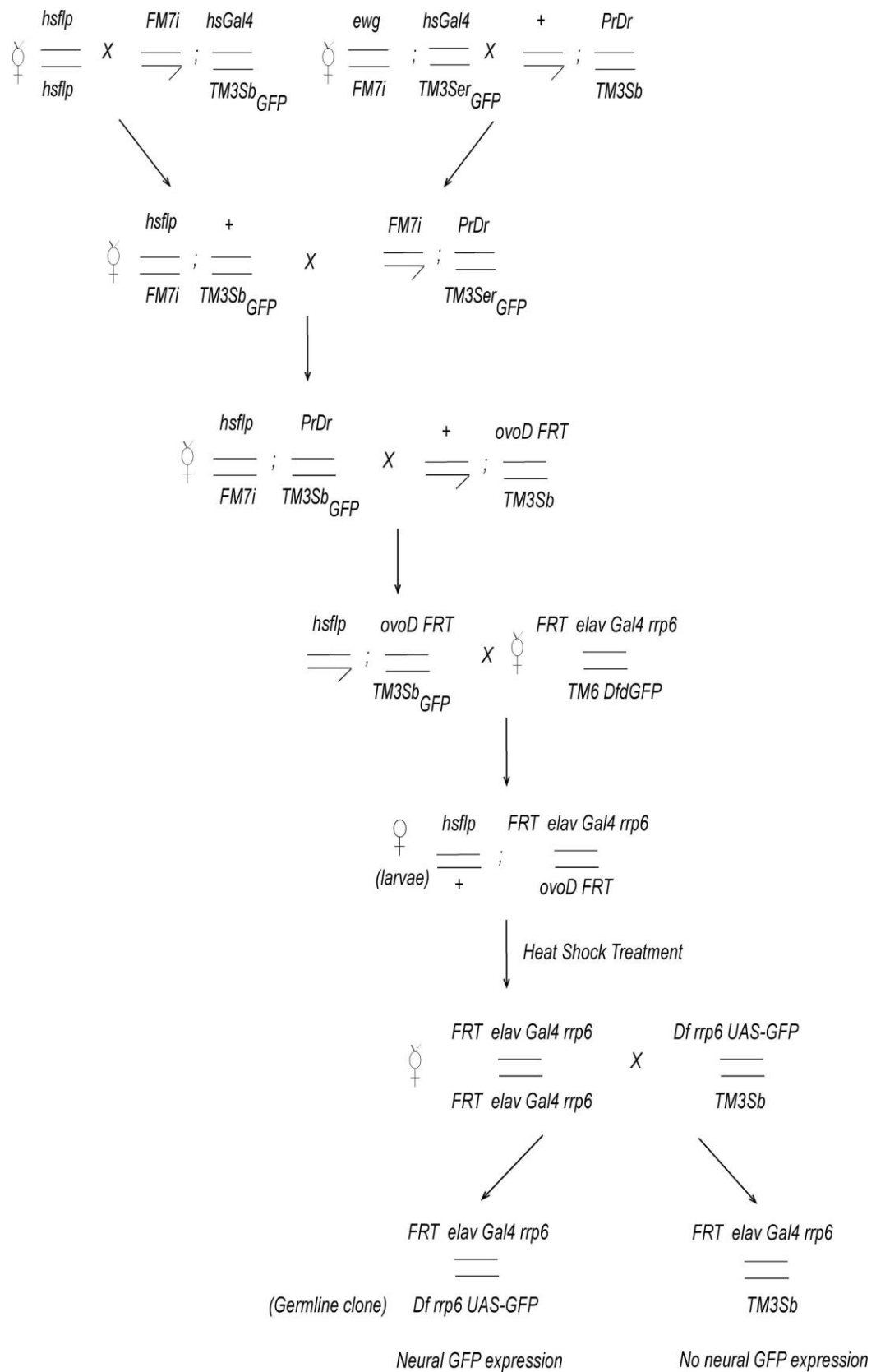
continued...



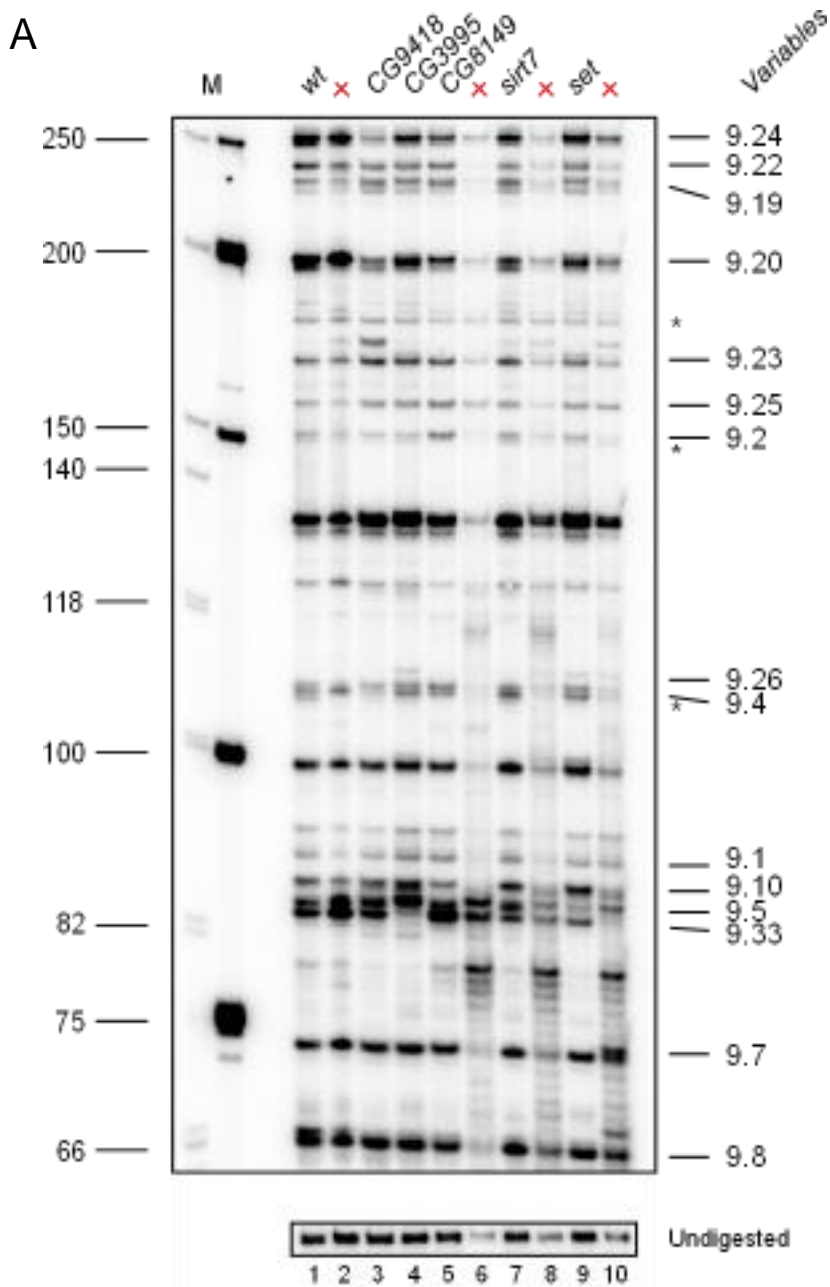
A10. Crossing scheme showing generation of *rrp6* zygotic and maternal mutants



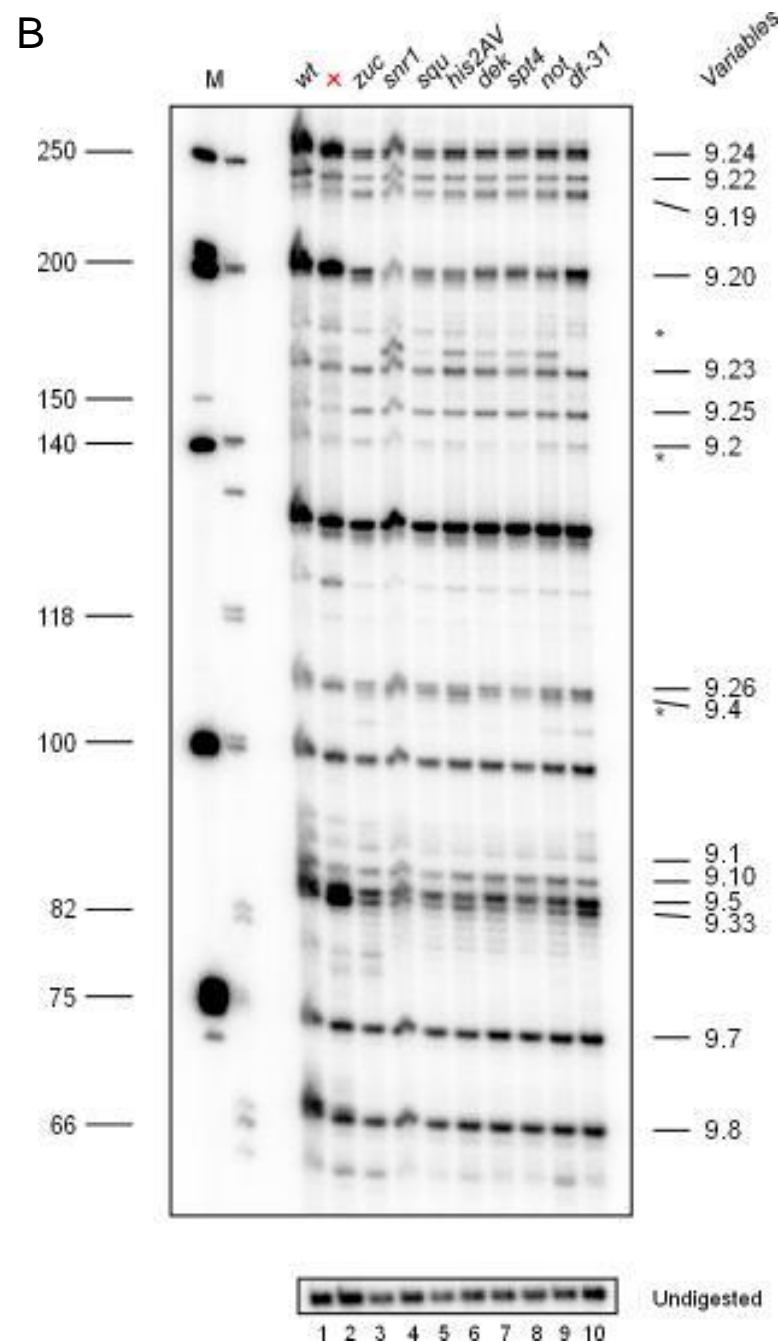
continued...



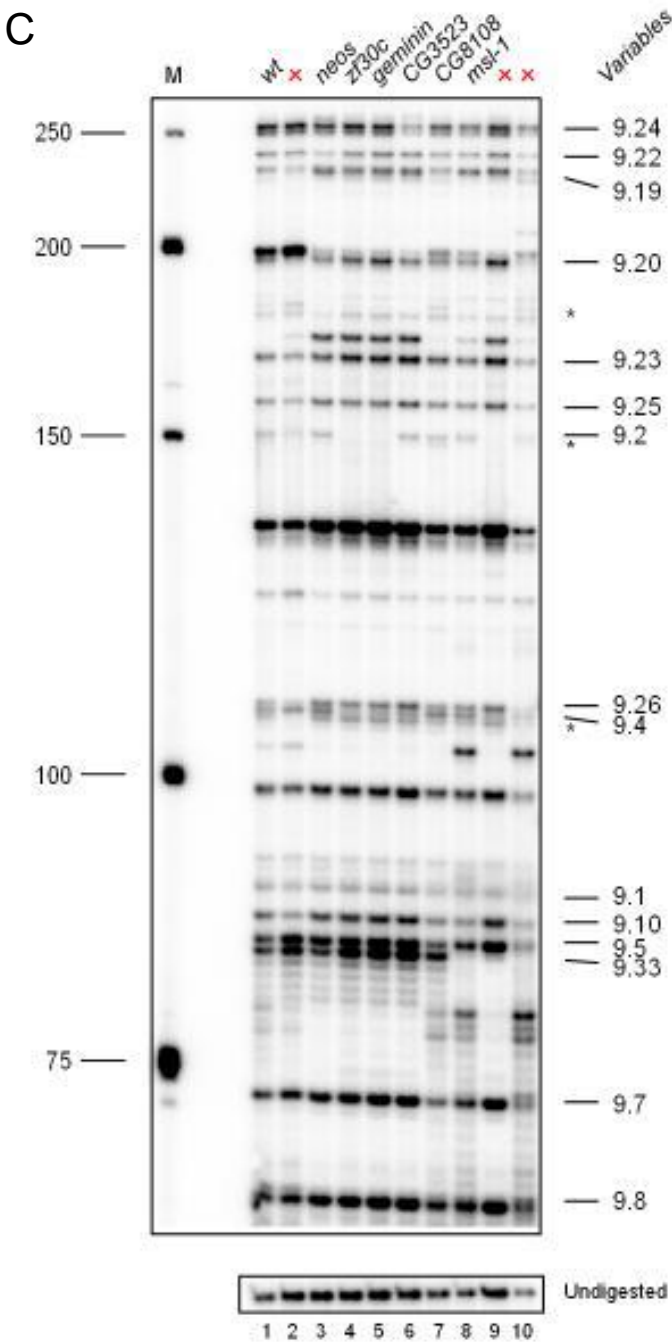
A11. Analysis of *Dscam* exon 9 splicing in mutants of genes that are differentially regulated in *elav* mutants. **(A)** Analysis of *Dscam* exon 9 splicing pattern using RNA extracted from 14-18 h old mutant embryos of *CG9418* (Lane 3), *CG3995* (Lane 4), *CG8149* (Lane 5), *sirt7* (Lane 7) and *set* (Lane 9). *Canton S* embryos served as control (Lane 1). Lanes with red crosses were not included in the analysis. *Dscam* exon variants were separated as explained in figure legend 22. Samples were run on an 8% denaturing polyacrylamide gel. M=phiX174 DNA/HinfI marker (Biotools).



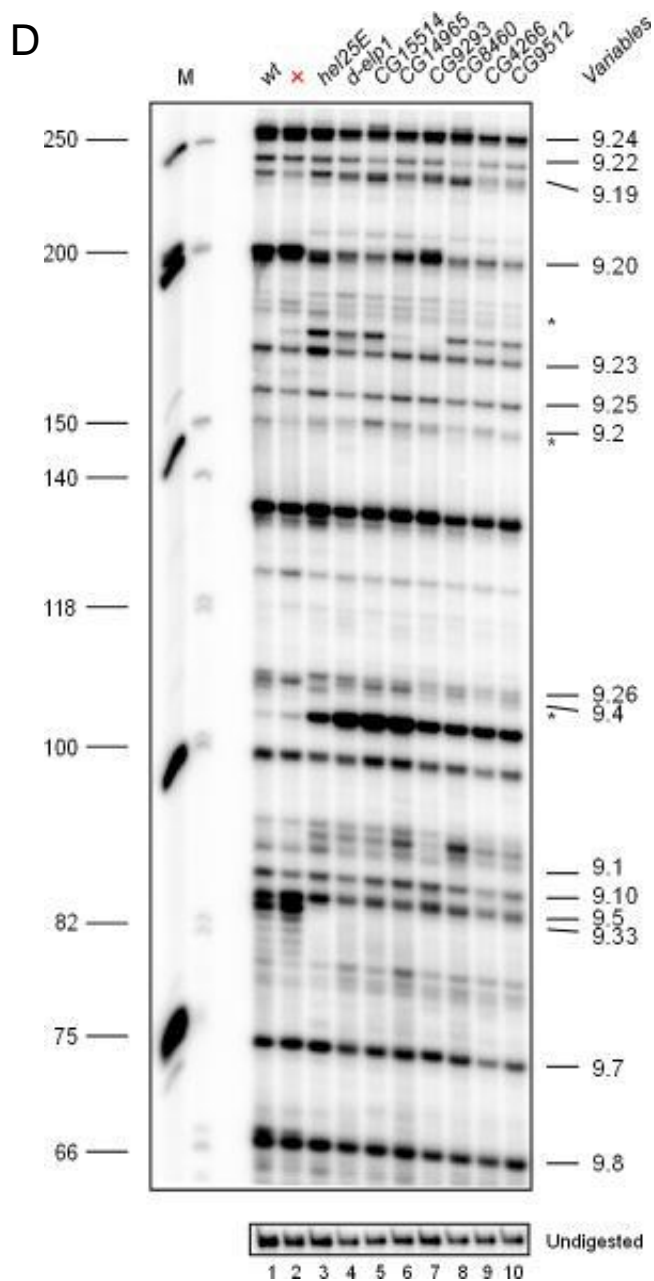
(B) Analysis of *Dscam* exon 9 splicing pattern using RNA extracted from 14-18 h old mutant embryos of *zuc* (Lane 3), *snr1* (Lane 4), *squ* (Lane 5), *his2AV* (Lane 6), *dek* (Lane 7), *spt4* (Lane 8), *not* (Lane 9) and *df-31* (Lane 10). *Canton S* embryos served as control (Lane 1). Lanes with red crosses were not included in the analysis. *Dscam* exon variants were separated as explained in figure legend 22. Samples were run on an 8% denaturing polyacrylamide gel. M=phiX174 DNA/HinfI marker (Biotools).



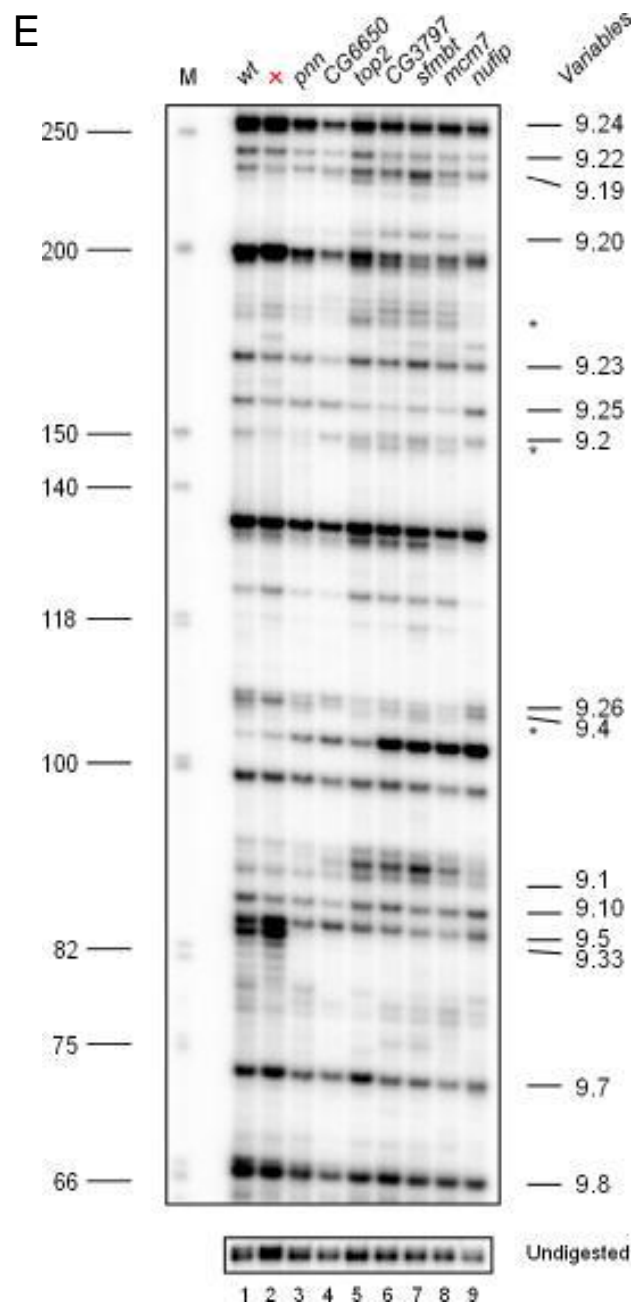
(C) Analysis of *Dscam* exon 9 splicing pattern using RNA extracted from 14-18 h old mutant embryos of *neos* (Lane 3), *zf30c* (Lane 4), *geminin* (Lane 5), *CG3523* (Lane 6), *CG8108* (Lane 7) and *msl-1* (Lane 8). *Canton S* embryos served as control (Lane 1). Lanes with red crosses were not included in the analysis. *Dscam* exon variants were separated as explained in figure legend 22. Samples were run on an 8% denaturing polyacrylamide gel. M=phiX174 DNA/HinfI marker (Biotools).



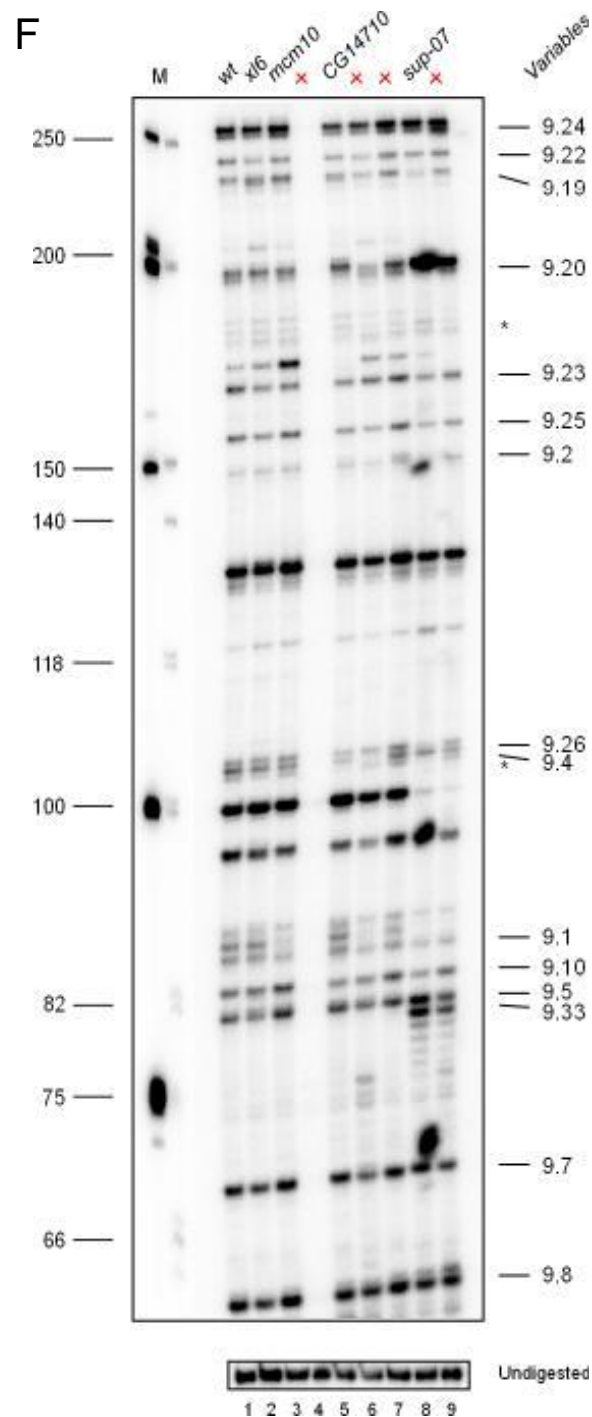
(D) Analysis of *Dscam* exon 9 splicing pattern using RNA extracted from 14-18 h old mutant embryos of *hel25E* (Lane 3), *d-elp1* (Lane 4), *CG15514* (Lane 5), *CG14965* (Lane 6), *CG9293* (Lane 7), *CG8460* (Lane 8), *CG4266* (Lane 9) and *CG9512* (Lane 10). *Canton S* embryos served as control (Lane 1). Lanes with red crosses were not included in the analysis. *Dscam* exon variants were separated as explained in figure legend 22. Samples were run on an 8% denaturing polyacrylamide gel. M=phiX174 DNA/Hinfl marker (Biotools).



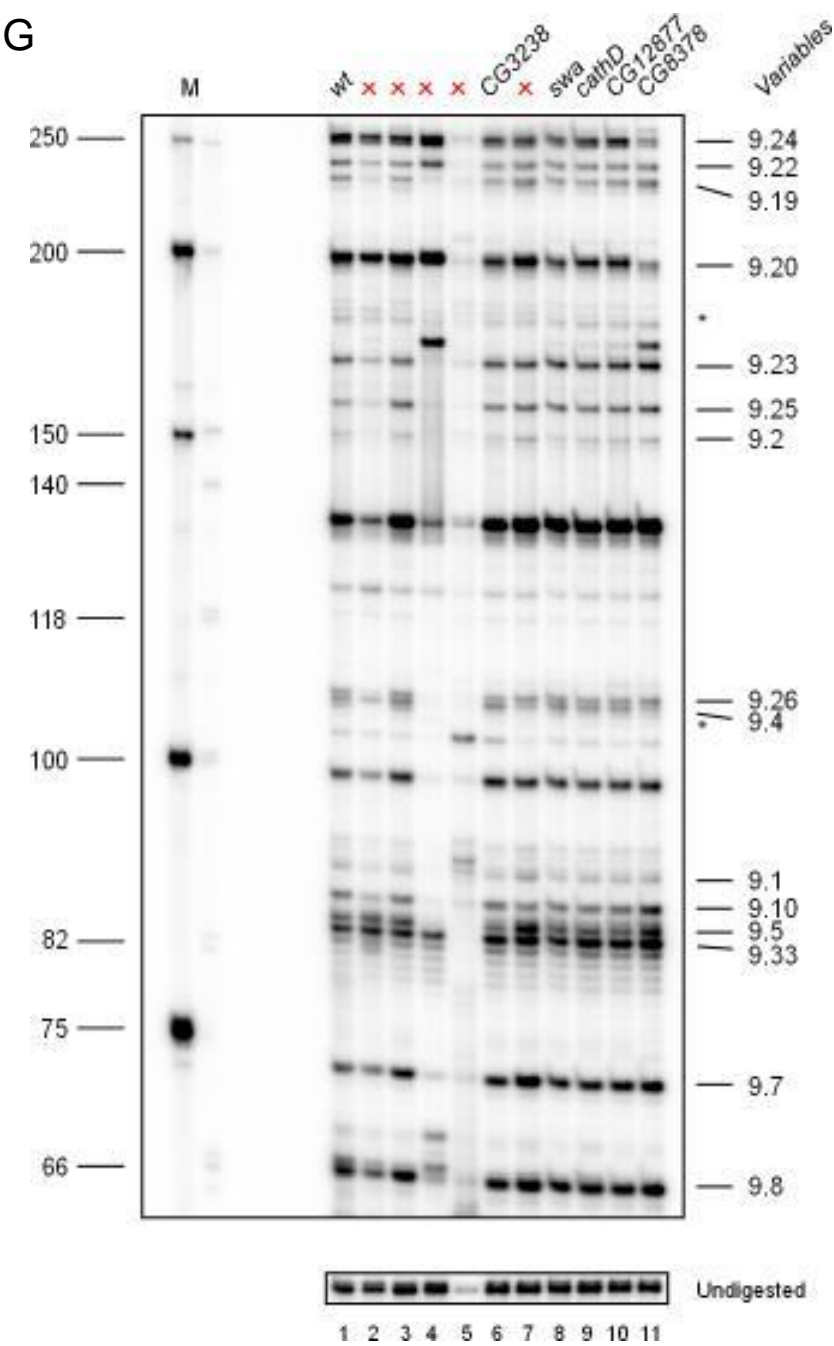
(E) Analysis of *Dscam* exon 9 splicing pattern using RNA extracted from 14-18 h old mutant embryos of *pnn* (Lane 3), *CG6650* (Lane 4), *top2* (Lane 5), *CG3797* (Lane 6), *sfmt* (Lane 7), *mcm7* (Lane 8) and *nufip* (Lane 9). *Canton S* embryos served as control (Lane 1). Lanes with red crosses were not included in the analysis. *Dscam* exon variants were separated as explained in figure legend 22. Samples were run on an 8% denaturing polyacrylamide gel. M=phiX174 DNA/HinfI marker (Biotools).



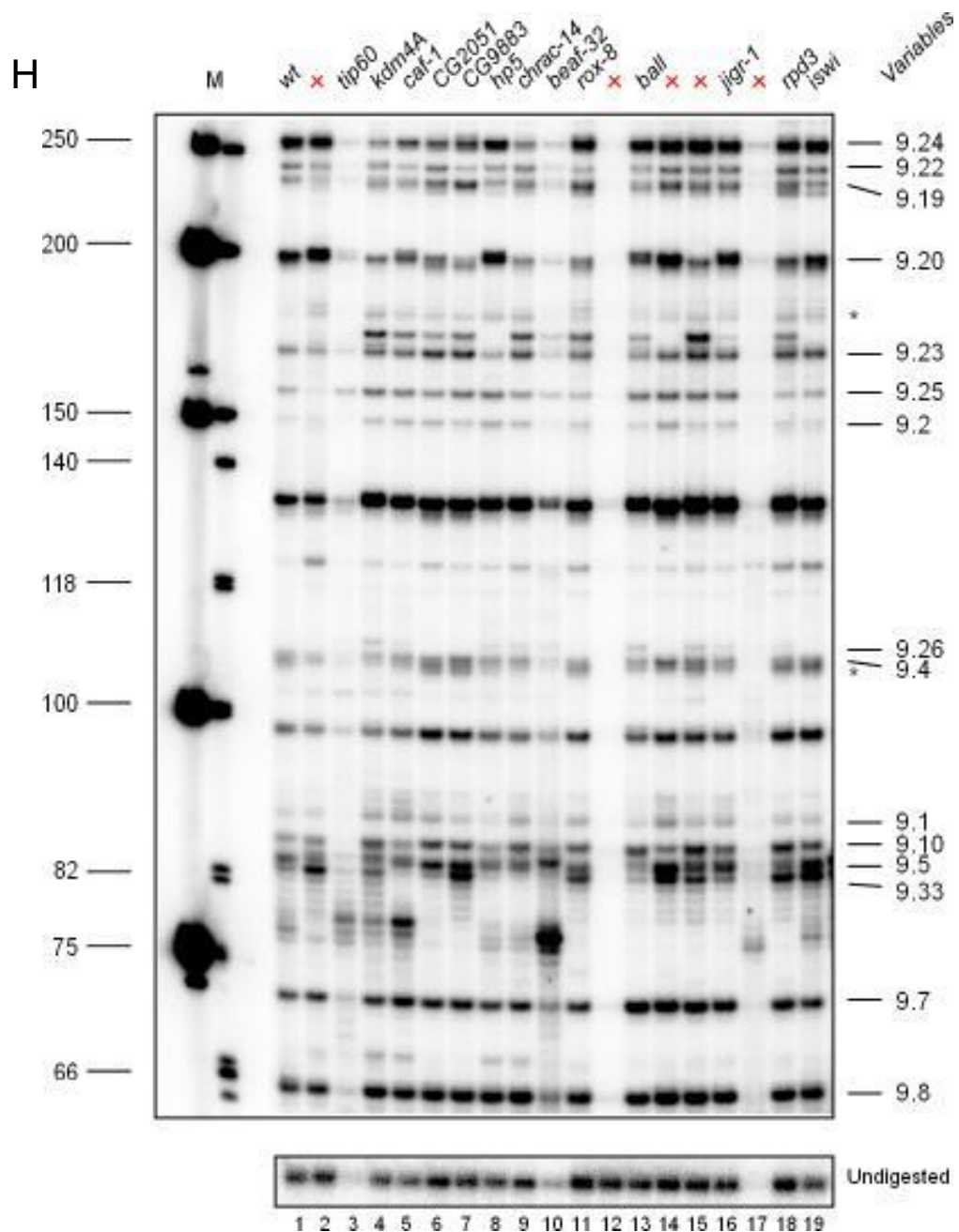
(F) Analysis of *Dscam* exon 9 splicing pattern using RNA extracted from 14-18 h old mutant embryos of *xl6* (Lane 2), *mcm10* (Lane 3), *CG14710* (Lane 5) and *sup-07* (Lane 8). *Canton S* embryos served as control (Lane 1). Lanes with red crosses were not included in the analysis. *Dscam* exon variants were separated as explained in figure legend 22. Samples were run on an 8% denaturing polyacrylamide gel. M=phiX174 DNA/Hinfl marker (Biotools).



(G) Analysis of *Dscam* exon 9 splicing pattern using RNA extracted from 14-18 h old mutant embryos of *CG3238* (Lane 6), *swa* (Lane 8), *cathD* (Lane 9), *CG12877* (Lane 10) and *CG8378* (Lane 11). *Canton S* embryos served as control (Lane 1). Lanes with red crosses were not included in the analysis. *Dscam* exon variants were separated as explained in figure legend 22. Samples were run on an 8% denaturing polyacrylamide gel. M=phiX174 DNA/HinfI marker (Biotools).



(H) Analysis of *Dscam* exon 9 splicing pattern using RNA extracted from 14-18 h old mutant embryos of *tip60* (Lane 3), *kdm4a* (Lane 4), *caf-1* (Lane 5), *CG2051* (Lane 6), *CG9883* (Lane 7), *hp5* (Lane 8), *chrac-14* (Lane 9), *beaf-32* (Lane 10), *rox-8* (Lane 11), *ball* (Lane 13), *jigr-1* (Lane 16), *rp3* (Lane 18) and *iswi* (Lane 19). *Canton S* embryos served as control (Lane 1). Lanes with red crosses were not included in the analysis. *Dscam* exon variants were separated as explained in figure legend 22. Samples were run on an 8% denaturing polyacrylamide gel. M=phiX174 DNA/HinfI marker (Biotools).



A12. List of primers

Primer Name	Primer sequence
Primers used to amplify Dscam variable exon clusters	
Dscam YH 3F2	GCAACCAGTTCGGAACCATTATCTCC
Dscam YH 5R1	CCAGAGGGCAATACCAGGTACTTTC
Dscam YH 5F1	GCCACAAAAGGACGATTGGTCATCACAG
Dscam YH 7R1	CGGGTTGTTCTACGATGAACTTGTACCAT
Dscam YH 8F1	GATCTCTGGAAGTGCAAGTCATGG
Dscam YH 10R1	GGCCTTATCGGTGGGCACGAGGTTCCATCTGGGAGGTA
Dscam YH 16F1	GAATACGACTTTGCCACCTTAACCGTTAC
Dscam YH 18R1	CCCATTGTCTGATTGTAACTACATCG
Dscam YH 11RT1	CGGAGCCTATTCCATTGATAGCCTCGCACAG
Primers used to clone <i>pAc5.1A Dscam Mut Exons 4-9</i>	
Dscam cDNA end F1 Not1 EcoRV	GTGCTGCGGCCGCGATATCCCGCCAACTGTGCCGAAGAGG ACCAATATCG
Dscam cDNA end R1	AAATGCCACGCCACCGCCGCGAGGGCGCTTACAAATTA CACTG
Dscam 6kb frag F1	AAATGTTTTTGTACATCAATTTTCGTGTCTGTGGTCCG
Dscam 6kb frag R1 Xho Spe	GCGTCCTCGAGACTAGTCTGATAACTGCTCCCGCTGATCCT GCTAATCCCTTG
Dscam 5'UTR1 F1 BsrGI SalI BglII	GCGTCTGTACAGTCGACAGATCTAGAACCGGATTTTCAGCGC TAGTCGGCG
Dscam 5'UTR1 R1	ATTGTTAACACTCACACACACACTTGTGAGAGTGGTG
Dscam 5'UTR2 F2	TAATCGCATTTAAAAACAATTTGGCCAGCCGCAG
Dscam 5'UTR2 R2 Not1 EcoRV	GCGTCGCGGCCGCGATATCTCGGGCATGGGATTGCCGCTG GCCTTG
Dscam Exon 1-4 F1 Xho NotI Xba HindIII Ase	GCGTCCTCGAGACGCGGCCGCGAGTCTAGAATAAGCTTGCA TTAATCGCATTTAAAAACAATTTGGCCAGCCGCAG
Dscam Exon 1-4 R1 BsrGI	GATATCGGCGCCGTAATACTGATTACAAACGGCTCGCACAT GTACATCCCGG
Dscam Exon 4-5 F1 BsrGI	CCGGGATGTACATGTGCGAGCCGTTGTGAATCAGTTTACG GCGCCGATATC
Dscam Exon 4-5 R1	GTCGTCTTTTGTGGCACTTAATCGGGTTTCTCCG
Dscam Exon 1-4 F1 Xho NotI Xba HindIII Ase	GCGTCCTCGAGACGCGGCCGCGAGTCTAGAATAAGCTTGCA TTAATCGCATTTAAAAACAATTTGGCCAGCCGCAG
Dscam Exon 4-5 R1	GTCGTCTTTTGTGGCACTTAATCGGGTTTCTCCG
Dscam Exon 5-7 F1	TAGTCATCACAGAGCCCGTTAGCAGTAGTCCGCCAAAATC AATG
Dscam Exon 5-7 R1 NgoMIV Spe Mlu BglII EcoRI	GCGTCGAATTCAGAGATCTGCACGCGTAGACTAGTGCGCC GGCGACGCACTTGAGGAATACACTTGGTCCGGGTTCCATG
Dscam Exon 7-8 F1 NgoMIV	GCGAGTGCTGAGCTGAAGCTCGGAGGCCGTTTCG
Dscam Exon 7-8 R1	GAGATCCTCGAGCAGAGTATCCTTCCTGATTCTTGGC
Dscam Exon 8-13 F1	TAGAAGTGCAAGTCATGGTTCCACCCAAAATTACGCCCTTC GACTTCG
Dscam Exon 8-13 R1 EcoRI	GTTGGCACTGAATTTCGACGCCCTTGATCTTCCATGTG
Primers used to validate presence of FRT sites	
pUChsneoF1	GCCGCTTTTCTGGATTCATCGACTGTG
pUChsneoR1	CGATTCCGAAGCCCAACCTTTCATAG
FRT F1	CAAAGCGTTTCCGAAAACGAGCGCTTCC
Car3'invR1	GCATGTCCGTGGGGTTTGAATTAAGTC

A13: List of fly stocks

Genotype of fly lines	Source
Genes differentially regulated in <i>elav</i> mutants	
$y^1 w^{67c23}; P\{SUPor-P\}CG9418^{KG05183}$	Bloomington
$y[1] w[67c23]; P\{w[+mC] y[+mDint2]=EPgy2\}CG3995[EY03827]$	Bloomington
$y[1] w[67c23]; P\{y[+t7.7] w[+mC]=wHy\}CG8149[DG19311]$	Bloomington
$y[1] w[67c23] P\{y[+m8]=Mae-UAS.6.11\}Tip60[GG01739]$	Bloomington
$w[1118]; Sirt7[5.Scer\Scel.RS]$	Bloomington
$y[1] w[67c23]; P\{y[+mDint2] w[BR.E.BR]=SUPor-P\}Kdm4A[KG04636]$	Bloomington
$y[1] w[67c23]; P\{w[+mC] y[+mDint2]=EPgy2\}Set[EY09821]$	Bloomington
$y[1] w[67c23]; P\{y[+t7.7] w[+mC]=wHy\}Caf1[DG25308]$	Bloomington
$y[1] w[67c23]; P\{w[+mC] y[+mDint2]=EPgy2\}CG2051[EY21697]$	Bloomington
$y[1] w[*]; P\{w[+mC]=EP\}CG9883[G17999]$	Bloomington
$y[1] w[67c23] P\{w[+mC] y[+mDint2]=EPgy2\}HP5[EY10901]$	Bloomington
$y[1] w[67c23]; P\{y[+mDint2] w[BR.E.BR]=SUPor-P\}mus201[KG01051] Chrac-14[KG01051]$	Bloomington
$y[1] w[67c23]; P\{y[+mDint2] w[BR.E.BR]=SUPor-P\}BEAF-32[KG06904]$	Bloomington
$y[1] w[67c23]; P\{w[+mC]=GSV1\}His2Av[GS3052]/TM3, Sb[1] Ser[1]$	Kyoto
$P\{ry[+t7.2]=PZ\}Rpd3[04556] ry[506]/TM3, ry[RK] Sb[1] Ser[1]$	Bloomington
$PBac\{RB\}Rpd3[e01851]$	Harvard
$y[1] w[67c23]; P\{y[+mDint2] w[BR.E.BR]=SUPor-P\}Iswi[KG03354]$	Bloomington
$P\{ry[+t7.2]=PZ\}Snr1[01319] ry[506]/TM3, ry[RK] Sb[1] Ser[1]$	Bloomington
$w[*]; His2Av[810]/TM3, Sb[1]$	Bloomington
$y[1] w[67c23]; P\{w[+mC]=lacW\}Dek[k09907]/CyO$	Bloomington
$y[1] w[67c23]; P\{w[+mC]=lacW\}spt4[k05316]/CyO$	Bloomington
$y1 w67c23; P\{wHy\}notDG24306/TM3, Sb1 Ser1$	Bloomington
$y1 w67c23; P\{GSV6\}GS16660/SM1$	Kyoto
$y[1] w[67c23]; P\{w[+mC]=lacW\}geminin[k14019]/CyO$	Bloomington
$msl-1[\gamma216] cn[1] bw[1]/CyO$	Bloomington
$y[1] w[*]; P\{y[+m8]=Mae-UAS.6.11\}Top2[LA00892]$	Bloomington
$y[1] w[*]; P\{w[+mC]=EP\}Sfmbt[G2280]/CyO$	Bloomington
$w[1118]; PBac\{w[+mC]=WH\}Mcm7[f03462]$	Bloomington
$y[1] w[67c23]; P\{y[+mDint2] w[BR.E.BR]=SUPor-P\}Mcm10[KG00233]$	Bloomington
$y[1] sc[*] v[1]; P\{y[+t7.7] v[+t1.8]=TRIP.HMS00608\}attP2/TM3, Sb[1]$	Bloomington
$PBac\{RB\}jigr1[e03251]$	Harvard
$y[1] w[67c23]; P\{w[+mC]=lacW\}zf30C[k02506]/CyO$	Bloomington
$w[1118]; P\{w[+mC]=EP\}CG15514[EP1005]/TM6B, Tb[1]$	Bloomington
$y[1] w[67c23]; P\{y[+mDint2] w[BR.E.BR]=SUPor-P\}CG14965[KG05766] ry[506]$	Bloomington
$w[1118]; PBac\{w[+mC]=WH\}CG14710[f06000]$	Bloomington
$w[1118]; P\{w[+mC] y[+mDint2]=EPgy2\}CG8378[EY04267]/CyO,$ $P\{ry[+t7.2]=sevRas1.V12\}FK1$	Bloomington
$w[*]; P\{GawB\}Rox8NP0528 / TM3, Ser1$	Kyoto
$w[1118]; PBac\{w[+mC]=WH\}CG12877[f01800]$	Bloomington
$zuc[RS49] cn[1] bw[1]/CyO, l(2)DTS513[1]$	Bloomington
$squ[PP32] cn[1] bw[1]/CyO, l(2)DTS513[1]$	Bloomington
$y1 w67c23; P\{lacW\}Hel25Ek11511/CyO$	Bloomington
$y1 w67c23; P\{EPgy2\}EY06979$	Bloomington
$y[1] w[67c23]; P\{y[+m8]=Mae-UAS.6.11\}Nufip[DP00363]/TM3, Sb[1]$	Bloomington
$y[1] w[*]; P\{w[+mC]=EP\}CG4266[G7664]$	Bloomington
$y[1] w[67c23]; P\{w[+mC]=lacW\}x16[k00230]/CyO$	Bloomington
$y1 w67c23; P\{EPgy2\}CG3238EY10295$	Bloomington
$v[1] swa[1]/FM3$	Bloomington
$w[1118]; P\{y[+mDint2] w[BR.E.BR]=SUPor-P\}CG3523[KG03696]/CyO,$ $P\{ry[+t7.2]=sevRas1.V12\}FK1$	Bloomington
$y[1] w[1118]; PBac\{y[+mDint2]=3HPy[+]\}CG6650[C151]$	Bloomington
$y[1] w[*]; P\{w[+mC]=EP\}CG3797[G8880]$	Bloomington
$y[1] w[*]; P\{w[+mC]=EP\}CG8460[G18835]$	Bloomington
$C(1;Y)1, y[1] P\{y[+mDint2] w[BR.E.BR]=SUPor-P\}Flo-2[KG00162]/C(1)DX, y[1] f[1]; ry[506]$	Bloomington
$w[1118]; P\{w[+mC]=EP\}cathD[EP2151]$	Bloomington

y ¹ w ^{67c23} ; P{w[+mC] y[+mDint2]=EPgy2}CG8108[EY14316]/TM3, Sb ¹ Ser ¹	Bloomington
y ¹ w ^{67c23} ; P{EPgy2}CG9293EY13364	Bloomington
PBac{PB}CG10535c00296	Harvard
y ¹ w ¹¹¹⁸ ; P{lacW}NeosL2249/TM3, Ser	Bloomington
Genes affecting cell signaling	
y [*] w [*] ; P{GawB}DscamNP3327/CyO, P{UAS-lacZ.UW14}UW14	Kyoto
w ¹¹¹⁸ ; P{RS3}DscamCB-0486-3	Kyoto
P{XP}Dscamd10584	Harvard
y ¹ w ^{67c23} ; P{EPgy2}DscamEY08820	Bloomington
y [*] w [*] ; P{neoFRT}40A P{FRT(whs)}G13 PBac{SAstopDsRed}LL01770 cn1 bw1/CyO, S [*] bw1	Kyoto
PBac{RB}Dscame04629	Harvard
Genes involved in mRNA methylation	
y ¹ v ¹ ; P{y[+t7.7] v[+t1.8]=TRiP.GL01126}attP2/TM3, Sb ¹	Bloomington
w ¹¹¹⁸ ; PBac{w[+mC]=RB}CG7818[e00875]	Bloomington
w ¹¹¹⁸ ; PBac{w[+mC]=PB}CG14906[c00109] CG14907[c00109]	Bloomington
y, w; dMTr1/dMTr1	Soller Lab
y, w; dMTr2/dMTr2	Soller Lab
RNA pol II processivity mutant	
v ¹ Rpl1215 ⁴	Bloomington
Dscam exon 9 reporter transgene	
w; UAS Dscam 9L	Y Hemani, this study
Lines used in generation of germline clones	
y ¹ w ^{67c23} ; P{lacW}AGO1 ^{K08121} /CyO	Bloomington
w ¹¹¹⁸ ; Df(2R)BSC307/CyO	Bloomington
PBac{WH}Rrp6f07001	Harvard
w ¹¹¹⁸ ; Df(3R)Exel6275, P{XP-U}Exel6275/TM6B, Tb ¹	Bloomington
w ¹¹¹⁸ ; P{FRT(w ^{hs})}G13 L/SM6a	Bloomington
y, w; Sco/CyO	Soller Lab
P{ry[+t7.2]=hsFLP}22, w[*]	Bloomington
w, elav ⁸⁵ , UAS CD8 GFP FRT19A/FM7iGFP; 201Y, RBP9/CyO _{GFP}	Soller Lab
w, elav ⁸⁵ , FRT19A/FM7iGFP; elav ELAV ^{OH NLS} /SM6 _{Roi}	Soller Lab
P{FRT(w ^{hs})}G13 P{ovoD1-18}2R/T(1;2)OR64/CyO	Bloomington
y ¹ w [*] ; P{neoFRT}82B Sb ¹ /TM6	Bloomington
Sco/SM6; PrDr/TM3Ser _{GFP}	Soller Lab
y, w, sn, ewg ¹¹ /FM7iGFP; hsGAL4/TM3Sb _{GFP}	Soller Lab
y, w, sn, ewg ¹¹ /FM7iGFP/Y ⁺ ; hsGAL4/TM3Ser _{GFP}	Soller Lab
FM7i/Y; PrDr/TM3Ser _{GFP}	Soller Lab
w [*] ; P{neoFRT}82B P{ovoD1-18}3R/st ¹ βTub85D ^D ss ¹ e ^s /TM3Sb ¹	Bloomington
y, w; Sco/CyO _{GFP} ; PrDr/TM3Sb	Soller Lab
Genes involved in small RNA processing	
y ¹ w ^{67c23} ; P{lacW}AGO1 ^{K08121} /CyO	Bloomington
w ¹¹¹⁸ ; Df(2R)BSC307/CyO	Bloomington
PBac{WH}Rrp6f07001	Harvard
w ¹¹¹⁸ ; Df(3R)Exel6275, P{XP-U}Exel6275/TM6B, Tb ¹	Bloomington
w [*] ; AGO2 ⁴¹⁴	Harvard
w [*] ; trf4 1-3	Soller Lab
elav[4] w[*]/FM6, w[*] ct[*]/Dp(1;Y)y[+]sc	Soller Lab
Lines expressing embryonic GFP marker	
w [*] baz ⁴ P{FRT(w ^{hs})}9-2/FM7a, P{Dfd-GMR-nvYFP}1	Bloomington
w [*] ; noc ^{Sco} /CyO, P{Dfd-GMR-nvYFP}2	Bloomington
w [*] ; ry ⁵⁰⁶ Dr ¹ /TM3, P{Dfd-GMR-nvYFP}3, Sb ¹	Bloomington
w [*] ; ry ⁵⁰⁶ Dr ¹ /TM6B, P{Dfd-GMR-nvYFP}4, Sb ¹ Tb ¹ ca ¹	Bloomington

List of references

- Allo, M., Buggiano, V., Fededa, J.P., Petrillo, E., Schor, I., de la Mata, M., Agirre, E., Plass, M., Eyra, E., Elela, S.A., *et al.* (2009). Control of alternative splicing through siRNA-mediated transcriptional gene silencing. *Nat Struct Mol Biol* 16, 717-724.
- Anastassiou, D., Liu, H., and Varadan, V. (2006). Variable window binding for mutually exclusive alternative splicing. *Genome Biol* 7, R2.
- Andersson, R., Enroth, S., Rada-Iglesias, A., Wadelius, C., and Komorowski, J. (2009). Nucleosomes are well positioned in exons and carry characteristic histone modifications. *Genome Res* 19, 1732-1741.
- Auboeuf, D., Honig, A., Berget, S.M., and O'Malley, B.W. (2002). Coordinate regulation of transcription and splicing by steroid receptor coregulators. *Science* 298, 416-419.
- Beck, G., and Habicht, G.S. (1996). Immunity and the invertebrates. *Sci Am* 275, 60-63, 66.
- Beckmann, J.S., and Trifonov, E.N. (1991). Splice junctions follow a 205-base ladder. *Proc Natl Acad Sci U S A* 88, 2380-2383.
- Belanger, F., Stepinski, J., Darzynkiewicz, E., and Pelletier, J. (2010). Characterization of hMTr1, a human Cap1 2'-O-ribose methyltransferase. *J Biol Chem* 285, 33037-33044.
- Bernstein, E., and Allis, C.D. (2005). RNA meets chromatin. *Genes Dev* 19, 1635-1655.
- Bharadwaj, R., and Kolodkin, A.L. (2006). Descrambling Dscam diversity. *Cell* 125, 421-424.
- Bisailon, M., and Lemay, G. (1997). Viral and cellular enzymes involved in synthesis of mRNA cap structure. *Virology* 236, 1-7.
- Bischof, J., Maeda, R.K., Hediger, M., Karch, F., and Basler, K. (2007). An optimized transgenesis system for *Drosophila* using germ-line-specific phiC31 integrases. *Proc Natl Acad Sci U S A* 104, 3312-3317.
- Black, D.L. (2003). Mechanisms of alternative pre-messenger RNA splicing. *Annu Rev Biochem* 72, 291-336.
- Bokar, J.A., Shambaugh, M.E., Polayes, D., Matera, A.G., and Rottman, F.M. (1997). Purification and cDNA cloning of the AdoMet-binding subunit of the human mRNA (N6-adenosine)-methyltransferase. *RNA* 3, 1233-1247.
- Brand, A.H., and Perrimon, N. (1993). Targeted gene expression as a means of altering cell fates and generating dominant phenotypes. *Development* 118, 401-415.
- Brodsky, A.S., Meyer, C.A., Swinburne, I.A., Hall, G., Keenan, B.J., Liu, X.S., Fox, E.A., and Silver, P.A. (2005). Genomic mapping of RNA polymerase II reveals sites of co-transcriptional regulation in human cells. *Genome Biol* 6, R64.
- Burnette, J.M., Miyamoto-Sato, E., Schaub, M.A., Conklin, J., and Lopez, A.J. (2005). Subdivision of large introns in *Drosophila* by recursive splicing at nonexonic elements. *Genetics* 170, 661-674.

- Callahan, K.P., and Butler, J.S (2010). TRAMP complex enhances RNA degradation by the nuclear exosome component Rrp6. *J Biol Chem* 285, 3540-3547.
- Camblong, J., Iglesias, N., Fickentscher, C., Dieppois, G., and Stutz, F. (2007). Antisense RNA stabilization induces transcriptional gene silencing via histone deacetylation in *S. cerevisiae*. *Cell* 131, 706-717.
- Carrillo Oesterreich, F., Bieberstein, N., and Neugebauer, K.M. (2011). Pause locally, splice globally. *Trends Cell Biol* 21, 328-335.
- Chang, W.C., Chen, Y.C., Lee, K.M., and Tarn, W.Y. (2007). Alternative splicing and bioinformatic analysis of human U12-type introns. *Nucleic Acids Res* 35, 1833-1841.
- Chen, B.E., Kondo, M., Garnier, A., Watson, F.L., Puettmann-Holgado, R., Lamar, D.R., and Schmucker, D. (2006). The molecular diversity of Dscam is functionally required for neuronal wiring specificity in *Drosophila*. *Cell* 125, 607-620.
- Chodavarapu, R.K., Feng, S., Bernatavichute, Y.V., Chen, P.Y., Stroud, H., Yu, Y., Hetzel, J.A., Kuo, F., Kim, J., Cokus, S.J., *et al.* (2010). Relationship between nucleosome positioning and DNA methylation. *Nature* 466, 388-392.
- Chodavarapu, R.K., Feng, S., Bernatavichute, Y.V., Chen, P.Y., Stroud, H., Yu, Y., Hetzel, J.A., Kuo, F., Kim, J., Cokus, S.J., *et al.* (2010). Relationship between nucleosome positioning and DNA methylation. *Nature* 466, 388-392.
- Chou, P.H., Chang, H.S., Chen, I.T., Lin, H.Y., Chen, Y.M., Yang, H.L., and Wang, K.C. (2009). The putative invertebrate adaptive immune protein *Litopenaeus vannamei* Dscam (LvDscam) is the first reported Dscam to lack a transmembrane domain and cytoplasmic tail. *Dev Comp Immunol* 33, 1258-1267.
- Chung, W.J., Okamura, K., Martin, R., and Lai, E.C. (2008). Endogenous RNA interference provides a somatic defense against *Drosophila* transposons. *Curr Biol* 18, 795-802.
- Churchman, L.S., and Weissman, J.S. (2011). Nascent transcript sequencing visualizes transcription at nucleotide resolution. *Nature* 469, 368-373.
- Claverie, J.M. (2001). Gene number. What if there are only 30,000 human genes? *Science* 291, 1255-1257.
- Cooper, E.L., and Roch, P. (1986). Second-set allograft responses in the earthworm *Lumbricus terrestris*. Kinetics and characteristics. *Transplantation* 41, 514-520.
- Cramer, P., Pesce, C.G., Baralle, F.E., and Kornblihtt, A.R. (1997). Functional association between promoter structure and transcript alternative splicing. *Proc Natl Acad Sci U S A* 94, 11456-11460.
- de la Mata, M., Alonso, C.R., Kadener, S., Fededa, J.P., Blaustein, M., Pelisch, F., Cramer, P., Bentley, D., and Kornblihtt, A.R. (2003). A slow RNA polymerase II affects alternative splicing in vivo. *Mol Cell* 12, 525-532.

- de la Mata, M., and Kornblihtt, A.R. (2006). RNA polymerase II C-terminal domain mediates regulation of alternative splicing by SRp20. *Nat Struct Mol Biol* 13, 973-980.
- Demir, E., and Dickson, B.J. (2005). fruitless splicing specifies male courtship behavior in *Drosophila*. *Cell* 121, 785-794.
- Dhami, P., Saffrey, P., Bruce, A.W., Dillon, S.C., Chiang, K., Bonhoure, N., Koch, C.M., Bye, J., James, K., Foad, N.S., *et al.* (2010). Complex exon-intron marking by histone modifications is not determined solely by nucleosome distribution. *PLoS One* 5, e12339.
- Dong, Y., Taylor, H.E., and Dimopoulos, G. (2006). AgDscam, a hypervariable immunoglobulin domain-containing receptor of the *Anopheles gambiae* innate immune system. *PLoS Biol* 4, e229.
- Donmez, G., Hartmuth, K., and Luhrmann, R. (2004). Modified nucleotides at the 5' end of human U2 snRNA are required for spliceosomal E-complex formation. *RNA* 10, 1925-1933.
- Du Pasquier, L. (2005). Immunology. Insects diversify one molecule to serve two systems. *Science* 309, 1826-1827.
- Faulhaber, L.M., and Karp, R.D. (1992). A diphasic immune response against bacteria in the American cockroach. *Immunology* 75, 378-381.
- Flaherty, S.M., Fortes, P., Izaurralde, E., Mattaj, I.W., and Gilmartin, G.M. (1997). Participation of the nuclear cap binding complex in pre-mRNA 3' processing. *Proc Natl Acad Sci U S A* 94, 11893-11898.
- Fortes, P., Inada, T., Preiss, T., Hentze, M.W., Mattaj, I.W., and Sachs, A.B. (2000). The yeast nuclear cap binding complex can interact with translation factor eIF4G and mediate translation initiation. *Mol Cell* 6, 191-196.
- Garcia-Blanco, M.A., Baraniak, A.P., and Lasda, E.L. (2004). Alternative splicing in disease and therapy. *Nat Biotechnol* 22, 535-546.
- Ghosh, J., Lun, C.M., Majeske, A.J., Sacchi, S., Schrankel, C.S., and Smith, L.C. (2011). Invertebrate immune diversity. *Dev Comp Immunol* 35, 959-974.
- Graveley, B.R. (2005). Mutually exclusive splicing of the insect Dscam pre-mRNA directed by competing intronic RNA secondary structures. *Cell* 123, 65-73.
- Gromak, N., Matlin, A.J., Cooper, T.A., and Smith, C.W. (2003). Antagonistic regulation of alpha-actinin alternative splicing by CELF proteins and polypyrimidine tract binding protein. *RNA* 9, 443-456.
- Han, J., Ding, J.H., Byeon, C.W., Kim, J.H., Hertel, K.J., Jeong, S., and Fu, X.D. (2011). SR proteins induce alternative exon skipping through their activities on the flanking constitutive exons. *Mol Cell Biol* 31, 793-802.
- Hapala, J., and Trifonov, E.N. (2011). High resolution positioning of intron ends on the nucleosomes. *Gene* 489, 6-10.
- Harpaz, Y., and Chothia, C. (1994). Many of the immunoglobulin superfamily domains in cell adhesion molecules and surface receptors belong to a new structural set which is close to that containing variable domains. *J Mol Biol* 238, 528-539.
- Hattori, D., Chen, Y., Matthews, B.J., Salwinski, L., Sabatti, C., Grueber, W.B., and Zipursky, S.L. (2009). Robust discrimination between self

and non-self neurites requires thousands of Dscam1 isoforms. *Nature* **461**, 644-648.

- Hattori, D., Demir, E., Kim, H.W., Viragh, E., Zipursky, S.L., and Dickson, B.J. (2007). Dscam diversity is essential for neuronal wiring and self-recognition. *Nature* **449**, 223-227.
- Hemani, Y., and Soller, M. (2012). Mechanisms of *Drosophila* Dscam mutually exclusive splicing regulation. *Biochem Soc Trans* **40**, 804-809.
- Hertel, K.J. (2008). Combinatorial control of exon recognition. *J Biol Chem* **283**, 1211-1215.
- Hnilicova, J., Hozeifi, S., Duskova, E., Icha, J., Tomankova, T., and Stanek, D. (2011). Histone deacetylase activity modulates alternative splicing. *PLoS One* **6**, e16727.
- Hnilicova, J., and Stanek, D. (2011). Where splicing joins chromatin. *Nucleus* **2**, 182-188.
- Hodges, C., Bintu, L., Lubkowska, L., Kashlev, M., and Bustamante, C. (2009). Nucleosomal fluctuations govern the transcription dynamics of RNA polymerase II. *Science* **325**, 626-628.
- Hofmann, Y., and Wirth, B. (2002). hnRNP-G promotes exon 7 inclusion of survival motor neuron (SMN) via direct interaction with Htra2-beta1. *Hum Mol Genet* **11**, 2037-2049.
- Hon, G., Wang, W., and Ren, B. (2009). Discovery and annotation of functional chromatin signatures in the human genome. *PLoS Comput Biol* **5**, e1000566.
- House, A.E., and Lynch, K.W. (2008). Regulation of alternative splicing: more than just the ABCs. *J Biol Chem* **283**, 1217-1221.
- Hrzenjak, A., Moinfar, F., Kremser, M.L., Strohmeier, B., Staber, P.B., Zatloukal, K., and Denk, H. (2006). Valproate inhibition of histone deacetylase 2 affects differentiation and decreases proliferation of endometrial stromal sarcoma cells. *Mol Cancer Ther* **5**, 2203-2210.
- Huff, J.T., Plocik, A.M., Guthrie, C., and Yamamoto, K.R. (2010). Reciprocal intronic and exonic histone modification regions in humans. *Nat Struct Mol Biol* **17**, 1495-1499.
- Hughes, M.E., Bortnick, R., Tsubouchi, A., Baumer, P., Kondo, M., Uemura, T., and Schmucker, D. (2007). Homophilic Dscam interactions control complex dendrite morphogenesis. *Neuron* **54**, 417-427.
- Hummel, T. (2007). Neuronal development: neighbors have to be different. *Curr Biol* **17**, R1050-1052.
- Hummel, T., Vasconcelos, M.L., Clemens, J.C., Fishilevich, Y., Vosshall, L.B., and Zipursky, S.L. (2003). Axonal targeting of olfactory receptor neurons in *Drosophila* is controlled by Dscam. *Neuron* **37**, 221-231.
- Hutvagner, G., and Simard, M.J. (2008). Argonaute proteins: key players in RNA silencing. *Nat Rev Mol Cell Biol* **9**, 22-32.
- Iglesias-Gato, D., Martin-Marcos, P., Santos, M.A., Hinnebusch, A.G., and Tamame, M. Guanine nucleotide pool imbalance impairs multiple steps of protein synthesis and disrupts GCN4 translational control in *Saccharomyces cerevisiae*. *Genetics* **187**, 105-122.

- Ip, J.Y., Schmidt, D., Pan, Q., Ramani, A.K., Fraser, A.G., Odom, D.T., and Blencowe, B.J. (2011). Global impact of RNA polymerase II elongation inhibition on alternative splicing regulation. *Genome Res* 21, 390-401.
- Izaurralde, E., Lewis, J., McGuigan, C., Jankowska, M., Darzynkiewicz, E., and Mattaj, I.W. (1994). A nuclear cap binding protein complex involved in pre-mRNA splicing. *Cell* 78, 657-668.
- Jones, R.B., Wang, F., Luo, Y., Yu, C., Jin, C., Suzuki, T., Kan, M., and McKeehan, W.L. (2001). The nonsense-mediated decay pathway and mutually exclusive expression of alternatively spliced FGFR2IIIb and -IIlc mRNAs. *J Biol Chem* 276, 4158-4167.
- Jurica, M.S., and Moore, M.J. (2003). Pre-mRNA splicing: awash in a sea of proteins. *Mol Cell* 12, 5-14.
- Kaprielian, Z., Imondi, R., and Runko, E. (2000). Axon guidance at the midline of the developing CNS. *Anat Rec* 261, 176-197.
- Kataoka, Y., Takeichi, M., and Uemura, T. (2001). Developmental roles and molecular characterization of a Drosophila homologue of Arabidopsis Argonaute1, the founder of a novel gene superfamily. *Genes Cells* 6, 313-325.
- Keren, H., Lev-Maor, G., and Ast, G. (2010). Alternative splicing and evolution: diversification, exon definition and function. *Nat Rev Genet* 11, 345-355.
- Khodor, Y.L., Rodriguez, J., Abruzzi, K.C., Tang, C.H., Marr, M.T., 2nd, and Rosbash, M. (2011). Nascent-seq indicates widespread cotranscriptional pre-mRNA splicing in Drosophila. *Genes Dev* 25, 2502-2512.
- Kogan, S., and Trifonov, E.N. (2005). Gene splice sites correlate with nucleosome positions. *Gene* 352, 57-62.
- Kolasinska-Zwierz, P., Down, T., Latorre, I., Liu, T., Liu, X.S., and Ahringer, J. (2009). Differential chromatin marking of introns and expressed exons by H3K36me3. *Nat Genet* 41, 376-381.
- Konig, J., Zarnack, K., Rot, G., Curk, T., Kayikci, M., Zupan, B., Turner, D.J., Luscombe, N.M., and Ule, J. (2011). iCLIP reveals the function of hnRNP particles in splicing at individual nucleotide resolution. *Nat Struct Mol Biol* 17, 909-915.
- Kornblihtt, A.R. (2005). Promoter usage and alternative splicing. *Curr Opin Cell Biol* 17, 262-268.
- Kornblihtt, A.R., de la Mata, M., Fededa, J.P., Munoz, M.J., and Nogues, G. (2004). Multiple links between transcription and splicing. *RNA* 10, 1489-1498.
- Koushika, S.P., Soller, M., and White, K. (2000). The neuron-enriched splicing pattern of Drosophila erect wing is dependent on the presence of ELAV protein. *Mol Cell Biol* 20, 1836-1845.
- Kreamling, J.M., and Graveley, B.R. (2005). The iStem, a long-range RNA secondary structure element required for efficient exon inclusion in the Drosophila Dscam pre-mRNA. *Mol Cell Biol* 25, 10251-10260.
- Kruse, S., Zhong, S., Bodi, Z., Button, J., Alcocer, M.J., Hayes, C.J., and Fray, R. (2011). A novel synthesis and detection method for cap-associated adenosine modifications in mouse mRNA. *Sci Rep* 1, 126.

- Kurata, S. (2006). Recognition and elimination of diversified pathogens in insect defense systems. *Mol Divers* 10, 599-605.
- Kurtz, J., and Armitage, S.A. (2006). Alternative adaptive immunity in invertebrates. *Trends Immunol* 27, 493-496.
- Kvell, K., Cooper, E.L., Engelmann, P., Bovari, J., and Nemeth, P. (2007). Blurring borders: innate immunity with adaptive features. *Clin Dev Immunol* 2007, 83671.
- Leclerc, V., Pelte, N., El Chamy, L., Martinelli, C., Ligoxygakis, P., Hoffmann, J.A., and Reichhart, J.M. (2006). Prophenoloxidase activation is not required for survival to microbial infections in *Drosophila*. *EMBO Rep* 7, 231-235.
- Lee, C.W., Chen, I.T., Chou, P.H., Hung, H.Y., and Wang, K.V. (2012). Heterogeneous nuclear ribonucleoprotein hrp36 acts as an alternative splicing repressor in *Litopenaeus vannamei* Dscam. *Dev Comp Immunol* 36, 10-20.
- Lewis, J.D., Izaurralde, E., Jarmolowski, A., McGuigan, C., and Mattaj, I.W. (1996). A nuclear cap-binding complex facilitates association of U1 snRNP with the cap-proximal 5' splice site. *Genes Dev* 10, 1683-1698.
- Lisbin, M.J., Qiu, J., and White, K. (2001). The neuron-specific RNA-binding protein ELAV regulates neuroglial alternative splicing in neurons and binds directly to its pre-mRNA. *Genes Dev* 15, 2546-2561.
- Little, T.J., O'Connor, B., Colegrave, N., Watt, K., and Read, A.F. (2003). Maternal transfer of strain-specific immunity in an invertebrate. *Curr Biol* 13, 489-492.
- Long, J.C., and Cáceres, J.F. (2009). The SR protein family of splicing factors: master regulators of gene expression. *Biochem J* 417, 15-27.
- Lopez, A.J. (1998). Alternative splicing of pre-mRNA: developmental consequences and mechanisms of regulation. *Annu Rev Genet* 32, 279-305.
- Luco, R.F., Allo, M., Schor, I.E., Kornblihtt, A.R., and Misteli, T. (2011). Epigenetics in alternative pre-mRNA splicing. *Cell* 144, 16-26.
- Luhrmann, R., and Stark, H. (2009). Structural mapping of spliceosomes by electron microscopy. *Curr Opin Struct Biol* 19, 96-102.
- Maniatis, T., and Tasic, B. (2002). Alternative pre-mRNA splicing and proteome expansion in metazoans. *Nature* 418, 236-243.
- Manoli, D.S., Foss, M., Villella, A., Taylor, B.J., Hall, J.C., and Baker, B.S. (2005). Male-specific fruitless specifies the neural substrates of *Drosophila* courtship behaviour. *Nature* 436, 395-400.
- Marmaras, V.J., and Lampropoulou, M. (2009). Regulators and signalling in insect haemocyte immunity. *Cell Signal* 21, 186-195.
- Matova, N., and Anderson, K.V. (2006). Rel/NF-kappaB double mutants reveal that cellular immunity is central to *Drosophila* host defense. *Proc Natl Acad Sci U S A* 103, 16424-16429.
- Matthews, B.J., Kim, M.E., Flanagan, J.J., Hattori, D., Clemens, J.C., Zipursky, S.L., and Grueber, W.B. (2007). Dendrite self-avoidance is controlled by Dscam. *Cell* 129, 593-604.
- May, G.E., Olson, S., McManus, C.J., and Graveley, B.R. (2011). Competing RNA secondary structures are required for mutually exclusive splicing of the Dscam exon 6 cluster. *RNA* 17, 222-229.

- McCracken, S., Fong, N., Rosonina, E., Yankulov, K., Brothers, G., Siderovski, D., Hessel, A., Foster, S., Shuman, S., and Bentley, D.L. (1997). 5'-Capping enzymes are targeted to pre-mRNA by binding to the phosphorylated carboxy-terminal domain of RNA polymerase II. *Genes Dev* 11, 3306-3318.
- McManus, C.J., and Graveley, B.R. (2011). RNA structure and the mechanisms of alternative splicing. *Curr Opin Genet Dev* 21, 373-379.
- Monsalve, M., Wu, Z., Adelmant, G., Puigserver, P., Fan, M., and Spiegelman, B.M. (2000). Direct coupling of transcription and mRNA processing through the thermogenic coactivator PGC-1. *Mol Cell* 6, 307-316.
- Moret, Y. (2006). "Trans-generational immune priming": specific enhancement of the antimicrobial immune response in the mealworm beetle, *Tenebrio molitor*. *Proc Biol Sci* 273, 1399-1405.
- Mori, K., and Stewart, J.E. (2006). Immunogen-dependent quantitative and qualitative differences in phagocytic responses of the circulating hemocytes of the lobster *Homarus americanus*. *Dis Aquat Organ* 69, 197-203.
- Murph, M.M., Hurst-Kennedy, J., Newton, V., Brindley, D.N., and Radhakrishna, H. (2007). Lysophosphatidic acid decreases the nuclear localization and cellular abundance of the p53 tumor suppressor in A549 lung carcinoma cells. *Mol Cancer Res* 5, 1201-1211.
- Nahkuri, S., Taft, R.J., and Mattick, J.S. (2009). Nucleosomes are preferentially positioned at exons in somatic and sperm cells. *Cell Cycle* 8, 3420-3424.
- Neves, G., Zucker, J., Daly, M., and Chess, A. (2004). Stochastic yet biased expression of multiple Dscam splice variants by individual cells. *Nat Genet* 36, 240-246.
- Nichols, C.D. (2006). *Drosophila melanogaster* neurobiology, neuropharmacology, and how the fly can inform central nervous system drug discovery. *Pharmacol Ther* 112, 677-700.
- Nogues, G., Kadener, S., Cramer, P., Bentley, D., and Kornblihtt, A.R. (2002). Transcriptional activators differ in their abilities to control alternative splicing. *J Biol Chem* 277, 43110-43114.
- Nogues, G., Kadener, S., Cramer, P., de la Mata, M., Fededa, J.P., Blaustein, M., Srebrow, A., and Kornblihtt, A.R. (2003). Control of alternative pre-mRNA splicing by RNA Pol II elongation: faster is not always better. *IUBMB Life* 55, 235-241.
- Okamura, K., Ishizuka, A., Siomi, H., and Siomi, M.C. (2004). Distinct roles for Argonaute proteins in small RNA-directed RNA cleavage pathways. *Genes Dev* 18, 1655-1666.
- Olson, S., Blanchette, M., Park, J., Savva, Y., Yeo, G.W., Yeakley, J.M., Rio, D.C., and Graveley, B.R. (2007). A regulator of Dscam mutually exclusive splicing fidelity. *Nat Struct Mol Biol*.
- Oltean, S., Gammons, M., Hulse, R., Hamdollah-Zadeh, M., Mavrou A., Donaldson, L., Salmon, A.H., Harper, S.J., Ladomery, M.R., and Bates, D.O. (2012). SRPK1 inhibition *in vivo*. modulation of VEGF splicing and potential treatment for multiple diseases. *Biochem Soc Trans* 40, 831-835.

- Osheim, Y.N., Miller, O.L., Jr., and Beyer, A.L. (1985). RNP particles at splice junction sequences on *Drosophila* chorion transcripts. *Cell* **43**, 143-151.
- Pagani, F., Stuani, C., Zuccato, E., Kornblihtt, A.R., and Baralle, F.E. (2003). Promoter architecture modulates CFTR exon 9 skipping. *J Biol Chem* **278**, 15111-15117.
- Pan, Q., Shai, O., Misquitta, C., Zhang, W., Saltzman, A.L., Mohammad, N., Babak, T., Siu, H., Hughes, T.R., Morris, Q.D., *et al.* (2004). Revealing global regulatory features of mammalian alternative splicing using a quantitative microarray platform. *Mol Cell* **16**, 929-941.
- Pane, A., Wehr, K., and Schupbach, T. (2007). zucchini and squash encode two putative nucleases required for rasiRNA production in the *Drosophila* germline. *Dev Cell* **12**, 851-862.
- Park, J.W., Parisky, K., Celotto, A.M., Reenan, R.A., and Graveley, B.R. (2004). Identification of alternative splicing regulators by RNA interference in *Drosophila*. *Proc Natl Acad Sci U S A* **101**, 15974-15979.
- Patel, A.A., and Steitz, J.A. (2003). Splicing double: insights from the second spliceosome. *Nat Rev Mol Cell Biol* **4**, 960-970.
- Paterson, W.D., and Stewart, J.E. (1979). Rate and duration of phagocytic increase in lobsters induced by *Pseudomonas perolens* endotoxin. *Dev Comp Immunol* **3**, 353-357.
- Perrimon, N. (1998). Creating mosaics in *Drosophila*. *Int J Dev Biol* **42**, 243-247.
- Pham, L.N., Dionne, M.S., Shirasu-Hiza, M., and Schneider, D.S. (2007). A specific primed immune response in *Drosophila* is dependent on phagocytes. *PLoS Pathog* **3**, e26.
- Price, D.H. (2000). P-TEFb, a cyclin-dependent kinase controlling elongation by RNA polymerase II. *Mol Cell Biol* **20**, 2629-2634.
- Proudfoot, N. (2004). New perspectives on connecting messenger RNA 3' end formation to transcription. *Curr Opin Cell Biol* **16**, 272-278.
- Prucca, C.G., Slavin, I., Quiroga, R., Elias, E.V., Rivero, F.D., Saura, A., Carranza, P.G., and Lujan, H.D. (2008). Antigenic variation in *Giardia lamblia* is regulated by RNA interference. *Nature* **456**, 750-754.
- Rahman, M.M., Roberts, H.L., Sarjan, M., Asgari, S., and Schmidt, O. (2004). Induction and transmission of *Bacillus thuringiensis* tolerance in the flour moth *Ephestia kuehniella*. *Proc Natl Acad Sci U S A* **101**, 2696-2699.
- Rothrock, C.R., House, A.E., and Lynch, K.W. (2005). HnRNP L represses exon splicing via a regulated exonic splicing silencer. *EMBO J* **24**, 2792-2802.
- Rowley, A.F., and Powell, A. (2007). Invertebrate immune systems specific, quasi-specific, or nonspecific? *J Immunol* **179**, 7209-7214.
- Sadd, B.M., Kleinlogel, Y., Schmid-Hempel, R., and Schmid-Hempel, P. (2005). Trans-generational immune priming in a social insect. *Biol Lett* **1**, 386-388.
- Sadd, B.M., and Schmid-Hempel, P. (2006). Insect immunity shows specificity in protection upon secondary pathogen exposure. *Curr Biol* **16**, 1206-1210.

- Saint-Andre, V., Batsche, E., Rachez, C., and Muchardt, C. (2011). Histone H3 lysine 9 trimethylation and HP1gamma favor inclusion of alternative exons. *Nat Struct Mol Biol* 18, 337-344.
- Sawaya, M.R., Wojtowicz, W.M., Andre, I., Qian, B., Wu, W., Baker, D., Eisenberg, D., and Zipursky, S.L. (2008). A double S shape provides the structural basis for the extraordinary binding specificity of Dscam isoforms. *Cell* 134, 1007-1018.
- Schmucker, D. (2007). Molecular diversity of Dscam: recognition of molecular identity in neuronal wiring. *Nat Rev Neurosci* 8, 915-920.
- Schmucker, D., and Chen, B. (2009). Dscam and DSCAM: complex genes in simple animals, complex animals yet simple genes. *Genes Dev* 23, 147-156.
- Schmucker, D., Clemens, J.C., Shu, H., Worby, C.A., Xiao, J., Muda, M., Dixon, J.E., and Zipursky, S.L. (2000). *Drosophila* Dscam is an axon guidance receptor exhibiting extraordinary molecular diversity. *Cell* 101, 671-684.
- Schmucker, D., and Flanagan, J.G. (2004). Generation of recognition diversity in the nervous system. *Neuron* 44, 219-222.
- Schor, I.E., Rascovan, N., Pelisch, F., Allo, M., and Kornblihtt, A.R. (2009). Neuronal cell depolarization induces intragenic chromatin modifications affecting NCAM alternative splicing. *Proc Natl Acad Sci U S A* 106, 4325-4330.
- Schutt, C., and Nothiger, R. (2000). Structure, function and evolution of sex-determining systems in Dipteran insects. *Development* 127, 667-677.
- Schwartz, S., Meshorer, E., and Ast, G. (2009). Chromatin organization marks exon-intron structure. *Nat Struct Mol Biol* 16, 990-995.
- Shapiro, L. (2007). Self-recognition at the atomic level: understanding the astonishing molecular diversity of homophilic Dscams. *Neuron* 56, 10-13.
- Shin, C., Feng, Y., and Manley, J.L. (2004). Dephosphorylated SRp38 acts as a splicing repressor in response to heat shock. *Nature* 427, 553-558.
- Shukla, S., Kavak, E., Gregory, M., Imashimizu, M., Shutinoski, B., Kashlev, M., Oberdoerffer, P., Sandberg, R., and Oberdoerffer, S. (2011). CTCF-promoted RNA polymerase II pausing links DNA methylation to splicing. *Nature* 479, 74-79.
- Simionato, E., Barrios, N., Duloquin, L., Boissonneau, E., Lecorre, P., and Agnes, F. (2007). The *Drosophila* RNA-binding protein ELAV is required for commissural axon midline crossing via control of commissureless mRNA expression in neurons. *Dev Biol* 301, 166-177.
- Smith, C.W. (2005). Alternative splicing--when two's a crowd. *Cell* 123, 1-3.
- Smith, C.W., and Nadal-Ginard, B. (1989). Mutually exclusive splicing of alpha-tropomyosin exons enforced by an unusual lariat branch point location: implications for constitutive splicing. *Cell* 56, 749-758.
- Smith, C.W., Patton, J.G., and Nadal-Ginard, B. (1989). Alternative splicing in the control of gene expression. *Annu Rev Genet* 23, 527-577.
- Smith, H.C., Gott, J.M., and Hanson, M.R. (1997). A guide to RNA editing. *RNA* 3, 1105-1123.

- Smith, P.H., Mwangi, J.M., Afrane, Y.A., Yan, G., Obbard, D.J., Ranford-Cartwright, L.C., and Little, T.J. (2011). Alternative splicing of the *Anopheles gambiae* Dscam gene in diverse *Plasmodium falciparum* infections. *Malar J* 10, 156.
- Soba, P., Zhu, S., Emoto, K., Younger, S., Yang, S.J., Yu, H.H., Lee, T., Jan, L.Y., and Jan, Y.N. (2007). *Drosophila* sensory neurons require Dscam for dendritic self-avoidance and proper dendritic field organization. *Neuron* 54, 403-416.
- Soller, M. (2006). Pre-messenger RNA processing and its regulation: a genomic perspective. *Cell Mol Life Sci* 63, 796-819.
- Soller, M., and White, K. (2003). ELAV inhibits 3'-end processing to promote neural splicing of ewg pre-mRNA. *Genes Dev* 17, 2526-2538.
- Spies, N., Nielsen, C.B., Padgett, R.A., and Burge, C.B. (2009). Biased chromatin signatures around polyadenylation sites and exons. *Mol Cell* 36, 245-254.
- Staley, J.P., and Guthrie, C. (1998). Mechanical devices of the spliceosome: motors, clocks, springs, and things. *Cell* 92, 315-326.
- Sumanasekera, C., Kelemen, O., Beullens, M., Aubol, B.E., Adams, J.A., Sunkara, M., Morris, A., Bollen, M., Andreadis, A. and Stamm, S. (2012). C6 pyridinium ceramide influences alternative pre-mRNA splicing by inhibiting protein phosphatase-1. *Nucleic Acids Res* 40(9), 4025-4039.
- te Poele, R.H., Okorokov, A.L., and Joel, S.P. (1999). RNA synthesis block by 5, 6-dichloro-1-beta-D-ribofuranosylbenzimidazole (DRB) triggers p53-dependent apoptosis in human colon carcinoma cells. *Oncogene* 18, 5765-5772.
- Technau, G.M., Berger, C., and Urbach, R. (2006). Generation of cell diversity and segmental pattern in the embryonic central nervous system of *Drosophila*. *Dev Dyn* 235, 861-869.
- Tilgner, H., Nikolaou, C., Althammer, S., Sammeth, M., Beato, M., Valcarcel, J., and Guigo, R. (2009). Nucleosome positioning as a determinant of exon recognition. *Nat Struct Mol Biol* 16, 996-1001.
- Urbach, R., and Technau, G.M. (2004). Neuroblast formation and patterning during early brain development in *Drosophila*. *Bioessays* 26, 739-751.
- Usui-Aoki, K., Ito, H., Ui-Tei, K., Takahashi, K., Lukacsovich, T., Awano, W., Nakata, H., Piao, Z.F., Nilsson, E.E., Tomida, J., *et al.* (2000). Formation of the male-specific muscle in female *Drosophila* by ectopic fruitless expression. *Nat Cell Biol* 2, 500-506.
- van Mierlo, J.T., Bronkhorst, A.W., Overheul, G.J., Sadanandan, S.A., Ekstrom, J.O., Heestermans, M., Hultmark, D., Antoniewski, C., and van Rij, R.P. (2012). Convergent evolution of argonaute-2 slicer antagonism in two distinct insect RNA viruses. *PLoS Pathog* 8, e1002872.
- Venkataraman, K., Brown, K.M., and Gilmartin, G.M. (2005). Analysis of a noncanonical poly(A) site reveals a tripartite mechanism for vertebrate poly(A) site recognition. *Genes Dev* 19, 1315-1327.

- Venken, K.J., He, Y., Hoskins, R.A., and Bellen, H.J. (2006). P[acman]: a BAC transgenic platform for targeted insertion of large DNA fragments in *D. melanogaster*. *Science* 314, 1747-1751.
- Venter, J.C., Adams, M.D., Myers, E.W., Li, P.W., Mural, R.J., Sutton, G.G., Smith, H.O., Yandell, M., Evans, C.A., Holt, R.A., *et al.* (2001). The sequence of the human genome. *Science* 291, 1304-1351.
- Voelker, R.B., Erkelenz, S., Reynoso, V., Schaal, H., and Berglund, J.A. (2012). Frequent Gain and Loss of Intronic Splicing Regulatory Elements during the Evolution of Vertebrates. *Genome Biol Evol* 4, 659-674.
- Wagner, E.J., and Garcia-Blanco, M.A. (2002). RNAi-mediated PTB depletion leads to enhanced exon definition. *Mol Cell* 10, 943-949.
- Wahle, E., and Ruegsegger, U. (1999). 3'-End processing of pre-mRNA in eukaryotes. *FEMS Microbiol Rev* 23, 277-295.
- Wang, J., Ma, X., Yang, J.S., Zheng, X., Zugates, C.T., Lee, C.H., and Lee, T. (2004). Transmembrane/juxtamembrane domain-dependent Dscam distribution and function during mushroom body neuronal morphogenesis. *Neuron* 43, 663-672.
- Wang, J., Zugates, C.T., Liang, I.H., Lee, C.H., and Lee, T. (2002). *Drosophila* Dscam is required for divergent segregation of sister branches and suppresses ectopic bifurcation of axons. *Neuron* 33, 559-571.
- Watson, F.L., Puttmann-Holgado, R., Thomas, F., Lamar, D.L., Hughes, M., Kondo, M., Rebel, V.I., and Schmucker, D. (2005). Extensive diversity of Ig-superfamily proteins in the immune system of insects. *Science* 309, 1874-1878.
- Watthanasurorot, A., Jiravanichpaisal, P., Liu, H., Soderhall, I., and Soderhall, K. (2011). Bacteria-Induced Dscam Isoforms of the Crustacean, *Pacifastacus leniusculus*. *PLoS Pathog* 7, e1002062.
- Werner, M., Purta, E., Kaminska, K.H., Cymerman, I.A., Campbell, D.A., Mitra, B., Zamudio, J.R., Sturm, N.R., Jaworski, J., and Bujnicki, J.M. (2011). 2'-O-ribose methylation of cap2 in human: function and evolution in a horizontally mobile family. *Nucleic Acids Res* 39, 4756-4768.
- Williams, A.F., and Barclay, A.N. (1988). The immunoglobulin superfamily--domains for cell surface recognition. *Annu Rev Immunol* 6, 381-405.
- Wojtowicz, W.M., Flanagan, J.J., Millard, S.S., Zipursky, S.L., and Clemens, J.C. (2004). Alternative splicing of *Drosophila* Dscam generates axon guidance receptors that exhibit isoform-specific homophilic binding. *Cell* 118, 619-633.
- Wojtowicz, W.M., Wu, W., Andre, I., Qian, B., Baker, D., and Zipursky, S.L. (2007). A vast repertoire of Dscam binding specificities arises from modular interactions of variable Ig domains. *Cell* 130, 1134-1145.
- Yamakawa, K., Huot, Y.K., Haendelt, M.A., Hubert, R., Chen, X.N., Lyons, G.E., and Korenberg, J.R. (1998). DSCAM: a novel member of the immunoglobulin superfamily maps in a Down syndrome region and is involved in the development of the nervous system. *Hum Mol Genet* 7, 227-237.

- Yang, Y., Zhan, L., Zhang, W., Sun, F., Wang, W., Tian, N., Bi, J., Wang, H., Shi, D., Jiang, Y., *et al.* (2011). RNA secondary structure in mutually exclusive splicing. *Nat Struct Mol Biol* 18, 159-168.
- Yu, H.H., Yang, J.S., Wang, J., Huang, Y., and Lee, T. (2009). Endodomain diversity in the *Drosophila* Dscam and its roles in neuronal morphogenesis. *J Neurosci* 29, 1904-1914.
- Zaharieva, E., Chipman, J.K., and Soller, M. (2012). Alternative splicing interference by xenobiotics. *Toxicology* 296, 1-12.
- Zhan, X.L., Clemens, J.C., Neves, G., Hattori, D., Flanagan, J.J., Hummel, T., Vasconcelos, M.L., Chess, A., and Zipursky, S.L. (2004). Analysis of Dscam diversity in regulating axon guidance in *Drosophila* mushroom bodies. *Neuron* 43, 673-686.
- Zhao, J., Hyman, L., and Moore, C. (1999). Formation of mRNA 3' ends in eukaryotes: mechanism, regulation, and interrelationships with other steps in mRNA synthesis. *Microbiol Mol Biol Rev* 63, 405-445.
- Zhong, S., Li, H., Bodi, Z., Button, J., Vespa, L., Herzog, M., and Fray, R.G. (2008). MTA is an *Arabidopsis* messenger RNA adenosine methylase and interacts with a homolog of a sex-specific splicing factor. *Plant Cell* 20, 1278-1288.
- Zhou, H.L., Hinman, M.N., Barron, V.A., Geng, C., Zhou, G., Luo, G., Siegel, R.E., and Lou, H. (2011). Hu proteins regulate alternative splicing by inducing localized histone hyperacetylation in an RNA-dependent manner. *Proc Natl Acad Sci U S A* 108, E627-635.
- Zhu, H., Hummel, T., Clemens, J.C., Berdnik, D., Zipursky, S.L., and Luo, L. (2006). Dendritic patterning by Dscam and synaptic partner matching in the *Drosophila* antennal lobe. *Nat Neurosci* 9, 349-355.
- Zipursky, S.L., Wojtowicz, W.M., and Hattori, D. (2006). Got diversity? Wiring the fly brain with Dscam. *Trends Biochem Sci* 31, 581-588.